Nanoscale Manipulation of Electrokinetic Transport for Iontronic Applications based on Surface Modification

by

Jun Li

A thesis
presented to the University of Waterloo
in fulfillment of the
thesis requirement for the degree of
Doctor of Philosophy
in
Mechanical and Mechatronics Engineering

Waterloo, Ontario, Canada, 2021

EXAMINING COMMITTEE MEMBERSHIP

The following served on the Examining Committee for this thesis. The decision of the Examining Committee is by majority vote.

External Examiner	
NAME	Pouya Rezai
Title	Professor
Supervisor(s)	
NAME	Dongqing Li
Title	Professor
Internal Examiner	
NAME	Bo Cui
Title	Professor
Internal Examiner	
NAME	C. Perry Chou
Title	Professor
Internal Examiner	
NAME	Mustafa Yavuz
Title	Professor

AUTHOR'S DECLARATION

I hereby declare that I am the sole author of this thesis. This is a true copy of the thesis, including any required final revisions, as accepted by my examiners.

I understand that my thesis may be made electronically available to the public.

Abstract

Electrokinetic transport demonstrates a lot of new physical behaviors in nanofluidic systems due to the high surface-to-volume ratios and interactions between the fluid and walls of nanofluidic systems. The unique properties of electrokinetic transport in nanoscale offer possibilities for applications in many fields, such as biological computing, sensing, and drug delivery. Fundamental studies of electrokinetic transport phenomena in nanoscale have been investigated numerically and experimentally. However, the precise manipulation of electrokinetic transport in nanoscale is still a great challenge. Traditional nanofluidic devices are difficult to achieve practical applications due to their low accuracy and sensitivity. Surface modification is a promising method to develop nanofluidic devices with more functionalities. Up to date, the experimental study of electrokinetic transport in modified nanochannels is still limited.

This thesis systematically studies the electrokinetic transport phenomena in surface-modified polydimethylsiloxane (PDMS) nanochannels, as well as applications of chip-scale nanofluidic devices with surface modifications. At the beginning of this thesis, electroosmotic flow (EOF) is measured in pristine PDMS single nanochannels by the current-slope method. This nanochannel is fabricated by using solvent-induced cracking method and used to form a nanofluidic chip. The effects of ion size, ion valence, and pH of electrolyte solutions on the velocity of EOF in the nanochannel are experimentally studied. These results will serve as control data for the following studies of electrokinetic transport phenomena in modified nanochannels.

Then two fundamental research projects are conducted in nanochannels modified with DNA and charged polyelectrolytes to study the effects of surface modifications on electrokinetic transport phenomena. Electroosmotic flow is systematically investigated in DNA grafted hard PDMS (h-PDMS) channels with the channel size ranging from 50 nm to 2.5 μm by using the current-slope method. The effects of the DNA types, the incubation time, the pH value, the ionic concentration of electrolyte solutions, and the UV (ultraviolet) illumination on the EOF velocity are experimentally studied. The comparisons between the EOF in pristine nanochannels and DNA grafted nanochannels indicate that the surface modification of nanochannel can significantly affect the electrokinetic transport. Furthermore, the transport of fluid can be regulated by UV illumination in DNA grafted nanochannels. The size and surface charge of nanochannels after the layer-by-layer (LBL) deposition of polyelectrolytes are experimentally measured. The results reveal that the increment of the coated multilayer thickness will be limited in small nanochannels. A minimum

size of nanochannel exists when the nanochannel is modified by using LBL deposition of polyelectrolytes. This minimum size depends on the salt additive in the polyelectrolyte solutions. In addition, the surface charge of the modified nanochannels is determined by the outmost coated layer. The EOF can be alternatively reversed in the modified nanochannels by repeatedly coating oppositely charged polyelectrolytes.

Based on the results from the fundamental studies, a nanofluidic diode is developed by modifying the surface charge and size of a nanochannel with charged polyelectrolytes. The surface charge-governed electrokinetic transport of mobile ions results in diode-like behaviors of ionic current in the modified nanochannel. The working principle of the nanofluidic diode is explained and experimentally verified. The effects of the operation parameters, including ionic concentration, nanochannel length, and frequency, are systematically investigated. Two applications of the nanofluidic diode are presented in this thesis: improved resistive pulse sensing (RPS) system and iontronic circuits. A nanofluidic diode is fabricated and integrated into a RPS system serving as the sensing gate. A mathematic model for the modified RPS system is developed to evaluate the RPS signals. Nanoparticles with a diameter of 5 nm are also experimentally detected in the modified nanochannel-based RPS system. The experimental results are in good agreement with the numerical simulation results. By comparing the RPS signals in the modified nanochannel with that in the pristine nanochannel, it is found that RPS signals can be enhanced by approximately 50% when a nanofluidic diode is used as the sensing nanochannel. By integrating multiple nanofluidic diodes into a PDMS chip, iontronic circuits are developed. The performances of the iontronic circuits working as bipolar junction transistor and full-wave rectifier are examined and demonstrated. Signal manipulation and current rectification with high accuracy can be achieved by these iontronic circuits.

This thesis develops simple methods to modulate electrokinetic transport in nanochannels by surface modifications. The fundamental research in this thesis expands the understanding of electrokinetic transport phenomena in nanochannels with various surface modifications. The iontronic devices fabricated by using modified nanochannels provide new possibilities in the development of nanofluidic systems with more functionalities, toward improved biological computing and sensing.

Acknowledgements

First and foremost, I would like to thank my supervisor, Prof. Dongqing Li for his solid support and patient advice. His enthusiasm and foresight in academic research led me and inspired me a lot. Under his guidance, I had a great life in my Ph.D. program. It is my fortune and great honor to work in his lab. I also would like to thank my committee members, Prof. Pouya Rezai, Prof. Bo Cui, Prof, Mustafa Yavuz, and Prof. Perry Chou for their valuable comments and suggestions.

Many thanks to my friends and lab partners. During the four years at the University of Waterloo, Mr. Ran Peng, Mr. Mengqi Li, Mr. Kai Zhao, Mr. Chengfa Wang, and Mr. Kaihsiang Lin always support and help me. With their company, life and work become enjoyable in Waterloo.

I would like to thank my parents and my sister for their love. Their support and encouragement are important motivations in my life. I am lucky to have a supportive family.

Finally, I would like to thank my wife, Xiao Li. Thanks for your support and encouragement. You are the light in my life.

Table of Contents

List of Figures

List of Tables

List of Abbreviations

AFM	Atomic force microscope
ATRP	Atom transfer radical addition polymerization
BJT	Bipolar-junction transistor
CE	Capillary electrophoresis
CNT	Carbon nanotube
DS	Dextran sulfate
EDL	Electric double layer
EOF	Electroosmotic flow
EP	Electrophoresis
LBL	Layer-by-layer
LCST	lower critical solution temperature
MD	Molecular dynamics
PAA	Poly(acrylic acid)
PAH	Poly(allylamine) hydrochloride
PB	Polybrene
PDMS	Polydimethylsiloxane
PDDA	Poly-(diallyldimethylammonium chloride)
PEG	Poly(ethylene glycol)
PEI	Poly(ethyleneimine)
PEM	Polyelectrolyte multilayers
PLA	Poly(lactic acid)
PLGA	Poly(L-glutamic acid)
PLL	Poly(L-lysine)
PNIPAm	Poly(N-isopropylacrylamide)
PPO	Poly(propylene oxide)
RPS	Resistive pulse sensing
UCST	Upper critical solution temperature
UV	Ultraviolet
UVO	Ultraviolet and Ozone
XPS	X-ray photoelectron spectroscopy

List of Symbols

a	Radius of a spherical particle
Ψ	Electric potential
c_b	Bulk ionic concentration
d_o	Depth of the original nanochannel
d_m	Depth of polyelectrolytes modified nanochannel
D	Electrical displacement
D_i	Diffusion coefficient of ion i
ε_0	Electric permittivity of vacuum
E	Electric field strength
ε_r	Dielectric constant
e	Unit charge
F	Faraday constant
H	Nanochannel depth
I	Electric current
L	Nanochannel length
k_b	Boltzmann constant
n	Normal vector directed from the surface to the fluid
$n_{i\infty}$	Number density of ions
t_{av}	Average decrease in the nanochannel depth
R	Universal gas constant
T	Temperature
V_{AV}	Average velocity of the electroosmotic flow
V_{EOF}	Velocity of the electroosmotic flow
v_{Ep}	Electrophoretic velocity
W	Nanochannel width
z_i	Valence
ρ	Liquid density
μ	Dynamic viscosity
σ_W	Surface charge density on the walls of nanochannel
σ_p	Surface charge density of nanoparticle
η_{up}	Upstream noise
η_{down}	Downstream noise

List of Publications

(1) **J. Li**, R. Peng, D. Li, Effects of ion size, ion valence and pH of electrolyte solutions on EOF velocity in single nanochannels, Anal. Chim. Acta. 1059 (2019) 68–79. (Impact factor: **5.977**)

(2) **J. Li**, D. Li, Electroosmotic flow velocity in DNA modified nanochannels, J. Colloid Interface Sci. 553 (2019) 31–39. (Impact factor: **7.489**)

(3) Y. Song, C. Wang, **J. Li**, D. Li, Vortex generation in electroosmotic flow in a straight polydimethylsiloxane microchannel with different polybrene modified-to-unmodified section length ratios, Microfluid. Nanofluidics. 23 (2019) 1–11. (Impact factor: **2.489**)

(4) **J. Li**, D. Li, Polyelectrolyte adsorption in single small nanochannel by layer-by-layer method, J. Colloid Interface Sci. 561 (2020) 1–10. (Impact factor: **7.489**)

(5) **J. Li**, D. Li, A surface charge governed nanofluidic diode based on a single polydimethylsiloxane (PDMS) nanochannel, J. Colloid Interface Sci. 596 (2021) 54–63. (Impact factor: **7.489**)

(6) **J. Li**, D. Li, A method to improve the resistive pulse sensing by modifying surface charge of nanochannels, Sensors Actuators, B Chem. 337 (2021) 129773. (Impact factor: **7.100**)

Chapter 1 Introduction

1.1 Problem statement

The electrokinetic transport demonstrates unique performances in nanofluidic systems with at least one-dimension size smaller than 100 nm due to the high surface-to-volume ratio. Recently, in nanofluidic, numerous applications have been suggested for the electrokinetic transport phenomena in the fields of biology[1], chemical analysis[2,3], and mechanical engineering[4]. For instance, the coherent and oscillatory signals in electric current can be observed when ions transport through a nanochannel. As the size of the nanochannel becomes smaller than 10 nm, stochastic oscillations can be observed in electroosmotic current. This phenomenon that ionic transport can generate waveform signals in small nanochannels supplies applications of sensors and nanoreactors[5]. Besides, the overlapped EDLs in nanochannels induce surface charge governed ion transport, which can significantly affect the ionic current through nanochannels[6].

Many aspects of the physics of electrokinetic transport in nanochannels have been studied with the advancement of nano-fabrication technology. However, the accurate manipulation of the electrokinetic transport is still a challenge for researchers. Since the electrokinetic transport phenomena are mainly determined by the surface properties in general microfluidic and nanofluidic devices, surface modification is one of the most popular methods to effectively modulate the surface properties of nanochannels and realize complex control of electrokinetic transport in nanofluidic systems. A series of surface modification techniques have been developed for nanochannel functionalization. The general strategy for nanochannel surface modification is decorating functional groups on the nanochannel surfaces, such as DNAs and polymers. These surface modification techniques mainly focus on the surface properties of the modified nanochannels. The size regulation of nanochannels is seldom reported, which is a key factor in electrokinetic transport phenomena. Therefore, a simple and productive technique for the modulation of nanochannel surface properties and sizes is needed for nanofluidic researchers.

Manipulation of electrokinetic transport phenomena plays an important role in nanofluidic systems. Surface modification of nanochannels is an effective way to modulate electrokinetic transport in nanoscale. A lot of numerical studies and some experimental studies have been conducted to investigate surface modifications in

nanofluidic systems. Most of these studies focus on the surface properties and dimensional features of the nanochannel. The experimental results of the transport of fluid and ions in the modified nanochannel are very limited. Therefore, comprehensive understandings of electrokinetic transport in nanochannels with surface modifications are highly desirable.

Due to the restrictions of surface modification techniques and understandings of electrokinetic transport phenomena, the development of nanofluidic systems for practical applications is still challenging. For example, typical surface modification methods require specific materials and extremely small nanochannels to complete effective surface charge regulation of nanochannels. Nanofluidic diodes fabricated by decorating asymmetric surface charges along nanochannels are commonly developed base on porous membranes. The vertical structures of these membrane-based nanofluidic devices make it highly challenging to further integrate them into a chip-scale nanofluidic system for meeting practical application requirements. In addition, the undefined number of nanochannels in these devices results in low reproducibility. Therefore, integrated nanofluidic systems with simple surface modification techniques are highly desirable and will broaden the applications of nanofluidic systems.

1.2 Research objectives

The purpose of this thesis is to investigate the electrokinetic transport phenomena in nanochannels with surface modifications and develop integrated nanofluidic devices for applications. To achieve the goals, studies about the characterization of electrokinetic transport in modified nanochannels, development of surface modification techniques, and applications of modified nanochannels are conducted. The detailed objectives include:

1) Analyze the influence factors of EOF in PDMS nanochannels.
2) Fabricate single nanochannels modified with DNAs and characterize the surface modification with an atomic force microscope (AFM).
3) Investigate the influence factors of EOF in DNA-modified nanochannels.
4) Develop a surface modification method for regulating the nanochannel size and surface charge. The minimum size and surface charge of the modified nanochannel are characterized.

5) Design and fabricate nanofluidic diodes based on the developed surface modification method. Investigate the influence factors of the nanofluidic diode performance and find optimal working parameters.

6) Develop a RPS detection system with a modified sensing nanochannel and investigate the effects of the surface modification on the resolution of the RPS system.

7) Design and fabricate chip-scale iontronic systems based on the manipulation of electrokinetic transport in modified nanochannels.

1.3 Thesis layout

The thesis includes 9 chapters, and the structure of the thesis is shown in Figure 1-1. Chapter 1 presents an overview of this thesis, including a research background, motivation, and objectives of the thesis.

Chapter 2 reviews the electrokinetic transport phenomena and surface modification techniques in nanochannels. The classic electrokinetic phenomena, including electroosmotic, electric double layer (EDL), and electrophoresis (EP) are introduced. A summary and comparison of surface modification techniques are made. Chapter 2 aims to present the fundamental background of electrokinetic transport phenomena and give information on surface modification techniques.

Chapter 3 demonstrates an experimental study of EOF in PDMS nanochannels. The current-slope method is employed to measure the EOF velocity in nanochannels. The effects of ion size, pH value, and ion valence on the EOF are investigated. A model is presented to explain these effects on EOF transport.

Chapter 4 and Chapter 5 systematically investigate the EOF in modified nanochannels. In Chapter 4, nanochannels modified with DNAs are developed, and the performance of the surface modification is characterized. The effects of the incubation time on the grafting density are experimentally analyzed. An experimental system with an ultraviolet (UV) source is built for EOF velocity measurement. The effects of DNA types, incubation time, pH value, ionic concentration, and UV illumination on the velocity of EOF are experimentally studied.

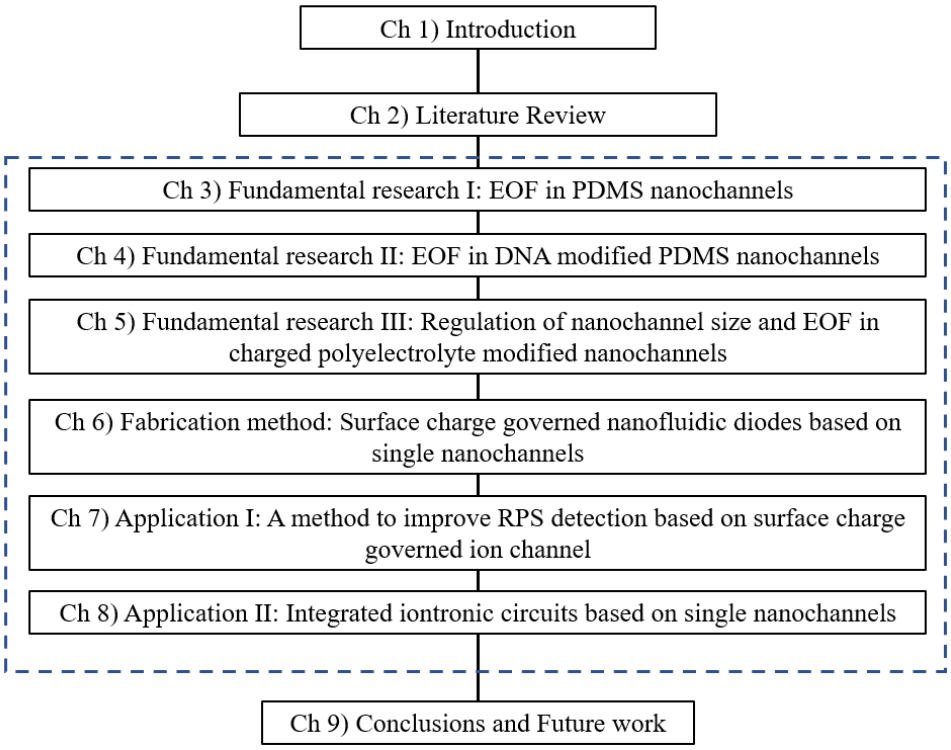

Figure 1-1. Thesis layout.

Chapter 5 investigates the modulation of size and surface properties of nanochannels by using layer-by-layer (LBL) deposition of polyelectrolytes. The thicknesses of the coated polyelectrolyte layer on flat surface and nanochannel wall are experimentally measured by AFM. The influence factors of the growth of the multiple polyelectrolyte layers on nanochannel surfaces are systematically investigated. The minimum size of nanochannels that can be achieved by this modification method is defined. EOF velocity is measured in the modified nanochannel by using the current-slope method. The surface charge of each polyelectrolyte layer on the modified nanochannel is characterized based on the measured EOF velocities.

Chapter 6 demonstrates nanofluidic diodes developed on single PDMS nanochannels by surface modification with charged polyelectrolytes. A method for generating asymmetric surface charges along nanochannels is presented in this chapter. The experimental visualization of ion distribution in the modified nanochannel is conducted with a florescent dye solution to explain the working principle of the nanofluidic diode. The parameters in the fabrication and operation of the nanofluidic diode, including nanochannel length, frequency, ionic

concentration, and applied electric field, are systematically studied. The optimal parameters for the design and fabrication of the single PDMS nanochannel-based nanofluidic diode are presented.

Chapter 7 and 8 present two applications, RPS detection system and inotronic circuits, by using nanochannels modified with charged polyelectrolytes. In Chapter 7, a RPS detection system with a single nanochannel serving as the sensing channel is built up. The sensing channel is modified with charged polyelectrolytes to generate positive surface charge, negative surface charge, or opposite surface at the two ends, respectively. The effects of the surface charge on the sensitivity of the RPS detection system are investigated. Based on the study, an effective method for the improvement of RPS detection sensitivity is provided. Chapter 8 demonstrates a novel design of an integrated iontronic device. This device can work as either a bipolar junction transistor or a full-wave bridge rectifier. The functions of this iontronic device are experimentally verified and displayed.

The last chapter, Chapter 9, concludes the major contributions, conclusions, and future research directions on electrokinetic transport and applications of nanochannels with surface modifications.

Chapter 2 Literature Review

This chapter provides an overview of classical electrokinetic transport phenomena and surface modification techniques in nanofluidics. The fundamental knowledge of electric double layer, electroosmotic flow, and electrophoresis is introduced. In surface modification techniques, the conventional strategies to develop functional nanochannels are introduced, including exposure to energy, modification with nonionic surfactants, charged polyelectrolytes, and stimuli-responsive polymers. The surface properties and structures of the nanochannels after surface modifications are also introduced. This chapter gives the fundamental background of the thesis.

2.1 Electrokinetic transport phenomena

2.1.1 Electric double layer theory

An electric double layer (EDL) is a rearrangement of free ions in the vicinity of a charged surface that is exposed to an aqueous electrolyte solution. Most materials acquire electrostatic charges when they are in contact with electrolyte solutions. The counterions in the solutions will be attracted to the charged surface, and the co-ions will be repelled away from the surface, leading to a net charge distribution near the surface. Theories have been developed to explain the charge distribution and the structure of EDL, and the Gouy-Chapman-Stern model is the most widely used model in the scientific community[7–9]. In this model, as shown in Figure 2-1, EDL is characterized by a Stern layer (also called compact layer) comprised immobile counterions attached to a charged surface, a diffuse layer of mobile ions that is symbolized by Debye-Huckel length (λ_D) and a zeta potential at the shear plane dividing the Stern layer and the diffuse layer. The Poisson-Boltzmann equation is usually used to describe the EDL field and the distribution of ions in microchannels[10].

$$\nabla^2\Psi = -\frac{\mathrm{e}}{\varepsilon_0\varepsilon_r}\sum z_i\, n_{i\infty} exp\left[-\frac{z_i e\Psi}{k_b T}\right] \tag{2-1}$$

Where Ψ is the electric potential, ε_r is the dielectric constant of the electrolyte, ε_0 is the electric permittivity of vacuum, e is the unit charge, k_b is the Boltzmann constant, $n_{i\infty}$ is the number density of ions in the bulk, z_i is the valence, and T is the temperature.

The stern layer with the typical thickness of one counterion diameter is very thin forming near the charged surface. In the stern layer, the concentration of the counter-ions is much more significant than that of the co-ions due to the strong electrostatic force, and these counter-ions are almost immobilized.

The diffuse layer forms after the stern layer, and its thickness is around three to five times of the Debye-Huckel length which can be calculated with the equation:

$$\lambda_D = \sqrt{\frac{\varepsilon_0 \varepsilon_r k_b T}{2 n_{i\infty} (ze)^2}} \tag{2-2}$$

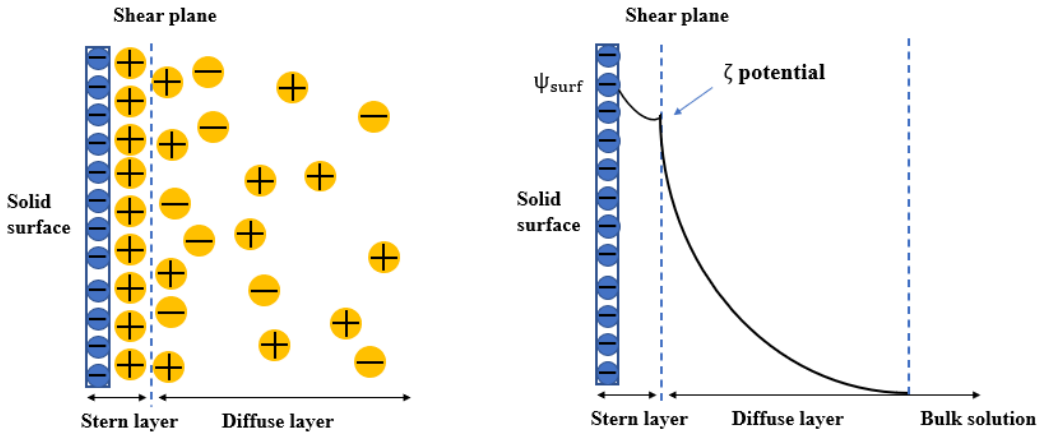

Figure 2-1. Schematic of electric double layer (left) and electrical potential distribution near a solid surface (right).

With the dimensional size of channels reducing to the submicron and nanoscale, the conventional theories are not applicable anymore for predicting the structure and capacitance of the EDL[11]. In nanochannels, the EDL will overlap, and the concentration of co-ions and counter-ions are not equal[12]. To analyze the steric effects in small nanochannels with overlapped EDL, the ion size is a very important criterion which is not considered in the conventional Poisson–Boltzmann equation. Recently, several studies have been developed to investigate the ionic correlation effects on the EDL in nanoscale, such as overscreening and crowding of the counter-ions near the charged surface[12–14]. Some modified Poisson–Boltzmann equations were presented to more accurately predict the distribution of electric potential and ion concentration in nanochannels with overlapped EDLs by taking into account ion size effects[15–17]. Based on these studies, both the structure and electric properties of EDL are related to the size of the counter-ions in the stern layer. Furthermore, the steric effects can enhance the extent of EDL overlap in nanochannels, thus affecting electrokinetic phenomena which depend on the EDL interactions.

2.1.2 Electroosmotic flow

Electroosmotic flow is a motion of flow caused by the interactions between electric double layer and applied electric field. The solid surface will attract counter-ions and repel co-ions when it is in contact with electrolyte solutions, forming electric double layer. The counter-ions in the stern layer are immobilized, and the excess counterions in the diffuse layer will move and drive the liquid to move with them under an external applied electric field. The rest of the liquid in the channel will be dragged to move with the movement of the liquid near the channel wall by the viscous force, generating electroosmotic flow. In most cases, the thickness of EDL is negligible compared with the size of microchannels. Generally, Helmholtz-Smoluchowski theory is utilized to calculate the electroosmotic flow velocity throughout microchannels.

$$v_{EOF} = \frac{\varepsilon_0 \varepsilon_r \zeta_w}{\mu} E_{ex} \tag{2-3}$$

where E_{ex} is the external applied electric field, ζ_w is the zeta potential of the channel wall and μ is the viscosity of the solution.

When the channel size reduces to the nanoscale and the thickness of EDL is comparable with the channel size, the interaction between EDLs has to be considered which can significantly influence the ion distribution and EOF velocity in the channel. As a result, the EOF velocity cannot be calculated accurately with the Helmholtz-Smoluchowski equation in nanochannels. Recently, extensive numerical and experimental studies of the effects of ion size[18–20], ion species[21–23], ion valence[24,25], pH value[26–28], ionic concentration[21,29–31], surface charge density[32,33], and channel size[34–37] on the distribution of EDL and EOF velocity in nanochannels have been conducted.

Numerical studies: Several models have been developed to predict EOF in nanoscale systems. Bazant et al.[38] presented a model including the finite ion size effects into a general continuum theory framework to analyzed the crowding effects on EOF velocity in nanochannels. Hatlo et al.[39] theoretically reported an improved model for predicting the double layer capacitance by including the excess ion polarizability into the Poisson-Boltzmann theory. Bonthus et al.[40] also derived a theoretical framework to show the dielectric profile near a surface and provided an improved understanding of electrokinetic phenomena. With the development of these models, a lot of molecular dynamics (MD) simulation studies have been conducted to investigate the ion distribution and EOF velocity profile in nanochannels, considering the finite ion size effects and steric effects. Qiao and Aluru[41] studied the velocity profiles of EOF in nanochannel by using molecular dynamics simulation

and showed that the velocity profile of EOF will be the “parabola type” instead of the “plunger type” in nanochannels. Freund[42] also investigated the electroosmotic flow in nanochannel by molecular simulation and found that the velocity profile is approximately flatted in the stern layer near the channel surface and parabolic in the middle of the channel. Rezaei et al.[43] presented the profile of ion concentration in a charged nanochannel and reported that EDL’s boundary is located at the plane where the ion concentrations of counterions and co-ions are equal. Joly et al.[44] also reported a similar ionic density profile near a charged wall. Some simulation studies reported that the phenomena of charge inversion and flow reversal in nanochannels. Qiao and Aluru[45] studied the electroosmotic flow reversal in very small nanochannels by using molecular dynamics simulations. Their results showed that the immobilized counterions adsorbed on the channel wall can cause a charge inversion phenomenon, thus leading to flow reversal. Rezaei et al.[46,47] analyzed the stern layer effects on charge inversion and flow reversal. When the total electric charges attracted by the charged surface in the stern layer exceed the surface charge, the shear plane charge will be opposite to the surface charge, and the electroosmotic flow will form in the opposite direction. Mashayak and Aluru[48] developed a study based on quasi-continuum theory to predict the charge inversion phenomenon more accurately. They stated that the electrostatic correlation effects and ion hydration are also very important to determine the ion distribution and the charge inversion in EDLs.

Experimental studies: With the advancement of nano-fabrication technology, several studies to experimentally examine electroosmotic flow in ultrafine channels have been reported. Jacobson et al.[49] evaluated the electroosmotic mobilities in a nanochannel with a depth of 98 nm and in some microchannels. By comparing the measured results of EOF velocity, they stated that there was a 35% reduction in the electroosmotic mobility in the nanochannel in comparison with that in microchannels. Peng and Li[50] fabricated single PDMS nanochannels and measured the EOF velocity in the single nanochannels as small as 20 nm in depth by the current-slope method[51,52]. They found that the overlapped EDL can significantly reduce the velocity of EOF, and the velocity depends on the ionic concentration and the applied electric field strength. Chou et al.[53] also measured the EOF velocity in a nanochannel of 50 nm and proposed that trivalent ions may adsorb on the negatively charged surface and cause a charge inversion, thus introducing a reverse flow in the nanochannel. Uba et al.[54] monitored the pH effects on the surface charge density in a PMMA channel with the depth of 120 nm and width of 120 nm. Their results showed that the surface charge density gradually increases when the pH of the electrolyte solution becomes larger.

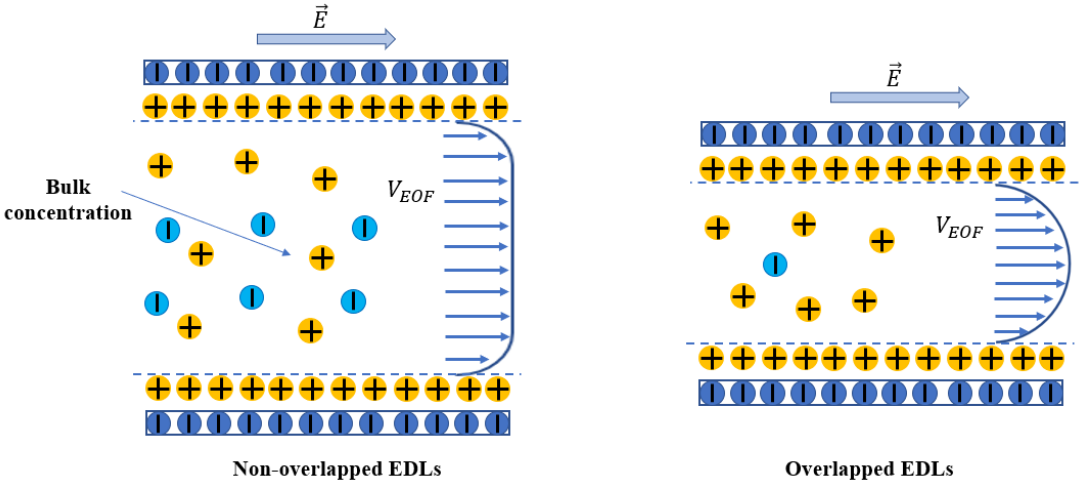

(a) (b)

Figure 2-2. Schematic of electroosmotic flow in (a) microchannel and (b) nanochannel with overlapped EDLs.

2.1.3 Electroosmotic flow in surface modified nanochannels

With the advancement of lab-on-a-chip technology, EOF is widely employed as a method of transporting liquids in microfluidic devices and nanofluidic devices due to its many advantages, such as ease to control and high reliability[55]. Although the transport phenomena and physics performances of electroosmotic flow have been well understood in microchannels, there still are many new challenges presented to researchers, such as the effects of surface roughness[56], and convective and absolute electrokinetic instability in electroosmotic flow[57].

Effective control of EOF is a crucial factor in both microfluidic and nanofluidic devices. For protein analysis, it typically requires suppressing the EOF to achieve a high-efficiency separation. For capillary electrochromatography, however, the EOF needs to be generated with high throughput to enhance the separation speed. Significant attention has been paid to EOF modulation in recent years. In EOF modulation, the surface coating is one of the most popular methods to effectively control EOF and minimize wall-analyte interactions in microchannels[58–62] and nanochannels[63–67]. The effects of the coated layer on electrokinetic transport have been investigated extensively. Theoretically, Harden et al.[68] set up a model to predict the qualitative features of EOF velocity in channels with end-grafted polyelectrolytes and reported that the EOF mobility is essentially determined by the electrokinetic

properties of the polymer in channels with densely grafted polymers. Adiga and Brenner[65] studied the EOF velocity distribution in a nanopore grafted with polymer brush by using molecular dynamics simulation method and showed that the EOF velocity depends on the coupling effects of polymer conformational dynamics induced by the drag force of fluid flow and electrohydrodynamics. Huang et al.[64] also investigated the electric properties of the surface on which polyelectrolyte brushes are grafted and reported that the surface charge is dependent on the grafting density, pH, electrolyte concentration, and the thickness of the brush layer. Cao et al.[66] stated that the maximum EOF velocity in the polymer-grafted nanochannel center region depends on the grafting density and solvent quality. Experimentally, the polymer or DNA chains can be irreversibly grafted onto the surface by chemical reactions between the inner surface and coated material to create covalent bonds[69–73], or reversibly adsorbed on the surface. Xia et al.[74] fabricated a pH-regulated smart nanochannel by coating DNA brushed onto the inner wall of the channel. Bello et al.[75] proposed that the EOF velocity could be progressively suppressed by absorbing polymer layers onto the channel wall. Hjerten[76] stated that the electroosmotic flow could be eliminated in channels by coating a layer of neutral polymer. Paumier et al.[77] measured the EOF velocity in channels grafted with neutrally charged polymers and reported that the thickness of the coated layer could control the development of EOF. When the polymer layer is thicker than the EDL, the EOF can be effectively prohibited even the channel surface with nonzero zeta potential. On the contrary, if the thickness of the coated polymer layer is smaller than that of EDL, the EOF could still occur unimpeded. Raafatnia[78] et al. further investigated the mobility of polyelectrolyte-grafted colloids in monovalent salt solutions. They presented that the mobility is dominated by the polyelectrolyte brush regime at high ionic concentrations. In Manning's theory, the neutralization of DNA charges is only determined by the valence of counterions in the solvent and independent of its type and concentration[79]. Guo et al. studied the effects on this issue and reported that the DNA charge neutralization is also dependent on the pH value of the solution or the concentration of hydrogen ions[71]. Moreover, the molecular structure of DNAs can be influenced by ultraviolet(UV) irradiation, thus changing the charges carried by DNAs[80–82]. Therefore, UV illumination can be an elegant way to modulate EOF in the DNA coated channels without any additives.

2.1.4 Electrophoresis

Electrophoresis is a motion that charged particles move in a bulk liquid driven by an external applied electric field. When an electric field is applied, charged particles will move along the electric field with the Coulomb force. The direction of the movement depends on the sign of the particles'

surface charges. The electrophoretic velocity of a charged particle in fluids can be calculated by the equation:

$$v_{Ep} = \frac{\varepsilon_0 \varepsilon_r \zeta_p}{\mu} E_{ex} \tag{2-4}$$

Where ζ_p is the zeta potential of the charged particle surface, E_{ex} is the applied electric field intensity.

With considering the viscous stress, the electrophoretic velocity is calculated by balancing the flow frictional force and the electrical force exerted on the charged particles.

$$v_{Ep} = \frac{2}{3} \frac{\varepsilon_0 \varepsilon_r \zeta_p E_\infty}{\mu} (1 + ka) \tag{2-5}$$

Where a is the radius of a spherical particle, When $ka \ll 1$, which mean the EDL is very thin, the equation can be reduced to:

$$v_{Ep} = \frac{2}{3} \frac{\varepsilon_0 \varepsilon_r \zeta_p}{\mu} E_{ex} \tag{2-6}$$

2.2 Surface modification techniques

2.2.1 Modification by exposure to energy

The PDMS surface properties can be altered, and some surface molecular groups can be activated by exposure to various energy sources, such as oxygen plasma[83–86] and ultraviolet light[87,88]. Plasma is a gas of positive and negative charges presenting in equal amount. It is a mixture of ions and electrons with high energy. When a plasma is applied to a PDMS surface, the reaction occurs at the surface, and surface oxidation is generated. The plasma treatment can significantly transfer the surface chemistry of PDMS because the surface is subjected to high energy species, such as ions, electrons, and radiation, during the treatment process. The reactions generated by plasma are complex, and the mechanisms behind the PDMS surface oxidation are not well understood. Generally, the effects of plasma exposure on PDMS surface can be defined as the following two stages. First, a silica layer of SiOx with more oxygen ions in the molecular structure than the PDMS will be formed on the PDMS surface after the application of plasma[89]. Second, the silica layer will disappear and be displaced by low molecular weight PDMS groups[84,90,91]. With the surface oxidation generated by plasma treatment, the PDMS surface wettability will increase, thus improving adhesion. This is because a silica-like layer produced by various plasma gases is wettable. However, the surface will recover the

hydrophobicity progressively due to the migration of untreated polymer chains from the bulk phase to the surface through the cracks of the silica-like layer[91]. Owen et al.[84,91] experimentally measured the thickness of the silica-like layer, which is about 10 nm, and the depth of the crack in the layer, which is ranging from 0.3 μm to 0.5 μm, by using X-ray photoelectron spectroscopy (XPS). The number of cracks is positively related to the plasma exposure time. When the exposure time is long, a larger number of cracks are generated in the treated polymer layer, causing a rapid diffusion of PDMS chains from the bulk PDMS to the surface.

Plasma treatment as a useful way of achieving wettability has been widely used in the microfluidic and nanofluidic systems. The high-energy plasma treatment provides an easy bonding method of a PDMS chip to a flat substrate. Wang el. al[92] investigated the oxidization of PDMS surfaces to form functional molecular groups by using a chemical force microscope and stated that the oxidized PDMS surface provides faster EOF than the native PDMS surface. Duffy et al. [93] also reported that the channels oxidized with plasma are filled easily with liquid. The channels oxidized by plasma are widely used in microfluidic electrophoresis because of their hydrophilicity and negatively charged surfaces when being in contact with aqueous solutions, which supporting EOF. The EOF in oxidized PDMS channels could be maintained for several days. However, because of the hydrophobicity recovery, the reliable analysis time by using an oxidized PDMS channel is only around 3h. This property restricted the applications of oxidized PDMS channels. To address this problem, continuous storage of PDMS channels in water is a good choice, which could stabilize EOF. Ren et al.[94] shown that the enhanced EOF can be preserved as long as the channels were stored in an aqueous solution.

UV illumination has similar effects on PDMS surface modification to plasma treatment that could initiate reactions on the surface and change its chemical properties. Some studies of UV polymerization on PDMS have been conducted recently[95–97]. The UV light can polymerize monomer solutions onto PDMS surfaces and form a gel-based structure. By grafting monomers with different chemical properties on PDMS, the PDMS surface can demonstrate significantly different performances. Hu et al.[98] achieved a high-quality separation in PDMS microchannel chips grafted with mixtures of monomers by using UV exposure. It is also reported that the UV graft polymerization can be significantly accelerated by preabsorbing Benzophenone on the PDMS surface. Compared with the plasma treatment method, an advantage of the UV illumination with monomer solutions for the surface modification of PDMS surface is that a covalent and stable polymeric coating can be formed on the surface in response to repeated hydration and air exposure[99]. Seong et al.[95] presented a method

that can fabricate hydrogel plugs in PDMS microchannels by using UV illumination and a photoinitiator. Their design provides an effective DNA manipulation tool and could be an important approach for analyzing gene expression in microfluidic chips. A combination of UV light and ozone (UVO) is also extensively used in the surface modification of PDMS. When a PDMS surface is exposed to UV/ozone, a photochemical process is induced, and a thin silicon oxide layer can be formed on the surface. The thickness of the layer on PDMS is around 20~30 nm[100]. As introduced above, UV illumination can cause a chain scission and create radicals on PDMS surfaces. The network formed with these radicals on PDMS surfaces has similar wetting properties to the untreated surface. In contrast to UV illumination, UVO modification method can generate a large number of hydrophilic groups both on the surface and the subsurface of PDMS[88]. UV and UVO can significantly change the chemical properties and structure of PDMS, thus manipulating the transport in PDMS channels. However, compared to plasma treatment, it typically requires a very long exposure time to fully achieve the transformation process.

2.2.2 Modification with nonionic surfactants

Nonionic surfactants can be adsorbed onto PDMS surfaces and create hydrophilic layers which can prevent the interactions between proteins and the surface and provide a stable electroosmotic flow in microfluidic and nanofluidic devices. Brij35 (PEO-dodecanol) is one of the most widely used nonionic surfactants in reducing the protein adsorption on the surface of microfluidic channels and capillaries due to its commercial availability, low cost, and simple coating process. The coating process can be achieved by incubating a PDMS surface into a coating solution directly. Then, the hydrophobic alkyl chains of Brij 35 will be adsorbed on the hydrophobic PDMS surface. The hydrophilic ends of PEO will be extruded to the free surface. It is reported that these hydrophilic ends could repel protein to a sufficient distance from the modified surface and residual silanol groups on the PDMS surface[101]. Dou et al. stated that the protein separation can be facilitated in the Brij 35 coated PDMS microchannels because the channel surface can be turned from hydrophobic interface to hydrophilic interface by the surface coating process. They also obtained that the electroosmotic mobility will decrease when the coating density of Brij 35 increases[102]. However, it requires at least 1 h of air drying to achieve the coating process. Otherwise, the surface properties are unstable.

Tween 20 and n-dodecyl- b-D-maltoside (DDM) also have been commonly used for PDMS channel surface coating. Tween 20 is poly(ethylene oxide) (PEO)-based copolymer containing a hydrophobic head group. The hydrophobic head group can work as an anchor to facilitate its adsorption on a hydrophobic PDMS surface. DDM is an alkyl polyglucoside that can strongly adsorb on

hydrophobic surfaces. Similar to Brij 35, these two surfactants can turn the PDMS surface to hydrophilic and nonionic, thus preventing protein adsorption. Boxshall et al.[103] experimentally studied the effects of coated Tween 20 layer on PDMS surface and reported that the surfactant can dramatically reduce the protein adsorption and fibroblast attachment. Besides, the reduction in protein adsorption is related to the solution concentration. The effects of DDM coating on PDMS were also investigated. The interactions between DDM alkyl chains and the PDMS surface generate bindings and make the surface become passivated, thus minimizing protein adsorption. Furthermore, the DDM coating could suppress the electroosmotic flow in coated channels because the surface charges are covered by the coated surfactants[103].

Other PEG-copolymers containing different blocks have been utilized for the surface modification of microfluidic devices. For instance, Pluronic is a series of surfactants that have the blocks of poly(propylene oxide) (PPO) and can be strongly adsorbed on hydrophobic materials by hydrophobic mechanism that makes it possible to be an ideal coating surfactant for PDMS surface. A method to micropattern Pluronic on various substrates, such as PDMS and glass, has been presented by Tan et al[103]. They pointed out that the surface wettability is a crucial factor for Pluronic adsorption that the Pluronic adsorption only occurs when the surface wettability is at intermediate to low. Hellmich et al. [104]experimentally studied the EOF in Pluronic F108 coated PDMS channels which are pretreated with plasma or UV light. Compared to the native PDMS channels, the mobility of EOF is relatively smaller in modified channels because the long polymer tails coated on the PDMS surface could extend through the double layer and increase the viscosity significantly. Poly(lactic acid)-poly(ethylene glycol)-biotin (PLA-PEG-biotin) is a degradable polymer that also shows effective protein resistance properties. It can rapidly create a biomimetic surface in aqueous media and is commonly used in the applications of tissue engineering[105,106].

2.2.3 Modification with charged polymers

Generally, a PDMS surface is negatively charged when being in contact with electrolyte solutions. Positively charged polyelectrolytes, such as Polybrene (PB), Poly(ethyleneimine) (PEI), Poly(allylamine) hydrochloride (PAH), Poly-(diallyldimethylammonium chloride) (PDDA), Poly-L-lysine (PLL) can be strongly attached to PDMS surfaces by electrostatic adsorption and inverse the surface charge of PDMS. Poly(L-lysine)-graft-poly(ethylene glycol) (PLL-g-PEG) is a copolymer with PEG side and polycationic PLL backbone. Lee and voros[107] reported a simple modification method of PDMS surfaces to achieve high-effective protein resistance by coating PLL-g-PEG. In this method,

the PDMS surface was pretreated with oxygen plasma and then immersed into an aqueous solution containing PLL-g-PEG. The polycationic PLL backbone can be attracted by the negative charges on the PDMS surface generated by oxygen plasma treatment, and the PEG side will be oriented to the liquid phase in the PDMS channel. The liquid/PEG interface showed excellent resistance to protein adsorption. This approach also can be applied to graft PEG on a network of PDMS channels, thus realizing protein patterning on the PDMS surface. Besides, the solvent swelling effects of PDMS channels can be relieved by using organic solvent-based PEG solution to modify the channel surface[108]. For the effects on fluid transport, the charged polyelectrolytes could repel equally charged molecules from the surface and revise the sign of the surface charge, leading to the flow reversal of EOF. Biddiss et al.[109] designed a PDMS microchannel with heterogeneous surface charge density by patterning polycationic polymer PB on a channel surface to enhance the mixing efficiency of different solutions inside the channel.

Although the physical adsorption of charged polymers is easy to achieve for surface modification, there is still a challenge in fabricating PDMS channels with long-term stability by using this method. To address this problem, an improved technique by exposing a PDMS surface to polycationic and polyanionic polymers alternately has been developed[110]. Typically, the adsorbed polyelectrolytes on the surface allow oppositely charged polyelectrolytes to be adsorbed on the coated surface that is called layer-by-layer (LBL) coating. The LBL process is achieved by the self-assembly of oppositely charged polyelectrolyte layers with electrostatic interactions or hydrogen-bonding interactions. Figure 2-3 (a) illustrates the LBL deposition process that depends on electrostatic interactions. Polycationic molecules, such as PLL, can be alternatively bonded with the polyanionic polymer of poly(L-glutamic acid) (PLGA) to form multilayers on the treated surface[111]. For the mechanism of hydrogen bonding, as shown in Figure 2-3 (b), the polycationic molecules with hydrogen acceptors and the polyanionic molecules with hydrogen donors can form the multilayer structure self-assembly by the attractive interaction between them[111,112].

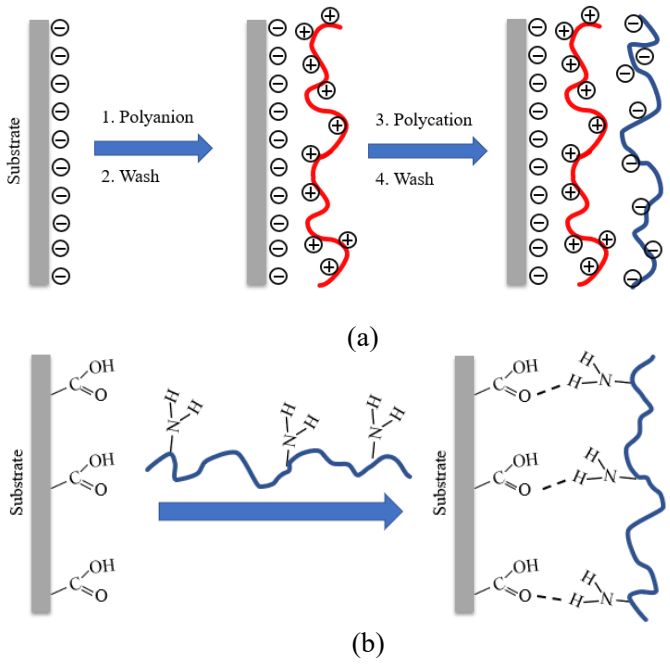

Figure 2-3. Scheme of LBL deposition process on a charge surface[110,112]. (a) Electrostatic interactions; (b) hydrogen-bonding interactions.

The charged polyelectrolytes are deposited from solutions to the surface that means this method can be carried out without requirements of the size and topology of the surface. Furthermore, the coated multiple layers can cover the defects on the underlying surface. Consequently, the modified surface properties are determined by the coated polyelectrolytes and the adsorption conditions. Decher[110] stated that similar surface properties can be obtained on various substrates as long as they are treated with the same polyelectrolytes. This method has been commonly used in EOF modulation by controlling the surface charges in microfluidics. Liu et al.[113] have shown that the PDMS microchannels coated with PB/DS multilayers exhibit a long-term stable and pH-independent EOF as pH is ranging from 5 to 10. The coating layer number of polyelectrolytes is a key factor for EOF reproducibility in this method. It is reported that the EOF mobility varies at low coating layer number and becomes essentially consistent at high coating layer number[114]. The variability of EOF at low coating layer number may be caused by the partial surface coverage and unstable coated film structure. When the layer number increases and the film becomes thicker, the overall consistency of the coated layer improves, and the surface charge density becomes more uniform. The layer number also affects the thickness of the coated film and the size of the channel which influences the EOF velocity in small

nanochannels. Dubas and Schlenoff [115] demonstrated that the thickness of polyelectrolyte multilayers (PEM) is related to the salt concentration. The presence of salt in the solution used for dynamic coating PEM on a surface increases the thickness of the layers. The changes in the layer thickness are caused by the coiling of polyelectrolyte chains with a high counterion concentration during the adsorption process. The adsorption process is achieved by ion exchange that the polyelectrolyte chains displace the counterions near the surface. Once the adsorption was completed, the structure and the thickness of the PEM cannot be changed anymore with changing salt concentration. Furthermore, the adsorption of PEM was irreversible, and only a small extent of desorption was observed after weeks[115]. Other data about the average PEM thickness with different polyelectrolytes was reported by Haselberg et al[116].

2.2.4 Modification with stimuli-responsive polymers

Chemical grafting is commonly used for developing stimuli-responsive surfaces and interfaces. Various stimuli-responsive polymers, such as binary polymer brushes[117–119], thermo-responsive polymers[120–122], and light-switchable polymers, can be used to manipulate the motion of the liquid in nanochannels by "grafting to" or "grafting from" the channel surfaces. In the approach of "grafting to" surfaces, stimuli-responsive polymers with end functional groups can covalently bond with the surface molecular groups and form a layer on the surface. Reversible addition-fragmentation chain transfer (RAFT) polymerization is a suitable technique for the synthesis of polymers in aqueous solutions with well-defined structures and molecular weights[123]. Furthermore, the polymers prepared by this mechanism usually have dithioester-end groups and narrow molecular weight distribution. As a result, the grafting layers on substrates are more homogeneous and allow further chemical reactions. In the "grafting from" approach, immobilized radical initiators are attached to the surface to initiate the polymerization. With this method, a surface with a high grafting density and thick grafting layer on the order of 100 nm can be obtained because the monomers can penetrate through the grafted polymer brushes easily[124]. Atom transfer radical addition polymerization (ATRP) is a versatile technique for the synthetic route of well-defined polymer in the "grafting from" approach[123].

Surfaces with binary brushes can be achieved by grafting two different and completely incompatible polymers onto the surface. The morphology and wettability of the surface can be reversibly changed by exposing it to different solvents[118]. As shown in Figure 2-4 (a), a confined solvent quality can affect the morphologies of grafted surfaces. In a poor solvent, binary brushes form a ripple structure, thus enhancing the lateral segregation. In a good solvent, the favorable brushes will

extend, and the unfavorable brushes form a dimple structure, generating perpendicular segregation[117]. The surface properties are governed by the grafted polymer type and its concentration. These surfaces are possibly used as templates for nanofluidic systems which respond to variable fluid conditions by their reversibly tunable wettability and surface structures.

Reversibly expanded and collapsed surfaces can be achieved by grafting responsive chains onto the surface, including polymers with lower critical solution temperature (LCST), upper critical solution temperature (UCST) [120–122], or critical pK_a value[74,125]. For example, Poly(N-isopropylacrylamide) ((PNIPAm) demonstrates a large swelling change in aqueous solution below LCST whereas a collapsed structure in an aqueous solution above LCST. It is also reported that the PNIPAm are hydrophilic below the LCST and hydrophobic above the LCST[121]. Figure 2-4 (b) illustrated the polymer transition in the surface structure. Some pH-responsive polyelectrolytes are also reported for surface grafting to fabricate a controllable gate in nanochannels. Polyvinylpyridine (PVP) could transfer from a positively charged, hydrophilic, and swollen state when pH is below 5.2 to a neutrally charged, hydrophobic, and collapsed state as pH is above 5.2. In contrast, Poly(acrylic acid) (PAA) could undergo the conformational changes from a neutrally charged, hydrophobic, and collapsed state when the pH is below 4.7, to a negatively charged, hydrophilic, and swollen state when the pH is above 4.7. The reversible phase transitions will induce significant changes in the topography, stiffness, adhesion, and morphology of the surface, exhibiting numerous new applications[126].

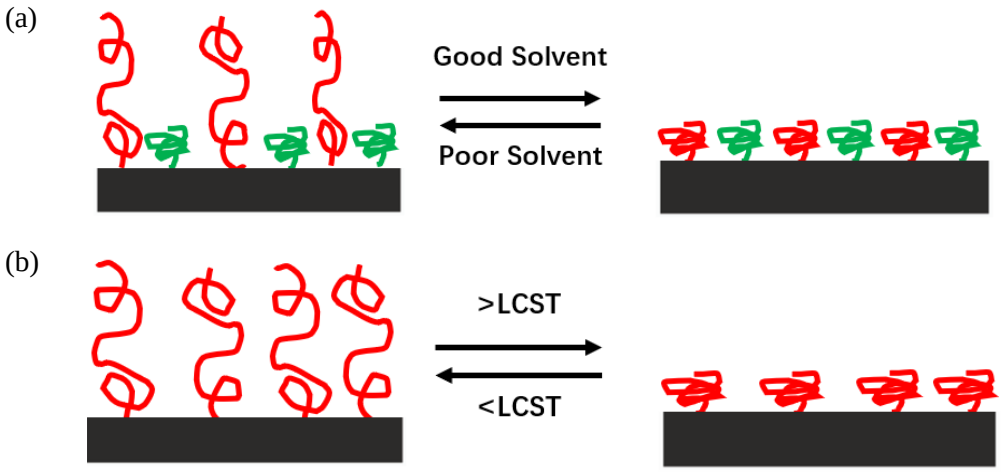

Figure 2-4. Schematic of morphological changes of stimuli-responsive polymer grafted surfaces. (a) Binary brushes grafted surface. (b) Thermo-responsive polymer grafted surface[124].

Reversible light-switching of surface properties offers unique opportunities for biological and tissue engineering applications because light intensity is easy to control and no additives are required. Grafting photochromic chains on substrates provide a method to create light-responsive surfaces. These chains can change their structure and polarity by photo-irradiation. Furthermore, unsymmetrical illumination can generate a gradient of free energy on the grafted surface, thus controlling the movement direction of a droplet over the surface[127]. Spiropyran is a well-known photochromic polymer and has been extensively used for surface modification[128–130]. As shown in Figure 2-5, the spiropyran has a closed oxygen-containing ring and is colorless in the native state. The closed state spiropyan undergoes a reversible transformation to the open and colored state by exposing it to UV light with a wavelength smaller than 400nm. This transformation induced by light can be reversed by irradiation of visible light[128]. Spiropyan can be covalently bonded on a surface, and reversible properties of hydrophilicity, isomerization, high solvent polarity can be obtained on the surface when the surface was alternatively illuminated by UV light and visible light[129].

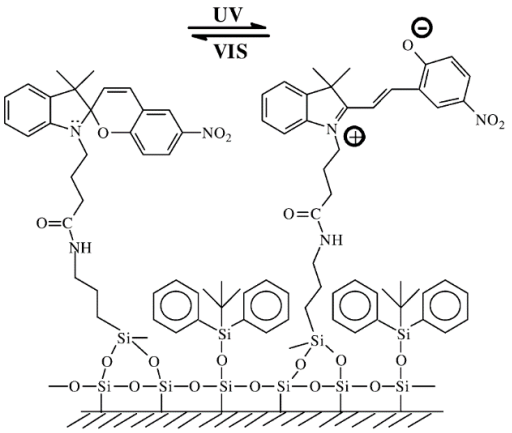

Figure 2-5.Schematic of a spiropyran monolayer on a surface in the closed (left side) and open (right side) state[128].

2.2.5 Summary

As reviewed in the above section, a variety of surface modification techniques has been developed. Each method has its advantages and disadvantages. Characteristics of these techniques such as stability of the coated layer, performance, and density of functional groups on modified surfaces are summarized. With the comparison of these methods, we can have the following conclusions:

(a) The techniques of exposure to energy sources, such as UV, UV/Ozone, and Plasma, can generate hydrophilic groups on modified surfaces. The procedures of the surface modification are simple and easy to achieve. UV and UV/Ozone can generate a large number of activated groups and achieve stable polymeric coating on modified surfaces. However, it generally requires a long exposure time. Plasma treatment can complete the surface modification in a short time while the stability and density of the functional group are low.

(b) Surface modification with surfactants and polyelectrolytes are able to generate coated layers and modulate surface properties. The modification process is achieved by physical adsorption due to electrostatic interactions between the charged surface and the mobile molecules in modification reagents. Furthermore, oppositely charged polymers can be alternatively coated on charged surfaces and reversibly change the surface charge. The procedures are relatively easy to achieve. However, it is still challenging to realize a long-term stability of the coated layers with these techniques.

(c) Chemical grafting can develop stable modified surfaces due to the functional groups are covalently bonded to the surfaces. The method of grafting to polymer coating can decorate end-functionalized polymers on the surface with a low grafting density. The method of grafting from polymer coating is able to generate a high grafting density of functional groups on substrates. However, initiators are required to achieve surface modification. By grating stimuli-responsive polymers, nanochannels with tunable surface properties can be developed. However, the procedures of these techniques are complex, and some stimuli-responsive polymers are only allowed to graft on specific materials.

Chapter 3 Fundamental Research I: Electroosmotic Flow in H-PDMS Nanochannels*

3.1 Introduction

Extensive numerical and experimental studies of the effects of ion size[18–20],, ion species[21–23], ion valence[24,25], pH value[26–28], electrolyte concentration[21,29–31], surface charge density[32,33], and channel size[34–37] on the distribution of EDL and EOF velocity in nanochannels have been conducted. Theoretically, the value of EOF velocity should be independent of the channel size in relatively large nanochannels without overlapped EDL. However, in reality, the distribution of EOF velocity in smaller nanochannels will change because the relative space occupied by the EDL in a small nanochannel is larger than that in a large nanochannel. Qiao and Aluru[41] studied the velocity profiles of EOF in nanochannel by using molecular dynamics simulation and showed that the velocity profile of EOF will be the "parabola type" instead of the "plunger type" in nanochannels. Freund[42] also investigated the electroosmotic flow in nanochannel by molecular simulation and found that the velocity profile is approximately flatted in the stern layer near the channel surface and parabolic in the middle of the channel. To analyze the steric effects in small nanochannels with overlapped EDL, the ion size is a very important criterion which is not considered in the conventional Poisson–Boltzmann equation. Borukhov et al. [15] developed a modified Poisson–Boltzmann equation that considered the ion size effect. From the numerical solution of their equation, the concentration profile of counterions near a charged surface strongly depends on the ion size. The counterions with the small size have a relatively high maximal ionic concentration near the charged surface, but also contribute to a thinner EDL. Storey and Bazant[17] also developed a fourth-order modified Poisson equation for evaluating the structure and capacitance of EDL. It is also reported that the high voltage will contribute to the crowding of counterions and form a condensed layer near the surface[131]. Qu and Li[132] proposed a model to compute the distribution of electrical potential and ionic concentration in the overlapped EDL field. Rezaei et al. [43] presented the profile of ion concentration in a charged nanochannel and EDL's boundary is located at the interface where the ion concentrations of counterions and co-ions are equal. Joly et al. [44]also reported a similar ionic density profile near a charged wall. From these MD

* A similar version of this chapter was submitted or published as:
J. Li, R. Peng, D. Li, Effects of ion size, ion valence and pH of electrolyte solutions on EOF velocity in single nanochannels, Anal. Chim. Acta. 1059 (2019) 68–79. https://doi.org/10.1016/j.aca.2019.02.008.

simulation results, the ion concentration of the co-ions is negligible in the stern layer compared with that of the counterions. These counterions in the stern layer are immobilized due to the strong electrostatic force. The potential drop across the stern layer and the zeta potential (ζ) at the shear plane layer are essentially determined by the amount of the electric charge of the counterions attracted in the stern layer when the surface charge is constant. Bohinc et al. [19] reported that the effective thickness of electric double layer depends on the concentration of ions, counterion size, and surface charge density. Coday et al. [133] also stated that the Debye length is associated with the hydration radius of counterions on the charged surface. Generally, when ions are dissolved in water, the water molecules will attach to the ions and create a spherical solvent shell surrounding the ions, which is referred to as the hydrated ion. The effective ionic size is referred to as the hydration radius of ions. It is understood that the hydration radius of ions has effects on the zeta potential value[134–136]. For a negatively charged surface, as the hydration radius increases, the zeta potential value becomes more negative without further change in the concentration of ions[133]. The zeta potential was also reported to be sensitive to the ionic valence. Yukselen and Kaya[137] proved that the zeta potential values with monovalent cations are relatively higher than those with divalent cations. Qiao and Aluru[45] studied the electroosmotic flow reversal in very small nanochannel by using molecular dynamics simulations. Their results showed that the immobilized counterions adsorbed on the channel wall can cause a charge inversion phenomenon, thus leading to flow reversal. Mashayak and Aluru[48] developed a study based on quasi-continuum theory to predict the charge inversion phenomenon more accurately. They stated that the electrostatic correlation effects and ion hydration are also very important to determine the ion distribution and the charge inversion in EDLs. For the SiO_2 surface, it is typically negatively charged because the silanol groups (Si-OH) are deprotonated to yield Si-O- when the surface is in contact with an ionic solution. The pH value of solutions can restrain this process and consequently change the surface charge density and zeta potential at the interface[138]. Yeh et al. [33] derived a new model to predict the surface charge property and showed that the surface charge and zeta potential can be regulated by changing the pH value and concentration of aqueous solutions.

With the advancement of nano-fabrication technology, several studies to experimentally examine electroosmotic flow in ultrafine channels have been reported. Jacobson et al. [49] evaluated the electroosmotic mobilities in a nanochannel of 98 nm in depth and in some microchannels. By comparing the measured results of EOF velocity, they stated that there was a 35% reduction in the electroosmotic mobility in the nanochannel in comparison with that in microchannels. Peng and

Li[50]fabricated single PDMS nanochannels and measured the EOF velocity in the single nanochannels as small as 20 nm in depth by the current-slope method[51,52]. They found that the overlapped EDL can significantly reduce the velocity of EOF, and the velocity depends on the ionic concentration and the applied electric field strength. Chou et al. [53] also measured the EOF velocity in a nanochannel of 50 nm in depth and proposed that trivalent ions may adsorb on the negatively charged surface and cause a charge inversion, thus introducing a reverse flow in the nanochannel. Uba et al. [54]monitored the pH effects on the surface charge density in a PMMA channel with the depth of 120 nm and width of 120nm. Their results showed that the surface charge density gradually increases when the pH of the solution becomes larger.

Although some investigations have been conducted to analyze the effects of ionic size, valence, and pH on EDL and EOF, they are mostly theoretical. Only a few studies experimentally looked at EOF particularly in nanochannels with overlapped EDL. There still be a lack of experimental studies to characterize the effects of stern layer with different counterions on EOF velocity. Therefore, this chapter will focus on the above-mentioned effects on the EOF velocity in nanochannels with overlapped EDL, and the results will be compared with that in a small microchannel. The current-slope method will be employed to evaluate the effects of ion size, ion valence, and pH value of solutions on the EOF velocity in nanochannels. Furthermore, models of the electric double layer are proposed to explain these effects.

3.2 Experimental section

3.2.1 Fabrication of a single nanochannel chip

To fabricate a single nanochannel chip, a single nanocrack is firstly created on a polystyrene surface by using the solvent-induced method[50]. Then, this negative nanocrack pattern is transferred to a photoresist layer with the photolithography method, thus forming a positive nanochannel mold. By using different photoresists, such as SU8 2075 and SU8 2150, and adjusting the heating temperature, the spin-coating speed, and the amount of chemical reagent in this step, nanochannel molds with different feature sizes can be obtained. A nanochannel can be made by casting a layer of PDMS on the positive nanochannel mold. As small nanochannels made by regular PDMS material are easily collapsed after the bonding process due to the deformation of PDMS, the nanochannel chip is produced with a bilayer of hard PDMS (h-PDMS) precisely replicating the mold's features and regular PDMS supporting the fragile h-PDMS layer[139]. The h-PDMS is spin-coated onto the nanochannel molds

and then heated in an oven with the temperature of 80 ^{o}C for 10 minutes. Finally, the regular PDMS is poured onto the layer of the h-PDMS and placed back in the oven for 2 hours. As an example, Figure 3-1 displays a h-PDMS nanochannel peeled off from the nanochannel mold measured with AFM (Multiode^{TM} SPM, Digital Instruments).

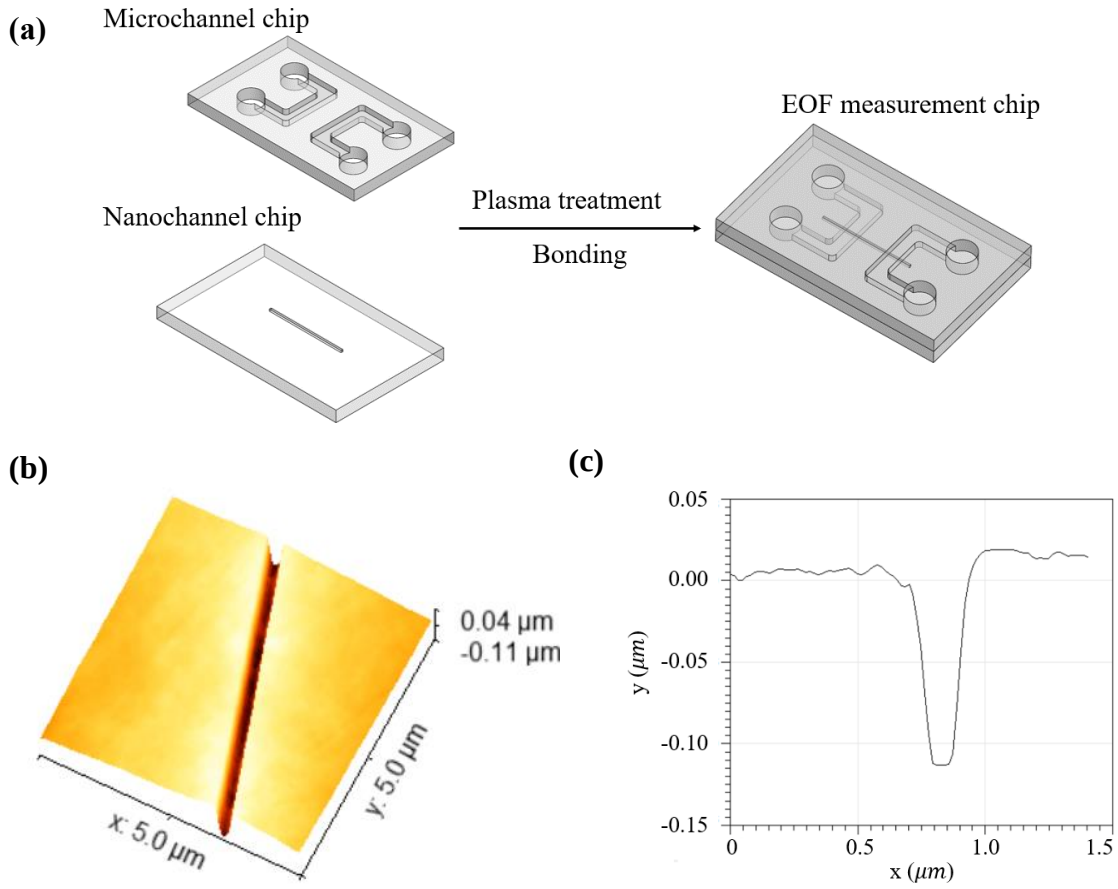

Figure 3-1. Schematic and examples of the nanofluidic chip. (a) Schematic of the EOF measurement chip bonding process; (b) 3D AFM image of a h-PDMS nanochannel replicated from the photoresist nanochannel mold; (c) Cross-section of the nanochannel with a depth 107 ± 7 nm and a width 260 ± 11 nm as measured by AFM.

To deliver the sample liquid to a nanochannel and measure the EOF velocity, the nanochannel has to be connected to a microchannel[140]. This PDMS microchannel chip is replicated from a SU8 photoresist microchannel mold which is fabricated on a silicon wafer with the standard photolithography method. In order to keep a consistent zeta potential value on all surfaces of the system,

the microchannel is also produced with a bilayer of h-PDMS and regular PDMS. As shown in Figure 3-1, this microchannel network is composed of two "U" shape microchannels with a depth of 30 μm and a width of 150 μm. The nanochannel bridges the two microchannels by bonding the PDMS nanochannel chip with the PDMS microchannel chip by plasma treatment (Harrick plasma, PDC-32G) for 60s, forming the final fluidic chip for EOF velocity measurement.

3.2.2 Measurement of EOF velocity by the current-slope method

Electric current monitoring method is a widely used technique that can evaluate the EOF velocity. As the conductivities of electrolyte solutions depend on the concentrations of electrolyte solutions, the EOF velocity could be evaluated by monitoring the electric current change in the process of replacing one electrolyte solution by another with a different conductivity. For instance, when a lower conductivity solution firstly fills a channel, and then is replaced by another solution with a higher conductivity driven by the electroosmotic flow, the electric current throughout the channel should increase from the initial steady value and finally reach a higher constant value when the solution with a higher conductivity fills the channel completely. The average velocity can be estimated by knowing the length of the channel and the replacement time. In order to increase the accuracy of this method, Ren et al. [52] proposed to use the slope of the current-time curve to evaluate the EOF velocity. Recently, Peng and Li[140] applied the current slope method to measure EOF velocity in a nanochannel. In this work, the electric resistance of nanochannel is much higher than that of microchannels due to the extremely small size of the nanochannel. Consequently, the voltage drop in the microchannels is negligible and the EOF velocity can be calculated by the following equation:

$$\mathrm{V}_{EOF} = \frac{k_{slope} L}{I_2 - I_1} \tag{3-1}$$

where V_{EOF} is the velocity of the electroosmotic flow; I_1 and I_2 are the initial electric current value and the final electric current value in the nanochannel, respectively; k_{slope} is the slope of the liner part of the current-time curve; L is the length of the nanochannel.

It should be noted that the ionic concentration not only changes the conductivity of the solution, but also affects the zeta potential which is associated with the EOF velocity. In order to minimize the concentration effects in the measurements, the concentration difference between the two displacing solutions should be small while making the initial electric current value I_1 and the final electric current

value I_2 clearly different. In addition, the EOF velocities measured for the process of using the high ionic concentration solution to replace the low ionic concentration solution and for the process of using the low ionic concentration solution to replace the high ionic concentration solution are averaged. The average velocity is given as:

$$V_{AV} = \frac{V_{EOF-inc}+V_{EOF-dec}}{2} \tag{3-2}$$

where V_{AV} is the average velocity of the electroosmotic flow; the $V_{EOF-inc}$ and $V_{EOF-dec}$ are the EOF velocities calculated for the increasing current process and decreasing current process, respectively.

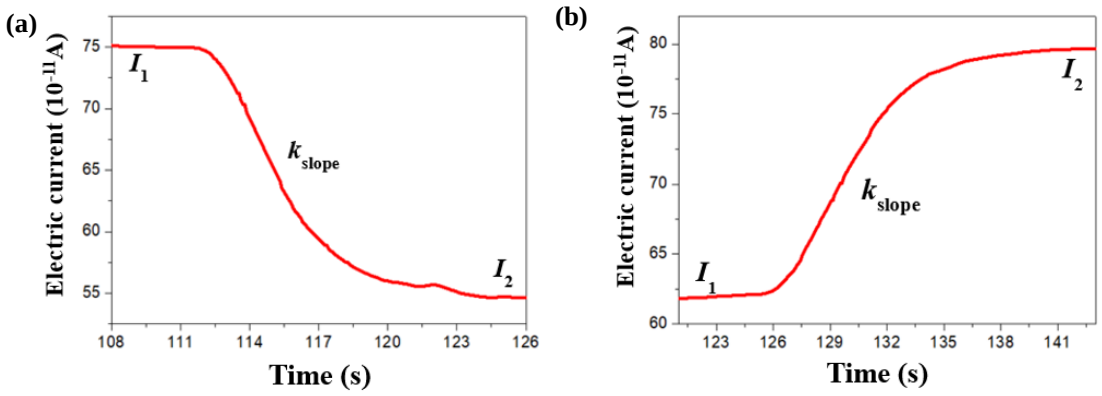

Figure 3-2. Examples of the current-time curves measured in a channel with the cross-section of 2.5 μm × 2.5 μm under the 50 V/cm applied electric field. (a) The curve of current change measured by replacing 2×10^{-3} M LiCl solution with 1×10^{-3} M LiCl solution. (b) The curve of current change measured by replacing 1×10^{-3} M LiCl solution with 2×10^{-3} M LiCl solution.

Figure 3-2 displays the examples of current change curves in the experiments for the case of the replacement between the 1×10^{-3} M LiCl solution and 2×10^{-3} M LiCl solution in a 2.5 μm deep and 2.5 μm wide channel under 50 V/cm electric field. In Figure 3-2 (a), the 2×10^{-3} M LiCl solution initially filled the nanochannel and the current I_1 was measured at the steady state. Then 1×10^{-3} M LiCl solution was added and driven into the nanochannel by the electroosmotic flow. Correspondingly, the electric current cross the nanochannel started decreasing gradually and eventually reached a constant value I_2 when the nanochannel is totally filled with the solution of the lower concentration. The linear section of the current-time curve is used as the slope of the curve for calculation of the EOF

velocity. Figure 3-2 (b) shows an example of the electric current-time curve in an opposite replacement process in the same channel used in Figure 3-2 (a). In this case, the 2×10^{-3} M LiCl solution was displacing the 1×10^{-3} M LiCl solution, and the electric current was increasing with time.

Figure 3-3 shows the schematic of the EOF velocity measurement system. This system consists of an electrometer (Keithley, Model 6517A) used to record and transfer the electric current signal to a computer by a LabVIEW program (National Instrument Corp.), an electric switch, and a nanofluidic chip. The electrometer also functions as a DC power supply providing the electric potential to the chip reservoirs through two Platinum electrodes (Sigma-Aldrich). The electrolyte solutions used in the work with ionic concentration of either 1×10^{-3} M or 2×10^{-3} M are prepared by dissolving KCl (Fisher Scientific), LiCl (Sigma-Aldrich), NaCl (Fisher Scientific), CaCl2 (Fisher Scientific), and AlCl3 (Fisher Scientific) in pure water (Mini Q, Direct-Q3), respectively. The pH of all solutions is 7 except for the KCl solutions. The KCl solutions with pH values ranging from 4 to 10 are regulated with the KOH (Fisher Scientific) solution and the HCl (Fisher Scientific) solution.

For each measurement, a new nanofluidic chip is assembled and initially filled with an electrolyte solution with a given ionic concentration. Afterward, the DC power is applied to the reservoir A and C of the nanochannel (shown in Figure 3-3), and the current is recorded with the LabVIEW program simultaneously. When the current reached a constant value, the same electrolyte solution with slightly different concentration is added to the reservoir B and start to replace the original liquid in the channel by switching the input voltage from reservoir A to reservoir B. With the applied electric field, the second solution in the reservoir B is pumped electroosmotically into the channel and eventually goes through the nanochannel. As a result, the electric current gradually changes until reaching the final constant value. For each set of conditions, the measurements were repeated at least 3 times in 3 independent nanofluidic chips. The EOF velocity was calculated by Eq. (3-1) and Eq. (3-2), and the results reported in this project are the averages of the calculated velocities. All the experiments were conducted at the room temperature of about 23 ^{o}C.

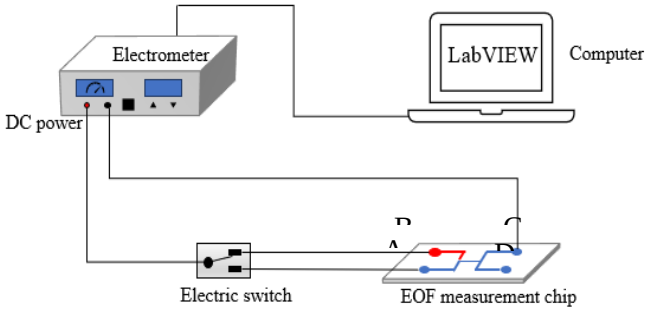

Figure 3-3. Schematic diagram of the EOF velocity measurement system

3.3 Results and discussion

3.3.1 Ion size effects

In aqueous solutions, most elements of electrolytes exist in the form of hydrated ions that are attached to water molecules to form a spherical shell surrounding the ions. Previous researchers have proposed that the distribution of zeta potential and the thickness of the EDL on a charged surface are related to the hydration radii of counterions at the stern layer[141,142]. Therefore, the hydration radius of the ion is considered as the effective ion size in this work. Generally, the hydration radius of the cation is contrariwise proportional to the original size of ion because the small ions have more hydration energy and can accept more water molecules. The sodium and potassium ions have relatively large ion size but are weekly hydrated, having a single water molecules shell. However, the smaller lithium ion can be hydrated more strongly and probably has a second hydration shell, leading to a large hydration radius[143].

Figure 3-4 (a) shows the experimental results of the hydration radius effects on the EOF velocity. EOF velocities of three monovalent electrolyte solutions, LiCl, NaCl, and KCl, are measured in channels with a depth ranging from 85 nm to 2.5 μm. In addition, most of the nanochannels used in this study have a much larger size in width direction than that in depth direction, and the EDL may overlap only in the depth direction of the nanochannels. For all cases, the applied electric field is 50 V/cm, and the pH is 7. By comparing the measured EOF velocities of these monovalent electrolyte solutions, it is clearly shown that the EOF velocity increases with the increasing size of hydrated ions (Li^+ > Na^+ >

K^+) in relatively large channels. However, when the nanochannels become smaller, particularly smaller than 150 nm, the EOF velocity is contrariwise proportional to the size of hydrated ions.

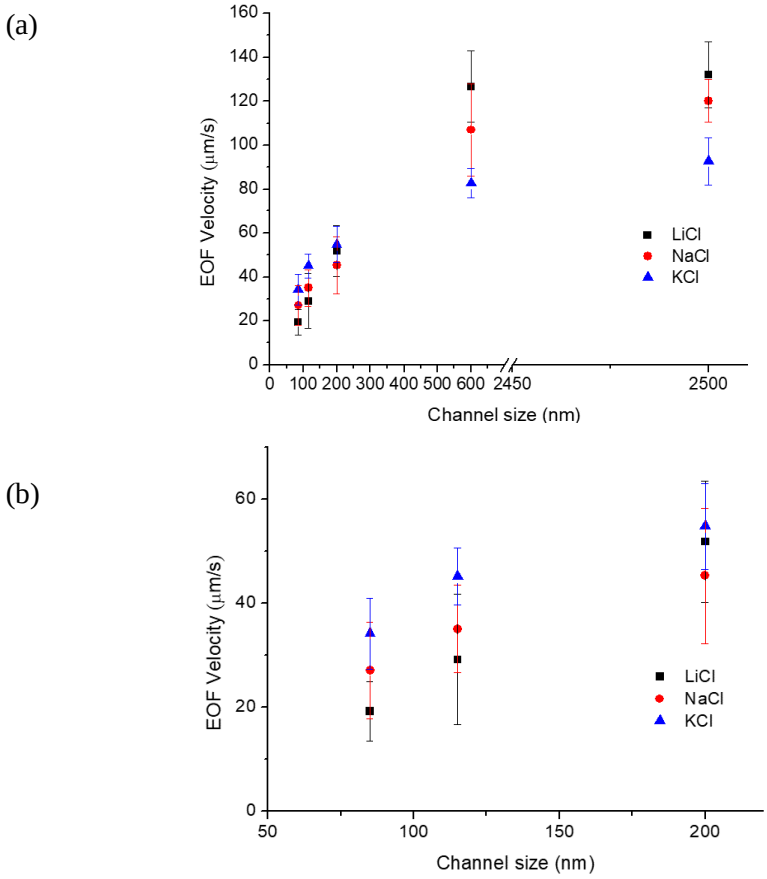

Figure 3-4. (a) Experimental results of ion size effects on EOF velocity in h-PDMS channels. The EOF velocities of three monovalent electrolyte solutions are measured in the channels with size ranging from 85 nm to 2.5 μm. The ionic concentrations of the solutions are 1×10^{-3} M and the applied electrical field strength is 50 V/cm. (b) Zoomed-in version of ion size effects on EOF velocity in small h-PDMS nanochannels.

The experimental results in Figure 3-5 indicate that the average EOF velocity has a decreasing trend when the depth of channel decreases from 600 nm to 200 nm which is still larger than the size required for EDL overlapping. For example, for 1×10^{-3} M KCl solution, the Debye length is about 9.6 nm, and the thickness of EDL may be approximately 50 nm. The maximum EOF velocity only occurs in the small central area of the nanochannels. Therefore, the average EOF velocity decreases

when the size of the channel decreases. Furthermore, when the channel size decreases from 110 nm to 85 nm, the EDLs overlap and the average EOF velocity is further reduced.

As shown in Figure 3-5, the potential distribution of EDL can be expressed as:

$$\psi_{surf} = \psi_{drop} + \zeta \tag{3-3}$$

Where ψ_{surf} is the surface charge of the nanochannel, ψ_{drop} is the potential drop in stern layer, and ζ is the zeta potential at the shear plane.

The surface potential is determined by the properties of the interface between the solid surface and electrolyte solution, and it should be a constant for the fixed pH value and concentration of the aqueous solution. However, as the ion size is considered, the limited area of the charged surface allows fewer counterions with a large size to be adsorbed on the surface in comparison with the small counterions. Consequently, the potential drop and zeta potential depend on the size of the counterions. As shown in Figure 3-5, the ψ_{surf} in these two models is the same under the same pH and ionic concentration. As illustrated by the model in Figure 3-5 (a), fewer counterions attach to the charged surface due to their large hydrated size, and the ψ_{drop} is smaller compared with that in Figure 3-5 (b). Consequently, the ζ of the interface with large hydrated ions is more negative than that with small hydrated ions. Because the EOF velocity is proportional to the zeta potential value in channels without overlapped EDL, the large hydration radius contributes to the larger velocity of EOF. For the three counterions tested in this work, the size of hydrated ions Li^+ is larger than that of Na^+ and K^+, and the size of hydrated ions Na^+ is larger than that of K^+, therefore, in larger channels, the EOF velocity of LiCl solution is the largest and the EOF velocity of the KCl solution is the smallest. In smaller nanochannels, however, the opposite trend is observed as shown in Figure 3-4. This may because the thicker EDL is formed with large hydrated ions and strongly overlapped EDLs may occur. Consequently, the overlapped EDLs result in a smaller EOF velocity. A previous theoretical study has demonstrated that the concentration distribution of the counterions in EDL depends on their size. The thickness of the stern layer is positively proportional to the ion size[15]. Furthermore, in small nanochannels, Freund reported that the EOF velocity is approximately zero in the stern layer and the velocity profile is parabolic in the middle of the channel [42]. Based on these studies, the mean EOF velocity should be proportional to the size of the counterions inversely in small nanochannel because

the immobilized stern layer composed of large counterions is thicker and occupies more space of the channel. The results of this experiment are in good agreement with these theoretical studies.

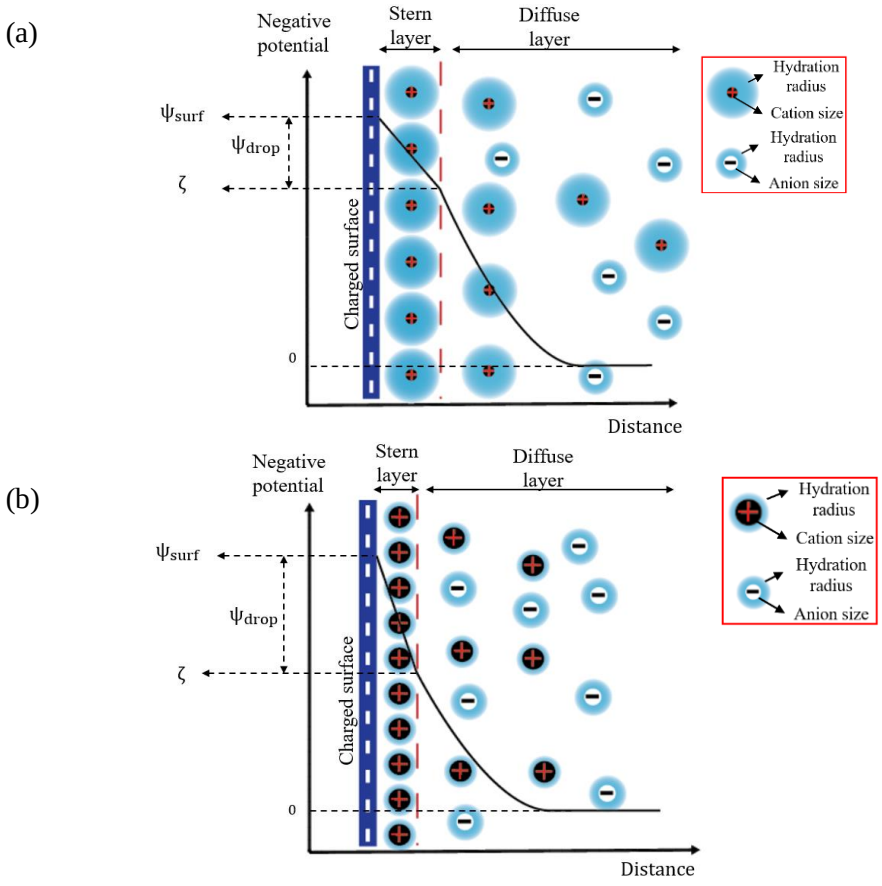

Figure 3-5. (a) Model for the potential distribution of EDL on a negatively charged surface with large hydrated counterions; (b) Model for the potential distribution of EDL on a negatively charged surface with small hydrated counterions.

3.3.2 Ion valence effects

Electrolyte solutions with different valences of cations and the same anion, KCl, $CaCl_2$, and $AlCl_3$, are utilized to measure EOF velocities in a series of channels by using the current-slope method. The applied electric field is 50 V/cm, and the pH of all solutions is regulated to 7. The experimental results of measured EOF velocities are shown in Figure 3-6. As can be seen from Figure 3-6, for the KCl solution and the $CaCl_2$ solution, the EOF velocity increases with the channel size and is a constant for larger nanochannels and the microchannels. In the comparison of the EOF velocity with the same ionic

concentration, it is found that the $CaCl_2$ solution has a slightly lower EOF velocity compared with the KCl solution. However, for the trivalent solution, $AlCl_3$, it demonstrates a reversed electroosmotic flow; that is, the flow is in the opposite direction to the direction of the applied electric field. Additionally, the speed of the flow increases with the channel size.

Similar to the above discussion, for all electrolyte solutions in this experiment, the EOF velocity slightly decreases in the large nanochannels because the EDL occupies more space of the channel, and significantly decreases in very small nanochannels due to the overlapped EDL. These channel size effects are related to the thickness of EDL. In the conventional EDL theory, the Debye length is correlated to the valence of the electrolyte and can be theoretically calculated with the following equation[144]:

$$\lambda_D = \sqrt{\frac{\varepsilon_0 \varepsilon_r k_b T}{2 n_{i\infty} (ze)^2}} \tag{3-4}$$

where ε_0 is the permittivity of vacuum, and ε_r is the dielectric constant of the electric solution; k_b is the Boltzmann constant; T is the temperature; $n_{i\infty}$ is the density of ions; z is the valence of electrolyte solution; e is the unit charge.

It is generally accepted that the thickness of the diffuse layer of EDL is about 3 to 5 times of the Debye length λ_D [144], which means the valence of electrolyte is contrariwise proportional to the thickness of EDL. However, the derivation of the above Debye length equation did not consider the effects of the hydrated ions. It is believed that the thickness of the diffuse layer is also strongly correlated and positively proportional to the size of hydrated counterions[133]. Therefore, the thickness of the EDL cannot be simply calculated by Eq. (3-4). For example, although the ion of aluminum has a high valence, it also has a large hydrated size (9.6 Å) compared with calcium (8.4 Å) and potassium (6.6 Å)[145].

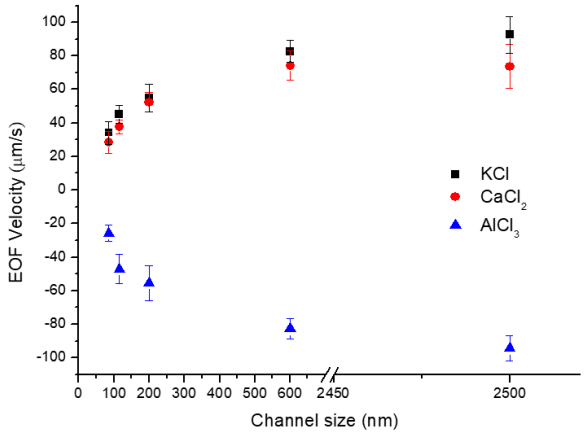

Figure 3-6. Experimental results of ion valence effects on EOF velocity in h-PDMS channels. The EOF velocities of three electrolyte solutions with different valence are measured in the channels with size ranging from 85nm to 2.5 μm. The ionic concentrations of the solutions are 1×10^{-3} M, and the pH is 7. The applied electric field strength is 50 V/cm.

As shown in Figure 3-6, the bivalent cations attached to the charged surface provide more counter-charges than the monovalent cations if these two kinds of cations have similar hydration sizes. As the ψ_{surf} is constant, the charged surface attached with the bivalent solution has a relatively large ψ_{drop} at the stern layer, thus generating a smaller ζ value at the shear plane. Therefore, the EOF velocity is contrariwise proportional to the valence of counterions adsorbed on the charged surface. Based on these two models in Figure 3-7, the electrolyte solution with a higher valence should have a smaller EOF velocity. However, as can been seen in Figure 3-6, only a slightly smaller EOF velocity of the $CaCl_2$ solution can be observed compared with that of the KCl solution. This is because the ion of calcium not only has a high valence, but also a larger hydration diameter (8.4 Å) than the ion of potassium (6.4 Å) [146]. As discussed above, the ψ_{drop} also depends on the hydration radius of ions. Thus, the difference of ζ between the KCl solution and $CaCl_2$ solution is smaller than expressed from the models in Figure 3-7. For the $AlCl_3$ solution, the high valence of electrolyte plays the leading role in the EOF velocity. When the ions of aluminum adsorb on the charged surface, overwhelming countercharges provided by the aluminum ions cause a charge inversion at the shear plane, thus leading to the reversed electroosmotic flow. The flow reversal has been investigated in some studies by molecular dynamics simulations[43,47]. They stated that the flow reversal occurs when the amount of electric charge attracted in the stern layer is larger than that of the surface charge. In this experiment, the multivalent

ions have similar effects on the flow reversal. The trivalent counter-ions, Al^{3+}, can contribute more positive charges than monovalent ions and bivalent ions when they are attracted in the stern layer. The amount of these positive charges could be more than the wall charges. Therefore, the flow reversal occurs.

(a)

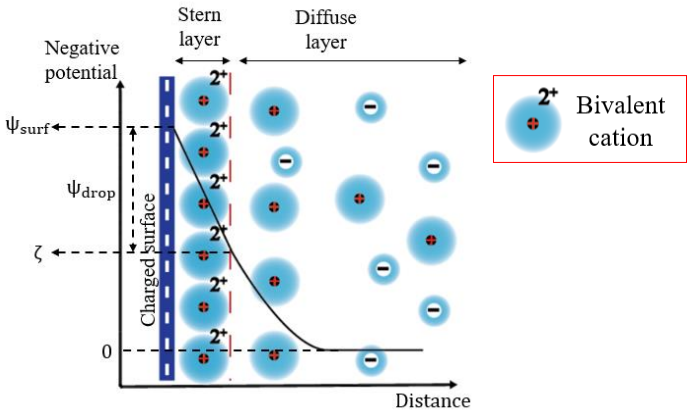

(b)

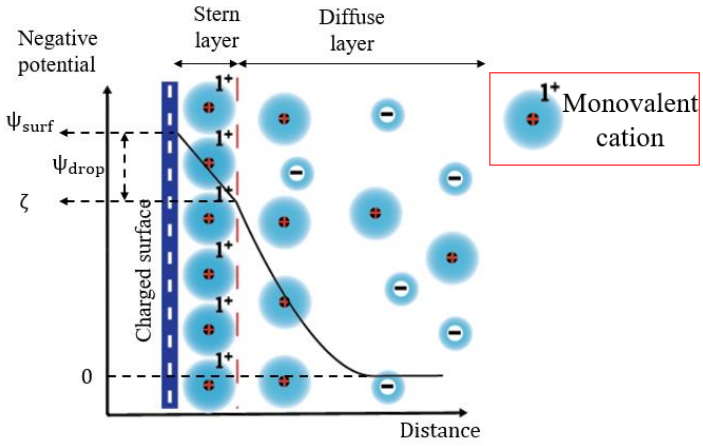

Figure 3-7. (a) Model for the potential distribution of EDL with bivalent counterions. (b) Model for the potential distribution of EDL with monovalent counterions.

3.3.3 pH value effects

The 1×10^{-3} M KCl solutions with pH value ranging from 4 to 10 were employed to analyze the effects of pH value on the EOF velocity. Figure 3-8 depicts the dependence of the measured EOF velocity on the pH value in h-PDMS channels with various sizes under the $50\ V/cm$ applied electric

field. The pH value of solutions is regulated with the 1×10^{-3} M KOH solution and 1×10^{-3} M HCl solution. As can be seen in Figure 3-8, for example, in the nanochannel with a depth of 85 nm, the EOF velocity of the KCl solution increases from around 13 $\mu m/s$ to 41 $\mu m/s$ as the pH increases from 4 to 10. The EOF velocity in other channels follows a similar trend.

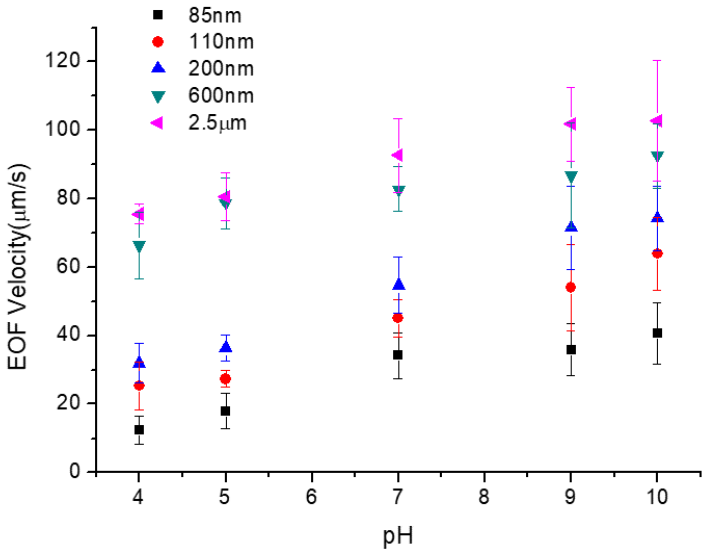

Figure 3-8. Experimental results of pH value effects on the EOF velocity in h-PDMS channels with depth ranging from 85 nm to 2.5 μm. The EOF velocities of 1×10^{-3} M KCl solutions are measured by using the current monitoring method under an applied electric field of $50\ V/cm$.

Uba et al. [54]reported that the surface charge increases monotonically with the increasing pH of solutions in PMMA nanochannels due to carboxyl groups on the channel surface deprotonated at high pH. In this experiment, similarly, the EOF velocity increases when the pH of the KCl solution increases. The models shown in Figure 3-9 can be used to explain the pH effects on EOF velocity. For h-PDMS-based channels, at a low pH, the relatively high ionic strength of hydrogen (H^+) in the solution restrains the deprotonation of silanol groups on the h-PDMS surface, reducing the negative surface charge and leading to a relatively lower ψ_{surf} , as shown in Figure 3-9 (a). In contrary, at a high pH, the h-PDMS surface has a higher ψ_{surf} , as shown in Figure 3-9 (b). As discussed above, the ψ_{drop} depends on the hydration radius and valence of counterions adsorbed on the surface. For the KCl solutions with pH ranging from 4 to 10, as the hydration radius and valence of counterions are the same, the ψ_{drop} can be regarded as a constant value. By using Eq. (3-3), it is easy to understand that there is a positive

correlation between the ζ and the pH value of solutions. Consequently, the EOF velocity is positively proportional to the pH value as well.

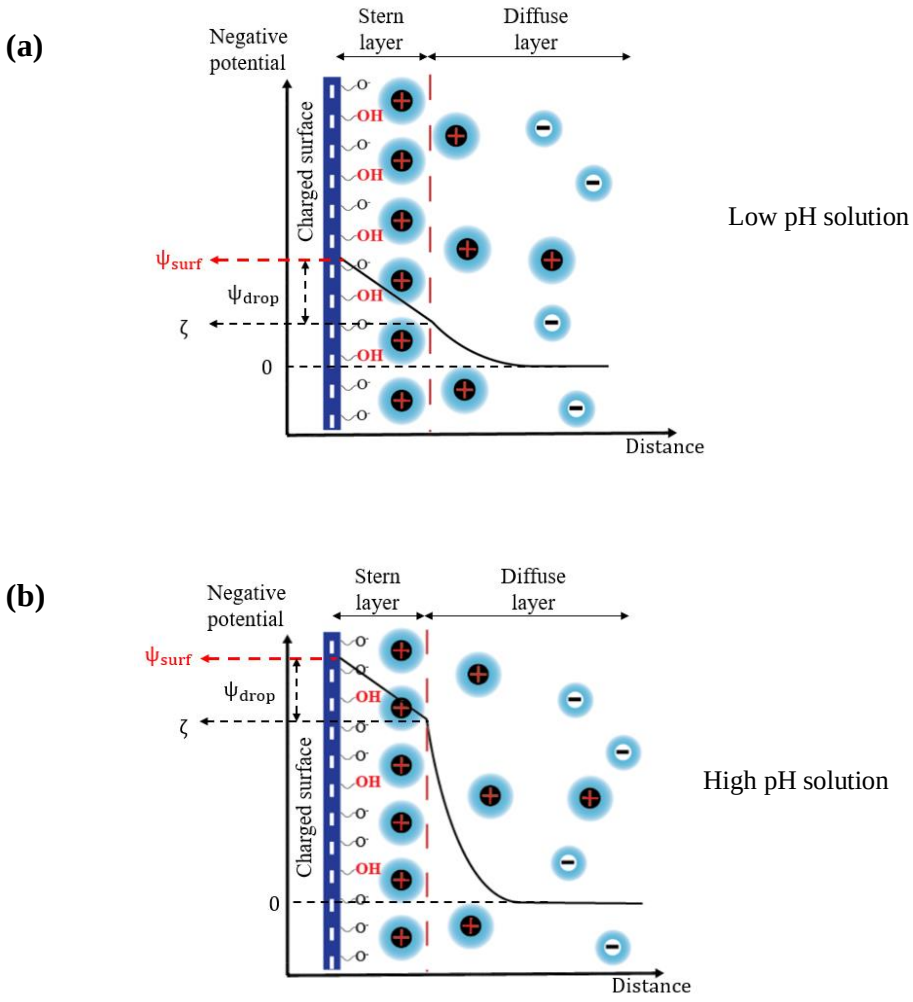

Figure 3-9. (a) Model for potential distribution of EDL at low pH; (b) Model for potential distribution of EDL at high pH.

3.4 Conclusions

In this chapter, the effects of ion size, ion valence and pH value of solutions on the electroosmotic flow velocity in various h-PDMS-based nanochannels are experimentally studied by using the current monitoring method. The experimental results indicate that the EOF velocity of electrolyte solutions with the same valence and ionic concentration is proportional to the hydration radius of ions in the

relatively large h-PDMS channels without overlapped EDL. On the contrary, this velocity is contrariwise proportional to the hydration radius of ions in small h-PDMS channels because the large size of hydrated ions contributes to form thicker EDL and generate strongly overlapped EDL, dramatically reducing the EOF velocity in nanochannels. Similarly, the high valence of cations also causes a decrease in EOF velocity, even can induce a reversal of EOF with trivalent cations in h-PDMS channels. The results also demonstrate that the increase of pH value will increase the EOF velocity by elevating the surface potential. These findings provide an improved understanding of EOF in nanochannels. These measured EOF velocities obtained in this chapter offer fundamental support for the future studies of electrokinetic transport processes in nanochannels.

Chapter 4 Fundamental Research II: Electroosmotic Flow in DNA Modified H-PDMS Nanochannels[†]

4.1 Introduction

Significant attention has been paid on EOF modulation in recent years. In EOF modulation, the surface coating is one of the most popular methods to effectively control EOF in microchannels[58–62] and nanochannels[63–67]. Some studies of the effects of the coated layer on electrokinetic transport have been conducted. Theoretically, Harden et al.[68] set up a model to predict the qualitative features of EOF velocity in channels with end-grafted polyelectrolytes and reported that the EOF mobility is essentially determined by the electrokinetic properties of the polymer in channels with densely grafted polymers. Adiga and Brenner[65] studied the EOF velocity distribution in a nanopore grafted with polymer brush by using molecular dynamics simulation method and showed that the EOF velocity depends on the coupling effects of polymer conformational dynamics induced by the drag force of fluid flow and electrohydrodynamics. Huang et al.[64] also investigated the electric properties of the surface on which polyelectrolyte brushes are grafted and report that the surface charge is dependent on the grafting density, pH, electrolyte concentration and the thickness of the brush layer. Paumier et al.[77] measured the EOF velocity in channels grafted with neutrally charged polymers and reported that the thickness of the coated layer could control the development of EOF. When the polymer layer is thicker than the EDL, the EOF can be effectively prohibited even the channel surface with nonzero zeta potential. On the contrary, if the thickness of the coated polymer layer is smaller than that of EDL, the EOF could still occur unimpeded. Raafatnia et al. [78] further investigated the mobility of polyelectrolyte-grafted colloids in monovalent salt solutions. They presented that the mobility is dominated by the polyelectrolyte brush regime at high ionic concentration. In Manning's theory, the neutralization of DNA charges only determined by the valence of counterions in the solvent and independent of its type and concentration[79]. Guo et al. studied the effects on this issue and reported that the DNA charge neutralization is also dependent on the pH value of solutions or the concentration of hydrogen ions[71]. Moreover, the molecular structure of DNAs can be influenced by ultraviolet(UV)

[†] A similar version of this chapter was submitted or published as:
J. Li, D. Li, Electroosmotic flow velocity in DNA modified nanochannels, J. Colloid Interface Sci. 553 (2019) 31–39. https://doi.org/10.1016/j.jcis.2019.06.002.

irradiation, thus changing the charges carried by DNAs[80–82]. Therefore, UV illumination can be an elegant way to modulate EOF in the DNA coated channels without any additives.

Although some experimental studies have been conducted to investigate the EOF modulation by using the surface modification methods, the complicated interactions between DNA and mobile counterions in the solution result in new questions about EOF in DNA modified channels. More efforts are need to be taken to further examine the fundamental characteristics of EOF influenced by the interactions between electrolyte solutions and the coated surface. At present, the experimental results of EOF velocity in PDMS nanochannels grafted with DNA brushes are very limited. In order to provide improved understandings of electrokinetic transport in nanochannels grafted with DNA brushes, in this chapter, EOF velocities are measured by using the current monitoring method in the microchannels, large nanochannels as well as very small nanochannels with overlapped EDLs [52]. The effects of the incubation time, the type of the coated layer, pH, and ionic concentration of electrolyte solutions on the performance of surface modification and EOF are studied in h-PDMS channels. The EOF velocities with UV illumination are also measured in DNA grafted channels. For comparison, corresponding measurements of EOF velocity in the pristine channels with UV illumination are also presented in this chapter.

4.2 Materials and methods

4.2.1 Chemicals and Oligonucleotides

The chemicals employed in this study include electrolytes of KCl (Fisher Scientific), NaCl (Fisher Scientific), LiCl (Sigma-Aldrich), $CaCl_2$ (Fisher Scientific) and $AlCl_3$ (Fisher Scientific), pure water (18.2 MΩ Mini Q, Direct-Q3) which is used to prepare all the electrolyte solutions, KOH (Fisher Scientific) solution and the HCl (Fisher Scientific) solution which are used to regulate the pH of KCl electrolyte solutions. Regular PDMS and hard PDMS (h-PDMS) are utilized to fabricated EOF measurement chips[50]. 1-ethyl-3-[3-(dimethylamino)propyl]carbodiimide hydrochloride (EDC) and N-hydroxysuccinimide (NHS) are used to treat the channel surface in the first step of the surface modification; single-stranded DNA (ssDNA) 5’-TTTTTTTTTTTTTTT-3’ (15T) and 3’-AAAAAAAAAAAAAAA-5’ (15A) are grafted on the channel surface in the second step of the surface modification.

4.2.2 Fluidic chip fabrication

In this study, the nanochannel molds were fabricated by using the solvent-induced cracking method[50]. The nanochannel chips were produced by casting a bilayer of hard PDMS (h-PDMS) and regular PDMS on the nanochannel molds. The h-PDMS can precisely replicate the molds' feature and minimize the deformation and collapse effects on channel size. The regular PDMS is relatively soft and used to support the fragile h-PDMS layer[139]. Firstly, the h-PDMS was spin-coated onto a nanochannel mold and then placed in an oven at 80 °C for 10 minutes. Afterward, the regular PDMS was cast onto the h-PDMS layer and heated with the same temperature for 2 hours. In order to easily deliver the testing liquid in a nanochannel, the nanochannel chip was connected to a microchannel which was replicated from a SU8 photoresist microchannel mold fabricated on a silicon wafer with the standard photolithography method. This PDMS microchannel chip was also produced with the bilayer of h-PDMS and regular PDMS so that the zeta potential value was constant on all surface of the system. The microchannel network was bonded with the nanochannel chip by Plasma treatment (Harrick plasma, PDC-32G). Figure 4-1 shows an example of the fluidic chip for EOF velocity measurement, where the nanochannel bridges the two "U" shape microchannels with a depth of 30 μm and a width of 150 μm.

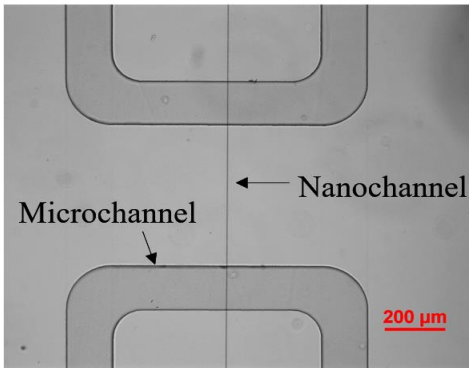

Figure 4-1. A picture of a h-PDMS nanofluidic chip for EOF velocity measurement captured by an optical microscope.

4.2.3 Surface modification

In this work, the surface modification process is achieved by the chemical reaction between the channel inner surface and the functional molecular groups to form covalent bonds. As shown in Figure 4-2, the nanochannel chip and microchannel chip were pretreated by oxygen plasma for 180 s, and then they were irreversibly bonded together. After leaving the chip standing for 30 minutes at room

temperature of about 23 °C, the inner surface modification can be achieved by a two-step chemical reaction and an incubation process. Firstly, 2 µl EDC solution (20 mM) and 2 µl NHS solution (20 mM) were filled into the chip to couple the carboxylic acid groups to amine-reactive groups on the channel surface. After that， 10 µl DNA 15T solution (10 µM) was added to the channel and bonded to the inner surface. Finally, the chip was fulfilled with 100 mM MES buffer solution and incubated at the temperature of 4 °C for a certain period before using. For the duplex DNAs modified nanochannels, 10 µl DNA 15A solution (1µM) was filled into the chip after the incubation process. By one extra hour incubation at the room temperature, the DNA 15A could hybridize with the grafted DNA 15T and formed dual-stranded structure[72,147].

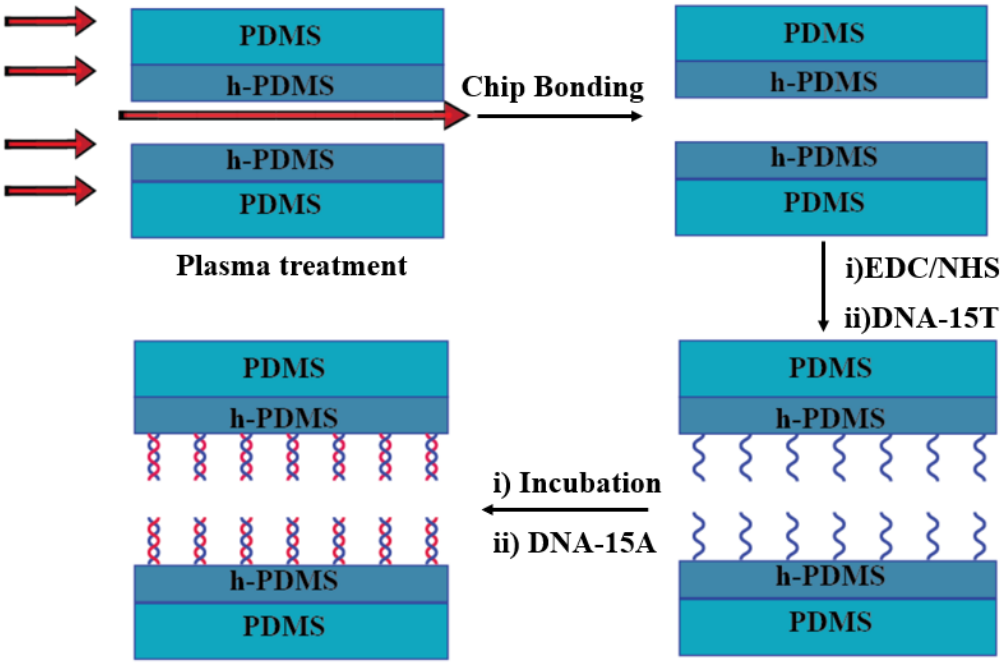

Figure 4-2. Schematic representation of the formation of grafted DNA layer on h-PDMS channel inner surfaces.

4.2.4 Measurement of EOF velocity

Electric current monitoring method is a widely used technique that can evaluate the EOF velocity in microchannels[148]. As the conductivities of electrolyte solutions are related to their ionic concentrations, the EOF velocity can be measured by monitoring the electric current change in the displacement process between two electrolyte solutions with slightly different ionic concentrations. The

time of a higher concentrated electrolyte solution displaced by a lower concentrated electrolyte solution can be recorded, the EOF velocity can be calculated by knowing the channel length and the replacement time. However, it is difficult to ascertain the exact starting time and the ending time of the displacement process in an experiment. To improve the measurement method and minimize the experimental error, Ren et al.[52] proposed to calculate the EOF velocity by using the slope of the current-time curve instead of the time period of the complete displacement process. Pend and Li[140] also measured the EOF velocity in nanochannels by using the current slope method. In this work, all channels initially were filled with an electrolyte solution of a high concentration and then the same electrolyte solution of a slightly lower concentration was filled into the channels to displace the original solution by EOF. For each set of conditions, the measurements are repeated at least 3 times in 3 independent nanofluidic chips. All the experiments are conducted at the room temperature of around 23 ^{o}C. Because the electrical resistance of the microchannel is much smaller than that of the nanochannel, the voltage drop in the microchannels is negligible compared with that in the nanochannel. According to the current slope method, the EOF velocity can be calculated by the following the equation：

$$V_{EOF} = \frac{k_{slope}\ L}{I_2 - I_1} \tag{4-1}$$

where V_{EOF} is the velocity of the electroosmotic flow; I_1 and I_2 are the initial electric current value and the final electric current value in the nanochannel, respectively; k_{slope} is the slope of the liner part of the current-time curve; L is the length of the nanochannel.

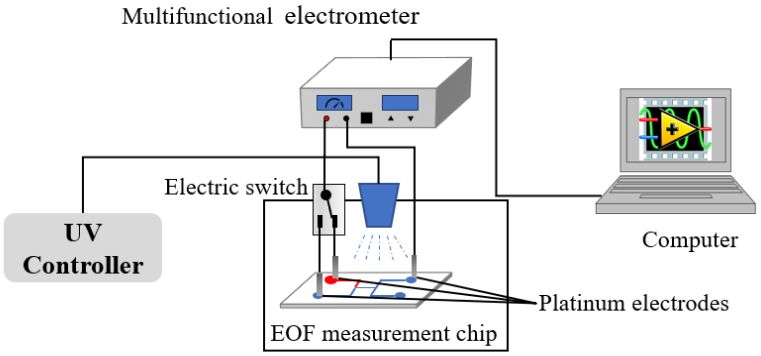

Figure 4-3. Schematic diagram of the EOF velocity measurement system.

The EOF measurement system, as shown in Figure 4-3, consists of a multifunctional electrometer (Keithley, Model 6517A) used to supply DC voltage and transfer the electric current signal to a computer by a LabVIEW program (National Instrument Corp.), platinum electrodes (Sigma-Aldrich), an electric switch, an UV controller, and a nanofluidic chip. The UV ray turns on only in the experiments of testing UV effects.

4.3 Results and discussion

4.3.1 Surface modification characterization by AFM

The quality of the modified h-PDMS surface and the grafting density of DNA attached on the surface were characterized by an AFM (MultiodeTM SPM, Digital Instruments). All images were captured in the conventional tapping mode. The DNA 15T modified h-PDMS chips were firstly treated with the surface modification process as described previously and then incubated at the temperature of 4 ^{o}C for 3 h and 24 h, respectively. The unmodified h-PDMS surface was used as a reference. The AFM height images of these surfaces modified with different conditions are shown in Figure 4-4. The surface profiles were measured correspondingly to the directions of the white lines on the AFM height images. The surface profile can indicate the surface structure and the grafting density of DNAs. As shown in the figure, the unmodified h-PDMS surface was very smooth. At the incubation of 3 h, the surface roughness increases, indicating DNA chains was grafted on the surface. Furthermore, the magnitudes of the peaks in the surface profile line are around 0.5 nm. At the incubation time of 24 h, the distance between the peaks of the surface profile is much smaller and the magnitudes of the peaks are larger than that at the incubation time of 3 h. These results illustrate that the grafting density of DNAs on the PDMS surfaces is proportional to the incubation time, and the high grating density will force the DNA chains transfer from folded to extended state, thus having a relatively long length.

4.3.2 Effects of incubation time

In general, the process that DNA molecules move from the bulk solution to the channel surface and the grafting density of DNA chains on the channel surface are related to the incubation time. In this work, the nanochannels modified with 15T ssDNA and incubated for 1h, 3 h, 6 h and 24 h were prepared, respectively. The electrolyte solution of 1×10^{-3} M KCl at pH 7 was utilized to investigate the effects of incubation time on EOF velocity in these nanochannels. It should be pointed out that most of the nanochannels used in this study have a much larger width than the depth, and the EDL may only overlap

in the depth direction of the nanochannels. Consequently, the EOF velocity is mainly dominated by the interaction between the modified channel surface and the bulk solution in the depth direction. Therefore, the depth is regarded as the effective size of the nanochannels. Theoretically, the EOF velocity should

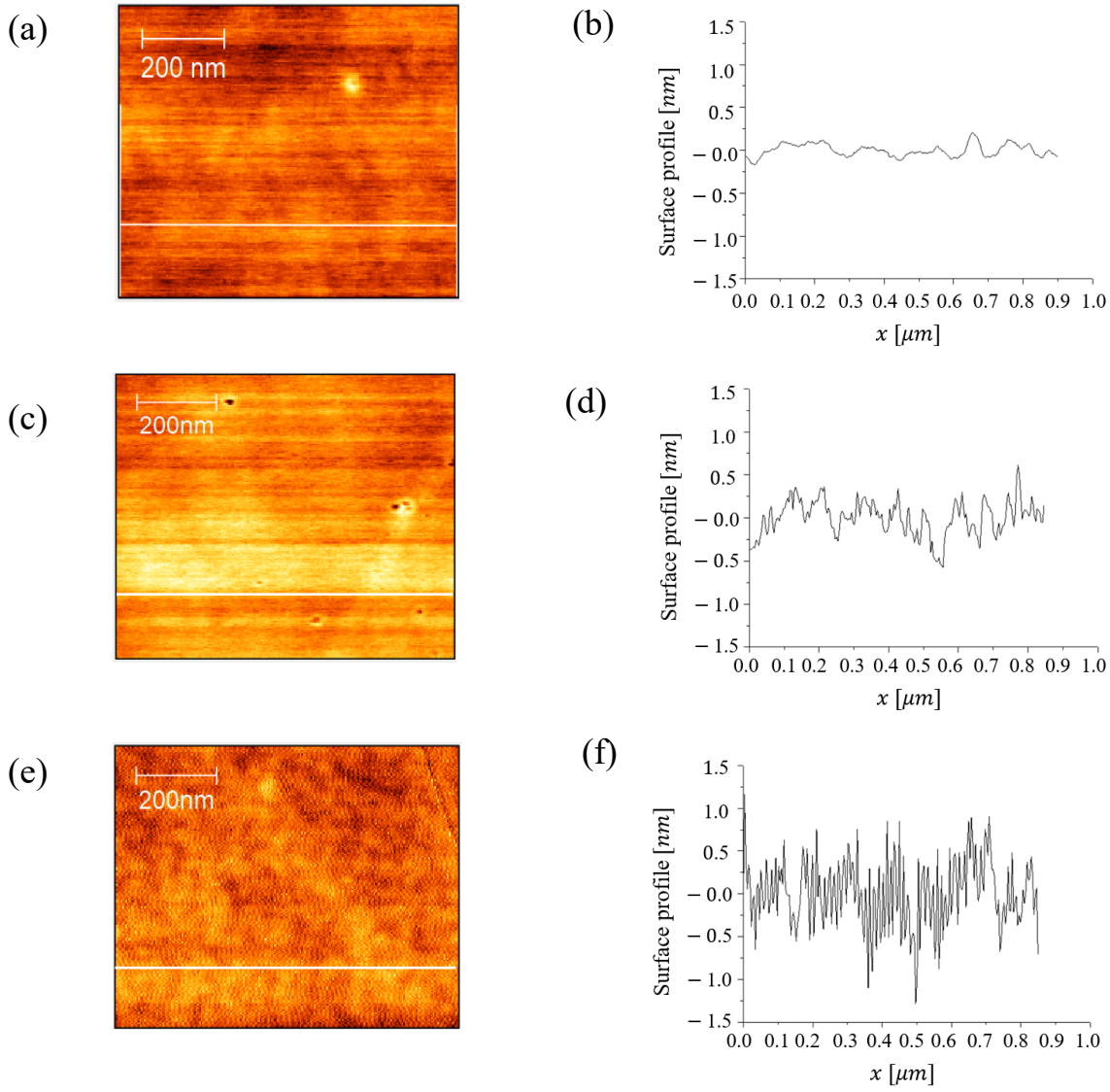

Figure 4-4. AFM images and surface profile of h-PDMS surfaces. (a) and (b) are the height image and surface profile of the unmodified h-PDMS surface, respectively; (c) and (d) are the height image and surface profile of DNA 15T modified h-PDMS surface with the incubation time of 3 h, respectively; (e) and (f) are the height image and surface profile of DNA 15T modified h-PDMS surface with the incubation time of 24 h, respectively.

be independent of the channel size in large nanochannels without overlapped EDL and reduced to a relatively small value in small nanochannel with overlapped EDL. However, as shown in Figure 4-5, the EOF velocity shows a decreasing tendency when the channel depth decreases from 2.5 μm to 650 nm which is still larger than the required size for EDL overlapping. This is because the relative space occupied by EDL increases in the nanochannel when the channel size becomes smaller although the size does not reach the critical value of overlapped EDL. For example, for the case of 1×10^{-3} M KCl solution, the calculated Debye length is approximately 9.6 nm, and the thickness of EDL may be approximately 30 ~ 50 nm. The maximum EOF velocity can only occur in a narrower center region in a small nanochannel compared with that in larger channels, even without overlapped EDL. As a result, the average velocity of EOF through the small nanochannel reduces.

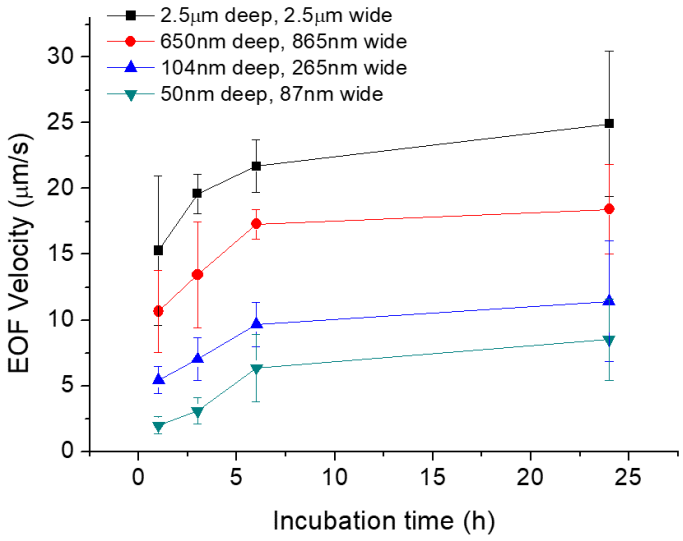

Figure 4-5. Measured EOF velocity as a function of the incubation time in ssDNA 15T modified nanochannels with size ranging from 50 nm to 2.5 μm. The applied electrical field strength is 20 V/cm. The solution used in the measurement is 1×10^{-3} M KCl at pH 7.

For the effects of the incubation time on EOF velocity, as shown in Figure 4-5, the EOF velocity initially increases rapidly when the incubation period increases from 1 h to 6 h and then increases only slightly as the incubation time increases from 6 h to 24 h. This is because more DNA chains will attach on the PDMS surface in a longer incubation process and this would generate a relatively higher surface charge density on the channels surface, thus increasing the EOF velocity. However, as the active surface groups that can be bonded with the DNA chains are limited on a fixed channel wall surface area, the

increase of the number of DNA chains attached on the channel surface will reach a limit with the further increase of the incubation time. Consequently, it is expected that the EOF velocity finally reach a maximum value and keep constant with the continuing increase of the incubation time.

4.3.3 Effects of the surface coating types

The properties of the grafted DNA layer on channel surface, such as surface charge, grafting density, and the thickness of the coated DNA layer, can critically affect the ion distribution in the EDL, thus influencing the distribution of EOF velocity in the modified channels[66]. In this work, the coated layer of DNAs is very thin (around 5nm), and the calculated thickness of EDL is 30~50 nm for 1×10^{-3}M KCl solution used in this measurement[149,150]. Therefore, the EDL extends far beyond the coated layer, and the EOF depends mostly on the electric properties of EDL[77]. However, these negative charges carried by DNA chains can increase the surface charge of the channel, thus resulting in a large zeta potential and increasing the EOF velocity. To confirm the effects of surface modification with DNAs of 15T and 15A on EOF velocity, the nanochannels with depth ranging from 50 nm to 2.5 μm were modified by only first chemical reaction step (EDC+NHS), two-step chemical reactions (EDC+NHS+15T), and duplex DNAs (EDC+NHS+15T+15A), respectively, by using the surface modification method described above. For comparison, the pristine PDMS channels are also prepared. All these channels were incubated with MES buffer solution at 4 ^{o}C for 24 h before using.

Figure 4-6 shows the experimentally measured EOF velocity of KCl solution with the ionic concentration of 1×10^{-3} M in modified nanochannels of different sizes. In comparison with the electroosmotic flow in pristine channels, the EOF velocity becomes smaller in all channels when the channel is modified only by the first chemical reaction step (EDC+NHS modification). In the 15T modified nanochannels, the EOF velocity shows a dramatic increase compared with that in the only EDC+NHS modified nanochannels. Because the molecular groups carried by DNAs are negatively charged in solutions, and they will increase the surface charge when they are attached on the channel surface, thus increasing the zeta potential and leading to a larger EOF velocity. The largest EOF velocity occurs in the duplex ssDNA modified nanochannels. The ssDNA 15A will hybridize with the immobilized ssDNA 15T on the channel surface and form the dual-stranded structure. As both ssDNA 15T and ssDNA 15A are negatively charged in pH 7 KCl electrolyte solution, the channel surface charge will be further increased after the hybridization, thus increasing the zeta potential and EOF velocity[147].

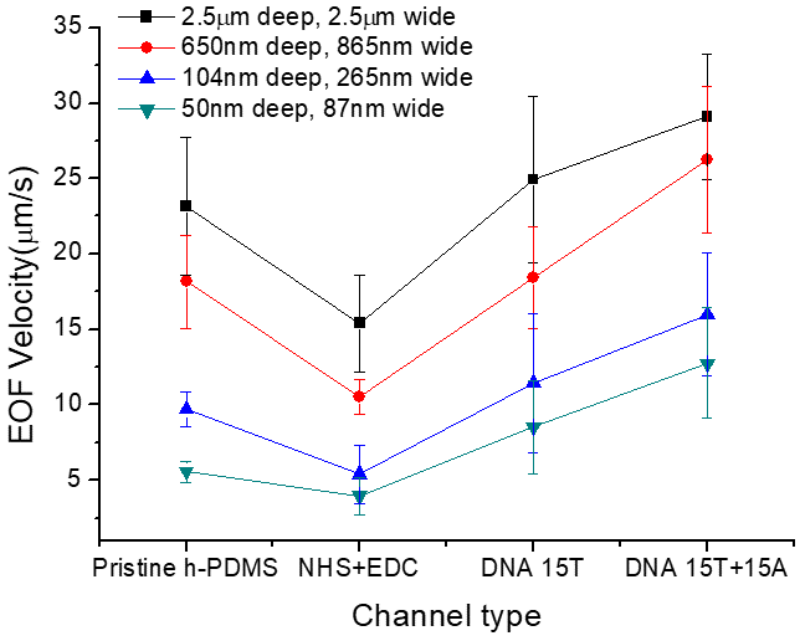

Figure 4-6**.** Experimental results of EOF velocity in nanochannels with different end-grafted layers. The applied electrical field strength is 20 V/cm. The solution used in the measurement is 1×10^{-3} M KCl solution at pH=7.

4.3.4 pH effects

Hydrogen ion plays an important role in determining the adsorption of metal cations on the channel surface, and its concentration influences the surface charge density and zeta potential on channel surfaces, thus influencing the electrokinetic transport in the channels[151,152]. In KCl solutions, the hydrogen ion is correlated to the pH value of the solution. In order to examine how pH value influences the EOF in 15T DNA modified nanochannels, the EOF velocity of 1×10^{-3} M KCl solution with pH value ranging from 4 to 10 were experimentally measured. In this work, all EOF measurement chips are incubated with MES buffer solution at 4 ^{o}C for 24 h before using. As a reference, the EOF velocity is also measured in a pristine h-PDMS channel which is also incubated with MES solution at 4 ^{o}C for 24 h before ready to use.

The measured EOF velocities of 1×10^{-3} M KCl solutions are shown in Figure 4-7. As can be seen from Figure 4-7, the EOF velocity of 1×10^{-3} M KCl solution increases monotonously in the unmodified h-PDMS channel when the pH increases from 4 to 10. However, in all ssDNA 15T modified channels, the EOF velocity of 1×10^{-3} M KCl solution only increases slightly when the pH rises from

5 to 10. The obvious change in EOF velocity can be observed only when the pH decreases from 5 to 4. These results indicate that the ssDNA 15T coated channels have a relatively stable surface charge when the pH of KCl electrolyte solution changes. For the pristine h-PDMS channels, the carboxyl groups and silanol groups will deprotonate when the concentration of hydrogen ions decreases, thus leading to a more negatively charged channel surface and larger EOF velocity. For the ssDNA 15T coated channels, the EOF velocity is also controlled by the DNA charge density when the coated DNA layer is engulfed by a thick EDL[71,153]. In the Manning theory, the fraction of the neutralized DNA charge is determined only by the valence of the counterions [71,154]. Consequently, for the 1×10^{-3} M KCl solution, pH effects on EOF velocity become less prominent in the ssDNA 15T modified channels.

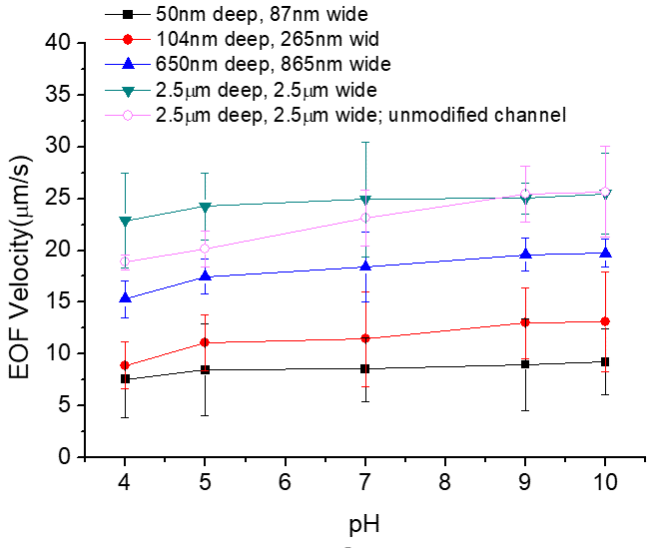

Figure 4-7. Measured EOF velocity as a function of the pH of 1×10^{-3} M KCl solution in DNA modified nanochannels with size ranging from 50 nm to 2.5 μm and an unmodified microchannel. The applied electric field strength is 20 V/cm.

4.3.5 UV illumination effects

The UV illumination could induce more negative charges on DNAs and affect the zeta potential of the DNA coated channel surface[82,147]. Moreover, the change in zeta potential caused by UV illumination is reversible that the zeta potential will turn back to the original value after the irradiation with visible light. To investigate the UV light effects on EOF velocity in DNA modified channels, the EOF velocity of KCl solution is measured in the channels with UV illumination. As a reference, the EOF velocity is also measured in the pristine h-PDMS channels with UV light illumination. The

concentration of KCl electrolyte used in the experimental is 1×10^{-3} M, and the calculated thickness of EDL is significantly larger than the coated DNA layer. Therefore, the EOF velocity mainly depends on the surface charge density. All measurement chips are incubated with MES buffer solution at 4 ^{o}C for 24 h before ready to use. The wavelength of UV light used in this experiment is 350 nm.

Figure 4-8 shows the EOF velocities response to UV illumination. To simplify the figure, only the depth of the channels is plotted as the x-axis in the figure. For h-PDMS channels, exposing channels to UV light could produce carboxyl groups on the surface and influence the surface charge density and EOF velocity[155]. However, all channels used in this experiment have been pretreated with a plasma device in the process of chips bonding. Most charged molecular groups of the channel surface have been activated by the plasma treatment.

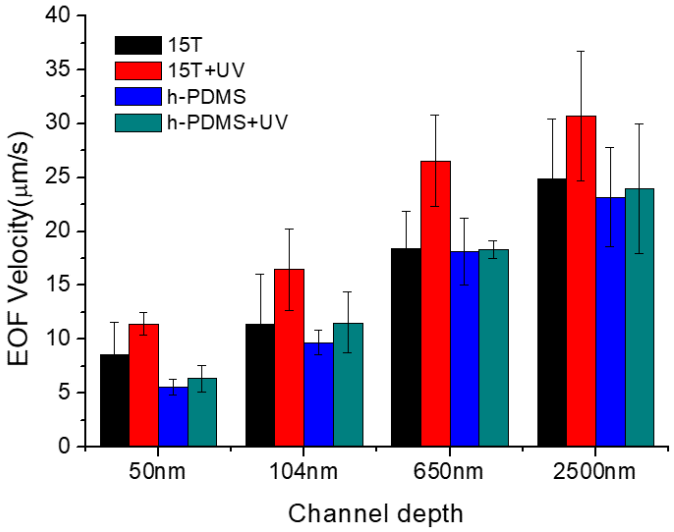

Figure 4-8. Measured EOF velocity response to UV illumination in pristine h-PDMS channels and ssDNA 15T modified h-PDMS channels. The applied electric field strength is 20 V/cm. The solution used in the measurement is 1×10^{-3} M KCl solution at pH=7.

According to Figure 4-8, the EOF velocity only increases slightly with the UV illumination compared that with visible light radiation in all pristine h-PDMS channels. These observations indicate the effects of UV illumination on EOF in the h-PDMS channels are inconspicuous. After ssDNA 15T coating, the negatively charged DNA brushes are grafted on the channel surface, and the surface charge density relates the negative charges carried by the DNAs. As UV illumination can affect the component and the surface charge of DNA, the EOF velocity should respond to the UV illumination in DNA

modified channels as well. From Figure 4-8, in comparison with the case of pristine h-PDMS channels, it can be seen that the EOF velocity is increased significantly in the ssDNA 15T modified channels with UV illumination compared that with visible light radiation, and the increment of the EOF velocity is larger than 20% in all size channels. The results show that the UV illumination could increase the surface charge of the ssDNA 15T and consequently increase the EOF velocity in the DNA modified channels.

4.3.6 Concentration effects

Figure 4-9 shows the experimental results of ionic concentration effects on EOF velocity in the pristine h-PDMS channels and ssDNA 15T modified channels. The electrolyte solutions of KCl with concentrations ranging from 0.2 M to 1×10^{-3} M were used to study the concentration effects in these channels. For the case of the pristine h-PDMS channels, shown in Figure 4-9 (a), the EOF velocity decreases monotonically in the microchannel and the large nanochannel, because the zeta potential of the channel surface is inversely proportional to the ionic concentration [140]. In the small nanochannels with depth 104 nm and 50 nm, the EOF velocity increases initially while the ionic concentration increases from 1×10^{-3} M to 1×10^{-2} M, and then shows a decreasing trend as the ionic concentration increases further. This is because the lower ionic concentration contributes to not only a higher zeta potential but also a larger thickness of EDL. For the 1×10^{-3} M KCl solution, the calculated EDL thickness can reach 50 nm. In the nanochannel with the depth of 104 nm, the EDL can extend almost to the whole channel. It is well-known that the electroosmotic flow field inside the electric double layer develops from zero velocity at the compact layer (immobile counter-ions adsorbed at the charged solid surface) to the maximum velocity at the outer boundary of the diffuse layer. For a channel with a relatively thick EDL, the maximum EOF velocity can occur only in a small portion of the space in the center of the channel. For such cases, the EOF velocity averaged over the channel cross section becomes much smaller although there is no overlapped EDL. When the EDL overlaps, the effective ionic concentration will be enhanced， contributing to a smaller zeta potential[156]. Therefore, in the 50 nm channel, the EOF velocity is further reduced due to the effects of the strongly overlapped EDL. From the Figure 4-9 (a), the EOF velocities of the 0.1 M and 0.2 M solution are essentially same in all the channels, because the EDL is very thin at these high ionic concentrations, and the EDL effects on EOF velocity are negligible.

(a)

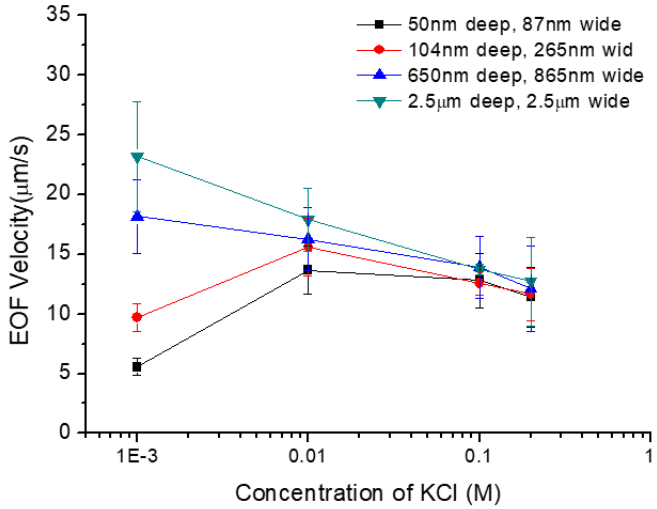

(b)

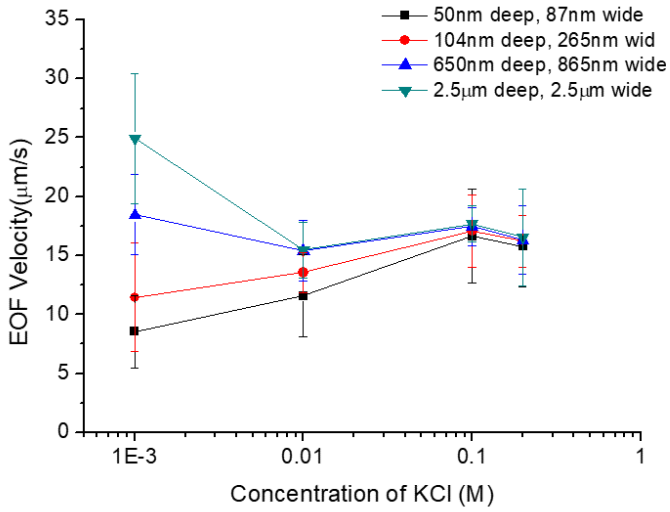

Figure 4-9. Measured EOF velocity as a function of the ionic concentration of KCl solution. (a) Measured EOF velocity in the unmodified h-PDMS channels. (b) Measured EOF velocity in ssDNA 15T modified h-PDMS channels. The applied electric field strength is 20 V/cm.

For the case of ssDNA 15T modified channels, the EOF velocity shows a similar trend to that in pristine h-PDMS channels at low ionic concentration. EOF velocity decreases in the large channels and increases in the small nanochannels when the ionic concentration increases from 1×10^{-3} M to 1×10^{-2} M. However, as the ionic concentration increases further, the EOF velocity increases firstly when the ionic concentration rises from 1×10^{-2} M to 0.1 M, and then decreases with the ionic concentration in all the channels. Similarly, the EOF velocities are essentially the same in all the

channels when the ionic concentrations of KCl solution are larger than 0.1 M due to the EDL is very thin. Previous theoretical works showed that the impact of the charge density of the coated brush layer is weak at a low ionic concentration (thick EDL), whereas the EOF velocity is dominated by the brush regime at a high ionic concentration (thin EDL)[78,153,157]. The aggregation of counterions within the brush layer could affect their contribution to the overall EOF velocity. Furthermore, the length of ssDNA will dramatically decrease when the ionic concentration of the monovalent salt solution is larger than 1×10^{-2} M [158]. This transformation in the structure of the coated DNA brushes could also influence the EOF velocity by changing the hydrodynamic screening of EOF[77].

4.4 Conclusions

This chapter presents an experimental study of electroosmotic flow (EOF) in DNA modified channels with size ranging from 50 nm to 2.5 μm by using the current-slope method. The influences of incubation time and type of DNAs on EOF velocity are investigated in the experiments. The EOF velocity of KCl electrolyte with various pH values and ionic concentrations are experimentally measured in the ssDNA 15T modified channels. Besides, the effects of ion size and ion valence on EOF velocity in DNA modified channels are studied. The effect of UV illumination on EOF velocity are also tested in the DNAs modified channels and the pristine h-PMDS channels. The results show that the surface coating with negatively charged DNAs can enhance the EOF in h-PDMS channels, and the EOF velocity is positively related to the grafting density of the coated DNAs. When the incubation time increases, EOF velocity increases initially and then approaches a constant. The EOF velocity relies strongly on the ionic concentration in the DNA modified channels as well as the pristine channels. The EOF velocity is relatively smaller in small nanochannels than that in large channels at a low ionic concentration, and independent of the channel size at a high ionic concentration. Different to the pristine channels, the EOF velocity becomes larger at the high ionic concentration of 0.1 M that the thickness of EDL is similar to the length of coated DNA brushes. The UV illumination also contributes to increase the EOF velocity in the DNA modified channels. For the effects of ion size and ion valence, they follow the similar trend in DNA modified nanochannels to that in bare h-PDMS nanochannels. However, the pH effects on EOF velocity are less prominent in these modified channels. The experimental results presented in this chapter facilitate the improvement in better understanding the electrokinetic transport and the EDL theory in DNA modified nanochannels.

Chapter 5 Fundamental Research III: Regulation of Nanochannel Size and EOF in Charged Polyelectrolyte Modified Nanochannels[‡]

5.1 Introduction

Recently, in nanofluidic, numerous applications have been suggested for the electrokinetic transport phenomena in the fields of biology[1], chemical analysis[2,3], and mechanical engineering[4]. Since the electrokinetic transport phenomena are mainly determined by the surface properties in general microfluidic and nanofluidic devices, it is a key factor that develops effective surface modification techniques for meeting the demands of applications[159]. Surface coating with self-assembly polyelectrolyte multilayers is a flexible and convenient method in the modulation of surface properties[73]. In this method, polyelectrolyte layer-by-layer (LBL) deposition is often employed to reversibly change surface charges and achieve nanoscale control in capillary electrophoresis (CE) due to its advantages of long-term stable properties and mechanical film integrity[116,160–162]. When polyelectrolyte attaches on an oppositely charged surface, the surface charges could be compensated or overcompensated by the charges carried by the polyelectrolyte molecules[163]. Generally, the LBL process is accomplished by alternately adsorbing polycationic and polyanionic molecules onto charged surfaces by hydrogen-bonding or electrostatic interactions[110].

Many papers studied the factors influencing the growth of polyelectrolyte multilayers on various substrates[111,115,116,163–165]. Dubas and Schlenoff[115] reported that the adsorption of charged polyelectrolytes on oppositely charged surfaces is an ion exchange process, and the thickness of coated layers on silicon substrates is proportional to the added salt concentration in polyelectrolyte solutions and the deposition cycles. Haselber et al.[116] investigated the morphology of the coated films on silica surfaces with the polyelectrolytes of polybrene (PB) and dextran sulfate (DS). They stated that a single polybrene (PB) coating could not cover the surface completely, and the full coverage of silica surfaces with PB-DS layers is achieved by at least triple-layer coating[116]. Guo et al.[166] also experimentally study the LBL deposition of polyelectrolytes on silicon wafers. Their results showed that the concentration ratio of positively charged polyelectrolytes to negatively charged polyelectrolytes is a key factor in determining the thickness and surface roughness of the coated layers[166]. With these

[‡] A similar version of this chapter was submitted or published as:
J. Li, D. Li, Polyelectrolyte adsorption in single small nanochannel by layer-by-layer method, J. Colloid Interface Sci. 561 (2020) 1–10. https://doi.org/10.1016/j.jcis.2019.11.116.

unique features, recently, the technique of LBL coating has been introduced into the field of microfluidic and nanofluidic to manipulate the fluid transport, and many studies have been developed [125,166–169].

In microscale, the change of channel size caused by the coated polyelectrolyte layers is negligible in comparison with the relatively large channel size. Therefore, LBL modulates the electrokinetic transport in microchannels mainly by regulating the surface charge. For example, Liu et al.[113] coated the PMDS capillary electrophoresis microchips by PB and DS. In their experiment, the direction of EOF is opposite in PB and PB-DS coated channels, indicating that the surface charge of the modified channels is determined by the outmost coated layer. Boonsong et al.[114] further studied the effects of LBL coating on EOF in PDMS microchannels and reported that the direction of EOF is determined by the charge properties of the outmost coated polyelectrolyte but the velocity may vary at a low coating layer number. This variability in the EOF velocity likely comes from the partial surface coverage at low layer number. As the layer number increases, the overall consistency of the surface charge will improve, and the EOF velocity will be a constant value with the same outmost layer[114]. According to the performances of surface coating, Biddiss et al. [109] developed a passive electrokinetic micromixer by patterning the microchannel surfaces with positively charged polyelectrolytes and generating heterogeneous surface charges.

In nanoscale, the steric effects have to be considered in determining the transport of polyelectrolyte molecules and the formation of multilayers [170]. Thomas et al.[171] investigated the growth of the G4-polyelectrolyte layer in nanopore by using LBL deposition. Their results proved that the size of nanopores is a dominant factor for the thickness of the polyelectrolyte layer deposited within nanopores, and the deposition can be completely suppressed when the nanopore is sufficiently small, even the pores are not filled. Roy et al.[172] also studied the effects of pore diameter on LBL deposition in nanopores with the pore diameter ranging from 100 to 500 nm by using Gas-flow porometry measurement and stated that the polyelectrolytes could form a more dense gel layer in small nanochannel due to the geometric constraints.

In summary, although these studies have been developed to analyze the growth of polyelectrolyte layer from the macro scale to nanoscale by using the LBL technique, they are mostly conducted on flat substrates and focus on the surface properties of the multilayers. Only limited data of size control in nanochannels can be found from the published results[171,172]. Therefore, this chapter aims to investigate the LBL coatings of polybrene (PB) and Dextran sulfate (DS) in single small nanochannels,

and the channel size change caused by the polyelectrolyte adsorption will be measured by using atomic force microscope (AFM).

5.2 Experimental section

5.2.1 Materials

The chemicals employed in this study include KCl (≥99%, Fisher Scientific), NaCl (≥99%, Fisher Scientific), LiCl (≥99%, Fisher Scientific), polybrene (PB, ≥94%, Sigma-Aldrich), Dextran sulfate (DS, molecular weight, 7000 – 20000, Sigma-Aldrich). Regular PDMS (Sylgard 184, Dow Corning) and hard PDMS (h-PDMS) are utilized to fabricated nanofluidic chips used in the experiment[139]. Deionized water (18.2 MΩ Mini Q, Direct-Q3) was used to prepare all the solutions.

5.2.2 Nanofluidic chip fabrication

In this experiment, the molds of nanochannels were fabricated by using the solvent-induced method[50]. To precisely replicate the features of nanochannels form the molds, a bilayer of h-PDMS and regular PDMS was employed to fabricate the nanochannel chips. Firstly, the h-PDMS was spin-coated on the nanochannel mold to replicate the nanochannels and minimize the deformation of the channel size. Following by a heating process in an oven at 80 °C for 10 minutes, the relatively soft regular PDMS was cast onto the h-PDMS layer to support the fragile h-PDMS and then heated in the oven at the same temperature for 2 hours [139]. Figure 5-1 shows the AFM height image and the profile of the nanochannel used in this study.

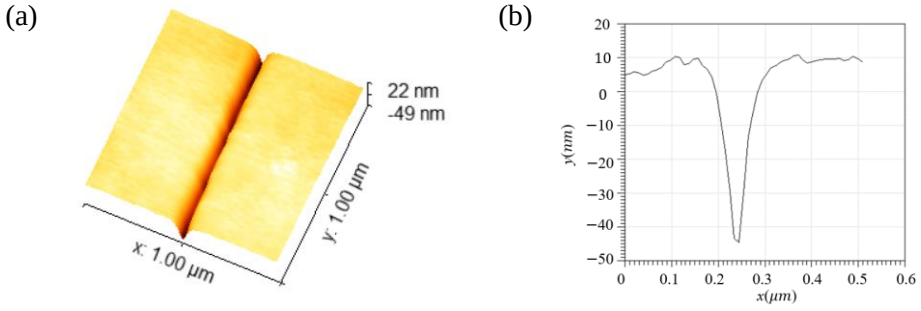

Figure 5-1. (a) The AFM images and (b) the profiles of the nanochannels with a depth of 54 ± 1 nm and a width 117 ± 9 nm.

To easily deliver the polyelectrolyte solutions and achieve the surface modification process in the nanochannels, the nanochannel was bonded with a microchannel which was replicated from a SU8 photoresist microchannel mold by Plasma treatment (Harrick plasma, PDC-32G). This mold was fabricated by casting SU8 photoresist on a silica wafer with the standard photolithography method. In order to keep the surface properties are constant on all the channel walls, the microchannel chip was also produced with the bilayer of h-PDMS and regular PDMS. Figure 5-2 shows the schematic of the bonding process (Figure 5-2(a)) and an example of the nanofluidic chip (Figure 5-2(b)). In the final nanofluidic chip, the nanochannel bridges the two microchannels which have a depth of 30 μm and a width of 100 μm.

(a)

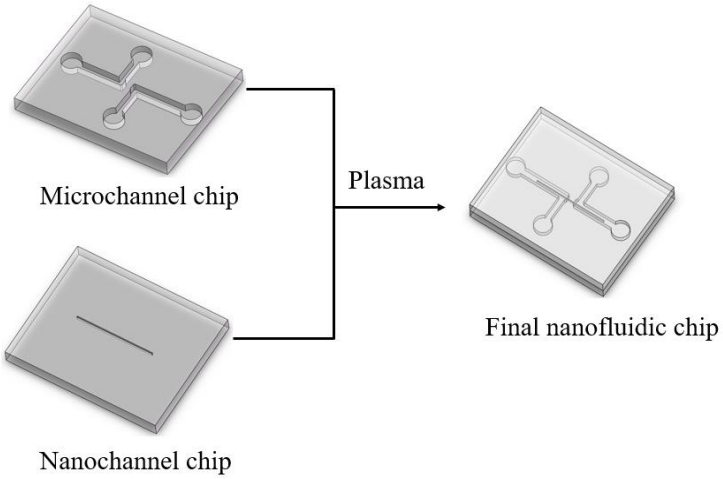

(b)

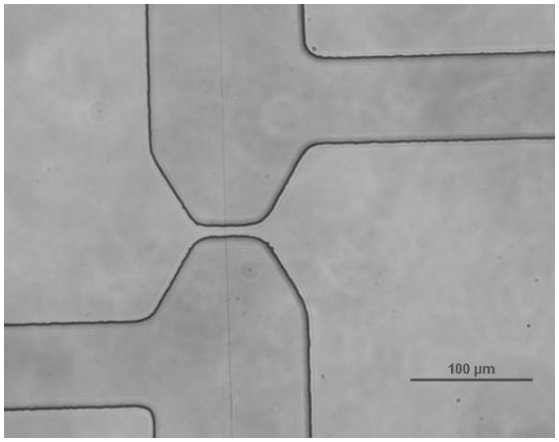

Figure 5-2. (a) The schematic of the nanofluidic chip bonding process. (b) An image of the nanofluidic chip captured by an optical microscope.

5.2.3 Surface modification

In this work, nanochannels were modified with 5% PB and 3% DS solutions according to the LBL self-assembly method [173]. Briefly, the nanochannel was initially filled and rinsed with 0.1 M NaOH solution for 30 min. Then, the nanochannel was rinsed with deionized water three times for 10 min each time. After the precondition steps, the nanochannel was rinsed by 5% PB solution for 30 min followed by three times rinsing with water for 10 min each. The solution of 3% DS was then utilized to rinse the nanochannel for 30 min, and the same rinse step with water was conducted to remove the residual polyelectrolyte solution. By repeating the above processes, multiple polyelectrolyte layers can be coated on the nanochannel inner surfaces. Figure 5-3 shows the scheme of the formation process of polyelectrolyte multilayers in nanochannels. All these procedures described above were conducted at the room temperature around 23 ^{o}C.

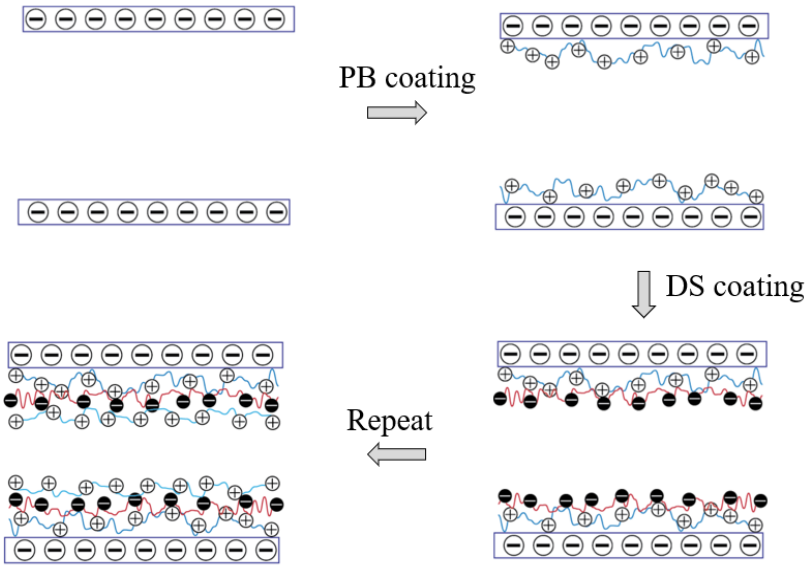

Figure 5-3. Schematic representation of the formation of PB-DS multilayers in a nanochannel.

5.2.4 Characterization

After the surface modification process, the nanochannels were blown to dry with an air pump. Then, a commercial instrument of atom force microscope (AFM, MultiodeTM SPM, Digital Instruments) was employed to measure the size of nanochannels coated with multiple layers. All images were captured in the conventional tapping mode by using silicon cantilevers. The experimental measurements of the nanochannel size were repeated at least 3 times in 3 independent chips.

5.2.5 Measurement of EOF velocity

In this study, the EOF velocity was measured by using the current-slope method[52]. The KCl solution of 1×10^{-3} M was used as the sample solution to conduct the EOF measurement in nanochannels. In the measurement, the nanochannel was filled with an KCl solution of 1×10^{-3} M initially, and an electric field was applied between the two ends of the nanochannel. Afterward, the same electrolyte solution, KCl, with a slightly higher concentration was added into the entrance of the nanochannel to displace the original solution by EOF. Because the ionic concentrations of electrolyte solutions determine their conductivities, an electric current change in the nanochannels can be obtained during the displacement process of electrolyte solutions[148]. This electric current change will be measured and recorded by an electrometer. Figure 5-4 (b) shows an example of the electric current-time curve. By knowing the length of the nanochannel and the slope of the electric current-time curve, the EOF velocity can be calculated. According to the current slope method, the EOF velocity can be expressed as the following equation.

$$\mathrm{V}_{EOF} = \frac{k_{slope}\ L}{I_2 - I_1} \tag{5-1}$$

where V_{EOF} is the velocity of the electroosmotic flow; I_1 and I_2 are the initial electric current value and the final electric current value in the nanochannel, respectively; k_{slope} is the slope of the linear part of the current-time curve; L is the length of the nanochannel.

Figure 5-4 (a) shows the schematic diagram of the EOF measurement system. This experimental system consists of an electrometer (Keithley, Model 6517A) which can supply DC voltage to generate EOF and measure the electric current, a computer that can receive and record the current signal from the electrometer by a LabVIEW program (National Instrument Corp.), an electric switch, and platinum electrodes (Sigma-Aldrich). In this work, all the experimental measurements of EOF were conducted at the room temperature of around 23 ^{o}C. and repeated for at least 3 times in 3 independent chips.

(a)

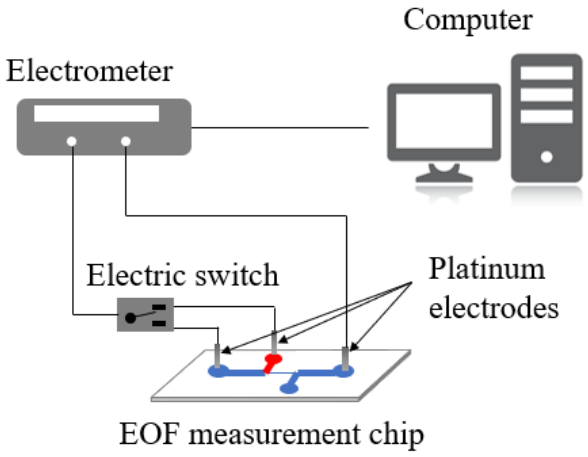

(b)

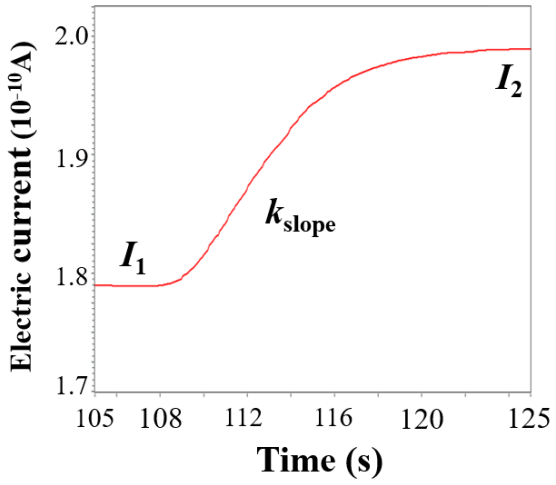

Figure 5-4. (a) Schematic diagram of the EOF velocity measurement system and (b) an example of the measured current-time curve by this system.

5.3 Results and discussion

5.3.1 Growth of polymer layers on flat h-PDMS surfaces

To obtain the reference thickness of the coated layers, polyelectrolytes are first coated on flat h-PDMS substrates. As shown in Figure 5-5(a), the h-PDMS flat substrates are reversibly bonded and partially covered with a PDMS chip. Then, the salt-free solutions of 5% PB and 3% DS of polyelectrolytes are utilized to modify the uncovered h-PDMS surfaces by using LBL method. Once the modification process is completed, the coverage on the surface is removed and the modified surfaces are examined by AFM. The height difference between the covered and uncovered portion of the

substrate surface indicates the thickness of the coated layer. Figure 5-5 (b) shows a representative 3D AFM image of a surface coated with two pairs of PB-DS layers. It can be observed that a significant height difference is generated between the covered and uncovered areas (shown in Figure 5-5 (c)).

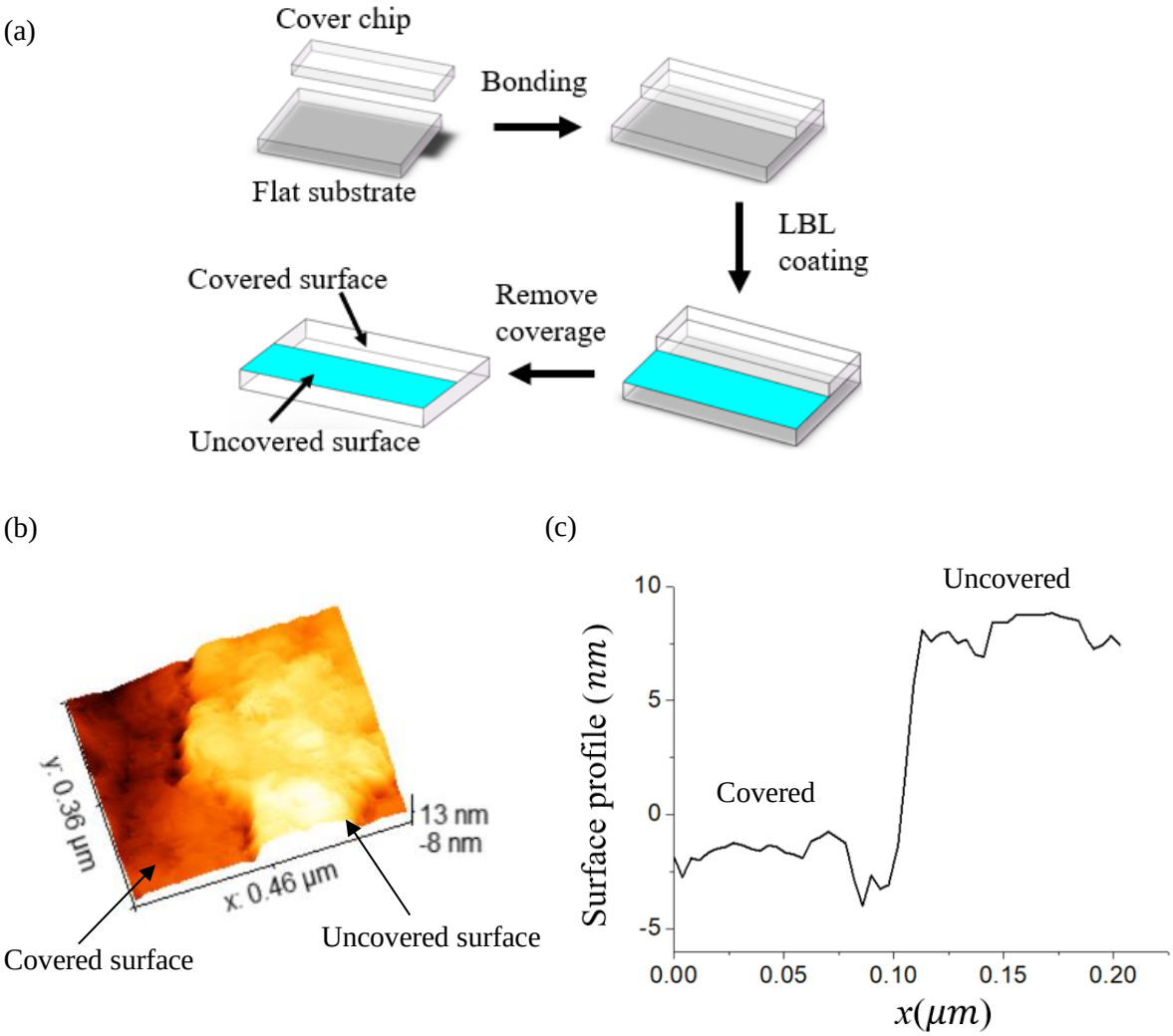

Figure 5-5. (a) Schematic diagram of the surface coating process; (b) AFM image and (c) surface profile of h-PDMS surfaces modified with two pairs of PB-DS layers.

The thicknesses of multilayers on flat substrates are shown in Table 5-1. From this table, one can see that the thickness of the multilayers is linearly proportional to the deposition cycles, and the average increment of the thickness of a pair of the polyelectrolytes (PB-DS) is essentially constant which is approximately 5.4 nm. It has been reported that the thickness of the polyelectrolyte layers on flat surfaces depends on the length of the polyelectrolyte chains, and the size of the polyelectrolyte chains

can be estimated by the standard theory of polyelectrolyte solutions[174]. Generally, the distance between the two ionized charges on the polyelectrolyte chains is described by the Bjerrum length, about 0.7 nm in water at room temperature. When the distance between the two ionized charges on the polyelectrolyte chains is smaller than the Debye length λ_d of the electric double layer at the substrate-solution interface, the polyelectrolyte chains are generally stiffened due to the electrostatic repulsion force. In our conditions, the Debye length λ_d of the salt-free solution is larger than 10 nm, significantly larger than the distance between the ionized charges of the polyelectrolyte chains. Therefore, these polyelectrolyte chains are likely adsorbed flatly on the substrate surface due to the electrostatic stiffening, and the thickness increment of the coated layers is linearly proportional to the layer number.

Table 5-1. The average thickness of polyelectrolyte multilayers on h-PDMS surface.

Deposition cycle[a]	Average thickness of the multilayers (nm)[b]
PB-DS	5.2 ± 0.3
$(PB\text{-}DS)_2$	10.7 ± 0.5
$(PB\text{-}DS)_8$	41.4 ± 2.0
$(PB\text{-}DS)_{14}$	75.5 ± 1.2

a $(PB\text{-}DS)_n$ means that n pairs of PB-DS polyelectrolytes are coated on the substrates.

b Average $\pm$ standard deviation.

5.3.2 Growth of polymer layers in nanochannels

5.3.2.1 Layer number effects

As discussed above, the formation of polyelectrolyte multilayers on flat surfaces is mainly affected by electrostatic interactions. However, in nanochannels, the dominant factors affecting the growth of polyelectrolyte multilayers are both electrostatic interactions and steric effects[171]. When the channel size becomes smaller than the length of the polymer chains, it is no surprise that the polymer molecules cannot transport through the nanochannel. As a result, there should be a saturation value in the minimum size of nanochannels modified with specific polymers by using this method. In addition, the thickness of electrical double layer is 3 ~ 5 times of λ_d , and the electric double layers (EDL) may overlap in small nanochannels. The overlapped EDL field will repel the electrolytes carrying the same

sign as that of the EDL field. Therefore, the transport of polyelectrolytes through nanochannels with overlapped electric double layers may not be realized even though the channel size is larger than the length of polyelectrolyte chains. Figure 5-6 shows the change of nanochannel size as a function of the layer number for PB/DS multilayer coating. In this case, the PB and DS are dissolved into pure water. Because the width of the nanochannel is relatively larger than the depth of the nanochannel used in this experiment, the nanochannel size will reach the saturation value in the width direction firstly. To simplify the figures, only the depth of the nanochannels is used to analyze the performance of the multilayer coating and plotted as the x-axis in the figures. According to Figure 5-6, for the condition of salt-free polyelectrolytes solutions, the average nanochannel size initially decreases linearly before the layer number 8 and finally approaches a constant with the increasing deposition layer number. In the initial decrease regime, the average decrease (t_{av}) in the depth direction of the nanochannel per pair of PB-DS layer is only around 2.7 nm which is calculated by:

$$t_{av} = (d_o - d_m)/2 \tag{5-1}$$

Where d_o is the depth of the original nanochannel, d_m is the depth of polyelectrolytes modified nanochannel.

In the linear regime, the thickness of the coated polyelectrolyte layer is very similar for each pair of layers. This indicates the thickness of the individual layer is additive when the coated layers are formed in this regime. This result is in good agreement with the previous studies of polyelectrolyte adsorption on flat substrates[116,175,176]. Clearly, the t_{av} (2.7 nm) in the nanochannel per pair of PB-DS layer is smaller compared with that (5.4 nm) on flat surfaces. The saturation value (the minimum nanochannel size) of the nanochannel in this condition is around 25 nm, and the nanochannel is far from being completely filled with the coated layers at this value. For the salt-free solutions, the electric double layer (EDL) has already overlapped in the depth direction of the original nanochannel which has a depth of 54 nm. These results indicate that the overlapped EDL will inhibit the growth of polyelectrolytes on the nanochannel inner surfaces and decrease the thickness of the coated layers. When the overlapped EDL exists, more counterions cumulate in the nanochannel than the co-ions and the transport of polyelectrolytes could be hindered electrostatically[171]. Besides, the strong electrostatic interactions also stretch the polyelectrolytes chains and generate thinner coated layers[177].

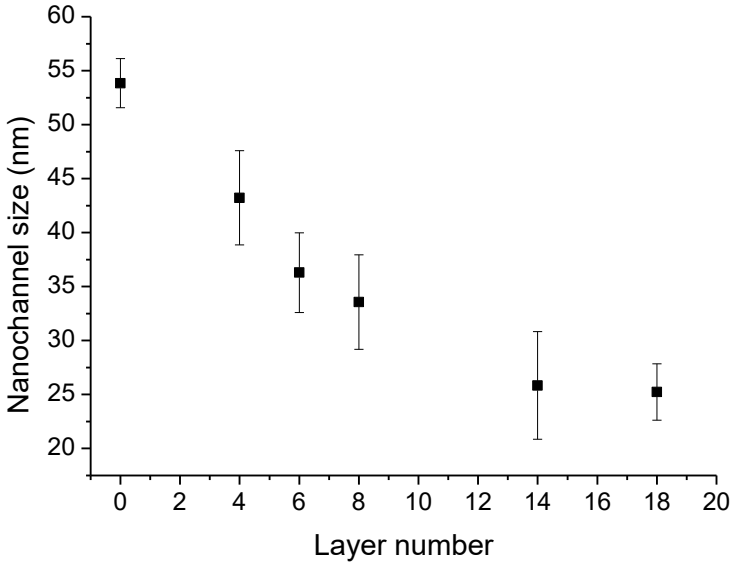

Figure 5-6. The change of nanochannel size as a function of the number of layers coated on the nanochannel surfaces. The point at layer number 0 is the original channel size.

5.3.2.2 Salt concentration effects

To further investigate the electrostatic interactions and steric effects on the adsorption of polyelectrolytes in nanochannels, the solutions of polyelectrolytes with different added salt concentrations were used to modify nanochannels. At low ionic concentration, the counterion condensation effects are dominated, and the polyelectrolyte chains will be stretched and lie to the substrate surfaces parallel due to the repulsive electrostatic interactions[174]. It should be realized that the Debye length is also a function of the ionic concentration and can be calculated by the following equation,

$$\lambda_d = \sqrt{\frac{\varepsilon_0 \varepsilon_r k_b T}{2 n_{i\infty} (ze)^2}} \tag{5-2}$$

Where ε_0 is the permittivity of vacuum, and ε_r is the dielectric constant of the electric solution; k_b is the Boltzmann constant; T is the temperature; $n_{i\infty}$ is the density of ions; z is the valence; e is the elementary charge.

Increasing ionic concentration will compress the Debye length and hence the thickness of EDL, thus affecting the electrostatic interactions. If the Debye length is small and comparable to the length of the monomer units, the electrostatic repulsion between the groups on the polyelectrolyte chains will be screened, and the polyelectrolyte chains will keep in random coil conformations with less electrostatic stiffening, thus increasing the adsorbed amount [163,172]. Therefore, the average thickness of the polyelectrolyte layers adsorbed on the channel surfaces becomes larger.

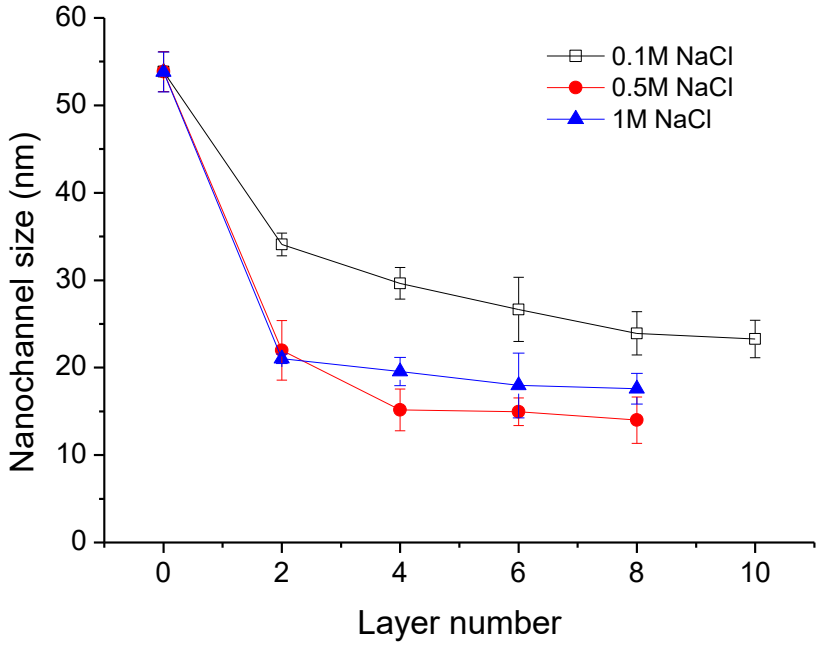

Figure 5-7. The change of nanochannel size as a function of the layer number deposited on the nanochannel surfaces.

Previous experimental study of PB and DS coating on flat surfaces has shown that the thickness of the coated layer is proportional to the added salt concentration[115]. In nanoscale, the changes in the structure of polyelectrolyte chains caused by the change of ionic concentration could also affect the saturation value of nanochannel size due to the steric effects and electrostatic repulsion effects. Figure 5-7 shows the effects of ionic concentration on the nanochannel size change over a range of NaCl concentrations (100 mM – 1 M). For the case of the solutions with 0.1 M NaCl, the nanochannel size decreases sharply after the coating of one pair of PB-DS layer. The t_{av} in nanochannel for the first pair of PB-DS layer is 9.9 nm which is increased around 4 times compared with that modified with salt-free solutions (Figure 5-6). As the layer number further increases, the nanochannel channel size gradually

decreases and finally reaches a saturation value. The saturation value of the nanochannel size is around 22 nm with 0.1 M NaCl added in the solutions and is relatively smaller than that without salt addition. This is because the high ionic concentration leads to a thinner EDL and weakens the electrostatic effects on polyelectrolyte transport. For the 0.1 M NaCl solution, the calculated Debye length is only around 1 nm, and the estimated thickness of EDL is 3-5 nm which is much smaller than the original channel size (depth) of 54 nm. Moreover, the coil conformations allow more polyelectrolyte chains adsorbed on the surfaces. As a result, the nanochannel size decreases significantly at the initial stage with the weaker electrostatic interactions. As the channel size further decreases, the thickness of EDL becomes comparable to the channel size, even not overlapped, the transport and adsorption of polyelectrolytes are inhibited, and the average thickness of the coated layer becomes smaller. Similarly, in the case of 0.5 M NaCl, the nanochannel size also dramatically decreases after coating the first PB-DS layer, and then gradually decreases to a saturation value. The t_{av} for the first pair of PB-DS layer rises to around 15.9 nm, and the nanochannel saturation value drops down to about 14 nm. When the salt concentration increases to 1 M, the t_{av} for the first layer of PB-DS coating shows a slight increase from 15.9 nm at 0.5 M to 16.4 nm, whereas the saturation value is relatively larger compared with that at 0.5 M. The results can be explained by the transformation of polyelectrolyte chains according to the salt environment [163,178]. As discussed above, the polyelectrolyte chains absorb on nanochannel surfaces in a relatively flatter conformation without salt addition. The average thickness of the coated layer will be smaller correspondingly. However, the low ionic concentration environment also contributes to building a strong electrostatic repulsion force surrounding the entrance of the nanochannel because the large Debye length will generate overlapped EDL. Consequently, it is difficult for the polyelectrolytes to transport into the nanochannel even their diameters are smaller than that of the channel entrance. Therefore, the saturation size of the nanochannel modified with “salt-free” polyelectrolyte solutions is larger. In the presence of salt, the polyelectrolyte chains become a loopier conformation, leading to thicker coated layers. In the meantime, the Debye length is compressed, and the electrostatic repulsion at the entrance will be screened. Hence the polyelectrolyte can be transported into the nanochannel easily, and the entering of polyelectrolyte to the nanochannel is mainly determined by the steric effects at the high ionic concentration. As a result, the saturation size becomes smaller. However, the saturation size demonstrates an opposite trend when the salt addition further increases to 1 M. The previous study described the adsorption of polyelectrolyte as an ion exchange process that the charged polyelectrolytes replace salt ions on the oppositely charged surfaces[115]. Since counterions have finite volumes, the salt ions will compete with the polyelectrolyte chains for the charged surface sites at high salt

concentration[115,163]. Moreover, the salt ions in the solution not only screen the electrostatic repulsion exerted on polyelectrolytes but affect the surface-polyelectrolyte attractions by compensating the surface charges. Therefore, the salt concentration effects on the adsorption of polyelectrolytes could be reversed at some point that the salt concentration is sufficiently high to displace polyelectrolytes from the surfaces[179]. Figure 5-8 demonstrates examples of AFM images of the modified nanochannels. From this figure, it is observed that the polyelectrolytes can be coated within nanochannels and form a uniform layer on the entire length of the channel inner surfaces. Furthermore, the nanochannels are not blocked by the coated polyelectrolyte layers at the saturation value (i.e., after 8 layers).

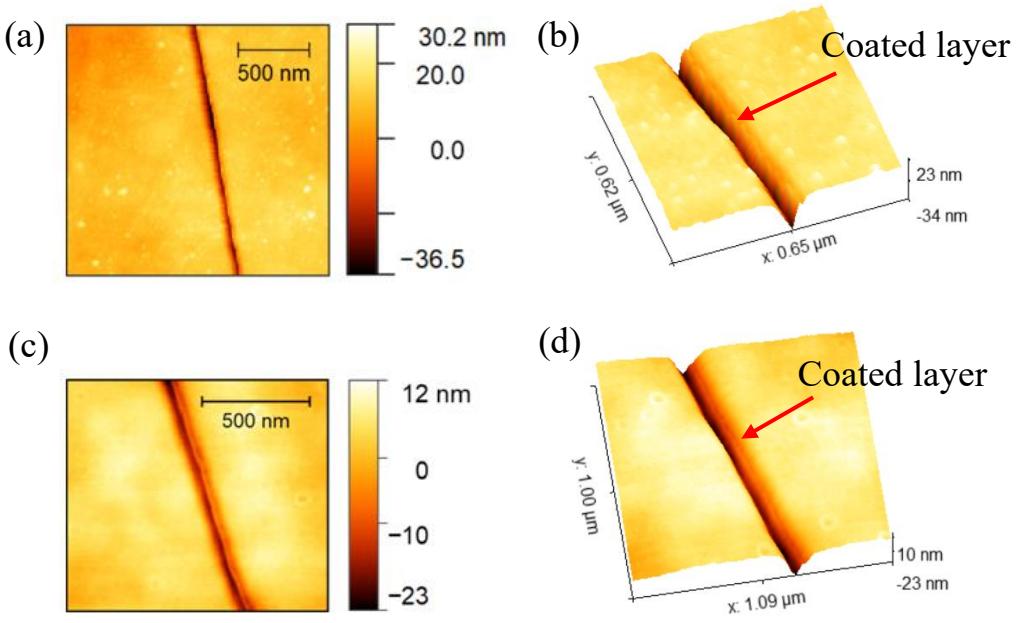

Figure 5-8. Examples of AFM images of PB/DS modified nanochannels. (a) and (b) are the AFM images of the nanochannel coated with 14 layers of PB/DS in salt-free solution, respectively; (c) and (d) are the AFM images of the nanochannel coated with 8 layers of PB/DS in the solution added with 0.5 M NaCl, respectively.

5.3.2.3 Ion type effects

Since the adsorption of polyelectrolyte is an ion exchange phenomenon, and the mechanism of the adsorption is electrostatic interactions, it is expected that different salt ions could affect the thickness

of the coated layer and modulate the adsorbed amount of polyelectrolyte. The bonding energy of ions could influence the solvation energy of the polyelectrolyte solutions which is a key factor for determining the driving force of polyelectrolyte to the interface[115]. In a crude approach, the ion that has less hydrated ion pair should bind more strongly and be more stable[115]. For example, among the ions of Li^+, Na^+, and K^+, the Li^+ attracts most hydrated ion and has the largest hydrated size while K^+ owns the least hydrated ion pair in aqueous solutions[145]. On flat surfaces, the polyelectrolyte layer prepared with the solution containing LiCl should have the least thickness compared with the other two salts at the given concentration and layer number. To examine the effects of ion type on the formation of polyelectrolyte layers in nanochannels, in this study, the 5% PB and 3% DS solutions containing 0.1 M LiCl, NaCl, KCl, respectively, were utilized to modify the nanochannels. Figure 5-9 shows the change in nanochannel size in different solvent conditions. For all solvent conditions, the nanochannel size changes follow a similar trend that the channel sizes decrease rapidly at low layer number, and then decrease gradually until reach a saturation value with the increasing layer number. It is to be noted that the t_{av} is inversely proportional to the hydrated size of ions at low layer number. However, the channel sizes modified with the solutions containing different salt ions are essentially the same at layer number of 8 where the channel size reaches the saturation value for the solution with 0.1 M NaCl. These results reveal that ion type effects on nanochannel size are prominent only when the layer number is low. The saturation value of nanochannel size is mainly determined by the added salt concentration and independent of salt types.

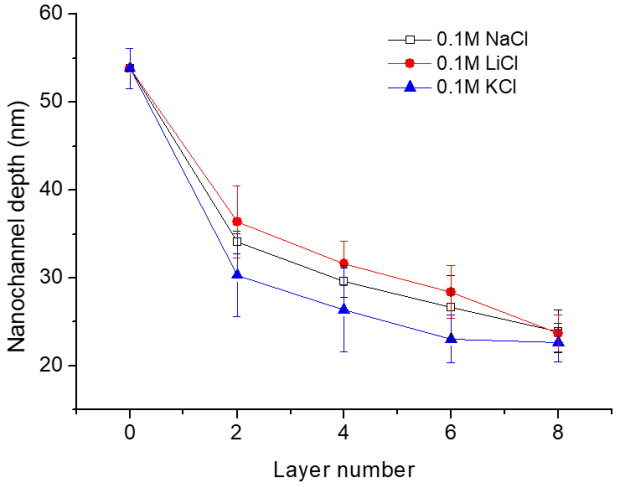

Figure 5-9. The change of nanochannel size as a function of the layer number deposited with different salt types.

5.3.3 Electroosmotic flow in nanochannels coated with polyelectrolyte multilayers

In order to analyze the effects of the LBL coating on the surface properties and electrokinetic transport in the modified nanochannels, EOF measurement was conducted in both the bare nanochannel and the modified nanochannels by using the current-slope method[52]. Because the electric current is very low and difficult to measure in extremely small nanochannels, therefore, a relatively large nanochannel with the smallest dimensional size of 104 nm was employed to measure the EOF velocity in this work. In this work, the presence of salt in the LBL deposition process could influence the thickness of the coated layer and the saturation size of the modified nanochannel. Boonsong et al.[114] investigated the salt addition effects on the EOF in microchannels and stated that EOF was not significantly influenced by the presence of salt compared with that without salt addition. Therefore, in this experiment, the nanochannel is modified by using 5% PB and 3% DS solutions without salt addition. Figure 5-10 shows the EOF velocity of 1×10^{-3} M KCl solution in the modified nanochannels at different layer numbers under the applied electric field of 50 V/cm. In the bare nanochannel, the point at layer number of 0 in Figure 5-10, the EOF velocity is positive (the direction of EOF is the same to the direction of the applied electric field). In the LBL deposition, the surface charge of the nanochannel will be alternatively changed corresponding to deposition numbers, thus influencing the EOF transport. As can be seen from the figure, the EOF velocity is positive in the nanochannels when the outmost coated layer is a DS layer whereas is negative when the outmost coated layer is a PB layer. This result indicates that the zeta potential of the channel surfaces which determines the EOF velocity depends on the electric properties of the outmost coated layer. For the cases that the outmost coated layer is a DS layer, it should be noted that the EOF velocity is relatively smaller at the layer number 2. This may be because the nanochannel surface was partially coated, and the EOF velocity is not very stable at low layer number. As the layer number further increases, the EOF velocity should become a constant value and independent of the layer number as the outmost coated layer has the same surface property, and the solution cannot permeate into the coated layer[114]. However, as seen in Figure 5-10, when the layer number increases further from layer number 4, and the nanochannel size becomes smaller, the EOF velocity demonstrates a gradually decreasing trend. This is because the effects of the space occupied by EDL on EOF velocity distribution has to be considered in small nanochannels. For the 1×10^{-3} M salt solution, the Debye length is 9.6 nm, and the thickness of the diffuse layer in EDL is 30-50 nm. The EDLs are likely to get overlapped in the modified nanochannel at large layer number. The velocity profile of EOF should be “parabola-like” shape in smaller nanochannels with overlapped EDL instead

of the “plunger-like” shape in large channels. The maximum EOF velocity could be reduced and only occurs in the center region of the smaller nanochannel. Therefore, the average velocity decreases accordingly as the channel size becomes smaller due to the coated multiple layers. The similar decreasing trend of EOF with layer numbers can be seen for the cases that the outmost coated layer is a PB layer.

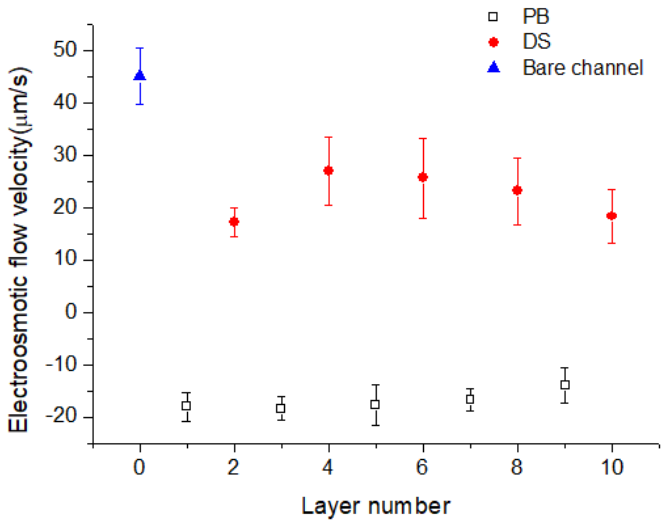

Figure 5-10. EOF velocity of 1×10^{-3} M KCl solution at various layer numbers (The applied electric field intensity is 50 V/cm).

5.4 Conclusions

This chapter studies LBL deposition of the charged polyelectrolytes PB and DS in small h-PDMS nanochannels. The influences of layer number, ionic concentration, and ion types on the growth and the thickness of the polyelectrolyte layer in nanochannel are investigated experimentally. EOF velocity of KCl solution is measured in the modified nanochannels with various deposition cycles of polyelectrolytes by using the current-slope method. Preliminary experiments of the polyelectrolyte adsorption on flat surfaces are also conducted and indicate that the increment of the layer thickness is linearly proportional to the layer number. In comparison with the growth of PB and DS layer on flat surfaces, the increments of the thickness per layer in nanochannels are inhibited and smaller than that on flat surfaces. The decrement of nanochannel size per deposition cycle of polyelectrolyte becomes smaller, and the nanochannel size approaches a saturation value with the increasing deposition layer number. In addition to the previous studies of LBL deposition in nanochannels[172,180,181], this

chapter systematically investigates the ion type effects and ionic concentration effects on the growth of the PB-DS layers and minimum nanochannel size with LBL deposition. At low layer number, both salt concentration and ion types could affect the average thickness of the coated layer in nanochannels. Conversely, the saturation value of the nanochannel size strongly depends on the salt concentration in the polyelectrolyte solutions whereas no significant dependence on the salt types. The LBL deposition could alternatively reverse the EOF velocity in nanochannels. In the meantime, the EOF velocity will gradually decrease in the small nanochannel as the deposition layer number increases due to the overlapped EDL. The experimental results presented in this chapter are valuable for nanochannel template fabrication and particularly important in investigating theories of electrokinetic and developing applications involving the requirements of suitable channel size. In the future, small nanochannels with heterogeneous surface charges will be fabricated. Based on this technique, functionalized nanochannels could be developed by precisely manipulating the surface charge and the nanochannel size.

Chapter 6 Fabrication Method: Surface Charged Governed Nanofluidic Diodes based on Single Nanochannels[§]

6.1 Introduction

It is well known that surface charges regulate electrokinetic effects[16,45,54,182,183] and induce electrostatic ion screen[184]. Surface charge-governed ion transport has gained widespread attention, and intense efforts on developing functional nanofluidic devices based on electrokinetic regulation have been taken in recent years[125,185,186]. These nanofluidic devices open up new possibilities in the development of ionic electronics and have demonstrated significant applications in logic computing[3,187], biological analysis[188,189], and sensing[5,190]. Example includes nanofluidic diode, transistors, and ionic pump. The two critical factors in constructing these nanofluidic devices are the geometry and surface charge distribution of nanochannels. Asymmetric geometry of nanopores can be used to control the ion transport that can mimic biological ion channels[74,168]. Heterogeneous surface charge distribution along the length of a nanochannel results in ion enhancement and depletion[191], thus rectifying ionic current.

Membrane-based nanopores with asymmetric geometries are commonly used in the development of nanofluidic diode-like devices. A nanopore with a conical structure and uniform surface charge can control the ion flow and rectify ionic current through the nanopore[192]. Functional polymers are often used to decorate the surface properties of the nanochannel, hence generating more effective ion gating. Vlassiouk et al. demonstrated a nanofluidic diode based on an asymmetric nanopore[193]. The surface charge on the sharp end of the nanopore was regulated to be positive and on the rest channel surface is negative. Their results showed that the degree of rectification is increased significantly after the surface charge regulation. Hou et al. presented that a nanochannel with asymmetric structure and surface charges can harvest controllable rectification behavior by ion-sputtering method[194]. Hsu et al. studied the performance of a nanofluidic diode with conical nanochannels and showed that the surface charge pattern can affect the current rectification behavior significantly. It is also reported that the ionic rectification in conical-shaped nanofluidic diodes depends on the pH, salt valence, temperature, and ionic concentration of the electrolytes solution[195–197]. Recently, a study showed that asymmetric

[§] A similar version of this chapter was submitted or published as:
J. Li, D. Li, A surface charge governed nanofluidic diode based on a single polydimethylsiloxane (PDMS) nanochannel, J. Colloid Interface Sci. 596 (2021) 54–63. https://doi.org/10.1016/j.jcis.2021.03.126.

double-gated nanochannel can also obtain fine ion rectification behavior by adjusting its surface properties[198]. Numerous kinds of tunable ion channels have also been developed by modifying the nanopores with stimuli-responsive polymer[199–201]. These ion channels have switchable conformational states by responding to specific stimuli that play an important role in cellular circuits. However, the thickness of membranes is generally small, thus resulting in low aspect ratios. As a result, it is difficult to generate opposite surface charges on the two ends of the nanopore during the wet modification due to the crosstalk of modification solutions. The short membrane-based nanochannels also contribute less effective charge modification, hence the corresponding rectification ratio is usually limited, which is a critical factor for certain applications. Carbon nanotubes (CNT) are promising candidates for the development of nanofluidic diodes due to their controllable inner diameters and high aspect ratios of silicon nanopores[202,203]. Recent studies have demonstrated some examples of CNT-based electronic channels. CNT-based transistors and high-speed logic integrated circuit have been developed for practical uses[204,205]. Cao et al.[206] presented a transistor scaled to 40 nanometers on high-density arrays of nanotubes which allow delivering high ionic current than silicon devices. Peng et al.[202] designed nanofluidic diode and circuits by horizontally aligned CNTs on PDMS chips. These CNT-based electronic devices display good performance due to the atomic inner diameter of CNT. Also, the long channel length of CNT is beneficial for the integration of Chip scale circuits. However, it is still challenging to pattern single CNT in chip-scale circuits. Multiple aligned CNT bundles result in uncertain ionic conductivities in the ionic diode that leads to low repeatability. This also generates new challenges to precisely control the performance of ionic diodes in integrated nanofluidic based electronic systems.

PDMS is one of the most popular materials in the fabrication of micrometer and sub-micrometer fluidic chips due to its advantages of mechanical flexibility and stability, transparency, biological compatibility, and gas permeability. Nanoimprint lithography method[207] and solvent-induced crack method[50] can fabricate PDMS nanochannels with dimensions less than 50 nm. However, such dimensions are not sufficiently small to build high-performance ionic diode. Our previous work demonstrated that the PDMS nanochannel size can be controlled by layer-by-layer deposition of charged polyelectrolytes[208]. The minimum nanochannel size can be reduced to smaller than 20nm, and the surface charge of the modified nanochannel is alternatively switchable, which is determined by the outmost coated layer. This modified nanochannel provides possibilities to fabricated PDMS-based ionic diode.

In summary, various nanofluidic diodes have been developed recently. Most of these nanofluidic diodes are fabricated by using membraned-based nanopores with asymmetric structure[192,193,209–212]. The rectification ratios of these nanofluidic diodes are generally limited. Composite membranes with modified nanopores were reported to develop nanofluidic diodes and achieve high rectification ratios recently[213,214]. However, the complex fabrication and structure of these nanofluidic diodes restrict their further integration in chip-scale circuits. It is still challenging to develop a nanofluidic diode with simple fabrication and high rectification ratio. Therefore, this chapter presents a novel nanofluidic diode with single PDMS nanochannels serving as ion channels is designed and fabricated. The replicated nanochannel chips are initially treated by using LBL deposition of polyelectrolytes to generate sufficiently small feature sizes. Then, the two ends of the channel are decorated with oppositely charged polyelectrolytes. The rectification of ionic current is achieved by surface charge-governed ion transport through the single PDMS nanochannels. The design and operation parameters of the nanofluidic diode are systematically investigated, and the electrical performance are evaluated. The studies of the performance of the nanofluidic diode provides necessary information to understand the electrostatic and electrokinetic interactions at the interfaces between salt solutions and polyelectrolytes modified channel walls. The advantages of PDMS chips provide high potentials of this ionic diode for constructing highly integrated nanofluidic electronic systems.

6.2 Materials and methods

6.2.1 Chemicals

In this experiment, all nanofluidic chips are fabricated by using regular PDMS (Sylgard 184, Dow Corning) and hard PDMS (h-PDMS)[139]. The regular PDMS consists of pre-polymer (base) and the cross linker (curing agent), and the mixing ratio of the base to curing agent is 10 in this work. The reagents employed in this study include polybrene (PB, Sigma-Aldrich), Dextran sulfate (DS, sodium salt, molecular weight, 7000 – 20000, Sigma-Aldrich), and KCl (≥99%, Fisher Scientific). Deionized water (18.2 MΩ · cm, Mini Q, Direct-Q3) was used to prepare all the solutions. The polyelectrolytes of PB and DS used in this study are cationic and anionic, respectively. 5% PB solution and 3% DS solution were prepared to modify the nanochannels with deionized water according to the method reported by Liu et al.[113]

6.2.2 Fabrication of nanofluidic chips for nanofluidic diodes

In this experiment, as shown in Figure 6-1 (b), the nanofluidic chip consists of a single PDMS nanochannel which serves as the ion channel and is connected by two microchannels. The nanochannel chips used in this work are replicated from a photoresist mode which is fabricated by using solvent-induced cracking method[50]. To precisely replicated the features and avoid deformations of the nanochannel, a bilayer of regular PDMS and h-PDMS are utilized to fabricate the nanochannel chips. Briefly, a h-PDMS layer is cast onto the nanochannel mode to replicate the features of the nanochannel firstly. After a heat process in an oven at 80 ^{o}C for 10 minutes and the h-PDMS is solidified, the regular PDMS is then cast on the h-PDMS layer to generate a relatively soft layer and support the fragile h-PDMS. Finally, the chip is placed back to the oven at the same temperature for 2 hours before ready to use. Figure 6-1 (c) and (d) show the AFM (Multimode™SPM, Digital Instruments) image and the height profile of a single nanochannel chip.

To connect the nanochannel to the testing system and easily deliver electrolyte solutions, this nanochannel chip is bonded with a microchannel chip by plasma treatment (Harrick plasma, PDC-32G), as shown in Figure 6-1 (a). This microchannel chip is replicated from a SU8 photoresist model, which is fabricated by patterning photoresist on a silica wafer with standard photolithography method. To keep the consistency of the surface properties of the bonded nanofluidic chip, the microchannel chip is also produced by using a bilayer of regular PDMS and h-PDMS with the same fabrication processes. Figure 6-1 (a) shows the schematic diagram of the chip bonding process.

6.2.3 Surface modification of ion channel for nanofluidic diode

Our previous study reported that the PDMS nanochannel size can be fine-tuned by LBL deposition of charged polyelectrolytes[208]. The modified nanochannel size is determined by the number of the coated layers of polyelectrolytes of PB and DS. For the nanochannel used in this work, the smallest feature size of nanochannels can be reduced from the original size to approximately 25 nm when the coated layer number is 14. As the coated layer number further increasing, the nanochannel size will not decrease anymore. This is because the steric effects and strong electric repulsion force prohibit the charged polyelectrolyte chains to enter the nanochannel when the coated multiple layers are sufficiently thick. This indicates that a minimum size exists when regulate the PDMS nanochannel size by using LBL deposition method. According to this phenomenon, a nanochannel with opposite surface charges at the two ends is designed and fabricated in this work. Since the polyelectrolytes are not allowed to

enter the nanochannel anymore after reaching the minimum size by the LBL deposition, and the nanochannel lengths are relatively long in this work, asymmetric surface charges can be generated by adding oppositely charged polyelectrolyte solutions at the two ends, respectively, without the crosstalk of modification fluids. The modification can be achieved by two steps of polyelectrolyte adsorption.

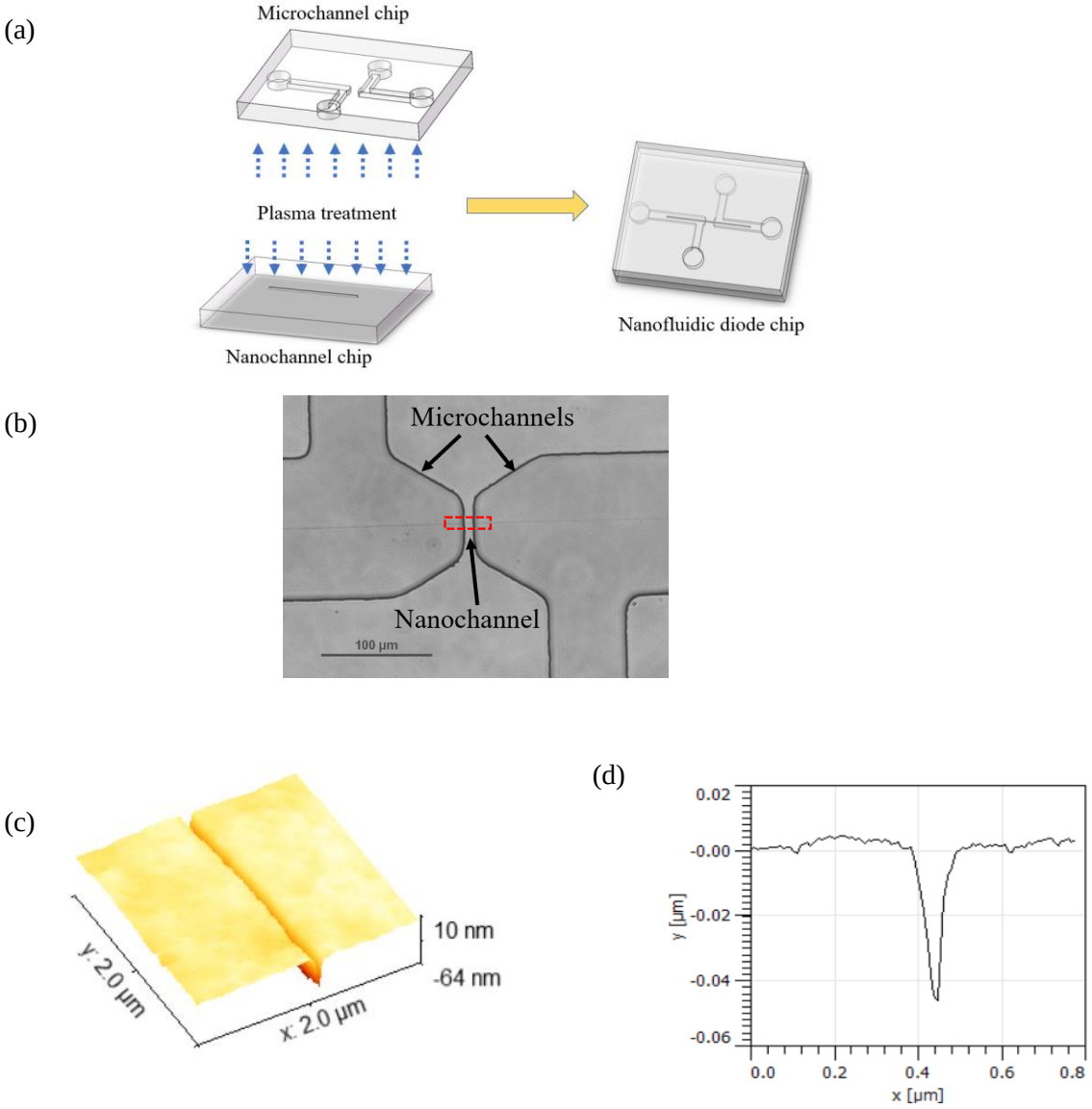

Figure 6-1. (a) A schematic diagram of a nanofluidic chip bonding process. (b) An image of the nanofluidic chip captured by an optical microscope. (c) 3D AFM image and (d) profile of a nanochannel with a depth of 54 ± 1 nm and a width of 117 ± 9 nm.

Figure 6-2 schematically shows the modification processes. In Step I, the nanochannel is pre-coated with multiple PB/DS layers until the nanochannel reaches the minimum size[208]. Briefly, the nanofluidic chip is rinsed with 0.1 M NaOH solution for 30 min to pretreat the surfaces and prepare for the further adsorption of polyelectrolyte layers. Then, 5% PB solution and 3% DS solution are used to rinse the chip alternatively according to the LBL self-assembly method. Between each rinse of polyelectrolyte solutions, three times of rinse with pure water are employed to remove the residuals. Once the nanochannel reaches the minimum size, the second step of polyelectrolyte adsorption is applied to generate asymmetric surface charges labeled at the two ends of the nanochannel. In the experiment, 5% PB solution and 3% DS solution are filled into the two sides of the nanochannel, respectively. As a result, the entrance and the outlet of the nanochannel will adsorb different polyelectrolyte chains, thus generating opposite surface charges at the two ends of the nanochannel.

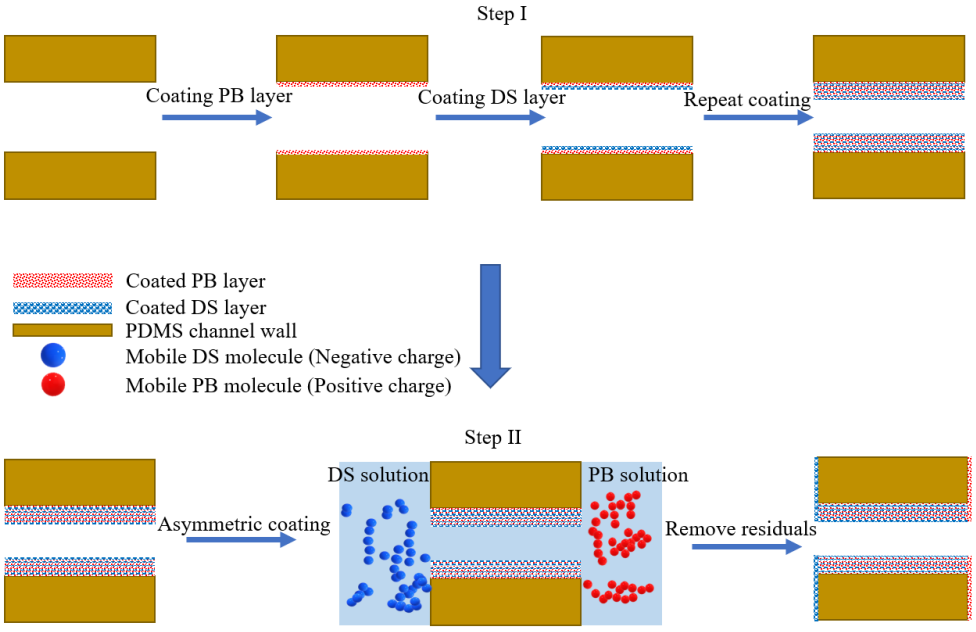

Figure 6-2. Schematic diagrams of the surface modification process of the nanofluidic diode.

6.2.4 Experimental measurement system

Figure 6-3 illustrates the ionic current measurement system used in the experiment. The nanofluidic diode chip is connected to an electrometer (Keithley, Model 6517A), which is used to collect the ionic current from the fluidic diode. This electrometer also serves as a programmable DC power supplying electric potential bias through two Platinum electrodes and driving the mobile ions

inside the nanochannel. The collected ionic current signal is then transferred to a computer via LabVIEW program (National Instrument Corp.) The electrolyte solutions of KCl with a series of ionic concentrations are employed as the working fluids in the ionic current measurement. All the experimental measurements are conducted at the room temperature of around 23 °C and repeated at least three times in three individual chips.

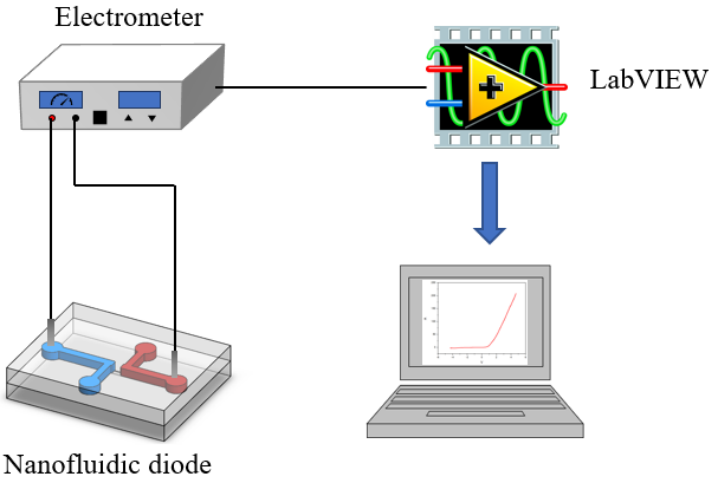

Figure 6-3. Schematic of the configuration of the electric measurement system.

6.3 Results and discussion

6.3.1 Working principle of the nanofluidic diode

Similar to semiconductor diodes, the current rectification in ionic diodes is achieved by the ion accumulation and depletion generated by asymmetric surface charges. In this nanofluidic diode, the cation of K^+ and anion of Cl^- serve as charge carriers. As illustrated in Figure 6-2, the modified nanochannel is able to immobilize oppositely charged polyelectrolyte chains on the two ends of the nanochannel via physical adsorption. When a forward or a reverse electric field is applied through the diode chip, the mobile ions will accumulate or deplete due to the electrostatic interactions between the mobile ions and immobilized polyelectrolyte chains at the two ends of the nanochannel.

As schematically shown in Figure 6-4 (a), the counterions are accumulated at the two ends of the nanochannel and generate ion depletion inside the nanochannel under a reverse electric field. As a result, the ion flow is prohibited, and the overall electric conductivity is reduced. On the contrary, the counterions approach each other and accumulate inside the nanochannel under a forward electric field,

as shown in Figure 6-4 (b). As a result, the mobile ions can transport through the nanochannel, and a continuous ionic current can be maintained.

To characterize the surface modification of the nanochannel, a negatively charged dye (FITC) was introduced into the nanochannel. The dye solution with a constant bulk concentration of 100 μM was diluted into 1×10^{-3} M KCl solution. The chosen dye solution provides mobile anions, and the fluorescence is observed from the anions which are supplied by the dye solution. Hence, the observed fluorescence intensity of the solution can represent the amount of anion in the nanochannel. The fluorescence intensity is proportional to the amount of anion. For example, a high fluorescence intensity indicates more anions exist in the observed area whereas a low fluorescence intensity indicates the depletion of the anion in the area. As discussed above, the accumulation or depletion of ions occurs under forward or reverse electric field due to the field-effect modulation of charge carrier density in the nanofluidic diode[186]. In the experiment, the nanofluidic chips are initially filled with KCl solution containing fluorescent dye. After the solution is loaded, as schematically shown in Figure 6-3, an electric field of 2 V/cm is applied at the two end reservoirs of the microchannels to drive the mobile ions in the chip by using an electrometer. The fluorescent intensity can be observed via a fluorescent microscope (Eclipse TE 2000, Nikon). As shown in Figure 6-4 (c), the fluorescent intensity is higher at the DS coated end (negatively charged) while is much lower at the PB coated end (positively charged) of the nanochannel. That is, the anions and cations get accumulated at the two ends of the nanochannel, respectively. As a result, the ion channel is blocked by the accumulated cations and anions, and only a very low leakage current exists under the reverse electric field. When a forward electric field is applied, cations and anions are driven to approach the nanochannel. Since the immobile surface charges on the two ends of the nanochannel only allow counter-ions to enter the nanochannel, cations and anions can enter the nanochannel from the entrance and outlet, respectively, due to the driving force of electric field. As shown in Figure 6-4 (d), both cations and anions can transport through the nanochannel under a forward electric field. Most ions are accumulated inside the nanochannel. As a result, a continuous ionic current can be maintained due to the ion transport. The fluorescence from the nanochannel is not obvious due to the extremely low volume of the fluorescent dye inside the small nanochannel. These phenomena, which are in good agreement with the theoretical model described above, result in the ionic diode behavior.

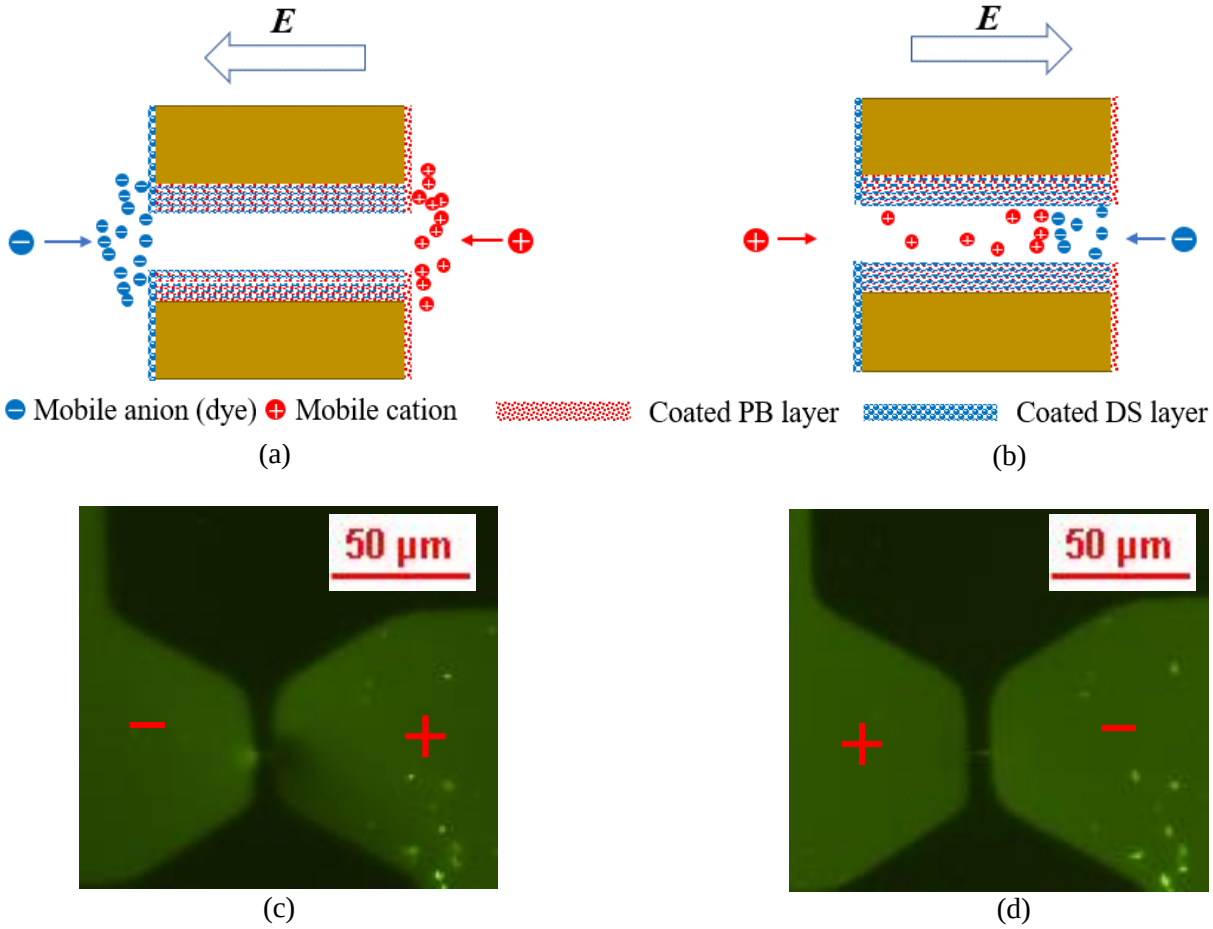

Figure 6-4. Schematic of ion depletion under a reverse electric filed (a) and ion accumulation under a forward electric field (b). Images of fluorescent intensity gradient of a negatively charged dye (FITC) solution in the nanofluidic diode under a reverse electric field (c) and a forward electric field (d), which are captured by an optical microscope.

To validate the design and evaluate the performance of the nanofluidic diode based on a single PDMS nanochannel, the experimental investigation of the ionic current rectification in the nanofluidic diodes is conducted. In the experiment, as shown in Figure 6-5, a trace sweep voltage which increases from −4.5 V to 4.5 V and a retrace sweep voltage which decreases from 4.5 V to −4.5V were applied to the nanofluidic diode, respectively. The sweep speed of the applied voltages is 300 mV/s. The ionic current changes corresponding to the applied voltage sweeps are demonstrated in Figure 6-5. The nanochannel length is 5 μm, and the working fluid is the KCl solution with a bulk ionic concentration of 1×10^{-4} M. As shown in the figure, the measured results demonstrate excellent diode behavior.

The ionic current is almost zero under a reverse potential bias whereas a continuous ionic current is obtained when a forward potential bias is applied. To be noted that the trace curve and retrace curves do not follow the same path. Compared to the retrace curve, a delay in the diode status change can be observed in the trace curve when the applied voltage changes from negative to positive. That is, a response time is required to change the nanofluidic diode from "off" status to "on" status. This is caused by the slow response of the ionic charges in aqueous solutions to the drive field due to the ion polarization and viscosity of fluids. As shown in Figure 6-4 (c), cation and anion are accumulated at two ends of the nanochannel, respectively, thus generating the ionic current blocking. When the applied voltage is transferred from negative to positive, it takes a certain time to remove the accumulated ion by the electric field and fluid flow.

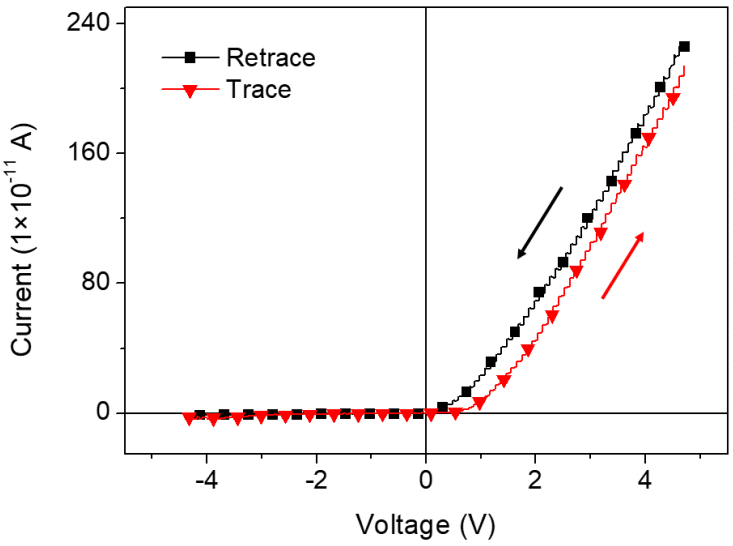

Figure 6-5. An example of current-voltage curves measured from nanofluidic diode with trace and retrace voltage sweep, respectively.

6.3.2 Effects of frequency of the applied electric field

To design an effective nanofluidic diode, the effects of the operation parameters on the diode performance are studied quantitatively in this chapter. The results show that the sweep speed of the applied voltage, that is the voltage frequency, is important in the nanofluidic diode operation. Previous study also reported that ionic diodes can only work effectively at a relatively low voltage frequency[215]. In this experiment, the response of the nanofluidic diode to the voltage frequency is experimentally examined by controlling the sweep speed of the applied voltage. In this study, the ionic

current rectification ratio is defined as the ratio of the absolute value of ionic current at the given forward voltage to reverse voltage, which can be expressed as $f_{rec} = \left|\frac{I_{@+V}}{I_{@-V}}\right|$. This rectification ratio is used to evaluate the performance of the nanofluidic diode working at different frequencies. Figure 6-6 (a) demonstrates I-V curves measured from the nanofluidic diode with a nanochannel length of 5 μm at different sweep speeds and Figure 6-6 (b) shows the corresponding rectification ratios at the applied voltage of $\pm 4\,V$. The KCl solution with a bulk concentration of 1×10^{-4} M is used as the working fluid. From Figure 6-6 (a), one can see that the nanofluidic diode can provide diode function while operating in a range of sweep speed from 130 mV/s to 400 mV/s. However, the higher sweep speed contributes to a larger delay in the electric potential to activate the nanofluidic diode from "off" status to "on" status. Moreover, as shown in Figure 6-6 (b), the rectification ratio gradually decreases from 124 ± 2.5 to 112 ± 2.3 with the sweep speed rise from 130 mV/s to 300 mV/s. By further increasing the sweep speed, the rectification ratio rapidly falls to 90 ± 6.6 as the sweep speed increases from 300 mV/s to 400 mV/s. This decrease in the rectification ratio is also caused by the slow response of the mobile ion in the aqueous solutions. These results indicate that the nanofluidic diode is more effective and suitable to operate at a low sweep speed of the applied voltage.

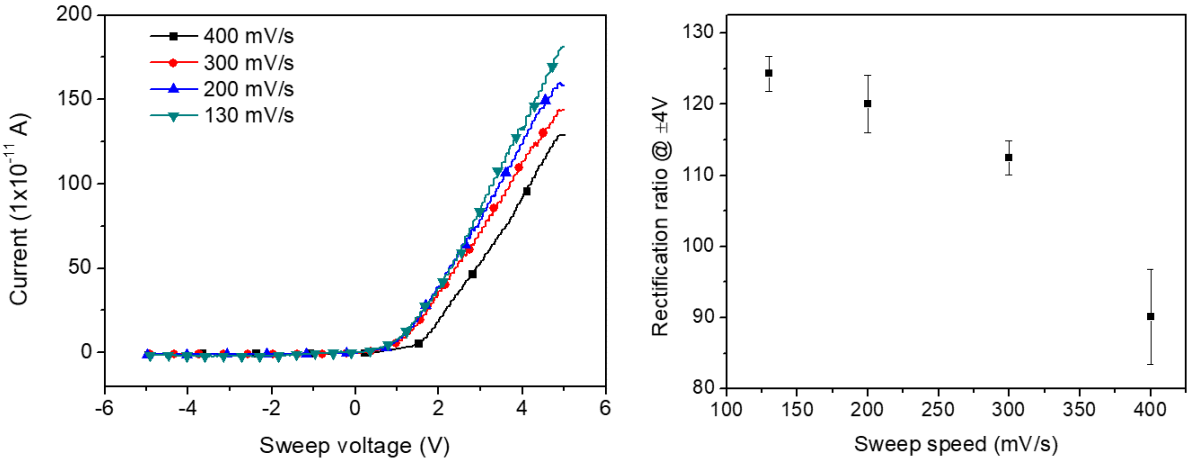

(a) (b)

Figure 6-6. (a) The measured current-voltage curves from nanofluidic diodes at different sweep speeds of applied voltage and (b) the corresponding rectification ratios under the applied voltage of $\pm 4\,V$.

6.3.3 Effects of the ionic concentration

In order to operate properly, the nanofluidic diode always requires a working fluid to provide charge carriers inside the nanochannel. The ionic concentration of the working fluid determines the amount of mobile ion and ionic conductivity of the ion channel. Moreover, the thickness of electrical double layer (EDL), which dominates the electrostatic interactions between the mobile ions and the charged surface of the nanochannel, depends on the ionic concentration[132]. It is expected that ionic concentration can significantly affect the performance of nanofluidic diodes. To study the effects of ionic concentrations of the working fluid on the diode operation, in this part of the experimental investigation, KCl solutions with the bulk concentrations of 1×10^{-4} M to 0.1 M were used in the nanofluidic diode from low to high ionic concentration sequentially, and the ionic current changes are then measured. The nanochannel length is 5 μm, and the sweep speed of the applied voltage is 300 mV/s. Figure 6-7 illustrates the I-V curves and corresponding rectification ratio under $\pm 4\ V$ of the nanofluidic diode at different KCl concentrations. In nanofluidic diode devices, charge carriers supplied by the electrolyte solution are required to generate ionic current. As shown in Figure 6-7, the ionic current increases with the ionic concentration of KCl solutions under forward bias electric potentials because more charge carriers (mobile ions) are provided. However, the rectification ratio increases initially when the KCl concentration decreases from 0.1 M to 1×10^{-3} M. As the KCl concentration further decreases, an inversion in the change of the rectification ratio can be observed that the rectification ratio starts to decrease. The maximum rectification ratio , which is the best rectification ratio of this nanofluidic diode, occurs at the concentration of 1×10^{-3} M, which is 218 ± 17.7. As the KCl concentration increases to 0.1 M, the nanofluidic diode almost lost the function of current rectification, and the rectification ratio reduce to 2.8 ± 0.3. These results display that the nanofluidic diode can be operated in a large range of applied voltage, and the rectification ratio is very high compared with those of common membrane-based nanofluidic diodes those are usually smaller than 100 [210,212,216–218]. As shown in Table 1, only a few of nanofluidic diodes can harvest a rectification ratio over 200[213,214]. However, these nanofluidic diodes owned such high rectification ratios are fabricated by using composite membranes. Their structures and fabrication methods are generally very complex and restrict further integration. Moreover, the nanochannel size of the nanofluidic diode reported in this chapter can be further reduced by modifying the nanochannel with salt-addition polyelectrolyte solutions instead of salt-free polyelectrolyte solutions as reported in our previous study[208]. As a result, it is possible to enhance rectification ratio of this nanofluidic diode.

Table 6-1. A comparison of recent reported nanofluidic diodes.

Structure	Surface charge	Materials	Rectification ratio over 200	Fabrication
Asymmetric	Homogeneous [192,209–212]	Porous membrane/track-etched nanopore	No	Simple
	Heterogeneous [185,193,200,213,214,219–222]	Composite membranes	No except Ref. 213 and 214	Complex
Symmetric	Heterogeneous[4,202]	Modified CNT/nanochannel	No	Relatively complex

The ionic concentration effects on the rectification ratio can be explained by EDL theory[132]. Theoretically, the thickness of EDL is 3-5 times of the Debye length (λ_d), which can be simply expressed as $\lambda_D = \frac{0.304}{\sqrt{M}}\ (nm)$ for KCl solution. Here M is the ionic concentration of KCl solution expressed in molar. At a high ionic concentration, 0.1 M, the calculated Debye length is approximately 1 nm, and the thickness of electric double layer is significantly small compared with the nanochannel size. The immobilized surface charges on the two ends of the nanochannel are screened. As a result, the electrostatic gating of mobile ions is less prominent, thus generating a large reverse ionic current and a low rectification ratio. When the KCl concentration decreases to 1×10^{-3} M, the calculated Debye length is approximately 10 nm which is comparable to the nanochannel size. The Debye lengths on the nanochannel surfaces essentially occupy the whole nanochannel. Therefore, a strong electrostatic gating of mobile ions can be formed. The immobile charges modified on the two ends of the nanochannel can effectively repel co-ions with a reverse electric field, thus generating a very low ionic current. When a forward electric field is applied, the transport of counter-ions is promoted, and ion accumulation is formed in the nanochannel. As a result, the ion exchange is accelerated, and large ionic current is obtained with a forward electric field. Hence, the rectification ratio increases. The previous study of nanofluidic diode with conical-shaped nanochannels was also showed similar results[193]. It was reported that the rectification ratio decreases by 2 orders of the magnitude with an increasing ionic concentration. However, as the KCl concentration further decreases, the rectification ratio stops increasing in the experiments. This is because the mobile ions have been fully gated when the KCl concentration is 1×10^{-3} M. When the KCl concentration further decreases to 1×10^{-4} M, the reverse current will not further decrease anymore which is almost zero. However, the forward current

becomes smaller due to fewer mobile ions are released by the KCl solution with a low ionic concentration. Consequently, the rectification ratio decreases at extremely low ionic concentrations.

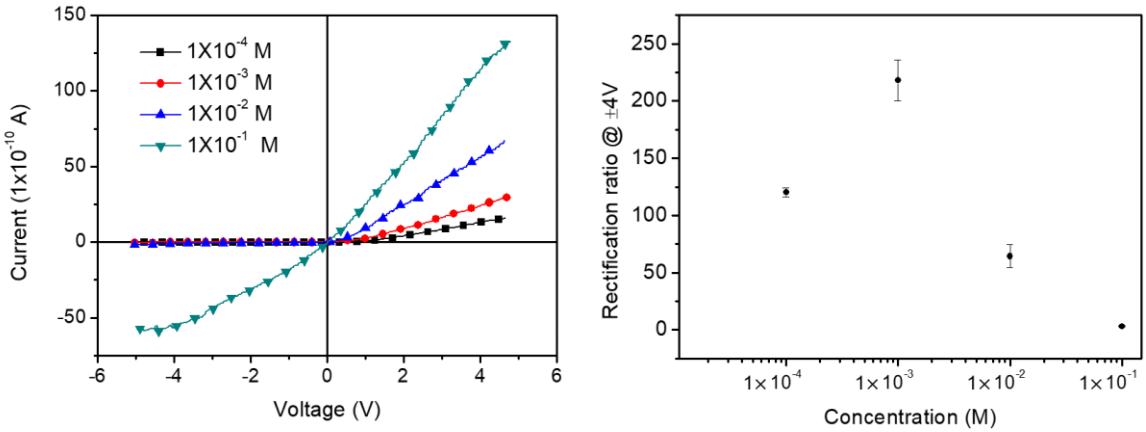

(a) (b)

Figure 6-7. (a) The measured current-voltage curves from nanofluidic diodes and (b) corresponding rectification ratios at different KCl concentrations.

6.3.4 Effects of nanochannel length

The nanochannel length can affect the effective electric field strength which is related to the ion distribution inside the nanofluidic diode. In addition, previous research reported that the shorter nanochannel length can improve the efficiency and expand the working frequency range of the nanofluidic diode[223]. As a result, the nanochannel length is a crucial factor in determining the performance of the nanofluidic diode. In this chapter, nanofluidic diodes with the nanochannel length ranging from 5 μm to 50 μm were designed and fabricated. To evaluate the nanochannel length effects on the performance of nanofluidic diodes, the ionic rectification ratios are measured from nanofluidic diodes, under a constant voltage difference, with different nanochannel lengths and ionic concentrations.

Figure 6-8 illustrates the current rectification ratios for nanofluidic diodes with various nanochannel lengths and KCl concentrations, under the applied voltage of 4 V. As one can see from the figure, the nanochannel length can significantly affect the rectification ratio of the nanofluidic diode. At the ionic concentration of 1×10^{-3} M, the rectification ratio is sharply reduced from 218 ± 17.7 to 93 ± 7.8 as the nanochannel length increases from 5 μm to 10 μm. By further increasing the

nanochannel length, the rectification ratio decreases gradually. When the nanochannel length reaches 55 μm, the nanofluidic diode becomes much less effective, and the rectification ratio is only 12 ± 2.6 at the KCl solution of 1×10^{-3} M. It can be observed that the rectification ratios for all nanofluidic diodes examined in this experiment follow a similar trend with KCl concentration, and the maximum rectification ratio occurs at the concentration of 1×10^{-3} M. However, by comparing the trend of rectification ratio with different channel lengths, the effects of ionic concentration on the diode performance become less prominent. For instance, the rectification ratio triples in the nanochannel of 5 μm whereas it only increases by 1.5 times in nanochannel of 55 μm while the KCl concentration decreases from 1×10^{-2} M to 1×10^{-3} M. These phenomena are caused by the lower effective electric field strength in nanofluidic diode with a long nanochannel. Typically, as shown in Figure 6-4 (c), the charged polyelectrolytes absorbed at the two ends of the nanochannel could repel co-ions effectively under a reverse electric field. These ions are accumulated at the entrance and the outlet of the ion channel due to the driven force of the electric field and the strong electrostatic repulsion force between the mobile ions and immobile charges decorated on the two ends of the nanochannel. As a result, only a few of ion leakage exists and a very low ionic current can be generated. However, it was reported that the degree of the ion enrichment depends on the electric field strength[191]. When a constant electric potential is applied, the effective electric field strength is larger in the nanofluidic diode with a shorter nanochannel. Hence, a higher degree of ion enrichment can be obtained, thus reducing the ion leakage. Furthermore, the weaker effective electric field contributes to a smaller ionic current in a forward biased nanofluidic diode. Therefore, the rectification ratio decreases.

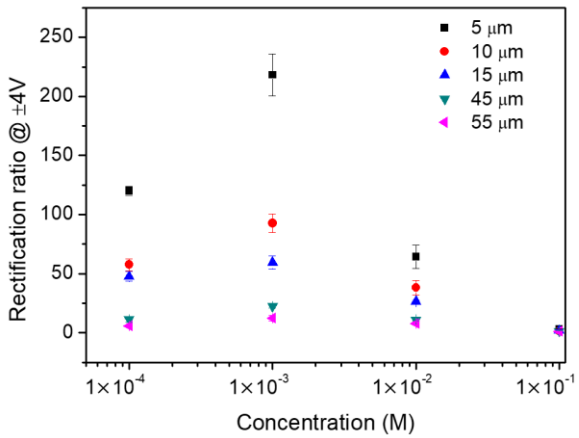

Figure 6-8. The dependence of rectification ratio at the applied voltage of ±4 V measured from nanofluidic diodes on the channel lengths and KCl concentrations (Sweep speed: 300 mV/s).

6.3.5 Effects of electric field strength

The electric field strength affects the movement of the mobile ions and the degree of the ion enrichment, thus influencing the rectification ratio. To examine the effects of electric field on the performance of the nanofluidic diode, the rectification ratios under different applied electric field strengths are measured. Since the best rectification ratio is observed at the ionic concentration of 1×10^{-3} M, in this experiment, the KCl solution of 1×10^{-3} M is used as the working fluid and the nanochannel length is $5\,\mu m$. The total length of the main microchannels is 2 cm. Theoretically, the ionic current is essentially zero under a reverse electric field and proportional to the applied electric field strength under a forward electric field. As a result, the rectification ratio should increase with an increasing electric field strength. As shown in Figure 6-9, the rectification ratio almost linearly increases while the applied electric field increases from 0.1 V/cm to 1.25 V/cm. However, the increment of the rectification ratio becomes smaller with further increase of the applied electric field strength.

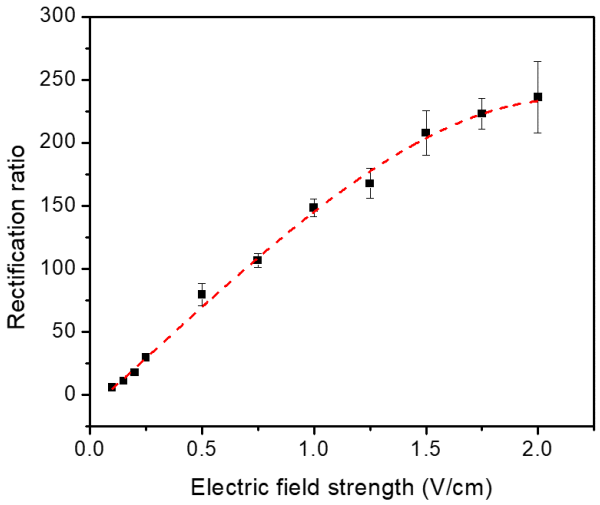

Figure 6-9. The dependence of the rectification ratio on the applied electric field strength measured from a nanofluidic diode with a 5 μm nanochannel.

The weaker growth of rectification ratio at the high electric field strength is caused by the breakdown effects and polarization effects[215]. When a strong electric field is applied, the Coulomb force may overwhelm the repulsion force generated by the immobile charges at the ends of the nanochannel and break the ion gating, thus generating a large leakage current under a reverse electric field. Besides, the high degree of ion enrichment at the entrance of the nanochannel can generate a thinner local EDL, resulting in less effective ion screening. In addition, previous studies also reported

that the increase of the forward ionic current in nanofluidic diodes can be weakened under an extremely strong electric field due to concentration polarization effects[202,215]. Consequently, the growth rate of the rectification ratio slows down at high electric field strength. The results indicate that it is possible to generate breakdown in the nanofluidic diode similar to that in a semiconductor diode.

6.4 Conclusions

Previously reported nanofluidic diode were commonly fabricated by using membrane-based nanopores[185,210,212,216–218]. The rectification ratios of these nanofluidic diodes are generally less than 100. A membrane-based nanofluidic diode with asymmetric structure and surface properties was reported harvesting distinctly high rectification ratios[224]. This nanofluidic diode comprises two types of nanochannels with different sizes and opposite surface charges. However, its inherent complex structure creates challenges in the integration of chip-scale electronic circuits. Aligned CNT bundles allow chip-scale integration, but generate relatively low rectification ratio and repeatability[202]. This chapter demonstrates a novel method to develop nanofluidic diodes based on single PDMS nanochannels. The operation parameters, including voltage frequency, working fluid concentration, and channel length, are systematically investigated by evaluating the ionic current rectification ratio. The nanofluidic diode chips used in this study were fabricated by standard photolithography method. The nanofluidic diodes possess excellent current rectification behaviors, and the rectification ratio can be as high as 218 with easily fabricated channel length and suitable ionic conditions. This rectification ratio decreases with an increasing sweeping frequency of the applied voltage, and the diode may lose effectiveness at extremely high voltage frequency. The results revealed that the nanochannel length is significant in the design of nanofluidic diodes. The rectification performance of nanofluidic diodes can be improved by shortening the nanochannel length. A higher electric field strength leads to a larger rectification ratio. However, an extremely strong electric field can degrade the ion transport or ion gating inside the nanofluidic diode, thus weakening the current rectification. This chapter presents a method to fabricate nanofluidic diode on typical PDMS-based chips. The best rectification of 218 can be obtained with a relatively low size requirement and simple modification process. The results about the performances of nanofluidic diodes provide better understandings of the interfacial electrostatic and electrokinetic interactions at the liquid-modified channel wall interfaces. Furthermore, the fabrication method of the nanofluidic diode based on layer-by-layer deposition of polyelectrolytes creates new possibilities to develop high-performance nanofluidic diode with relatively large ion channels for future researchers who are interested in nanofluidic electronics. In future work, we will focus on integrating

multiple PDMS-based nanofluidic diodes on a chip and develop nanofluidic electric circuits for practical uses.

Chapter 7 Application I: A Method to Improve RPS Detection based on Surface Charge Governed Ion Channel[**]

7.1 Introduction

Resistive pulse sensing (RPS) is a measurement technique capable of analysis of submicron bioparticles and particle-by-particle sizing and detection[225–228]. RPS method was developed for sensing and counting cells by Coulter in the 1950s[229]. Submicron particles and viruses were studied since 1970s[230,231]. In recent years, with the advancement of nanofabrication technologies, RPS method has been widely used in detecting and analyzing nanoscale particles as small as single molecules, such as proteins[225,232] and DNAs[190,233,234]. Particularly, intensive studies of nanopore-based DNA sequencing[235–237] and nuclei acid analysis[234,238] in biological nanopores have been conducted by using RPS method.

In a typical RPS system, a single micrometer- or nanometer-sized pore or channel separating two reservoirs is filled with an electrolyte solution as the sensing gate. An electric potential applied across the sensing gate can drive a steady ionic current passing through the gate. When a particle enters the sensing gate, the ionic current is disrupted, and a pulse signal can be observed. To improve the sensitivity of RPS systems, a lot of methods have been developed. Wu et al.[239] demonstrated that the noises can be reduced significantly in a microfluidic RPS chip with a design of two symmetric mirror detection channels positioned before and after the sensing gate, and by using differential amplification. Song et al.[240] further improved the signal-to-noise ratio by using two-stage differential amplification. Their results showed that particles as small as 220 nm can be detected by using a microfluidic chip. Zhou et al.[241] presented a new RPS sensor without requiring particles passing through the sensing gate. In their study, an orifice located on the side of the main channel is worked as the sensing gate to count particles, and the detected signal amplitude can be increased by turning the orifice size. Liu et al.[242] also presented a method to improve the detection sensitivity of a RPS system by fabricating focusing stream channels on the chip, thus narrowing the effective sensing gate.

[**] A similar version of this chapter was submitted or published as:
J. Li, D. Li, A method to improve the resistive pulse sensing by modifying surface charge of nanochannels, Sensors Actuators, B Chem. 337 (2021) 129773. https://doi.org/10.1016/j.snb.2021.129773

The detection sensitivity of a RPS system is mainly determined by the volume ratio of the particles to the sensing gate (or sensing channel). As the sensing gate, the nanochannel or nanopore is a key component in RPS systems and provides confined space to covert nanosized objects to measurable electric signals. The first solid-state nanopore has been successfully fabricated by using a technique of ion beam sculpting in 2001[243]. After that, nanopores have been fabricated by using multiple techniques over the past decades, such as focused ion beams[243], dielectric breakdown[244], and focused electron beams[245]. To develop high-performance nanopores or nanochannels with desired dimensions, many novel methods have been reported [246–249]. For example, elastic membranes have been used as a tool in RPS systems to form tunable nanopore. The advantage of this method is the adjustable pore size which is able to detect a range of particle sizes by sing a single tunable pore[250,251]. Biological nanopores are also promising tools in building nano-RPS systems, particularly in DNA sequencing, due to their advantages of good specificity and high throughput[252–254]. Carbon nanotube (CNT) provides a platform in the analysis of nanoparticles, signal molecules, and ions by using nano-RPS systems as well[190]. CNT-based nano-RPS devices are relatively easy to fabricate, and the inner diameters are controllable. With these advantages, studies about ion selection, DNA sequencing, and single molecule analysis have been reported[255–258].

Apart from the technologies for fabricating the sensing nanopores and nanochannels and the structure of RPS chips, there are alternative techniques that can improve the performances of the nanopores in RPS detection. For example, the nanopore dimensions can be fine-tuned by using atomic layer deposition[259]. Wei et al.[260] showed that nanopore surfaces can be metalized by deposition of a gold layer, resulting in lower electrical noise and reduced nanopore diameter. Ayub et al.[261] further studied the nanopore size control for diameters below 20 nm by using electrodeposition and demonstrated the capability of the modified nanopore in single biomolecule analysis.

In addition, many methods can be utilized to further improve the properties of nanopores and RPS systems, such as surface modification of nanopores and localize electrodes in and around nanopores. In nano-RPS systems, different from micro-RPS systems, the space occupied by the electrical double layer (EDL) cannot be ignored. When the sensing channel is sufficiently small and the EDL overlaps, the surface charge property of the nanochannel can govern the ion transport and determine the ionic conductance[262,263]. It is known that the detected electric signal is the change of the potential bias along the sensing nanochannel in a RPS system when a particle is passing through the sensing nanochannel. The surface charged governed ionic conductance is related to the potential bias along the

sensing channel and can affect the measured RPS signals significantly. Moreover, by modifying the inner surfaces of the sensing nanopores/nanochannels, the surface charge, wettability, and receptors can be manipulated. These surface effects can be employed to achieve and adjust the selective sensing of charged particles, ions, and DNAs[264–267]. Modifying chemical and electrical properties of the nanopore interior surfaces is particularly appealing in single molecule analysis since they allow the nanopore equipped with desired functions. However, there are significant challenges. Most of these reported studies focus on the fabrication of nanopores with small inner diameters and specific geometry to improve the resolution and sensitivity of RPS systems. These fabrication techniques often require novel materials and advanced equipment. Only a few of them studied the effects of chemical properties of nanopore interior surfaces in the RPS detections[248,265].

As discussed above, to improve the sensitivity of RPS systems, previous studies mainly focused on reducing the size of the sensing nanochannel. However, it is still challenging to fabricate a sensing nanochannel with a size smaller than 10 nm and a short length. This chapter demonstrates an approach to enhance the detected signals and the sensitivity of RPS devices by controlling the surface charge of the inner surface of the sensing nanochannel. The approach presented in this chapter aims to further increase the sensitivity of RPS systems and reduce the size requirement in nano-scale detection. In this work, the effects of the surface charges and the length of the sensing nanochannel were investigated theoretically. A nano-RPS device with the sensing nanochannel decorated with different surface charges was designed and fabricated. To analyze the surface charge effects on the RPS detection, detection of nanoparticles with a diameter of 5 nm was conducted experimentally. The results show that the detected RPS signal amplitudes can be improved significantly when the sensing nanochannel has opposite surface charges on the two ends.

7.2 Materials and method

7.2.1 Chemical reagents

Gold nanoparticles (Sigma-Aldrich) of 5 nm in diameter suspended in citrate buffer are used as sample nanoparticles in RPS measurements. In the experiment, all nanoparticle solutions are diluted in KCl (≥99%, Fisher Scientific) solutions by 1000 times. Polybrene (PB, Sigma-Aldrich), Dextran sulfate (DS, sodium salt, molecular weight, 7000 – 20000, Sigma-Aldrich) dissolved in deionized water (18.2 MΩ, Mini Q, Direct-Q3) are used to modify nanochannel surfaces. Regular PDMS (Sylgard 184, Dow Corning) and hard PDMS (h-PDMS) are used to fabricate the nanofluidic chips.

7.2.2 Experimental system and fabrication of nano-RPS chips

As shown in Figure 7-1 (a), the nano-RPS chip consists of a single sensing nanochannel connected by two microchannels. An electric voltage difference (as indicated by V+ and V− in the figure) is applied at the two ends of the microchannels to generate an electric current and drive the transport of particles in the chip. Two detecting microchannels are located on the two sides of the nanochannel and connected to a differential signal amplifier (AD 620) via two platinum electrodes. The change in the electric potential along the nanochannel will be collected by the detecting microchannels, amplified by the amplifier, and finally exported to a computer through LabView program.

The nanochannel used in the system is fabricated by using the solvent-induced method[50]. The nanochannel chip is replicated from a nanochannel mold by using a bilayer of regular PDMS and hard PDMS. Firstly, a thin h-PDMS layer is spin-coated on the nanochannel mold and following a heating in an oven at 80 ^{o}C for 10 min. This h-PDMS layer can precisely replicate the features of the nanochannel and minimize the deformation of the nanochannel. Afterward, regular PDMS is casted onto the h-PDMS layer and placed back to the oven for 2 hours at 80 ^{o}C. The relatively soft regular PDMS layer can support the fragile structure of the hard PDMS layer. The nanochannel chip can be easily peeled off from the mold after the heating process. Figure 7-1 (b) and (d) shows the AFM image and the profile of the nanochannel used in this work.

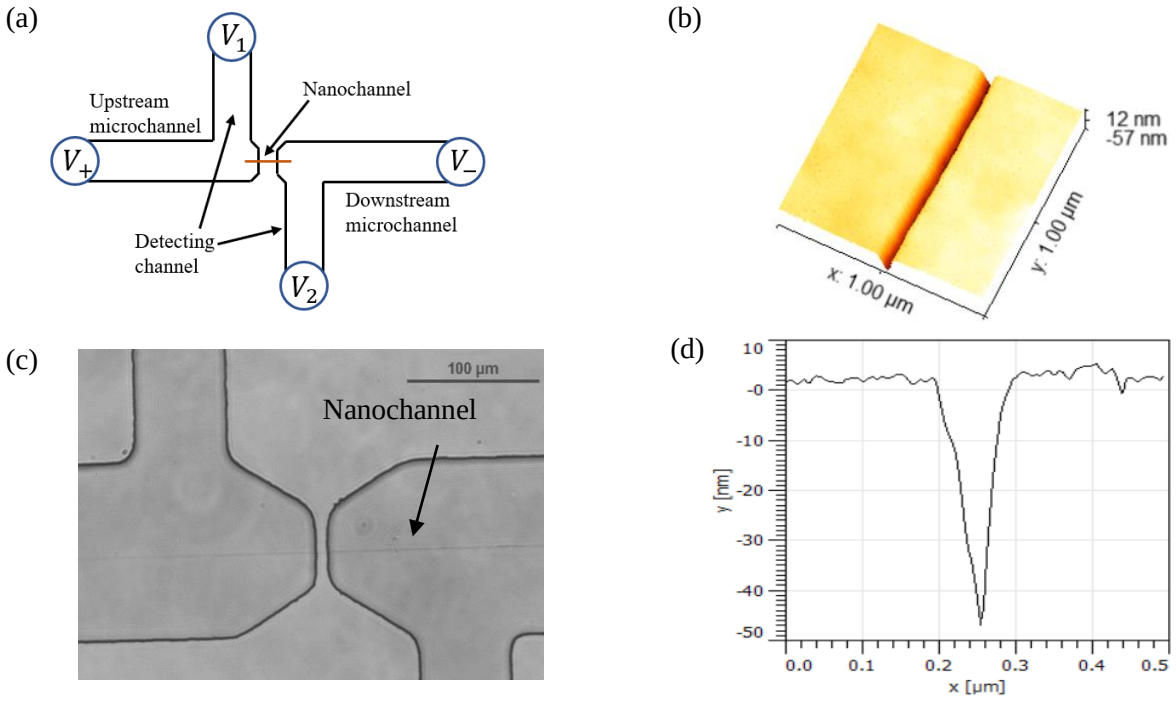

Figure 7-1. (a) A schematic diagram of nano-RPS system. (b) The AFM image and (c) An image of the nanofluidic chip captured by an optical microscope. (d) profile of a nanochannel with a depth of 54 ± 1 nm and a width of 117 ± 9 nm.

To form the final nanofluidic chips, as shown in Figure 7-1 (c), the nanochannel is bonded with a microchannel which is replicated from a SU8 photoresist mold by Plasma treatment (Harrick plasma, PDC-32G). The microchannel mold is fabricated on a silica wafer by using standard photolithography method. To keep the chemical properties of all chip interior surfaces are consistent, the microchannel is also fabricated by using a bilayer of hard-PDMS and regular PDMS.

7.2.3 Surface modification of sensing nanochannels

Our previous study has shown that the PDMS nanochannel size and surface charge can be controlled by using layer-by-layer (LBL) deposition of polyelectrolytes[208]. By modifying the nanochannel with charged polyelectrolytes, multiple polyelectrolyte layers can be coated on the channel interior surfaces. These coated polyelectrolyte layers will reduce the nanochannel size. When the coated multiple layers are sufficiently thick, the charged polyelectrolyte chains cannot enter the nanochannel anymore due to the steric effects and strong electric repulsion force. As a result, the nanochannel reaches a minimum size which is referred to as saturated size by using this LBL deposition method.

For the nanochannel used in this study, the nanochannel size will be reduced from the original nanochannel size to the saturated size by coating multiple PB/DS layers. The saturated nanochannel has a size of approximately 25 nm in the depth [208]. In this work, the nanochip interior surface charge is alternatively regulated by using 5% PB and 3% DS solutions according to the LBL self-assembly method. Briefly, the nanofluidic chip is firstly rinsed with 100 mM NaOH solution for 30 min to pretreat the surfaces and prepare for the further adsorption of polyelectrolyte layers. Once the precondition steps are completed, the 5% PB solution and 3% DS solution are used alternatively to rinse the chip and generate multiple layers on the channel inner walls. Between each rinse of polyelectrolyte solutions, three times of water rinse are employed to remove the residual polyelectrolyte solutions. The thickness of a single polyelectrolyte layer in the nanochannel is approximately 1 nm.

To compare the surface charge effects on RPS detections, in this work, the sensing nanochannels of RPS devices with different surface charges are produced by the above modification method. As the sensing nanochannel size is about reaching the saturated size, specific polyelectrolyte solutions are added into the chips to complete the final surface modification process and generate an outmost coated layer. This outmost coated layer will determine the surface charge properties of the sensing nanochannel. The surface charge properties of the modified nanochannel are schematically shown in Figure 7-2. For the sensing nanochannel with a coated PB layer as the outmost layer, the surface charge is positive, and this sensing nanochannel is referred to as positive nanochannel. On the contrary, the sensing nanochannel with a coated DS layer as the outmost layer has negative surface charges and is referred to as negative nanochannel. The third type of nanochannel is pre-coated with PB and DS solutions to the saturated size. Then, 5% PB solution is added into one reservoir of the chip, while 3% DS solution is filled into another reservoir in order to keep the pressure balance between the two reservoirs and make sure the entrance and the outlet of the nanochannel are fully covered with oppositely charged polyelectrolyte layers, Since the nanochannel has reached the saturated size, the polyelectrolyte molecules cannot enter the nanochannel. Only the surface charge of the entrance region of the nanochannel with a limited length is regulated to be positive by the positively charged PB molecules. The rest of the nanochannel walls remain a negative surface charge density. This sensing nanochannel is referred to as bipolar nanochannel in this chapter.

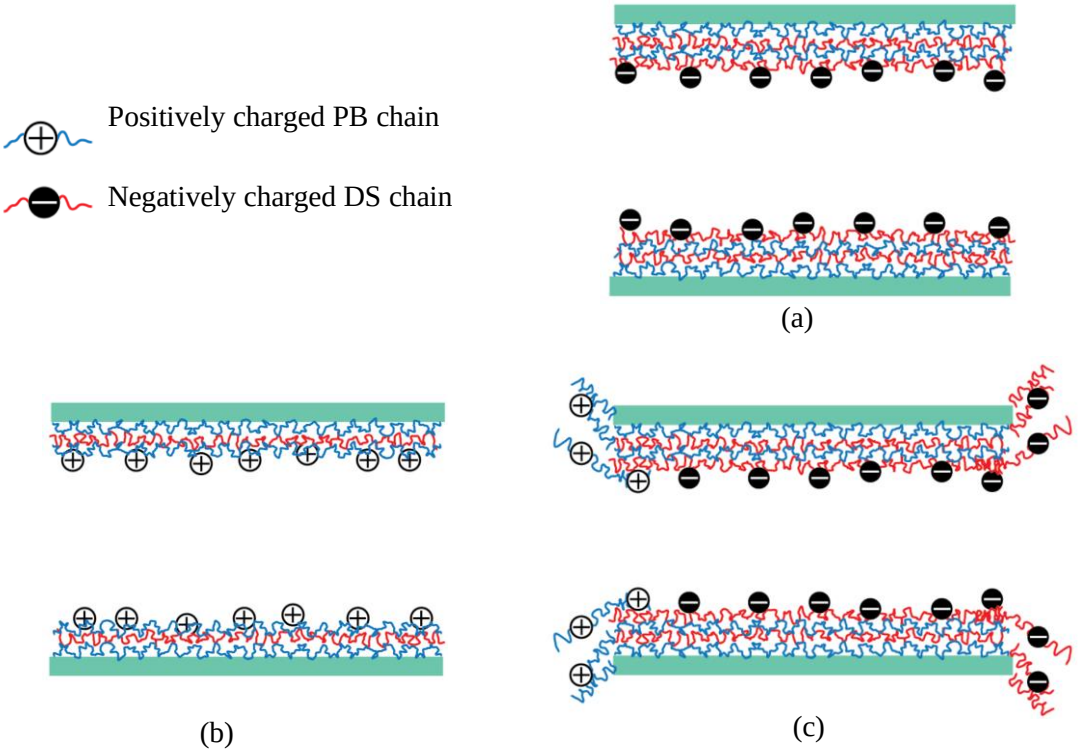

Figure 7-2. Schematic diagrams of modified nanochannels. (a) Negative nanochannel with a coated DS layer as the outmost layer. (b) Positive nanochannel with a coated PB layer as the outmost layer. (c) Bipolar nanochannel with positive surface charge at the entrance region of one end of the nanochannel.

7.3 Mathematical model

Consider a nanochannel with a length of L, width of W, and height of H, connecting two reservoirs, as schematically shown in Figure 7-3. These two reservoirs and the nanochannel are initially filled with a KCl solution with a bulk concentration c, density ρ, dynamic viscosity μ, and relative permittivity ε_r. An electric potential ϕ is applied between the two ends of the two reservoirs and generates an ionic current along the nanochannel.

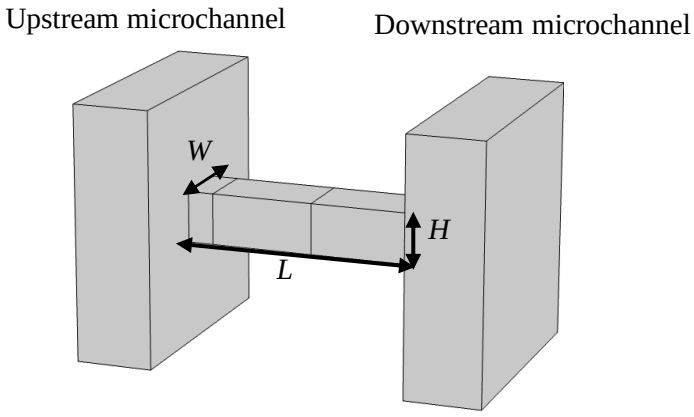

Figure 7-3. The schematic diagram of the nanofluidic chip used in the model and numerical simulation.

7.3.1 Electric filed

Once an external electric filed is applied, the distribution of electric potential in the computational domain can be obtained by solving Poisson equation

$$-\nabla(\varepsilon_o \varepsilon_r \nabla\phi) = F\sum z_i c_i \tag{7-1}$$

The local applied electric field strength can be expressed as:

$$E = -\nabla\phi \tag{7-2}$$

The electrical displacement is given as:

$$D = \varepsilon_o \varepsilon_r E \tag{7-3}$$

The boundary condition of the surface charge on the walls of the nanochannel is described as:

$$n \cdot D = \sigma_W \tag{7-4}$$

The surface charge on the nanoparticle is:

$$n \cdot D = \sigma_p \tag{7-5}$$

Where *n* is the normal vector directed from the surface to the fluid.

For other boundaries of the model, zero charge condition is applied:

$$n \cdot D = 0 \tag{7-6}$$

The electric potential at the left side of upstream reservoir is set as the following:

$$\phi = \phi_1 \tag{7-7}$$

At the right side of downstream reservoir:

$$\phi = \phi_2 \tag{7-8}$$

7.3.2 Ionic concentration field

Nernst-Planck equation is used to describe the ionic mass transport in the nanofluidic chip[268]:

$$\nabla N_i + \frac{\partial c_i}{\partial t} = 0, \quad \text{i= 1 and 2} \tag{7-9}$$

The ionic flux density of i ion species is given as:

$$N_i = uc_i - D_i \nabla c_i - z_i \frac{D_i}{RT} F c_i \nabla \phi \tag{7-10}$$

In Eq. (7-10), the first term (uc_i) is the electroosmosis effects. The second and the third terms of Eq. (7-10) are the ionic fluxes generated by the concentration gradient and electric potential gradient, respectively.

The channel walls and particle surfaces are set as impermeable for ionic mass transport, and the boundary condition is given as:

$$n \cdot N_i = 0 \tag{7-11}$$

The bulk ionic concentration is assumed at the two reservoirs:

$$c_1 = c_2 = c_b \tag{7-12}$$

7.3.3 Flow field

In this model, the flow field can be expressed by the Naiver-Stokes equations:

$$\rho(u \cdot \nabla)u = \nabla \cdot [-pI + \mu(\nabla u + (\nabla u)^T] + f \tag{7-13}$$

and

$$\nabla u = 0 \tag{7-14}$$

Here p is the pressure of the fluid, f is the electrostatic body force which can be expressed：

$$f = -F(z_1 c_1 + z_2 c_2)\nabla \phi \tag{7-15}$$

The boundaries at the two ends of the two reservoirs are assumed as the open boundary condition. For an open boundary condition, the flow can both enter or exit from this type of boundary. The applied pressure is zero, no viscous stress at these boundaries. The boundary condition is governed by:

$$[-pI + \mu(\nabla u + (\nabla u)^T]n = 0 \tag{7-16}$$

No slip boundary condition is employed on the nanochannel walls and the nanoparticle surface:

$$u = 0 \tag{7-17}$$

For the sensing nanochannel with opposite surface charges at the two ends, the surface charge densities of the nanochannel are set as $+\sigma_W$ at the walls of the nanochannel entrance with a limited length of 20 nm and $-\sigma_W$ at the rest of the nanochannel walls, respectively. For the sensing nanochannels with homogeneous surface charges, the nanochannel walls have a constant surface charge density σ_W for positively charged nanochannel and $-\sigma_W$ for negatively charged nanochannel. The ionic current can be calculated as the following:

$$I = \int F \sum(Z_i N_i)\, ndS \tag{7-18}$$

where I is the ionic current, S is the cross-sectional area of the nanochannel.

In this numerical simulation, we mainly focus on the variation of the electric current when a nanoparticle passes through the nanochannel and replaces ionic solution. Generally, the amplitude of the ionic current change is determined by the volume ratio of the nanoparticle to the sensing nanochannel. In nanoscale, the particle surface charge also affects the ionic current due to the exist of electric double layer. Theoretically, the transport velocity of the nanoparticle will not influence the amplitudes of ionic current change. To simplify the model, the drag forces exerted on the nanoparticle are not considered, and a stationary solver is utilized in the simulations. Initially, there is not any nanoparticles inside the channel. The initial ionic current I_1 can be calculated by using Eq. (7-18). Then a nanoparticle is placed in the left reservoir and start to move forward 5 nm by each step in the direction of the nanochannel length. By calculating the ionic current of each step by using Eq. (7-19), a series of ionic current can be obtained:

$$I(x) = \int F \sum Z_i N_i(x)\, ndS \tag{7-19}$$

where x is the displacement of the nanoparticle along the direction of the nanochannel length.

The minimum ionic current I_2 when a nanoparticle passes through the nanochannel can be obtained:

$$I_2 = I(x)_{min} \tag{7-20}$$

The amplitude of the ionic current change is used to evaluate the RPS signal, which can be expressed as:

$$\nabla I = I_1 - I_2 \tag{7-21}$$

In a RPS system, the electric potential bias along the sensing nanochannel without any particles passing through can be expressed as:

$$V_1 = V - I_1 R_1 - I_1 R_2 \tag{7-22}$$

where V is the applied electric potential across the RPS chip, R_1 and R_2 are the electrical resistance of the upstream microchannel and downstream microchannel, respectively.

Assume that the electrical resistance of the upstream microchannel is constant when a nanoparticle leaves upstream main microchannel and enters the sensing nanochannel, the electric potential bias along the sensing nanochannel with a particle passing through it is:

$$V_2 = V - I_2 R_1 - I_2 R_2 \tag{7-23}$$

The RPS signal can be simply expressed as:

$$V_{out} = V_2 - V_1 = \nabla I(R_1 + R_2) \tag{7-24}$$

Clearly, the amplitude of the RPS signal should be proportional to the ionic current change ∇I in the sensing nanochannel. Therefore, to simplify the calculation in the simulation of this chapter, the change amplitude of the ionic current is used to evaluate the RPS signal.

Numerical simulations based on the theoretical model as described above are conducted by using Comsol Multiphysics 5.4. The simulations consider a nanochannel with a rectangular cross section connected to two reservoirs. A nanoparticle with a diameter of 5 nm transports through the nanochannel. The Poisson-Nernst-Plank equation, Navier-Strokes equation are used to simulate the fluid flow, ionic concentration, and the electric potential, simultaneously. A physics-controlled mesh is used in the simulations. To obtain the reliable results, different numbers of grids are examined. The number of the

grids are used when the simulated results do not change if the mesh was further fined. The relative tolerance is set as 0.001. The parameter values used in the simulation are listed in Table 7-1.

Table 7-1. The parameter values used in the simulations.

Parameter	Value/Range	Unit
ε_r (Relative permittivity)	80	−
ε_0 (Absolute permittivity)	8.85×10^{-12}	F/m
ρ (Liquid density)	1000	$\mathrm{kg/m^3}$
μ (Dynamic viscosity)	1×10^{-3}	$\mathrm{Pa \cdot s}$
σ_W (Surface charge density on the walls of nanochannel)	5×10^{-3}	$\mathrm{C/m^2}$
σ_p (Surface charge density of nanoparticle)	-2×10^{-3}	$\mathrm{C/m^2}$
ϕ_1 (Electric potential on the left)	$-4 \sim 4$	V
ϕ_2 (Electric potential on the right)	0	V
R (Universal gas constant)	8.314	J/(mol·K)
T (Temperature)	300	K
L (Nanochannel length)	500~5000	nm
W (Nanochannel width)	25	nm
H (Nanochannel depth)	20	nm
D_1 (Diffusion coefficient of K^+)[187]	1.96×10^{-9}	$\mathrm{m^2/s}$
D_2 (Diffusion coefficient of Cl^-) [187]	2.03×10^{-9}	$\mathrm{m^2/s}$
Z_1 (Valence of K^+)	1	−
Z_1 (Valence of Cl^-)	-1	−
c_b (Bulk ionic concentration)	10	$\mathrm{mmol/m^3}$

In the experimental RPS system, as schematically shown in Figure 7-1 (a), a DC electric voltage is applied to the main microchannel, and the nanochannel connecting the upstream and downstream microchannel channel serves as the sensing gate of the system. A voltage difference between the two detecting microchannels can be amplified and observed when a particle passes through the nanochannel. The voltage difference amplified by the differential amplifier with a gain A can be expressed as:

$$V_{out} = A\left(\eta_{up} - \eta_{down}\right) + A(\nabla V_2 - \nabla V_1) \tag{7-25}$$

Where η_{up} and η_{down} are the noises detected by the upstream detecting channel and downstream detecting channel, respectively; ∇V_1 and ∇V_2 are the electric potential bias between the two ends of the nanochannel without any particle passing through and with a particle passing through, respectively.

7.4 Results and discussion

7.4.1 Surface charge effects on the ionic current

In the numerical simulations, KCl solution with a bulk concentration of 10 mM is used. All three types of nanochannels are considered. For the bipolar nanochannel, the surface charge density on the nanochannel entrance walls with a limited length of 20 nm is set as $5 \times 10^{-3}\ C/m^2$, and the surface charge density on the rest of the nanochannel walls is $-5 \times 10^{-3}\ C/m^2$. For the positive nanochannel, the surface density is set as a uniform positive value of $5 \times 10^{-3}\ C/m^2$. For the negative nanochannel, the surface charge density is set as a uniform negative value of $5 \times 10^{-3}\ C/m^2$. The electric potential difference between the two reservoirs is ranging from -4 V to 4 V. The temperature is 300 K. Figure 7-4 shows numerical results for the ionic current-potential curves through the nanochannels with different surface charge densities and in the same KCl solution of 10 mM bulk concentration. As shown in Figure 7-4, in the bipolar nanochannel, the ionic current increases with the increasing applied electric potential in forward bias whereas it is almost zero in reverse bias. For the nanochannels with homogeneous surface charges, the ionic current increases monotonically with the increasing applied electric potential. Furthermore, the ionic current is larger in the bipolar nanochannel compared with the other two types of nanochannels when the electric potential is forward bias. This promotion in ionic current is getting larger as the applied electric potential increases.

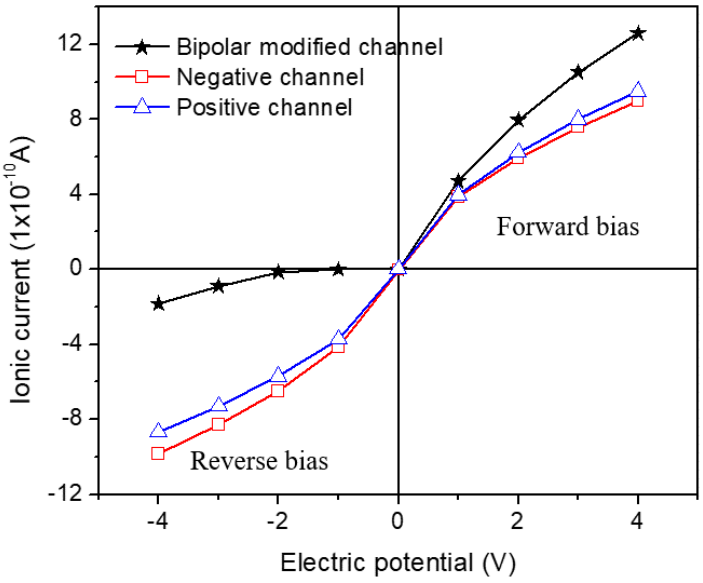

Figure 7-4. Numerical simulation of the current-potential curve for three different types of nanochannels. The bulk concentration of KCl solution is 10 mM. The nanochannel dimensional size is $500 \times 25 \times 20$ nm (L × W × H).

Behavior of the current-voltage curve for the bipolar nanochannel as shown in Figure 7-4 can be explained by the surface charge governed ion distribution in the nanochannel. As shown in Figure 7-5 (b), the counterions inside the electric double layers, K^+ and Cl^-, are dragged to the junction of the oppositely charged channel walls with a forward potential bias. Consequently, these counterions are accumulated in the nanochannel, and a continuous current can be generated. This ion accumulation will accelerate the transport of ions through the nanochannel due to the concentration gradient of counterions. As a result, the ionic current becomes larger. With the reverse bias of electric potential, the counterions approach to the two ends of the nanochannel, and an ion depletion is formed at the junction of oppositely charged channel surface, as shown in Figure 7-5 (c). As a result, the nanochannel is blocked, and the current ceases. Figure 7-5 (d) shows potential profiles alone the nanochannel centerline in the length direction under the applied electric voltage ranging from -3 to 3. In forward bias, large potential drops occur at the two ends of the nanochannel. However, in reverse bias, the potential changes largely at the entrance of the nanochannel where the surface charges change from the positive to the negative value. This is because the total flux of ions is constant along the nanochannel, and the largest potential change will occur in the lowest-density region that is the ion depletion region.

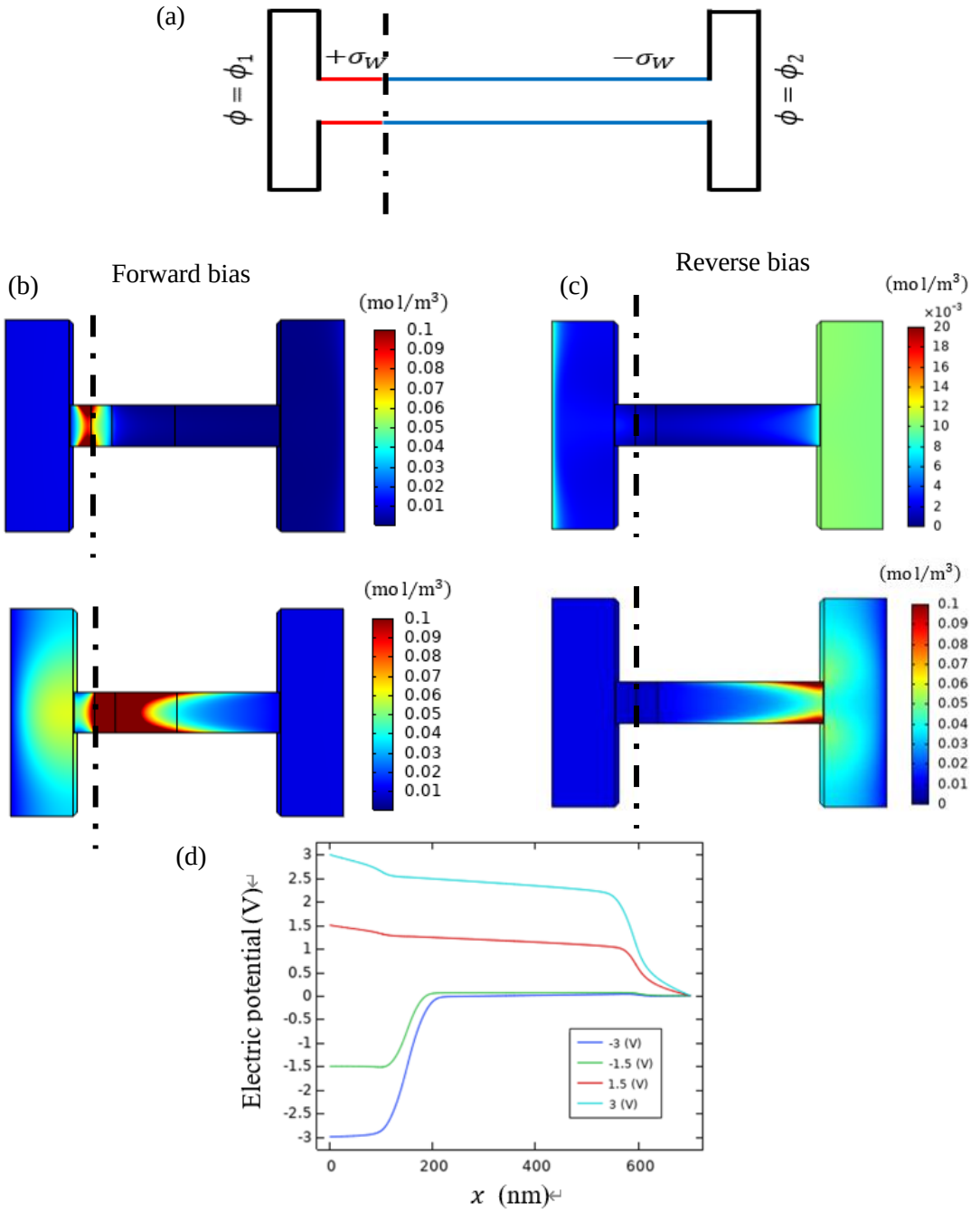

Figure 7-5. (a) A schematic diagram of the surface charge pattern and applied electric potentials. (b)Distribution of K^+ (top)and Cl^-(bottom) in the bipolar nanochannel with a forward-biased electric potential. (c) Distribution of K^+ (top)and Cl^-(bottom) in the bipolar nanochannel with a reverse-biased electric potential (Bulk concentration: 10 mM. The color gradient illustrates the concentration

gradient of ions. The black dash line shows the interface of the positive and negative walls of the nanochannel). (d) Potential profile along the nanochannel centerline with the applied electric potential ranging from −3 V to 3 V (Bulk concentration: 10 mM).

In RPS systems, the detected signals are proportional to the ionic current change along the sensing nanochannel when a particle passes through it. In positive and negative nanochannels, the nanoparticle will replace a certain amount of ionic solution and reduce the ionic conductivity. As a result, the ionic current decreases, and a RPS signal can be observed. As mentioned above, the ionic current is larger in the bipolar nanochannel due to the ion accumulation. Figure 7-6 demonstrates the ionic concentration distribution in the bipolar nanochannels without and with a nanoparticle passing through it under a forward potential. The surface charge density of the nanoparticle is $-2 \times 10^{-3}\ C/m^2$. In the bipolar nanochannel, as shown in Figure 7-6 (b), the nanoparticle not only replace ionic solution but also disrupt the ion accumulation due to the electrostatic force. The disruption in the ion accumulation will further decreases the ionic current in bipolar nanochannel. Therefore, the amplitude of the ionic current change is larger in the bipolar nanochannel compared with the other two types of nanochannels.

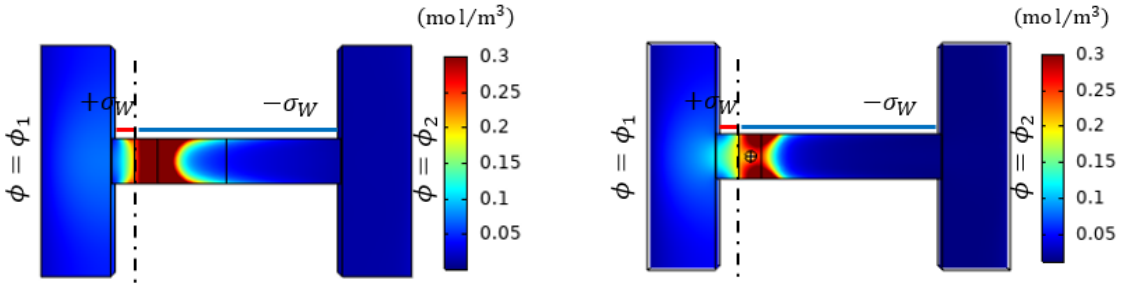

Figure 7-6. The concentration gradient of total ions (K^+ and Cl^-) in the nanochannel without particle (a) and with a particle passing through the junction (b) under a forward electric potential ($\phi_1 = 3\ V; \phi_2 = 0$; bulk concentration 10 mM).

7.4.2 Surface charge effects on RPS detection

As discussed above, the ionic current is larger in the bipolar nanochannel with a forward potential. As shown in Equation (7-24), the electric current change is related to the detected signal amplitude in a RPS system. To investigate the surface charge effects on RPS detection, a numerical simulation is

conducted. In this simulation, ionic current changes in the three types of nanochannels, including positive nanochannel, negative nanochannel, and bipolar nanochannel, are investigated, respectively. The nanoparticle in this model is non-conductive and negatively charged with the surface charge density of $-2 \times 10^{-3}\ C/m^2$. The amplitude of the ionic current change when a nanoparticle with a diameter of 5 nm passes through the nanochannel is simulated and used to evaluate the RPS signals.

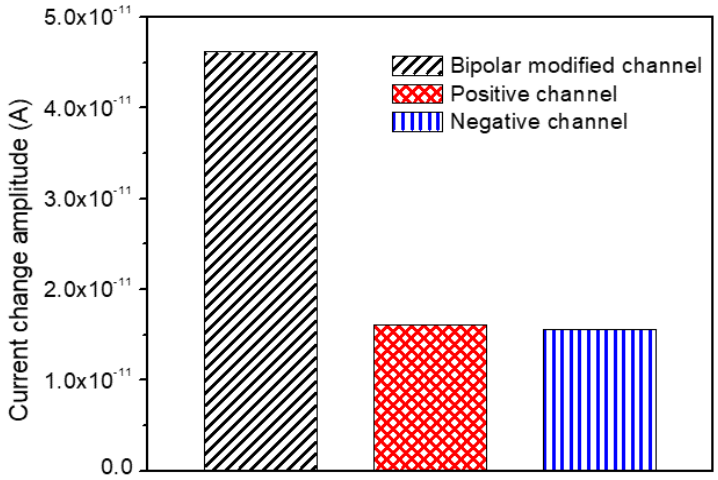

Figure 7-7. The simulated amplitudes of the ionic current change when a 5 nm nanoparticle passes through three types of modified nanochannels (nanochannel length: 500 nm).

Figure 7-7 shows the simulated amplitudes of the ionic current change when a 5 nm nanoparticle passes through nanochannels with different surface charges. From this figure, one can see that the amplitude of the ionic current change in the bipolar channel is significantly larger than that in the positive channel and the negative channel. The amplitude of the ionic current change of the bipolar sensing nanochannel is approximately 3 times of that of the other two types of nanochannels. As discussed above, the ionic conductivity will decrease when a nanoparticle is passing through the nanochannel due to the replacement of ionic solution by the nanoparticle. For positive and negative nanochannels, the nanochannel is mainly filled with counterions with the applied electric field due to the surface charge effects. The ionic current change is determined by the amount of ion replaced by the nanoparticle. For bipolar nanochannel, the ionic current also decreases due to the ion replacement. Moreover, the ion accumulation in bipolar nanochannel will accelerate the ion exchange at the junction due to the concentration gradient, leading to a larger ionic current. This ion accumulation will be disrupted when a nanoparticle passes through it. Therefore, the ionic current decreases more significantly in a bipolar nanochannel.

7.4.3 Effects of nanochannel length on the ionic current and RPS signals

As discussed above, the increase in ionic current caused by the ion accumulation will affect the ionic current change, and consequently the detected RPS signals. It should be noted that the nanochannel length may also affect the degree of ion accumulation and depletion in the modified nanochannels, hence influence the ionic current and RPS signal. In addition, the space occupied by a nanoparticle in a longer nanochannel will become relatively smaller, thus weakening the pulse signal in RPS detection. To investigate the channel length effects, the ionic current in the bipolar nanochannels with different nanochannel lengths are calculated. The nanochannels with the same width of 25 nm, height of 20 nm, and different lengths ranging from 500 nm to 5000 nm are analyzed. The surface charge densities at the entrance wall and the rest walls of the nanochannel are set as $\pm 5 \times 10^{-3}\ C/m^2$, respectively. The KCl solution with a bulk concentration of 10 mM is used as the charge carriers.

Figure 7-8 shows simulated current-potential curves for the modified nanochannels with different lengths at the potential bias of $\pm 1.5\ V$. As shown in Figure 7-8, the ionic current under forward biased potential decreases with the channel length because of the lower electric field strength in longer nanochannels. The reverse bias current is almost zero and essentially constant for all nanochannel lengths due to the co-ions are repelled and gated effectively by electrostatic force. When a reverse bias electric field is applied across the nanochannel, the entrance of the nanochannel with immobilized positive surface charges will repel co-ions and block the channel, thus stopping the ionic current. On the contrary, with a forward bias electric field, the counterions accumulate in the nanochannel, and the degree of the accumulation of ions depends on the electric field strength. With a constant applied potential across the nanochannel, the shorter nanochannel has a larger electric field strength, leading to a higher enrichment of counterions in the nanochannel. As a result, the ionic current is higher. As a result, the nanochannel length is an important factor in determining the magnitude of RPS signals in the surface modified nanochannels.

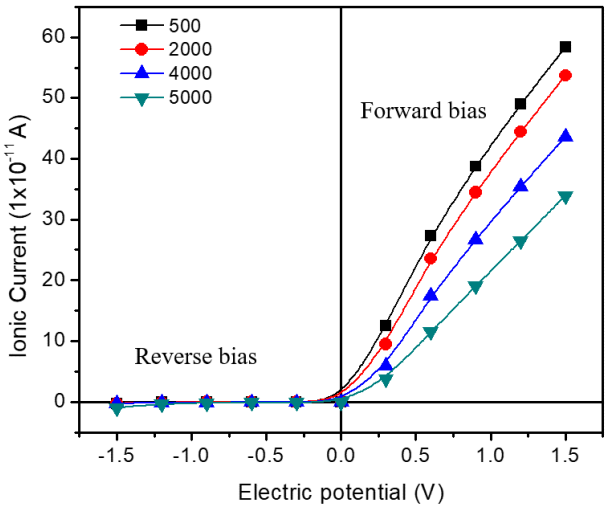

Figure 7-8. Numerical simulation results of the current-potential curves for the bipolar nanochannels with different nanochannel lengths. (Bulk concentration: 10 mM).

To evaluate the channel lengths effects on pulse signals of nanoparticles, the ionic current changes when a nanoparticle passes through the nanochannel are calculated for different channel lengths. The nanochannel is filled with KCl solution with a bulk concentration of 10 mM, and the surface charge densities at two ends of the bipolar nanochannel are $\pm 5 \times 10^{-3}\ C/m^2$, respectively. For the positive and negative nanochannel, the surface charge densities are $5 \times 10^{-3}\ C/m^2$ and $-5 \times 10^{-3}\ C/m^2$, respectively. The surface charge density of the nanoparticle is $-2 \times 10^{-3}\ C/m^2$, and the particle diameter is 5 nm. Figure 7-9 demonstrates the amplitude of the ionic current change of the surface modified nanochannels with different lengths when a nanoparticle passes through. From Figure 7-9 (a), one can see that the amplitude of the ionic current change (hence, the RPS pulse) of the bipolar nanochannel is the highest in comparison with the other two nanochannels with homogeneous surface charges. Furthermore, the amplitude of the ionic current change decreases monotonically with the nanochannel length from 500 nm to 5000 nm for all types of nanochannels. By comparing the ratio of the ionic current change amplitude in bipolar nanochannels to that in homogeneously charged channels, as shown in Figure 7-9 (b), it is observed that the signal ratio decreases rapidly as the nanochannel length increases from 500 nm to 1000 nm and then gradually decreases with the increasing nanochannel length. This is because a long nanochannel length will reduce the stable ionic current and the degree of ion enrichment inside the channel due to the lower electric field strength in longer nanochannels. As a result, the promotion in the ionic current change amplitudes by the surface modification becomes less

prominent with a larger length. Since the forward ionic current does not increase linearly with an increasing electric field strength in a bipolar modified nanochannel. The increment in ionic current becomes gentle at high electric field strength due to the concentration polarization. That means the promotion in ionic current in the modified nanochannel decreases as the applied electric field exceed a critical value. When the length of the bipolar modified nanochannel becomes larger than 3000 nm, the ionic current reduces more significantly at the low effective electric field. Therefore, it is also observed that the decrease in the RPS signal ratio is slightly steeper in long nanochannels.

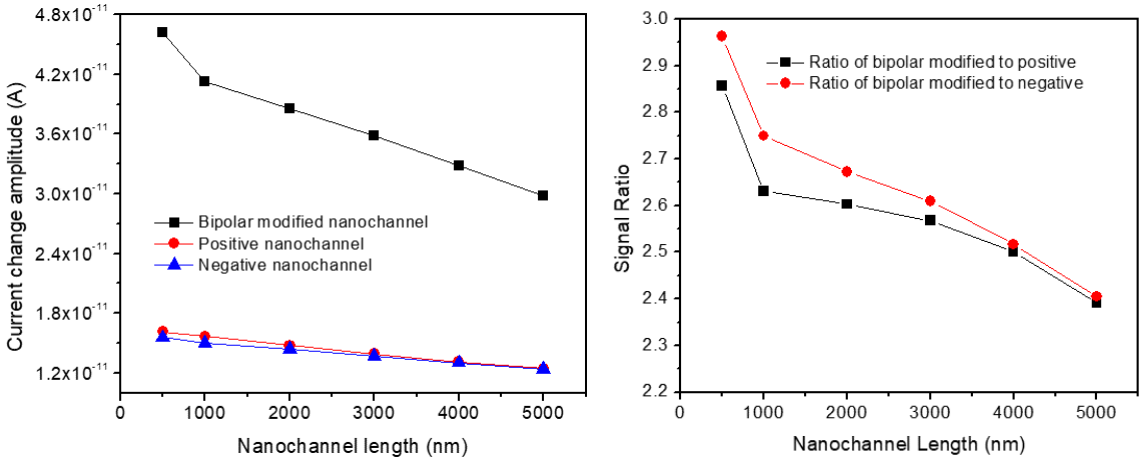

Figure 7-9. (a) The magnitude of ionic current change as a function of the nanochannel length. (b) The ratio of ionic current change in bipolar nanochannel to homogeneously modified channels at the applied potential of 1.5 V and different channel lengths.

7.4.4 Experimental characterization of the surface charge pattern effects on RPS detection

In the experiments, the nanofluidic chips as shown in Figure 7-1 are modified with the polyelectrolyte solutions of PB and DS by using the LBL method until the nanochannel depth reaches the minimum size of 25 nm[208]. In the experimental RPS system, two detecting microchannels are located at the two ends of the sensing nanochannel. To stably bond the nanochannel chip to the microchannel chip without leakage, a sensing nanochannel with a relatively large length of 5 μm is used in this study. According to the results shown in Figure 7-9, the RPS signals amplitude is inversely proportional to the nanochannel channel length. In the measurements, a voltage difference ranging from −2 V to 2 V is applied between the two reservoirs, and the electric current is measured by an

electrometer (Keithley, Model 6517A). Each experimental measurement is repeated at least three times in three individual chips. Figure 7-10 shows an example of the measured electric current-potential curve of the KCl solution with a bulk concentration of 10 mM in the bipolar nanochannel. It is observed that the current increases with the increasing electric potential in forward bias whereas almost be zero in reverse bias. The experimental current is relatively larger compared with the calculated results in Figure 7-8. This is because the nanochannel size used in this experiment has a relatively larger width than depth. Only the depth of the nanochannel can be reduced to the minimum size by using the LBL deposition method, and the width of the nanochannel is larger compared with that in the numerical simulation. However, the ion accumulation and depletion are determined by the minimum size of the sensing nanochannel. Therefore, excellent ionic current rectification behaviors can be obtained in the modified nanochannels.

.

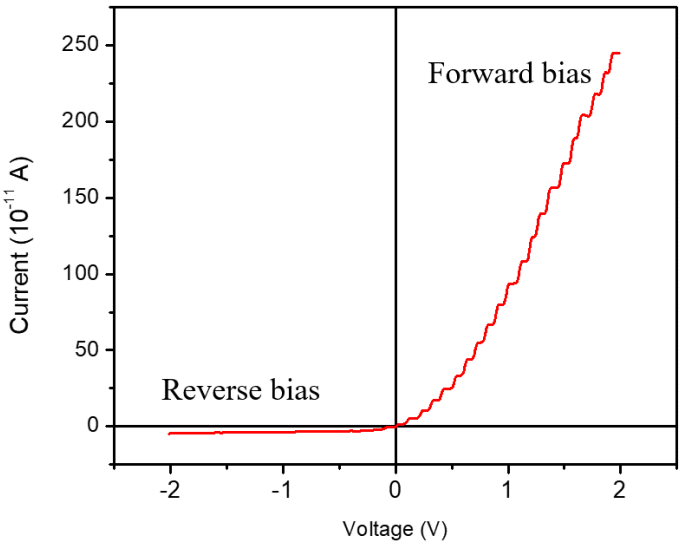

Figure 7-10. The experimentally measured current-potential curve of KCl solution with a bulk concentration of 10 mM in a bipolar nanochannel.

To examine the effects of surface modified sensing nanochannels on RPS signals, the nanoparticles are detected in bipolar nanochannel and nanochannels with constant surface charges. To keep the consistency of the channel size in the experiment, all nanochannel are precoated with PB/DS multiple layers to the saturated size. The outmost coated layer on the sensing nanochannel inner walls is PB layer for positive nanochannels whereas it is DS layer for negative nanochannels. Before the RPS

detection, all channels are rinsed with DI-water to remove the residual polyelectrolyte solutions. Then, 100 mM KCl solution containing 5 nm gold nanoparticles is loaded into the chips, and an electric potential of 1.5 V is applied between the two reservoirs. Figure 7-11 shows the examples of measured voltage signals generated by the nanoparticles and the histograms of the signal amplitudes. Each downward peak represents an individual nanoparticle passing through the nanochannel. The signal amplitudes are calculated by:

$$\nabla V = \left| V_{peak} - V_{base} \right| \tag{7-26}$$

Where the V_{peak} is the voltage at the peak point, and V_{base} is the average voltage of the baseline.

From the histograms shown in Figure 7-11, one can observe that the mean signal amplitudes are $1.51 \pm 0.30 \times 10^{-3}\, V$ for bipolar nanochannel, $1.00 \pm 0.30 \times 10^{-3}\, V$ for the PB layer coated nanochannel and $1.01 \pm 0.30 \times 10^{-3}\, V$ for the DS layer coated nanochannel, respectively. It is obvious that the measured signal amplitudes are relatively larger in the bipolar nanochannel than that in the other two types of nanochannels. The enhancement ratios of RPS signals for bipolar channel to PB channel and DS channel are calculated to be 1.51 and 1.50, respectively. In the numerical simulation, the KCl solution with a bulk concentration of 10 mM is used. The enhancement ratios of the current change (equivalent to the RPS signals as indicated by Eq. (7-24)) predicted by the model simulation as shown in Figure 7-7 can be as large as 3 in the surface modified nanochannels with a length of 500 nm. According to Figure 7-9, the long nanochannel length results in smaller RPS signals and smaller enhancement ratios. The calculated enhancement ratio of the RPS signal is 2.4 when the 10 mM KCl solution and 5000 nm length nanochannel are employed. In experiments, the signal-to-noise ratio is too small to accurately analyze the enhancement at such low ionic concentration due to the low ionic conductivity. To generate a stable ionic current and gain large RPS signals in the RPS chip with a long sensing nanochannel, the KCl solution with a relatively higher bulk concentration of 100 mM is used in this experimental study. As one can see from Figure 7-11, the experimental results of the enhancement ratio of the detected RPS signals, approximately 1.5, are smaller in comparison with the model prediction. This is primarily due to the nanochannel length effects and ionic concentration effects. It is known that ionic concentration not only influences the conductivity of the electrolyte solution but also affects the thickness of the EDL. As a result, the ionic current and the enhancement of RPS signals based on the surface charge governed ions transport can be changed significantly with a higher bulk concentration. To better analyze the experimental results, a numerical simulation of the ionic concentration effects on the ionic current change amplitude was conducted in the 500 nm nanochannels

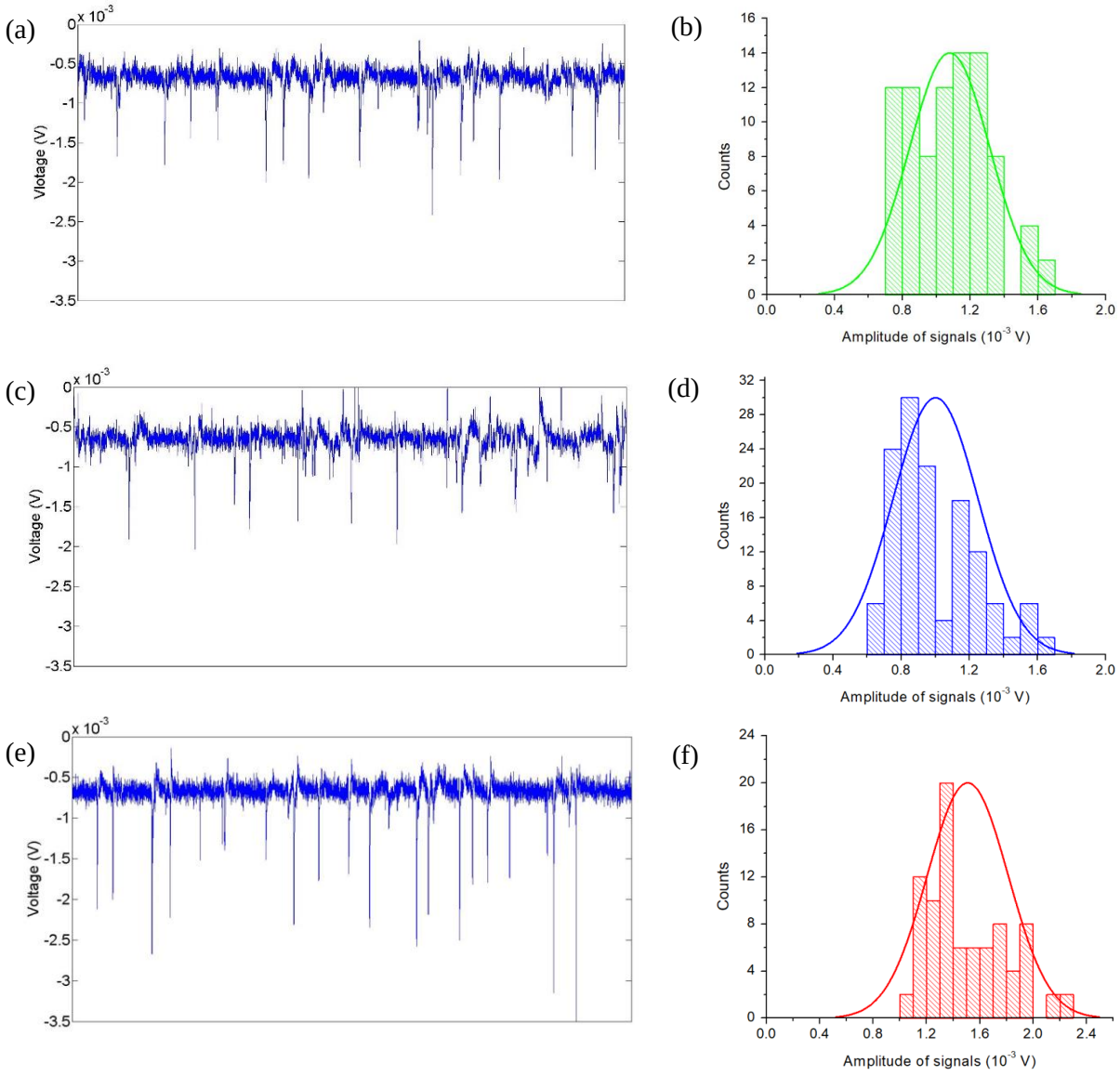

Figure 7-11. Examples of measured RPS signals and histograms generated by the 5 nm gold nanoparticles in (a) and (b) positive channels (PB layer as the outmost coated layer); (c) and (d) negative channels (DS layer as the outmost coated layer); (e) and (f) bipolar channels (one end is coated with PB layer and the rest of channel is coated with DS layer), respectively.

with different surface charges. As shown in B-1 (Appendix B), the amplitude of the ionic current change increases due to the larger stable ionic current in the nanochannel at a higher ionic concentration. However, the enhancement ratio of the amplitudes for the bipolar modified nanochannel to the positive nanochannel decreases from around 2.75 to 1.86 as the bulk ionic concentration increases from 10 mM

to 100 mM. The results indicate that a high ionic concentration of KCl solution leads to large RPS signal amplitudes but small enhancement ratios of RPS signals. By considering the channel length effects and the ionic concentration effects, the experimental results are reasonable and in good agreement with the simulated results.

7.5 Conclusions

The effects of the sensing nanochannel surface charge on the detection of nanoparticles by RPS method are studied in this chapter both numerically and experimentally. The influence factors in RPS detections, such as the length and surface charge pattern of the sensing nanochannel, are investigated by numerical simulation. The results show that the detected RPS signals of nanoparticles can be enhanced by decorating opposite charges on the two ends of the sensing nanochannel. The increase in the detected RPS signal amplitudes in the bipolar sensing nanochannel can be as higher as 3 times to that in normal sensing channels. This signal enhancement rate decreases as the sensing nanochannel length increases. In the experimental study, the bipolar sensing nanochannel with a length of 5 μm is fabricated by coating charged polyelectrolytes on the two ends of the sensing nanochannel. Nanoparticles of 5 nm are detected in the modified nanochannels. The experimental results are in good agreement with the theoretical model prediction. To the best of the authors' knowledge, this is the first time the surface charged governed current rectification effects are used in the signal enhancement in resistive-pulse sensing. This study provides a method to significantly improve the sensitivity and resolution of RPS detection of nanoparticles by using bipolar sensing nanochannels.

Chapter 8. Application II: Integrated Iontronic Circuits based on Single Nanochannels

8.1 Introduction

Integrated circuits are ubiquitous in our daily lives and widely used in all electronic devices, such as computers, laptops, and cell phones. Traditional integrated circuits consist of diodes, transistors, and other electronic components, and are used for electric signal process and manipulation. Recently, a new type of ionic device based on electrokinetic regulation of ion transport has attracted significant interest. These ionic devices may have applications in logic computing[187], biological analysis[188,189], and physiological process of living organisms[269] because they function in aqueous environment. The key functional component in ionic devices is the ion channel which can facilitate or block the exchange of ions and molecules depending on the polarity of the applied electric field. With the advancement of nanotechnology and material science, various materials, including membranes, carbon-nanotubes (CNTs) and polymers, have been used to mimic biological ion channels and regulate ion transport in ionic devices.

Examples of man-made ion channels have been reported. The regulation of ion transport through these ion channels is generally achieved by asymmetric geometry and opposite surface charges[4,216,270]. Membrane-based nanopores are commonly used in the development of artificial ion channels. Typically, a surface modification process is required for the membrane-based nanopores in order to have opposite surface charges for ion-flow regulation. Different kinds of ionic diode-like devices have been developed by using these nanopores or nanochannels[192,193,199–201]. For instance, ion channels with switchable conformational states have been reported and developed by surface functionalization with stimuli-responsive polymers[125,169,222]. The tunable properties of these ionic devices provide convenience in delicate signal manipulation and are important in cellular circuits. However, the low aspect ratio and small membrane thickness often cause less effective surface charge modification, thus resulting in low rectification ratios[188]. Moreover, the structure of the membrane-based ion channels makes the integration into chip-scale circuits highly challenging.

In the past few years, CNT technology has been pushed forward and gain broader attention in iontronics industry[204,271,272]. Increasing research efforts have been taken on the possibility of building complex integrated circuits with CNT-based ion channels. Several examples of integrated circuits fabricated with aligned CNT-bundles have already been reported[202,204,206]. Zhu et al.

presented a radiation-hardened CNT field-effect transistor (FET) with ion gel gates, which exhibited high radiation tolerance. Li and Zhou[273] examined the effects of air and temperature on the performance of ionic gel gated CNT circuits. In these CNT-based circuits, aligned CNT bundles are patterned to serve as p-channel and n-channel, similar to traditional semiconductor devices. One major uncertainty is that the final devices contain an undefined number of CNTs in each semiconductor component. One critical factor of ionic integrated circuits to achieve logic computing is that both p-channel and n-channel in FETs are working with similar current rectification performances. The undefined CNT number will cause variations between different ion channels[204].

To develop the iontronic circuit technology, single nanochannels or nanopores would be a better choice for the fabrication of iontronic devices. Intensive studies about nanofluidic diodes based on a single nanochannel have been conducted and some good examples were reported[185,194,199]. However, the solid-state nanopores serving as ion channels in these devices are generally constructed on membranes or other wafers by reactive-ion etching, chemical etching, or deposition method[188]. It is challenging to integrate these vertically aligned nanopores in a solid substrate into a circuit with in-plane arranged architecture on a chip. Up to date, there is no integrated iontronic circuit made of single nanochannel-based nanofluidic ionic diodes.

Desirable in-plane channel patterns in micrometer and sub-micrometer can be easily developed by photolithography method and nano-imprint lithography method[207]. Polydimethylsiloxane (PDMS) is a popular material to replicate these channel structures from designed molds onto chips and has the advantage of mechanical flexibility and stability, transparency, and biological compatibility. However, these technologies cannot satisfy the dimensional requirement for ion flow regulation. Generally, nanochannels with sizes smaller than 50 nm are required to achieve effective rectification for ionic diodes. It is impossible to fabricate such small nanochannels with traditional photolithography methods. Recently, Jun Li et al.[274] reported a PDMS-based nanofluidic diode that can achieve a high current rectification ratio. This nanofluidic diode is made by using wet modification of polyelectrolytes to nanochannels. The nanochannel was constructed by combining the solvent-induced crack method[50] and layer-by-layer (LBL) deposition method[208]. This method opens the possibility of PDMS nanochannel as a promising candidate for constructing iontronic integrated circuits.

In this chapter, a nanofluidic chip with integrated iontronic circuits is designed and fabricated with modified PDMS nanochannels serving as ion channels. In contrast to the CNT-based ionic circuits, the device presented in this chapter is based on single PDMS nanochannels. The PDMS nanochannels

fabricated on the chip have similar dimensional features, leading to similar performance after surface charge modification. The performances of the integrated iontronic circuit chip working as ionic bipolar transistors and full-wave ionic rectifiers were demonstrated. Multiple-functional circuits can be integrated on a PDMS nanofluidic chip by the method reported in this chapter. All processes developed in this work are scalable and lead to promising potentials of entirely PDMS-based chips for constructing complex iontronic devices.

8.2 Experimental section

8.2.1 Chemical reagents and instruments

KCl solution with an ionic concentration of 1 mM was prepared by dissolving KCl powder (≥99%, Fisher Scientific) with deionized water (DI water, 18.2 MΩ · cm, Mini Q, Direct-Q3). The nanofluidic chips were fabricated by using regular PDMS (Sylgard 184, Dow Corning) and hard PDMS (h-PDMS). Regular PDMS was prepared by mixing pre-polymer (base) and the crosslinker (curing agent) and the mixing ratio of the base to the curing agent is 10. Hard PDMS (h-PDMS) is prepared by the mixture of 3.4 g of (7 -8% vinylmethylsiloxane)–(dimethylsiloxane) copolymer (VDT-731, Gelest), 50 mg platinum -divinyltetramethyldisiloxane (SIP 6831.2, Gelest), 100 mg of 2, 4, 6, 8-tetramethyl-2, 4, 6, 8-tetravinylcyclotetrasiloxane (Sigma-Aldrich), and 1 g (25-35% methylhydrosiloxane)-(dimethylsiloxane) copolymer (HMS-501, Gelest) [139]. The nanofluidic chips were formed by bonding a nanochannel chip with a microchannel chip via Plasma treatment (Harrick plasma, PDC-32G). SU-8 2015, SU-8 2005 photoresists (MicroChem), and SU-8 developer were prepared to fabricate the molds for nanochannel chip and microchannel chip. Polybrene (PB, Sigma-Aldrich) and Dextran sulfate (DS, sodium salt, molecular weight, 7000 – 20000, Sigma-Aldrich) were dissolved with DI water to achieve the wet modification of nanochannels. The microchannel and nanochannel are characterized by optical microscope (Eclipse TE 2000, Nikon) and atomic force microscope (AFM, Multimode™SPM, Digital Instruments), respectively. A source meter (Keithley, Model 2602A) and a function generator (Tabor electronics 8550) were applied for the nanofluidic chip operation. The output signals were acquired by an electrometer (Keithley, Model 6517A) via Pt electrodes (Sigma-Aldrich).

8.2.2 Fabrication of nanofluidic chips and surface modification

The nanofluidic chip, as shown in Figure 8-1 (a), was composed of two chips. The bottom chip was the nanochannel chip constructed with two nanochannels that have similar dimensional features.

This nanochannel chip was duplicated from a photoresist mold fabricated by solvent-induced cracking method[50]. In the mold fabrication, two artificial defects were created on a polystyrene slab to dictate the locations of the nanocracks. Ethanol was used to fully vaporize and condense on the polystyrene surface. After absorption and release of the reagent vapor, two nanocracks can be generated on the polystyrene surface across the artificial defect points. The patterns of these nanocracks were transferred to a SU-8 photoresist layer as a positive nanochannel mold [275]. Then, a bilayer of h-PDMS and regular PDMS was utilized to replicate the nanochannel chip from the photoresist mold [182]. Briefly, a thin layer of h-PDMS was spin-coated on the photoresist mold of nanochannels. After a solidification process in an oven at 80 ^{o}C for 10 minutes, a regular PDMS layer is cast on the mold to support the brittle h-PDMS layer, and the chip is placed back in the oven at 80 ^{o}C for 90 minutes to be completely solidified. Figure 8-1 (b) and (c) show the AMF images and corresponding height profiles of these two nanochannels on the chip, respectively. The top chip was a microchannel chip duplicated from a silicon wafer constructed with microchannel mold. This channel mold was fabricated by using standard photolithography method, and the designed microchannel structure was transferred to a photoresist layer on the silicon wafer via a photomask printed at the resolution of 3.5 μm. To keep the consistency of surface properties, the microchannel chip was fabricated by using a bilayer of PDMS as well. Finally, the nanochannel chip was bonded with the microchannel chip to form a nanofluidic chip for experimental measurements by plasma treatment (45 s). As shown in Figure 8-1 (a), these two nanochannels bridge the microchannels forming four gates with a length of 30 μm in the chip that can serve as ionic diodes after surface modification with charged polyelectrolytes.

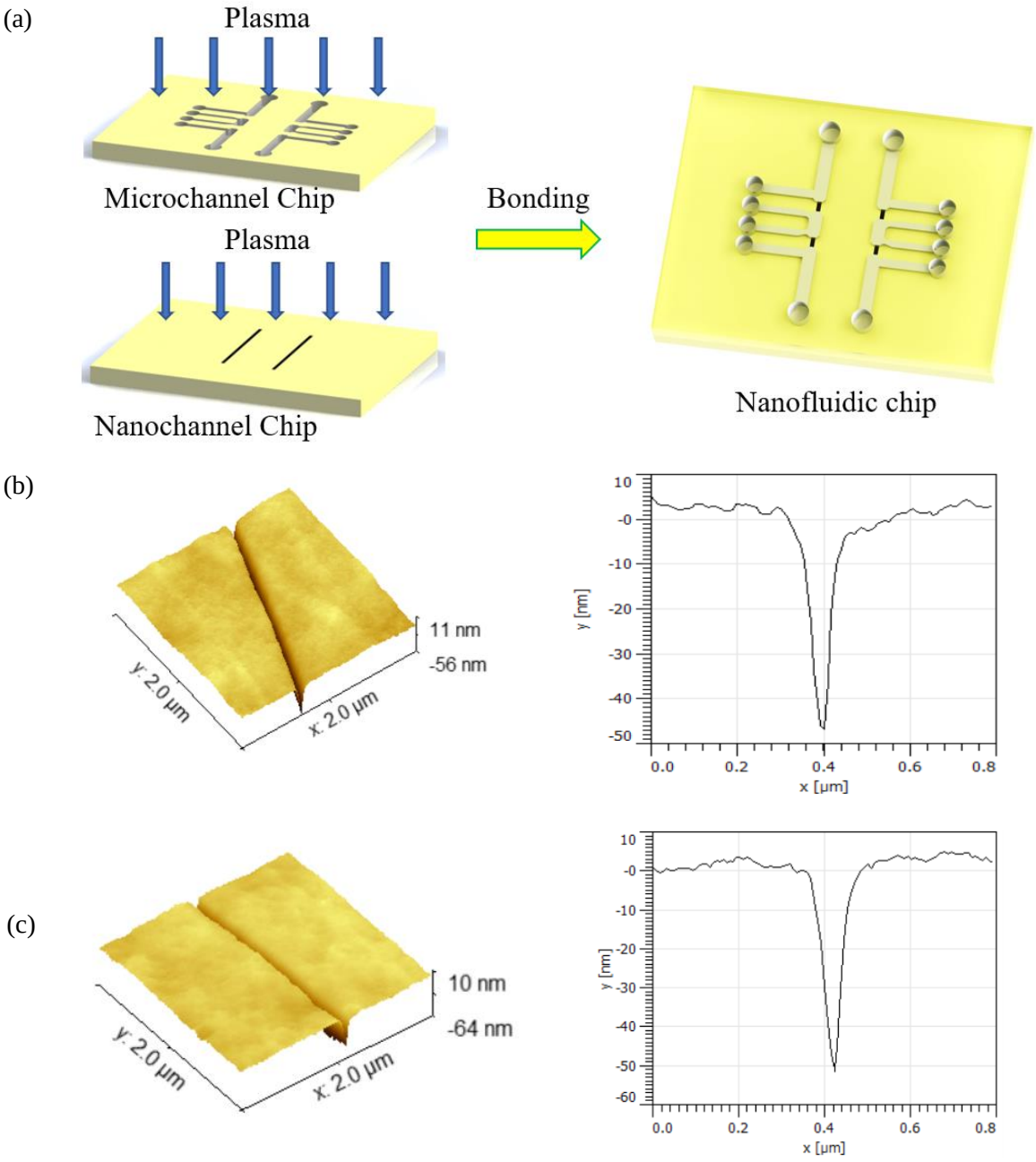

Figure 8-1. (a) Schematic of the bonding process of the nanofluidic chip. (b) 3D AFM images and corresponding height profiles of the nanochannel (left) with a depth of 50.6 ± 2.2 nm and a width of 110 ± 5.2 nm and (c) the nanochannel (right) with a depth of 53.2 ± 2.1 nm and a width of 125 ± 8.7 nm.

To develop multiple ionic diodes and integrate them into a nanofluidic chip, surface modification was required to generate asymmetric surface charges at the two ends of the nanochannels. Our previous studies have reported the method for the regulation of surface charge and size of PDMS nanochannels by a layer-by-layer (LBL) method [208,274]. As shown in Figure 8-2, the surface modification can be completed by two steps, including nanochannel size regulation and surface charge modification. In step one, the nanofluidic chip was firstly incubated with 0.1 M NaOH solution for 3 min to pretreat the channel walls and prepare for the adsorption of charged polyelectrolytes. Then, the NaOH solution was removed by a rinse of DI water, and the positively charged 5% PB solution was added to the chip to complete the first coating since the surface charges of pristine PDMS walls were electrostatically negative. Afterward, 3% DS solution was used to rinse the chip forming PB-DS layer on the channel walls. The modification procedure was repeated to alternatively coat multiple PB and DS layers on the channel walls until the nanochannel reached the minimum size. The minimum channel size was reported as approximately 25 nm when the coated layer number is 14. Three rinses of DI water for 10 min each time were applied to remove the residuals of polyelectrolyte solutions between each layer adsorption. Once the size regulation process was completed, 5% PB and 3% DS solutions were filled into the selected microchannels for generating positive or negative surface charges on the two ends of nanochannels, respectively. As shown in Figure 8-2, 5% PB solution was filled in the red microchannels, and 3% DS solution was filled in the blue microchannels followed by an incubation of 30 min to allow fully adsorption of charged polyelectrolyte molecules. Since the nanochannel size was pre-regulated to sufficiently small, the polyelectrolyte molecules were not able to transport through the nanochannels anymore due to steric effects. Consequently, selected microchannels were modified as positively charged or negatively charged depending on the added polyelectrolyte solutions. Opposite surface charges at the two ends of the nanochannels can be obtained without crosstalk of different polyelectrolyte solutions inside during the wet modification process. DI water was used to rinse channels to remove residual polyelectrolyte solutions then. Finally, a nanofluidic chip consisting of four nanochannels with asymmetric surface charges is developed.

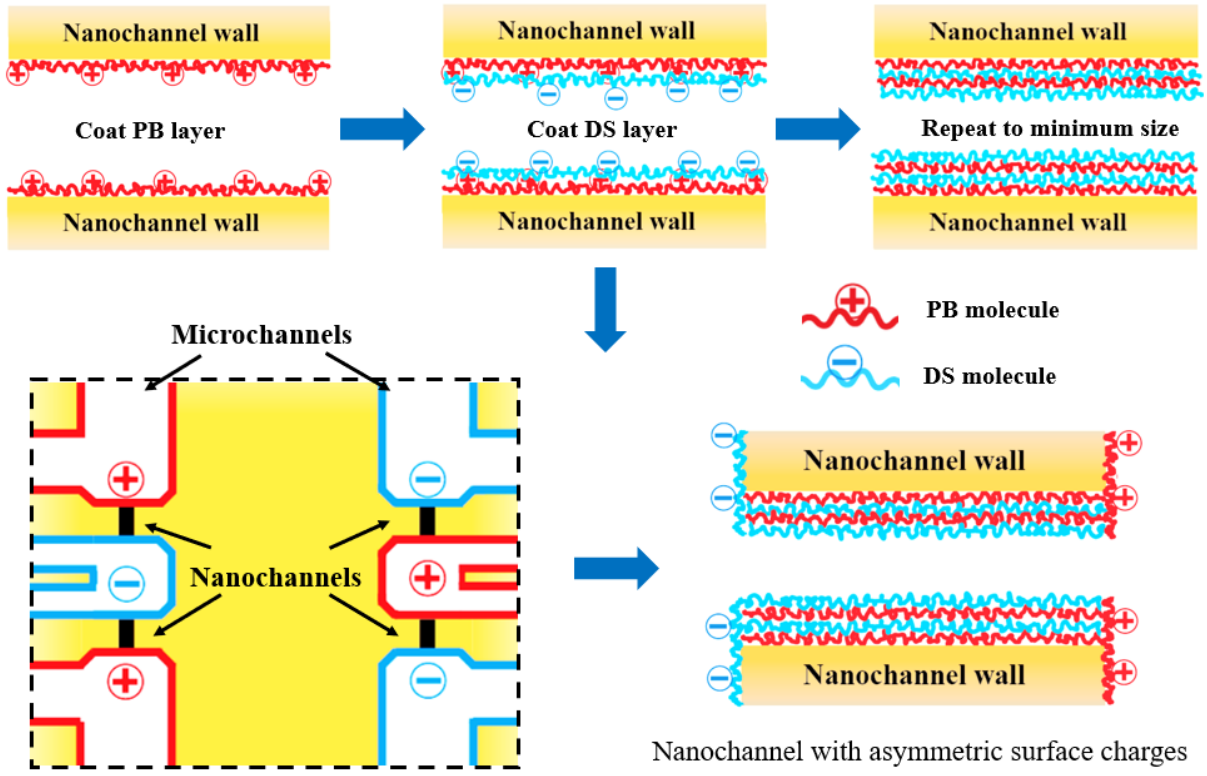

Figure 8-2. Schematic of the surface modification procedures of the nanofluidic chip.

8.2.3 Experimental data acquisition

For ionic devices, a certain amount of charge carries is necessary to enable functions. In this work, KCl solution of 1 mM was used to fill in the nanofluidic chip to provide mobile ions during the measurements. For ionic diodes, transistors, and full-wave ionic rectifier, function generator and source meter were employed to supply input signals and characterize the electric properties of the devices. The output data was measured from the chips by using an electrometer and then transferred to a computer via LabVIEW program (National Instrument Corp). Our previous study has investigated the effects on sweep speed of input voltage on ionic diodes[274]. Hence, here a proper sweep voltage at 250 mV/s was applied in the current-voltage (I-V) curve measurements for ionic diodes and transistors. For ionic rectifier, input signals with an amplitude of 3 V generated by a function generator were used to characterize the device performance. The nanofluidic chips were connected to the equipment through Pt electrodes. All the experiments were repeated at least three times to assure reproducibility and conducted at room temperature of 23 ^{o}C and atmospheric pressure in ambient conditions.

8.3 Results and discussion

8.3.1 Characterization of the performance of ionic diodes in the chip

Ionic diode is a key component in iontronic devices. To develop functional iontronic systems, the working principle and rectification performance of ionic diodes must be understood. One of the key features in producing ionic diodes is decorating asymmetric surface charges along nanochannels. It was reported that the nanochannel with opposite polarity of surface charge can rectify ionic current through it, leading to diode-like behaviors[187]. The current rectification behaviors in the nanochannel are achieved by ion accumulation and ion depletion caused by the electrostatic interactions between nanochannel surface charge and mobile ions, which is so-called field-effect nanofluidic ionic diode[211,219,276]. To investigate the working principle and characterize the performance of the ionic diode, a nanochannel was modified with PB and DS solutions to coat opposite surface charges at the two ends by using LBL method in this work. KCl solution was used as the sample solution, and the cation K^+ and anion Cl^- serve as charge carriers. When a forward electric field is applied, as shown in Figure 8-3 (a), immobilize surface charges at two ends allow counterions transport through the nanochannel. Cations and anions will approach each other under the driving force of electric field, resulting in ion accumulation and continuous ion flow in the nanochannel. When a reverse electric field is applied, the ion transport through the nanochannel is blocked due to the electrostatic repulsion between the immobilized surface charges and mobile ions. As a result, the ions deplete in the nanochannel and only a leakage ion flow exists in the nanochannel. To verify the current rectification behaviors of the modified nanochannel, the ionic current across the nanochannel was measured under a sweep voltage. In the experiment, a voltage bias was applied to the DS modified terminal of the nanochannel (negatively charged) while the PB modified terminal of the nanochannel (positively charged) was grounded. Figure 8-3 (b) shows a current-voltage (I-V) curve measured from the modified nanochannel with an applied voltage ranging from -5 V to 5 V. The forward electric field indicates a positive voltage was applied to the PB modified terminal whereas the reverse electric field indicates the applied voltage is negative. As one can see from the measured I-V curve, the ionic current is essentially zero when a reverse electric field is applied whereas is proportional to the applied voltage bias under a forward electric field. This is because immobilized polyelectrolytes repulse the mobile ions and ion flow in the nanochannel is blocked under the reverse electric field. As a result, only a very small leakage current can be obtained. In forward bias, the mobile ions are allowed to transport through the nanochannel, thus leading to a stable ionic current. This result verifies the proposed working

principle of the ionic diode. The polyelectrolyte modified nanochannel can server as an ionic diode to rectify ionic current.

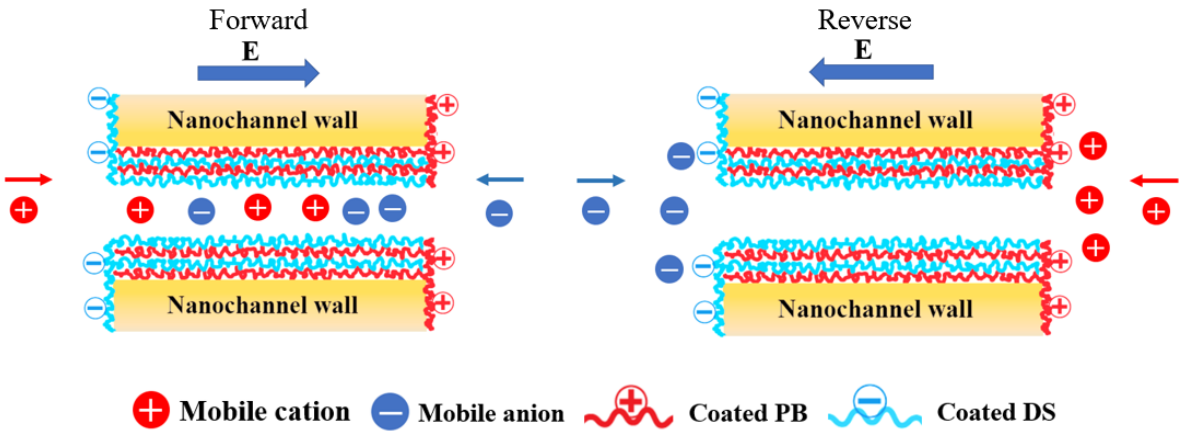

(a)

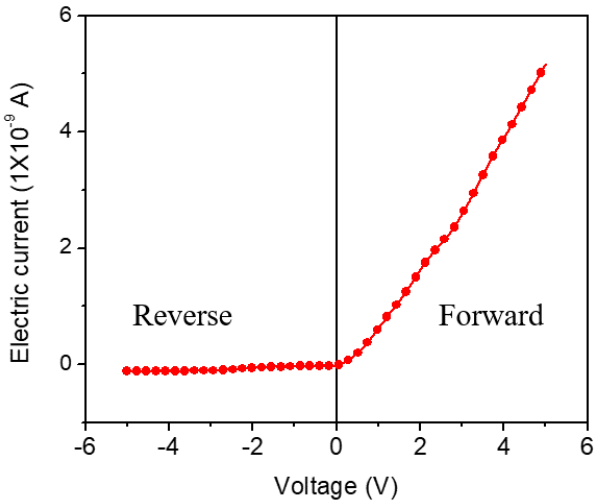

(b)

Figure 8-3. (a) A schematic of the working principle of ionic diode. (b) An example of current-voltage curve measured from an ionic diode with a channel length of 30 μm.

8.3.2 Ionic bipolar junction transistors

The polyelectrolyte modified nanochannel performs current rectification behaviors similar to traditional semiconductors. The nanofluidic chip can work as a bipolar junction transistor (BJT) by connecting the two back-to-back ionic diodes located on the same nanochannel. As shown in Figure 8-4 (a), here we demonstrated an NPN-type ionic transistor by connecting the three terminals with the

left nanochannel. The nanofluidic chip was modified with polyelectrolyte solutions to generate positive surface charge on terminal A and terminal C while negative surface charge on terminal B. Therefore, nanochannels B-A and B-C have opposite surface charges at two ends and can form two back-to-back ionic diodes The ionic transistor can be used as an ionic switch to regulate ion flow. Similar to traditional semiconductor transistors, the status, "ON" or "OFF", between two terminals of the ionic transistor should be regulated by the third terminal. An input voltage, V_B, is applied to terminal B, and terminals A and C are connected to an electrometer to measure the output ionic current I_A . By adjusting the DC voltage, V_{AC}, through terminal A and C, the BJT can serve as a switch to regulate the output ionic current. Figure 8-4 (b) illustrates the experimentally measured I-V curves for the NPN-type BJT operating at different V_B values. These curves indicate that the ionic current, I_A, flowing out from terminal A, is related to the applied voltage V_{AC}. When $V_B < V_{AC}$, the ion current flow through terminals A and B is blocked, and I_A can be considered as the leaking current which is essentially zero. As the sweep voltage decreases to $V_B > V_{AC}$, it is found that I_A becomes proportional to the applied voltage V_{AC}, indicating the transistor is "ON". The experimental results demonstrate that the nanofluidic device, NPN-type ionic BJT, can serve as a single pole single throw (SPST) switch circuit.

(a)

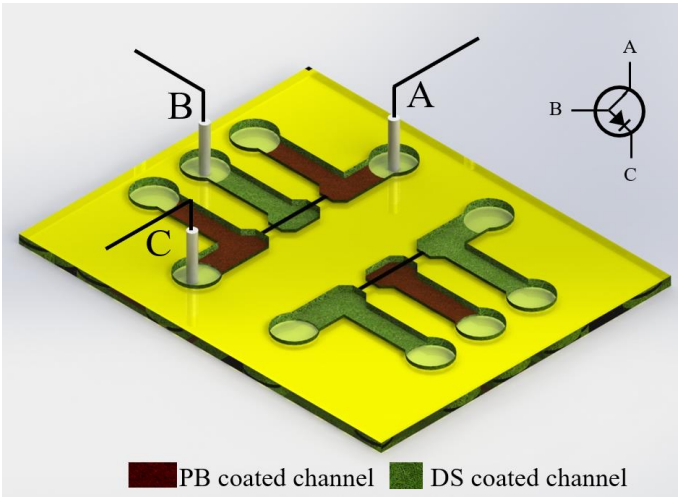

(b)

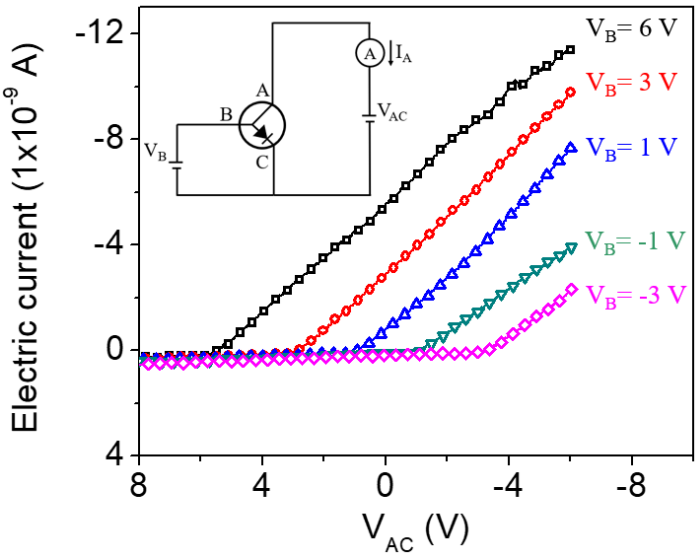

Figure 8-4. (a) Schematic diagram of the nanofluidic chip working as a BJT and the corresponding circuit connection. The nanochannel connects microchannels A and B, B and C. (b) Experimental results of the ionic current change when the BJT is serving as an ionic switch.

Traditional transistors are commonly used to switch or amplify signals. To investigate the performance of the ionic BJT in current signal manipulation, a constant ionic current, I_B, is applied as the input signal to terminal B, as shown in Figure 8-5 (a). Figure 8-5 (b) demonstrates the I-V curves across terminals A and C with a bias voltage of V_C at various I_B values. Here $I_B = 0$ indicates terminal B is open, and the measured I-V curve is essentially horizontal. In this case, the output ionic current I_A can be considered as the leakage current flowing through terminals A and C. When I_B injected to the

terminal is not zero, this current can be directed to terminal A or C by adjusting the bias voltage applied on terminal C, V_C. It is found that the output current I_A can be defined as three regimes in the curves based on the value and polarity of the applied voltage. In regime one, when a high negative V_C is applied, the ion channel across terminal A and B turns off, and the measured current I_A is essentially zero regardless of the value of I_B on terminal B. This indicates the ionic current is fully directed to terminal C in this regime. In regime two, I_A is proportional to the applied voltage V_C. In this regime, the input current I_B is directed to both terminal A and C, and $I_B = I_A + I_C$ since both ion channels turn on within the range of the given V_C. It is also observed that a larger I_B leads to a high current level of I_A in this regime with the same given value of V_C. As V_C further increases, I_A will saturate at a point with a positive V_C and according to input current I_B. I_A will not further increases after reaching the saturated point while a highly positive V_C is applied in regime three. In addition, a larger I_A can be obtained and saturate at a higher applied voltage with a larger I_B. In this saturation regime, it has $I_A = I_B + I_C$.

To consider the possibility of the nanofluidic ionic device serving as an amplifier, the saturated output current I_A is compared with the input current I_B to calculate the amplification gain (I_A/I_B). Figure 8-5 (c) and (d) demonstrate the measured I_A values at various I_B values with a given voltage bias of 5 V and the corresponding amplification gains, respectively. The results show that the current level of I_A is higher at larger I_B. Only a small amplification gain can be observed at low input current level that is approximately 1.4 when I_B is 0.5 nA. While I_B is larger than the 4 nA, the amplification gain almost drops to 1, and no significant amplification is achieved anymore. This is because the ionic current, I_C, flowing from terminal C to B is the leakage current through the reversed ionic diode, which is extremely low, in this regime. A previous study reported that it is possible to harvest high amplification gains with nanofluidic transistor only if the base area between two ion channels was shorter sufficiently to enable the mobile ions to migrate without caught by the applied electric field[215]. However, unlike charge carriers in metal semiconductors, the ion mobility in aqueous solutions is very low. As a result, it requires an extremely short length of the base area in the nanofluidic chip to realize significant amplification of signals through ionic devices.

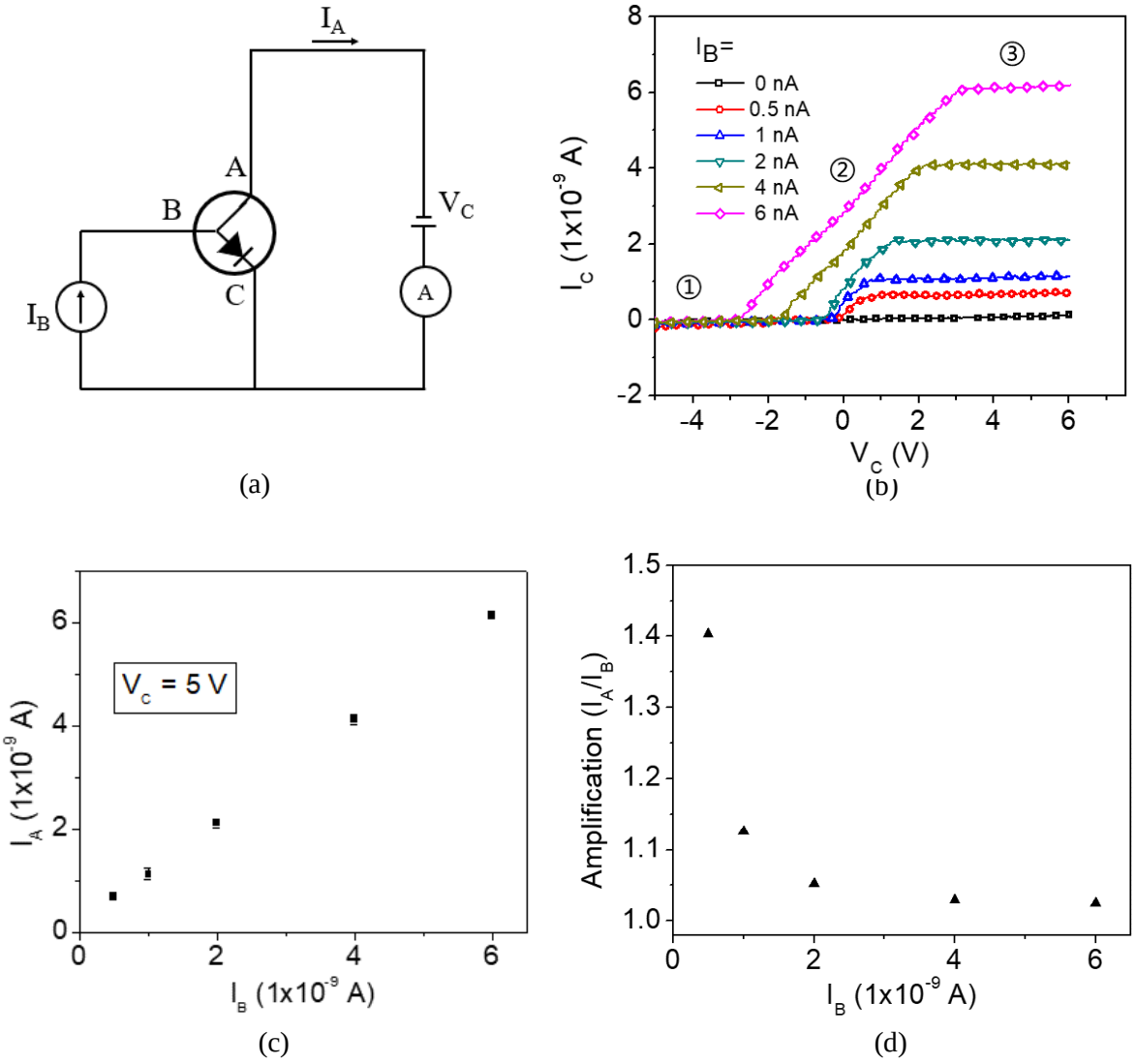

Figure 8-5. (a) Schematic of the BJT circuit connection. (b) Experimental I-V curve with different input current values. (c) Output ionic current values and (d) corresponding amplification gains of the transistor at various input current values.

8.3.3 Demonstration of full-wave ionic rectifier

Using the method developed in this work, a full-wave rectifier in the PDMS-based nanofluidic chip was designed and built. The rectifier consists of four ionic diodes, D_1, D_2, D_3, and D_4, as shown in Figure 8-6 (a) below. To characterize the performances of ionic diodes in the chip, current-voltage curves were tested for each ionic diode with KCl solution of 1 mM, respectively. To minimize errors

in measurements triggered by the sweep path of the applied voltage, the voltage was applied to the solution next to the DS modified channel (negatively charged) while the PB modified channel was grounded for all measurements. Figure 8-6 (b) demonstrates the experimental I-V curves measured from corresponding ionic diodes. These curves clearly show that the modified nanochannels have excellent diode behaviors. The ionic current is essentially zero when a reverse electric field is applied, indicating the ionic diode state is "OFF". While a forward electric field is applied, the ionic diode state is "ON". To build ionic circuits or rectifiers with proper operation, the performance consistency of ionic diodes is critical in the design. As shown in Figure 8-6 (b), the I-V curves for ionic diodes located on the same nanochannel are essentially following the same path with the applied sweep voltage, indicating a good consistency in ionic current rectification between them. The rectification ratio, which is defined as the ratio of the forward electric current to the reverse electric current at $\pm 5\ V$, is measured to evaluate the ionic diode performance. Figure 8-6 (c) displays the rectification ratios measured from different diodes in the nanofluidic chip. The rectification ratios are approximately 60 and similar for all diodes. That indicates all ionic diodes perform excellent rectification behavior and operate with similar rectification efficiency. A slight discrepancy in electric current between the ionic diodes on different nanochannels is caused by the inconsistency of sizes of the two paralleled nanochannels. The two nanochannels have similar widths but a slight difference in depths. The inconsistency of nanochannel size affects the ionic conductivity and generates a discrepancy in ionic current through the diode.

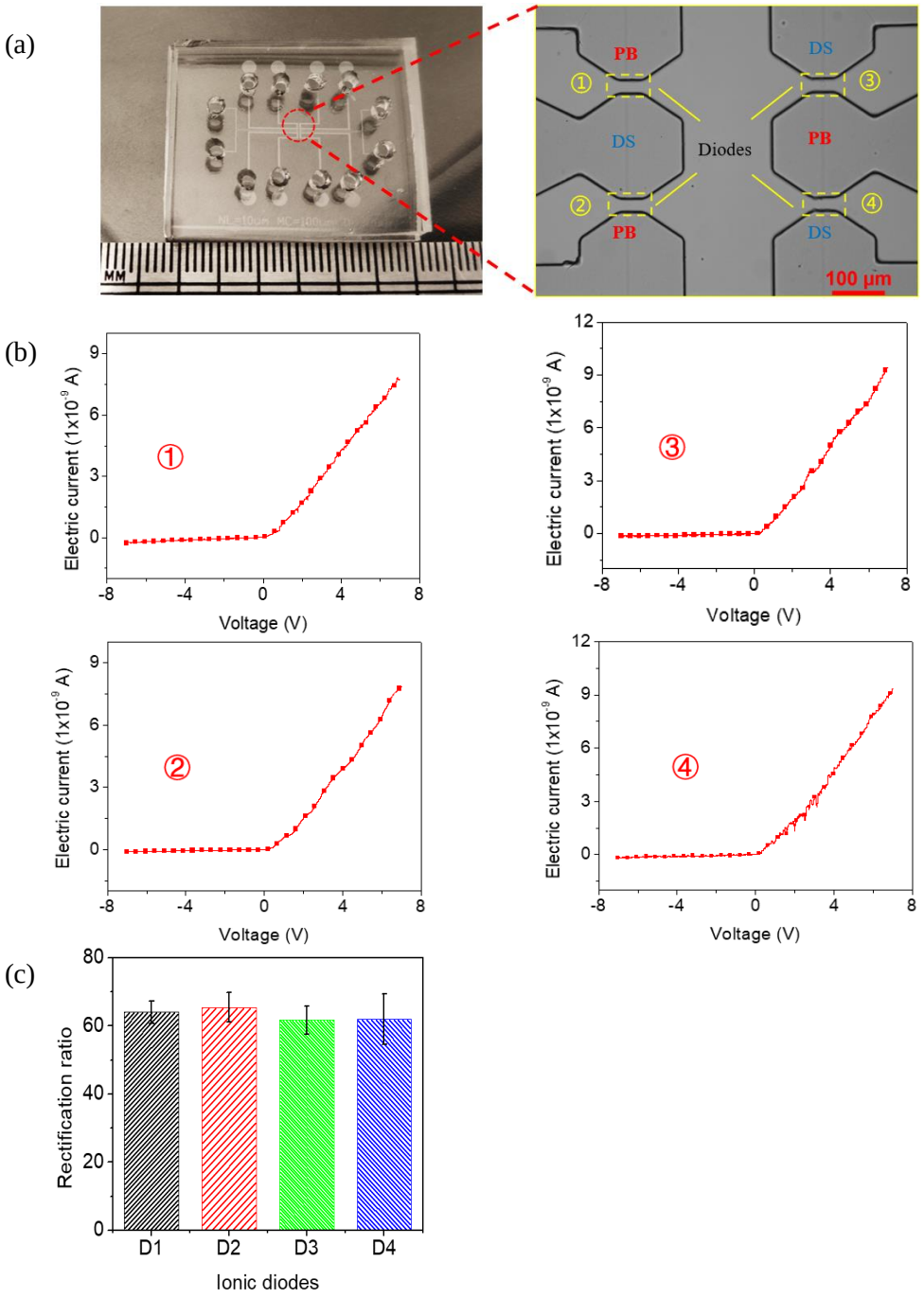

Figure 8-6. (a) A picture of the nanofluidic chip and the zoom-in view of the four ionic diodes of D_1, D_2, D_3, and D_4 captured by an optical microscope. (b) I-V curves of D_1, D_2, D_3, and D_4 under a sweep voltage of 250 mV/s. (c) Rectification ratios of ionic diodes (D_1, D_2, D_3, and D_4) at the bias voltage of $\pm 5\ V$.

Typically, a full-wave rectifier is used to convert AC signals to DC output. Figure 8-7 (a) demonstrates a schematic diagram of the ionic rectifier integrated into the nanofluidic chip and the corresponding circuit. To clarify the circuit connections, only the six working microchannels are schematically shown in this figure. There are two additional branches of microchannels on a real nanofluidic chip used to remove residual polyelectrolyte solutions from the middle junction area. The input AC signals were applied on terminals A, D, and C, F, and the output signals were measured by an electrometer through terminals B and E. Sine-wave and square-wave voltages were applied to the rectifier to characterize its performance by using a function generator. Both the input signal (V_{in}) and the output current (I_{out}) were monitored with an electrometer. To evaluate the working frequency limit of the rectifier, the output signals were measured at a series of square-wave voltages with various frequencies as well. The electrolyte solution, KCl of 1 mM was filled into the chip serving as the sample solution to supply mobile ions.

Figure 8-7 (b) and (c) show the experimental results of rectification of input signals with an amplitude of 3 V by using the full-wave ionic rectifier. As one can see from Figure 8-7 (b), as expected from a diode bridge circuit, the negative half cycles of are rectified to positive cycles, generating an output current with the same polarity when a sine-wave voltage was applied to the device. Similarly, as shown in Figure 8-7 (c), this ionic rectifier can rectify the square-wave input to a constant current output with a positive polarity regardless of the polarities of V_{in}. Moreover, the ionic rectifier circuit indicates that the output current flows different diodes when the polarity of V_{in} switches. For instance, the ionic diodes of D_1 and D_4 operate, and the ionic diodes of D_2 and D_3 are "OFF" while the polarity of V_{in} is positive. The current level across the operating ionic diodes will determine the value of I_{out}. It can be observed that the values of I_{out} at positive polarity and negative polarity of V_{in} are very close at the steady state due to the excellent performance consistency of ionic diodes on the same nanochannel. Such a performance is difficult to achieve in CNT bundle-based and porous membrane-based iontronic circuits because of the diode-to-diode variations caused by the undefined number of nanochannels.

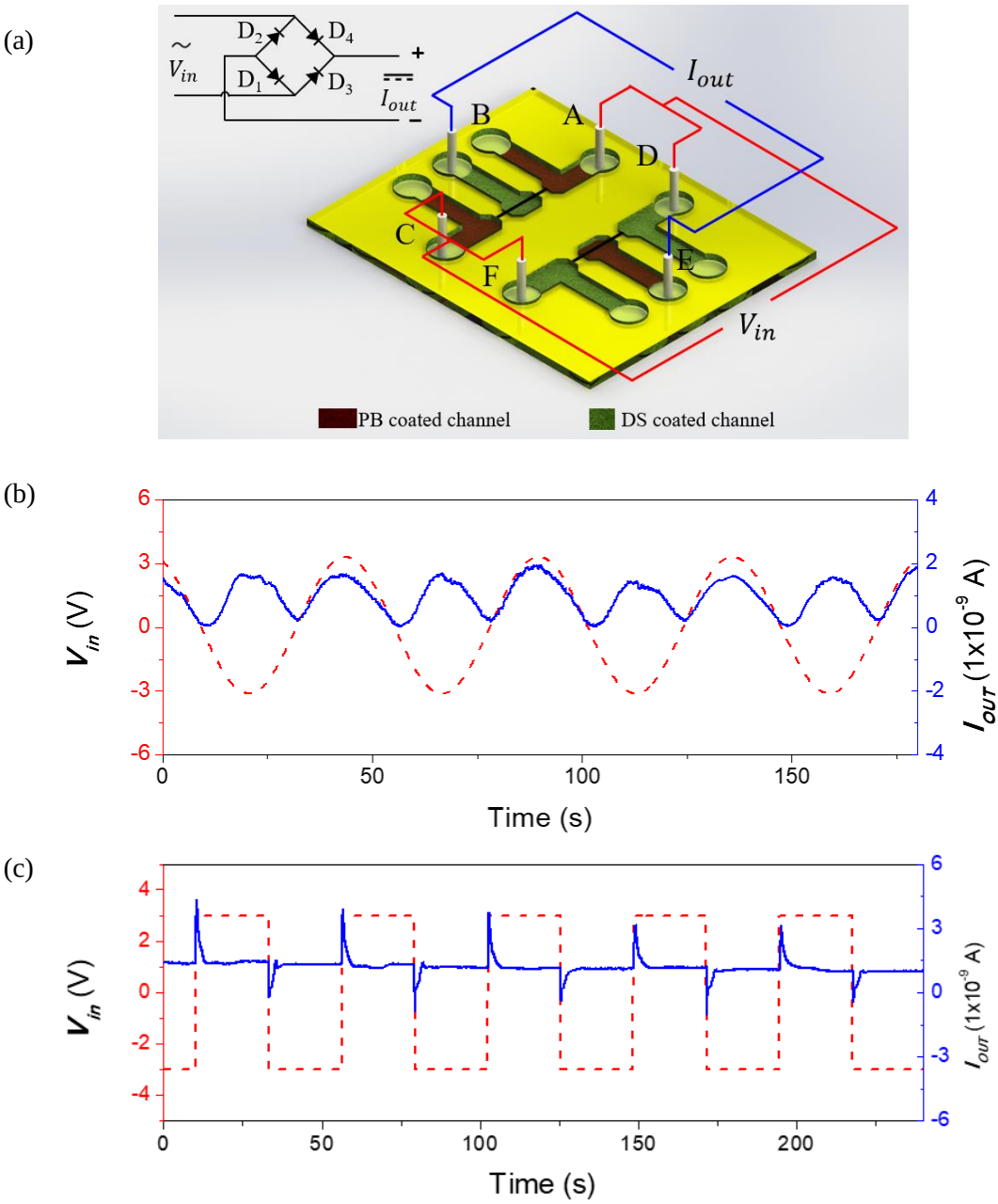

Figure 8-7. (a) A schematic of the nanofluidic chip working as an ionic rectifier and the corresponding circuit connection. (b) Full-wave rectified current signals of the Sine-wave input voltage and (c) the square-wave input voltage with an amplitude of 3 V (Red dash lines: input voltage; blue solid lines: output current).

It should be mentioned that a response time is required to re-build a stable ionic current when the polarity of the input voltage changes. This is because, as discussed above, the mobile ions in aqueous electrolyte solutions respond slower to the applied electric field than electrons and holes in semiconductors. Figure 8-8 (a) demonstrates a measured output current curve while the ionic rectifier it is rectifying a 0.07 Hz square-wave signal with an amplitude of 3 V. As can be seen from the figure, a peak will be generated in the output current curve when the polarity of V_{in} switches. The time, which takes to recover the output current to the constant value, is defined as the response time in this work. This response time is dominated by the speed of ion field construction under the driving electric field. Figure 8-8 (b) and (c) show examples of input polarity change-induced ionic current change while the ionic rectifier is rectifying a 0.07 Hz square-wave signal. As shown in Figure 8-8 (b), a downward peak was generated in the ionic current when the polarity of V_{in} switches from positive to negative. On the contrary, the ionic current increases rapidly and then recover to a constant value when the V_{in} changes to a positive value (Shown in Figure 8-8 (c)). The calculated response time is approximately 1.5 s for each switch of the input polarity. It is expected that the ionic rectifier is more suitable to work at low frequency and is possible to lose effectiveness when the input signal frequency is significantly high. To investigate the frequency effects on the performance of the ionic rectifier, square-wave signals with higher frequencies were applied to the rectifier. Figure 8-8 (d) and (e) show the experimentally measured output currents with square-wave signals at the frequencies of 0.1 Hz and 0.2 Hz, respectively. One can see that the rectifier can rectify the input signals to a positive output current at both applied frequencies. However, the stable state of the output current, where the output current can maintain a constant value, becomes short as the frequency increases. This is because the response time is essentially constant under different working frequencies. The response period, in which the rectifier eliminates the current change caused by the switch of polarity, will occupy a relatively large portion of the output current curve. When the frequency increases to 0.2 Hz, as shown in Figure 8-8 (e), the stable state is relatively shorter compared with the response period. The results indicate that the ionic rectifier operates more properly at low frequency. It was reported that the response range of the output signal can be shortened by improving the conductivity of the electrode, using ions with higher mobilities, and reducing the length of the nanochannel[223]. Our previous study also presented that the rectification performance of the ionic semiconductors can be improved by narrowing the micro-nano junctions of chips[274].

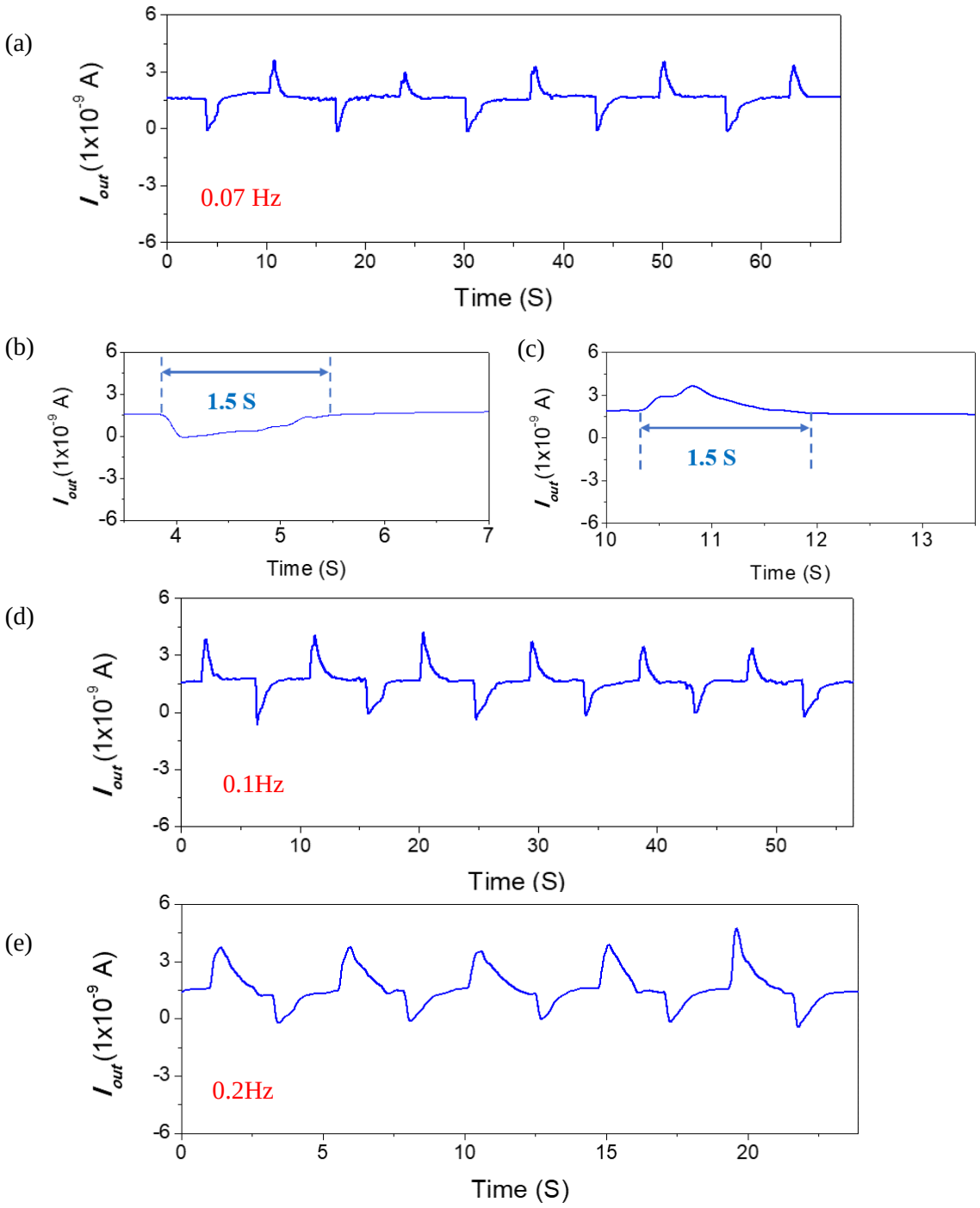

Figure 8-8. (a) Experimentally measured output current with an input square-wave voltage of 0.07 Hz. Examples of the current change when the input polarity switches to negative (b) and positive (c), respectively, at the working frequency of 0.07 Hz. (d) Experimentally measured output current at the

working frequency of 0.1 Hz. (e) Experimentally measured output current at the working frequency of 0.1 Hz.

8.4 Conclusions

This chapter reported a novel integrated iontronic circuit based on PDMS nanofluidic chips. Compared with previous technologies of iontronic devices, single PDMS nanochannels with well-defined dimensional features were utilized to build ionic diodes in this work, avoiding the diode-to-diode variations and leading to excellent performances in signal rectification through the designed circuits. An individual chip developed with the technology reported in the chapter can operate as either a bipolar junction transistor or full-wave bridge rectifier by modulating the circuit connections. The performances of multiple ionic diodes in the chip were characterized individually. All ionic diodes in the chip have the similar rectification behaviors. For the chip serving as a transistor, the mode of ionic switch and amplifier were both investigated. The results demonstrated that the ionic device can properly switch the ionic current flowing across the circuit by modulating the base voltage. Slight amplification can be achieved at low input signals. The full-wave rectifications of sine-wave signals and square-wave signals were demonstrated and confirmed by measuring the output ionic current. The presented PDMS-based iontronic devices are simple in fabrication and cost-friendly. By taking advantage of this method, it is easy to construct complex iontronic devices by integrating multiple iontronic components (i.e., diode, transistor) on a chip. The design provides promising potentials to improve biological computing and biochemical sensing.

Chapter 9 Conclusions and Future Work

This chapter presents a summary of the contributions of this thesis. Based on the conclusions, future research on the development of modified nanofluidic systems, the manipulation of electrokinetic transport in nanoscale, as well as the potential applications of the modified nanofluidic devices is introduced.

9.1 Summary of Contributions

This thesis systematically investigates the effects of surface modification on electrokinetic transport phenomena in nanoscale and presents their applications. The thesis starts with a fundamental research project on EOF measurement in PDMS nanochannels. By following this research, two fundamental research projects on EOF in modified PDMS nanochannels are conducted to investigate how the modified surfaces affect the electrokinetic transport phenomena. In the first project, EOF in PDMS nanochannels, the effects ion size, ion valence, and pH on EOF transport are analyzed. A comprehensive understanding of EOF in pristine PDMS nanochannels is provided. The followed projects experimentally investigate the EOF transport in DNA modified nanochannels and polyelectrolytes modified nanochannels. The surface charge regulation and size reduction of the nanochannel caused by surface modifications are experimentally measured. New properties of electrokinetic transport phenomena in the modified nanochannels are demonstrated and explained. Based on these properties of electrokinetic transport regulated by surface modifications, a nanofluidic diode is developed, and the working parameters of the nanofluidic diode are examined. By integrating nanofluidic diodes into nanofluidic chips, two applications are developed, including improved RPS detection systems and iontronic circuits. The working parameters involved in the improvement of the RPS system sensitivity by modified nanochannels are studied. For the iontronic circuits, the functions of the modified nanofluidic chip serving as a transistor or a rectifier are demonstrated, respectively. Overall, the major contributions of this thesis are summarized and listed as follows:

1） The influence factors of EOF transport in PDMS nanochannel were experimentally investigated with considering ion size. A better understanding of the EOF transport in nanoscale was provided.

2） PDMS nanochannels modified with DNAs were developed. EOF transport in DNA modified nanochannels was experimentally measured. UV illumination regulated EOF transport can be achieved in these modified nanochannels.

3） A method for modulating the surface charge and size of nanochannels was developed. This method can reduce the PDMS nanochannels size to smaller than 20 nm and alternatively change the polarity of the channel surface charge.

4） The manipulation of EOF transport in nanochannels modified with charged polyelectrolytes was achieved and demonstrated, experimentally.

5） A method for generating asymmetric surface charges along nanochannels was developed. Opposite polarities of surface charges at the two ends of the nanochannel were obtained. The ion distribution at the modified nanochannel ends was visualized under an applied electric field by using a fluorescent dye solution.

6） By using the developed surface modification method, a nanofluidic diode was designed and fabricated. The working principle of the nanofluidic was explained, and the working parameters were systematically investigated.

7） A numerical model for the nanofluidic diode was developed. The current rectification in the nanofluidic diode was simulated.

8） A numerical model for the RPS system with a modified sensing channel was developed. The ionic current changes caused by nanoparticle transport were simulated in nanochannels with different surface charges.

9） Based on the numerical results, the surface charge effects on the RPS detection were investigated. The effects of the polarity and value of surface charges on the RPS signal amplitudes were demonstrated.

10） With the surface modification method of polyelectrolyte adsorption, a improved RPS detection system with a nanofluidic diode serving as the sensing nanochannel was designed and fabricated. The enhancement in RPS signal amplitude by the modified RPS system was demonstrated experimentally.

11） A nanofluidic chip consists of two paralleled single nanochannels was fabricated for the development of iontronic circuits by using the solvent-induced cracking method.

12） By using the nanofluidic chip with surface modification, chip-scale integrated iontronic circuits were developed. Multiple nanofluidic diodes were fabricated and integrated into the nanofluidic

chip. This chip can work as either a bipolar junction transistor or a full-wave bridge ionic rectifier. The performances of the iontronic device were demonstrated experimentally.

9.2 Future work

This thesis has demonstrated the electrokinetic transport phenomena in nanochannels modified with DNAs and charged polyelectrolytes. The electrokinetic transport can be effectively manipulated with the modified nanochannels, and applications were developed based on the new transport properties of the modified nanochannels. Possible extensions of the present work are listed below.

9.2.1 Fabrication of smart nanochannels with stimuli-responsive polymers

We have demonstrated that electrokinetic transport phenomena can be manipulated by modifying the surface charge of nanochannels. Iontronic devices were developed based on the modified nanochannels. Improvements are still needed for the development of nanofluidic devices with multiple functions to meet the requirements of practical applications, including:

1) Develop nanochannels modified with stimuli-responsive polymers. In this thesis, the modified nanochannels have fixed surface properties and size once the surface modification is completed. In practical application, nanochannels with tunable properties are better choices to achieve more functions and meet multiple requirements. Polymers with tunable conformation and surface properties could be used to produce smart nanochannels that can respond to applied stimuli.

2) Develop nanochannels that can respond to the pH value of the working solution. Polymers with switchable surface charges and size, such as PVP or PAA, may be used to modify PDMS-based nanochannels and graft functional groups on the nanochannel walls. The modified nanochannel could change its interior size and polarity of surface charge according to the pH value.

3) Develop nanochannels that can respond to temperature. Temperature is a critical factor in the operation of nanofluidic devices. A method for grafting thermo-responsive polymers on PDMS surfaces can be developed. The operation status of the modified nanochannel can be controlled by temperature without any additives in the working solution.

4) Develop nanochannels that can respond to multiple stimuli. Multiple stimuli-responsive polymers can be used to decorate different areas of a nanochannel. A nanochannel with tunable surface charge, size, and ion selectivity can be formed with proper surface modification. This smart nanochannel has high potentials in developing new multiple-functional nanofluidic devices.

9.2.2 Characterization of electrokinetic transport phenomena in the nanochannels modified with stimuli-responsive polymers.

In the fundamental part, the electrokinetic properties in the modified nanochannel are studied, including EOF field and ion distribution under applied electric field. The brush structure and tunable electrokinetic properties of stimuli-responsive polymers could generate new transport phenomena in the modified nanochannel. To fully take advantage of nanochannels modified with stimuli-responsive polymers, a comprehensive understanding of the electrokinetic transport in the modified nanochannels is essential. Studies of influence factors of electrokinetic transport phenomena in the modified nanochannel should be conducted, including

1) Characterization of the surface modification of nanochannels. The density and uniformity of the coated polymer determine the surface properties of the modified nanochannel directly. Therefore, the characterization of surface modification is essential, and the optimal parameters for effective surface modification will be found.

2) Study the effects of ion size, ion valence, and ionic concentration on the EOF transport in the modified nanochannel. EOF is related to the channel size and surface charge in small nanochannels. In addition, the brush structure of the coated polymers also affects the EOF transport due to viscosity effects. Therefore, the study of EOF transport in the modified nanochannels is suggested.

3) Study the effects of temperature, pH value, and UV illumination on the EOF transport in the modified nanochannel. The nanochannels are modified with stimuli-responsive polymers. Hence, the electrokinetic properties vary according to the change of environment. The study of the EOF transport at different environments provides a guideline for the manipulation of electrokinetic transport phenomena in the modified nanochannels.

4) Study the ion distribution and selectivity in the modified nanochannel. The interactions between the mobile ions and immobilized polymer molecules on the nanochannel are key factors in determining the electrokinetic transport in the modified nanochannels. A comprehensive understanding of ion field distribution under the driving force of an applied electric field is essential. The results provide useful information for the application development of modified nanochannels.

5) Study the effects of channel length on the electrokinetic transport in the modified nanochannel. In this thesis, it is proved that the nanochannel length can affect the ion flow and ionic current in nanochannels with asymmetric surface charges. A long nanochannel results in a smaller rectification ratio. A shorter nanochannel is possible to generate crosstalk of different polymers in the wet surface modification, leading to less effective regulation of surface charges. Therefore, a suitable nanochannel length is a key factor in the development of smart nanochannels.

6) Study the integration of multiple modified nanochannels in a nanofluidic chip. The modified nanochannels have the potentials in building complex iontronic systems. With a good assembly of different modified nanochannels in a nanofluidic chip, an iontronic device with multiple functions can be developed.

9.2.3 Applications of the modified nanochannels

1) Improve the sensitivity and selectivity of RPS detection systems. Traditional RPS detection systems are functioned by detecting the signal pulse caused by the transport of nanoparticles or molecules. The resolution of RPS systems is determined by the volume ratio of the detected nanoparticles to the sensing nanochannel. The tunable size of the modified nanochannel enables a RPS detection system to measure a series of nanoparticles with different sizes while maintaining a high resolution. Furthermore, the switchable surface charges of coated polymers on the nanochannel regulate the selectivity of RPS detection systems.

2) Fabricate nanofluidic systems to achieve complex logic computing. Stimuli-responsive polymers with switchable surface charges and structures can be used to modified nanochannels. By controlling the aqueous environment in the modified nanochannel, the nanochannel can serve as a logic gate. The status of the nanochannel, such as block, open for selected ions, and fully open, can be tunable by switching the surface charge and structures of the immobilized polymer on the nanochannel.

3) Integrate multiple modified nanochannels in a chip. Individual nanochannel in the chip can be modified with a specific polymer and functionalized. Consequently, a complex nanofluidic system with multiple functions can be developed.

References

[1] W. Sparreboom, A. Van Den Berg, J.C.T. Eijkel, Principles and applications of nanofluidic transport, Nat. Nanotechnol. 4 (2009) 713–720. doi:10.1038/nnano.2009.332.

[2] J.C. Hulteen, K.B. Jirage, C.R. Martin, Introducing chemical transport selectivity into gold nanotubule membranes, J. Am. Chem. Soc. 120 (1998) 6603–6604. doi:10.1021/ja980045o.

[3] X.C. Xuan, Ion separation in nanofluidics, Electrophoresis. 29 (2008) 3737–3743. doi:10.1002/elps.200800098.

[4] R. Karnik, C. Duan, K. Castelino, H. Daiguji, A. Majumdar, Rectification of ionic current in a nanofluidic diode, Nano Lett. 7 (2007) 547–551. doi:10.1021/nl062806o.

[5] S.C. Nanotube, A. Agcl, Coherence Resonance in a Single-Walled Carbon Nanotube Ion Channel, Science (80-.). 329 (2010) 1320–1324. doi:10.1126/science.1193383.

[6] D. Stein, M. Kruithof, C. Dekker, Surface-Charge-Governed Ion Transport in Nanofluidic Channels, Phys. Rev. Lett. 93 (2004) 035901. doi:10.1103/PhysRevLett.93.035901.

[7] J. Sonnefeld, Surface charge density on spherical silica particles in aqueous alkali chloride solutions - Part 2. Evaluation of the surface charge density constants, Colloid Polym. Sci. 273 (1995) 932–938. doi:10.1007/BF00660370.

[8] T. Hiemstra, M. Wolthers, A Surface StructuralAapproach to Ion Adsorption: The Charge Distribution (CD) Model, J. Colloid Interface Sci. 179 (1996) 488–508. doi:10.1006/jcis.1996.0242.

[9] K.B. Oldham, A Gouy-Chapman-Stern model of the double layer at a (metal)/(ionic liquid) interface, J. Electroanal. Chem. 613 (2008) 131–138. doi:10.1016/j.jelechem.2007.10.017.

[10] D. Li, Electrokinetics in microfluidics, Academic Press, 2004.

[11] S. Movahed, D. Li, Electrokinetic transport through nanochannels, Electrophoresis. 32 (2011) 1259–1267. doi:10.1002/elps.201000564.

[12] A.A. Kornyshev, Double-layer in ionic liquids: Paradigm change?, J. Phys. Chem. B. 111 (2007) 5545–5557. doi:10.1021/jp067857o.

[13] M. V. Fedorov, A.A. Kornyshev, Towards understanding the structure and capacitance of

electrical double layer in ionic liquids, Electrochim. Acta. 53 (2008) 6835–6840. doi:10.1016/j.electacta.2008.02.065.

[14] S. Das, S. Chakraborty, Steric-effect-induced enhancement of electrical-double-layer overlapping phenomena, Phys. Rev. E - Stat. Nonlinear, Soft Matter Phys. 84 (2011) 2–5. doi:10.1103/PhysRevE.84.012501.

[15] I. Borukhov, D. Andelman, H. Orland, Adsorption of large ions from an electrolyte solution: A modified Poisson-Boltzmann equation, Electrochim. Acta. 46 (2000) 221–229. doi:10.1016/S0013-4686(00)00576-4.

[16] M. V. Fedorov, A.A. Kornyshev, Ionic liquid near a charged wall: Structure and capacitance of electrical double layer, J. Phys. Chem. B. 112 (2008) 11868–11872. doi:10.1021/jp803440q.

[17] B.D. Storey, M.Z. Bazant, Effects of electrostatic correlations on electrokinetic phenomena, Phys. Rev. E - Stat. Nonlinear, Soft Matter Phys. 86 (2012) 1–11. doi:10.1103/PhysRevE.86.056303.

[18] E. González-Tovar, M. Lozada-Cassou, W. Olivares, Electrokinetic flow in ultrafine slits: Ionic size effects, J. Chem. Phys. 94 (1991) 2219–2231. doi:10.1063/1.459892.

[19] K. Bohinc, V. Kralj-Iglič, A. Iglič, Thickness of electrical double layer. Effect of ion size, Electrochim. Acta. 46 (2001) 3033–3040. doi:10.1016/S0013-4686(01)00525-4.

[20] D. Ellwood, Americanisation or globalisation?, Hist. Today. 52 (2002) 18. doi:10.1016/j.jcis.2014.11.059.

[21] B.J. Kirby, E.F. Hasselbrink, Zeta potential of microfluidic substrates: 1. Theory, experimental techniques, and effects on separations, Electrophoresis. 25 (2004) 187–202. doi:10.1002/elps.200305754.

[22] E.E. Saka, C. Güler, The effects of electrolyte concentration, ion species and pH on the zeta potential and electrokinetic charge density of montmorillonite, Clay Miner. 41 (2006) 853–861. doi:10.1180/0009855064140224.

[23] A.M. El Badawy, T.P. Luxton, R.G. Silva, K.G. Scheckel, M.T. Suidan, T.M. Tolaymat, Impact of environmental conditions (pH, ionic strength, and electrolyte type) on the surface charge and aggregation of silver nanoparticles suspensions, Environ. Sci. Technol. 44 (2010)

1260–1266. doi:10.1021/es902240k.

[24] Z. Zheng, D.J. Hansford, A.T. Conlisk, Effect of multivalent on electroosmotic flow in micro- and nanochannels, Electrophoresis. 24 (2003) 3006–3017. doi:10.1002/elps.200305561.

[25] S. Pennathur, J.G. Santiago, Electrokinetic transport in nanochannels. 2. Experiments, Anal. Chem. 77 (2005) 6782–6789. doi:10.1021/ac0508346.

[26] M. Takahashi, ζ Potential of microbubbles in aqueous solutions: Electrical properties of the gas - Water interface, J. Phys. Chem. B. 109 (2005) 21858–21864. doi:10.1021/jp0445270.

[27] V. Tandon, S.K. Bhagavatula, W.C. Nelson, B.J. Kirby, Zeta potential and electroosmotic mobility in microfluidic devices fabricated from hydrophobic polymers: 1. The origins of charge, Electrophoresis. 29 (2008) 1092–1101. doi:10.1002/elps.200700734.

[28] Y.S. Choi, S.J. Kim, Electrokinetic flow-induced currents in silica nanofluidic channels, J. Colloid Interface Sci. 333 (2009) 672–678. doi:10.1016/j.jcis.2009.01.061.

[29] K. Da Huang, R.J. Yang, Electrokinetic behaviour of overlapped electric double layers in nanofluidic channels, Nanotechnology. 18 (2007) 115701. doi:10.1088/0957-4484/18/11/115701.

[30] J.P. Gillet, R. Sauvetre, J.F. Normant, Preparation et reactivite de fluorovinylzincs, Tetrahedron Lett. 26 (1985) 3999–4002. doi:10.1016/S0040-4039(00)98708-2.

[31] S. Tseng, Y.H. Tai, J.P. Hsu, Electrokinetic flow in a pH-regulated, cylindrical nanochannel containing multiple ionic species, Microfluid. Nanofluidics. 15 (2013) 847–857. doi:10.1007/s10404-013-1185-x.

[32] C.W. Outhwaite, L.B. Bhuiyan, An improved modified Poisson-Boltzmann equation in electric-double-layer theory, J. Chem. Soc. Faraday Trans. 2 Mol. Chem. Phys. 79 (1983) 707–718. doi:10.1039/F29837900707.

[33] L.H. Yeh, S. Xue, S.W. Joo, S. Qian, J.P. Hsu, Field effect control of surface charge property and electroosmotic flow in nanofluidics, J. Phys. Chem. C. 116 (2012) 4209–4216. doi:10.1021/jp211496b.

[34] M. Sadeghi, M.H. Saidi, A. Moosavi, A. Sadeghi, Geometry effect on electrokinetic flow and ionic conductance in pH-regulated nanochannels, Phys. Fluids. 29 (2017) 062002.

doi:10.1063/1.5003694.

[35] C. Largeot, C. Portet, J. Chmiola, P.L. Taberna, Y. Gogotsi, P. Simon, Relation between the ion size and pore size for an electric double-layer capacitor, J. Am. Chem. Soc. 130 (2008) 2730–2731. doi:10.1021/ja7106178.

[36] S. Chakraborty, A.K. Srivastava, Generalized model for time periodic electroosmotic flows with overlapping electrical double layers, Langmuir. 23 (2007) 12421–12428. doi:10.1021/la702109c.

[37] S. Das, A. Guha, S.K. Mitra, Exploring new scaling regimes for streaming potential and electroviscous effects in a nanocapillary with overlapping Electric Double Layers, Anal. Chim. Acta. 804 (2013) 159–166. doi:10.1016/j.aca.2013.09.061.

[38] M.Z. Bazant, M.S. Kilic, B.D. Storey, A. Ajdari, Towards an understanding of induced-charge electrokinetics at large applied voltages in concentrated solutions, Adv. Colloid Interface Sci. 152 (2009) 48–88. doi:10.1016/j.cis.2009.10.001.

[39] M.M. Hatlo, R. Van Roij, L. Lue, The electric double layer at high surface potentials: The influence of excess ion polarizability, Epl. 97 (2012). doi:10.1209/0295-5075/97/28010.

[40] D.J. Bonthuis, S. Gekle, R.R. Netz, Profile of the static permittivity tensor of water at interfaces: Consequences for capacitance, hydration interaction and ion adsorption, Langmuir. 28 (2012) 7679–7694. doi:10.1021/la2051564.

[41] R. Qiao, N.R. Aluru, Ion concentrations and velocity profiles in nanochannel electroosmotic flows, J. Chem. Phys. 118 (2003) 4692–4701. doi:10.1063/1.1543140.

[42] J.B. Freund, Electro-osmosis in a nanometer-scale channel studied by atomistic simulation, J. Chem. Phys. 116 (2002) 2194–2200. doi:10.1063/1.1431543.

[43] M. Rezaei, A.R. Azimian, D. Toghraie, Molecular dynamics study of an electro-kinetic fluid transport in a charged nanochannel based on the role of the stern layer, Phys. A Stat. Mech. Its Appl. 426 (2015) 25–34. doi:10.1016/j.physa.2015.01.043.

[44] L. Joly, C. Ybert, E. Trizac, L. Bocquet, Hydrodynamics within the Electric Double Layer on slipping surfaces, 257805 (2004) 1–4. doi:10.1103/PhysRevLett.93.257805.

[45] R. Qiao, N.R. Aluru, Charge inversion and flow reversal in a nanochannel electro-osmotic

flow, Phys. Rev. Lett. 92 (2004) 1–4. doi:10.1103/PhysRevLett.92.198301.

[46] M. Rezaei, A.R. Azimian, D. Toghraie, Molecular dynamics study of an electro-kinetic fluid transport in a charged nanochannel based on the role of the stern layer, Phys. A Stat. Mech. Its Appl. 426 (2015) 25–34. doi:10.1016/j.physa.2015.01.043.

[47] M. Rezaei, A.R. Azimian, D.T. Semiromi, The surface charge density effect on the electro-osmotic flow in a nanochannel: a molecular dynamics study, Heat Mass Transf. Und Stoffuebertragung. 51 (2015) 661–670. doi:10.1007/s00231-014-1441-y.

[48] S.Y. Mashayak, N.R. Aluru, A multiscale model for charge inversion in electric double layers, J. Chem. Phys. 148 (2018). doi:10.1063/1.5026975.

[49] S.C. Jacobson, J.P. Alarie, J.M. Ramsey, Electrokinetic Transport Through Nanometer Deep Channels, Micro Total Anal. Syst. (2001) 57–59.

[50] R. Peng, D. Li, Fabrication of polydimethylsiloxane (PDMS) nanofluidic chips with controllable channel size and spacing, Lab Chip. 16 (2016) 3767–3776. doi:10.1039/c6lc00867d.

[51] S. Arulanandam, D. Li, Determining ζ potential and surface conductance by monitoring the current in electro-osmotic flow, J. Colloid Interface Sci. 225 (2000) 421–428. doi:10.1006/jcis.2000.6783.

[52] L. Ren, C. Escobedo-Canseco, D. Li, A new method of evaluating the average electro-osmotic velocity in microchannels, J. Colloid Interface Sci. 250 (2002) 238–242. doi:10.1006/jcis.2002.8299.

[53] K.H. Chou, C. McCallum, D. Gillespie, S. Pennathur, An Experimental Approach to Systematically Probe Charge Inversion in Nanofluidic Channels, Nano Lett. 18 (2018) 1191–1195. doi:10.1021/acs.nanolett.7b04736.

[54] F.I. Uba, S.R. Pullagurla, N. Sirasunthorn, J. Wu, S. Park, R. Chantiwas, Y.K. Cho, H. Shin, S.A. Soper, Surface charge, electroosmotic flow and DNA extension in chemically modified thermoplastic nanoslits and nanochannels, Analyst. 140 (2015) 113–126. doi:10.1039/c4an01439a.

[55] H.A. Stone, A.D. Stroock, A. Ajdari, Engineering Flows in Small Devices, Annu. Rev. Fluid Mech. 36 (2004) 381–411. doi:10.1146/annurev.fluid.36.050802.122124.

[56] Y. Hu, C. Werner, D. Li, Electrokinetic Transport through Rough Microchannels, Anal. Chem. 75 (2003) 5747–5758. doi:10.1021/ac0347157.

[57] C.H. Chen, H. Lin, S.K. Lele, J.G. Santiago, Convective and absolute electrokinetic instability with conductivity gradients, J. Fluid Mech. 524 (2005) 263–303. doi:10.1017/S0022112004002381.

[58] H. Makamba, J.H. Kim, K. Lim, N. Park, J.H. Hahn, Surface modification of poly(dimethylsiloxane) microchannels, Electrophoresis. 24 (2003) 3607–3619. doi:10.1002/elps.200305627.

[59] J. Zhou, D.A. Khodakov, A. V. Ellis, N.H. Voelcker, Surface modification for PDMS-based microfluidic devices, Electrophoresis. 33 (2012) 89–104. doi:10.1002/elps.201100482.

[60] D. Belder, M. Ludwig, Surface modification in microchip electrophoresis, Electrophoresis. 24 (2003) 3595–3606. doi:10.1002/elps.200305648.

[61] D. Wu, J. Qin, B. Lin, Self-assembled epoxy-modified polymer coating on a poly(dimethylsiloxane) microchip for EOF inhibition and biopolymers separation, Lab Chip. 7 (2007) 1490–1496. doi:10.1039/b708877a.

[62] J.M. Goddard, J.H. Hotchkiss, Polymer surface modification for the attachment of bioactive compounds, Prog. Polym. Sci. 32 (2007) 698–725. doi:10.1016/j.progpolymsci.2007.04.002.

[63] Z. Zhang, C. Zuo, Q. Cao, Y. Ma, S. Chen, Modulation of electroosmotic flow using polyelectrolyte brushes: A molecular dynamics study, Macromol. Theory Simulations. 21 (2012) 145–152. doi:10.1002/mats.201100081.

[64] J. Huang, Y. Wang, M. Laradji, Flow control by smart nanofluidic channels: A dissipative particle dynamics simulation, Macromolecules. 39 (2006) 5546–5554. doi:10.1021/ma060628f.

[65] S.P. Adiga, D.W. Brenner, Flow control through polymer-grafted smart nanofluidic channels: Molecular dynamics simulations, Nano Lett. 5 (2005) 2509–2514. doi:10.1021/nl051843x.

[66] Q. Cao, C. Zuo, L. Li, Y. Ma, N. Li, Electroosmotic flow in a nanofluidic channel coated with neutral polymers, Microfluid. Nanofluidics. 9 (2010) 1051–1062. doi:10.1007/s10404-010-0620-5.

[67] H. Huang, E. Ruckenstein, Double layer interaction between two plates with polyelectrolyte brushes, J. Colloid Interface Sci. 275 (2004) 548–554. doi:10.1016/j.jcis.2004.02.058.

[68] J.L. Harden, D. Long, A. Ajdari, Influence of end-grafted polyelectrolytes on electro-osmosis along charged surfaces, Langmuir. 17 (2001) 705–715. doi:10.1021/la000594j.

[69] D.J. Anderson, A. Ralph, A Framework for Studying Emotions Across Phylogeny David, Cell. 157 (2014) 1–23. doi:10.1088/1367-2630/15/1/015008.Fluid.

[70] Y. Mao, D. Liu, S. Wang, S. Luo, W. Wang, Y. Yang, Q. Ouyang, L. Jiang, Alternating-electric-field-enhanced reversible switching of DNA nanocontainers with pH, Nucleic Acids Res. 35 (2007) 2–9. doi:10.1093/nar/gkl1161.

[71] Z. Guo, Y. Wang, A. Yang, G. Yang, The effect of pH on charge inversion and condensation of DNA, Soft Matter. 12 (2016) 6669–6674. doi:10.1039/c6sm01344a.

[72] G. Liu, Y. Shao, J. Peng, W. Dai, L. Liu, S. Xu, F. Wu, X. Wu, Highly thymine-dependent formation of fluorescent copper nanoparticles templated by ss-DNA, Nanotechnology. 24 (2013). doi:10.1088/0957-4484/24/34/345502.

[73] J. Zhou, A.V. Ellis, N.H. Voelcker, Recent developments in PDMS surface modification for microfluidic devices, Electrophoresis. 31 (2010) 2–16. doi:10.1002/elps.200900475.

[74] F. Xia, W. Guo, Y. Mao, X. Hou, J. Xue, H. Xia, L. Wang, Y. Song, H. Ji, Q. Ouyang, Y. Wang, L. Jiang, Gating of single synthetic nanopores by proton-driven DNA molecular motors, J. Am. Chem. Soc. 130 (2008) 8345–8350. doi:10.1021/ja800266p.

[75] M.S. Bello, P. De Besi, R. Rezzonico, P.G. Righetti, E. Casiraghi, Electroosmosis of polymer solutions in fused silica capillaries, Electrophoresis. 15 (1994) 623–626. doi:10.1002/elps.1150150186.

[76] S. Hjertén, High-performance electrophoresis, J. Chromatogr. 347 (1985) 191–198. doi:10.1016/S0021-9673(01)95485-8.

[77] G. Paumier, J. Sudor, A.M. Gue, F. Vinet, M. Li, Y.J. Chabal, A. Estève, M. Djafari-Rouhani, Nanoscale actuation of electrokinetic flows on thermoreversible surfaces, Electrophoresis. 29 (2008) 1245–1252. doi:10.1002/elps.200700396.

[78] S. Raafatnia, O.A. Hickey, C. Holm, Mobility reversal of polyelectrolyte-grafted colloids in

monovalent salt solutions, Phys. Rev. Lett. 113 (2014) 1–5. doi:10.1103/PhysRevLett.113.238301.

[79] G.S. Manning, The molecular theory of polyelectrolyte solutions with applications to the electrostatic properties of polynucleotides, Q. Rev. Biophys. 11 (1978) 179. doi:10.1017/S0033583500002031.

[80] J.L. Ravanat, T. Douki, J. Cadet, Direct and indirect effects of UV radiation on DNA and its components, J. Photochem. Photobiol. B Biol. 63 (2001) 88–102. doi:10.1016/S1011-1344(01)00206-8.

[81] J. Liu, C. Roussel, G. Lagger, P. Tacchini, H.H. Girault, Antioxidant sensors based on DNA-modified electrodes, Anal. Chem. 77 (2005) 7687–7694. doi:10.1021/ac0509298.

[82] S.K.M. Nalluri, J. Voskuhl, J.B. Bultema, E.J. Boekema, B.J. Ravoo, Light-responsive capture and release of DNA in a ternary supramolecular complex, Angew. Chemie - Int. Ed. 50 (2011) 9747–9751. doi:10.1002/anie.201103707.

[83] A.D. Tserepi, M.E. Vlachopoulou, E. Gogolides, Nanotexturing of poly(dimethylsiloxane) in plasmas for creating robust super-hydrophobic surfaces, Nanotechnology. 17 (2006) 3977–3983. doi:10.1088/0957-4484/17/15/062.

[84] J.L. Fritz, M.J. Owen, Hydrophobic recovery of plasma-treated polydimethylsiloxane, J. Adhes. 54 (1995) 33–45. doi:10.1080/00218469508014379.

[85] Q. He, Z. Liu, P. Xiao, R. Liang, N. He, Z. Lu, Preparation of hydrophilic poly(dimethylsiloxane) stamps by plasma-induced grafting, Langmuir. 19 (2003) 6982–6986. doi:10.1021/la020785h.

[86] J.Y. Lai, Y.Y. Lin, Y.L. Denq, S.S. Shyu, J.K. Chen, Surface modification of silicone rubber by gas plasma treatment, J. Adhes. Sci. Technol. 10 (1996) 231–242. doi:10.1163/156856196X00364.

[87] H. Ye, Z. Gu, D.H. Gracias, Kinetics of ultraviolet and plasma surface modification of poly(dimethylsiloxane) probed by sum frequency vibrational spectroscopy, Langmuir. 22 (2006) 1863–1868. doi:10.1021/la052030r.

[88] K. Efimenko, W.E. Wallace, J. Genzer, Surface modification of Sylgard-184 poly(dimethyl siloxane) networks by ultraviolet and ultraviolet/ozone treatment, J. Colloid Interface Sci. 254

(2002) 306–315. doi:10.1006/jcis.2002.8594.

[89] A. Tóth, I. Bertóti, M. Blazsó, G. Bánhegyi, A. Bognar, P. Szaplonczay, Oxidative damage and recovery of silicone rubber surfaces. I. X-ray photoelectron spectroscopic study, J. Appl. Polym. Sci. 52 (1994) 1293–1307. doi:10.1002/app.1994.070520914.

[90] H. Hillborg, J.F. Ankner, U.W. Gedde, G.D. Smith, H.K. Yasuda, K. Wikström, Crosslinked polydimethylsiloxane exposed to oxygen plasma studied by neutron reflectometry and other surface specific techniques, Polymer (Guildf). 41 (2000) 6851–6863. doi:10.1016/S0032-3861(00)00039-2.

[91] M.J. Owen, P.J. Smith, Plasma treatment of polydimethylsiloxane, J. Adhes. Sci. Technol. 8 (1994) 1063–1075. doi:10.1163/156856194X00942.

[92] B. Wang, Z. Abdulali-Kanji, E. Dodwell, J.H. Horton, R. Oleschuk, Surface characterization using chemical force microscopy and the flow performance of modified polydimethylsiloxane for microfluidic device applications, Electrophoresis. (2003) 1442–1450.

[93] D.C. Duffy, J.C. McDonald, O.J.A. Schueller, G.M. Whitesides, Rapid prototyping of microfluidic systems in poly(dimethylsiloxane), Anal. Chem. 70 (1998) 4974–4984. doi:10.1021/ac980656z.

[94] X. Ren, M. Bachman, C. Sims, G.P. Li, N. Allbritton, Electroosmotic properties of microfluidic channels composed of poly(dimethylsiloxane), J. Chromatogr. B Biomed. Sci. Appl. 762 (2001) 117–125. doi:10.1016/S0378-4347(01)00327-9.

[95] G.H. Seong, W. Zhan, R.M. Crooks, Fabrication of microchambers defined by photopolymerized hydrogels and weirs within microfluidic systems: Application to DNA hybridization, Anal. Chem. 74 (2002) 3372–3377. doi:10.1021/ac020069k.

[96] J. Moorthy, D.J. Beebe, In situ fabricated porous filters for microsystems, Lab Chip. 3 (2003) 62–66. doi:10.1039/b300450c.

[97] C. Yu, M. Xu, F. Svec, J.M.J. Fréchet, Preparation of monolithic polymers with controlled porous properties for microfluidic chip applications using photoinitiated free-radical polymerization, J. Polym. Sci. Part A Polym. Chem. 40 (2002) 755–769. doi:10.1002/pola.10155.

[98] S. Hu, X. Ren, M. Bachman, C.E. Sims, G.P. Li, N. Allbritton, Cross-linked coatings for

electrophoretic separations in poly(dimethylsiloxane) microchannels, Electrophoresis. 24 (2003) 3679–3688. doi:10.1002/elps.200305592.

[99] S. Hu, X. Ren, M. Bachman, C.E. Sims, G.P. Li, N.L. Allbritton, Surface-Directed, Graft Polymerization within Microfluidic Channels, Anal. Chem. 76 (2004) 1865–1870. doi:10.1021/ac049937z.

[100] M. Ouyang, C. Yuan, R.J. Muisener, A. Boulares, J.T. Koberstein, Conversion of some siloxane polymers to silicon oxide by UV/ozone photochemical processes, Chem. Mater. 12 (2000) 1591–1596. doi:10.1021/cm990770d.

[101] J.K. Towns, F.E. Regnier, Capillary Electrophoretic Separations of Proteins Using Nonionic Surfactant Coatings, Anal. Chem. 63 (1991) 1126–1132. doi:10.1021/ac00011a013.

[102] Y.H. Dou, N. Bao, J.J. Xu, F. Meng, H.Y. Chen, Separation of proteins on surface-modified poly(dimethylsiloxane) microfluidic devices, Electrophoresis. 25 (2004) 3024–3031. doi:10.1002/elps.200405986.

[103] K. Boxshall, M.-H. Wu, Z. Cui, Z. Cui, J.F. Watts, M.A. Baker, Simple surface treatments to modify protein adsorption and cell attachment properties within a poly(dimethylsiloxane) micro-bioreactor, Surf. INTERFACE Anal. 20 (2005) 68–69. doi:10.1002/sia.

[104] W. Hellmich, J. Regtmeier, T.T. Duong, R. Ros, D. Anselmetti, A. Ros, Poly(oxyethylene) based surface coatings for poly(dimethylsiloxane) microchannels, Langmuir. 21 (2005) 7551–7557. doi:10.1021/la0510432.

[105] A. Lucke, J. Teßmar, E. Schnell, G. Schmeer, A. Göpferich, Biodegradable poly(D,L-lactic acid)-poly(ethylene glycol)-monomethyl ether diblock copolymers: Structures and surface properties relevant to their use as biomaterials, Biomaterials. 21 (2000) 2361–2370. doi:10.1016/S0142-9612(00)00103-4.

[106] A.K. Salem, S.M. Cannizzaro, M.C. Davies, S.J.B. Tendler, C.J. Roberts, P.M. Williams, K.M. Shakesheff, Synthesis and characterisation of a degradable poly(lactic acid)-poly(ethylene glycol) copolymer with biotinylated end groups, Biomacromolecules. 2 (2001) 575–580. doi:10.1021/bm010030+.

[107] S. Lee, J. Vörös, An aqueous-based surface modification of poly(dimethylsiloxane) with poly(ethylene glycol) to prevent biofouling, Langmuir. 21 (2005) 11957–11962.

doi:10.1021/la051932p.

[108] A. Papra, A. Bernard, D. Juncker, N.B. Larsen, B. Michel, E. Delamarche, Microfluidic Networks Made of Poly(dimethylsiloxane), Si, and Au Coated with Polyethylene Glycol for Patterning Proteins onto Surfaces, Langmuir. 17 (2001) 4090–4095. doi:10.1021/la0016930.

[109] E. Biddiss, D. Erickson, D. Li, Heterogeneous surface charge enhanced micromixing for electrokinetic flows, Anal. Chem. 76 (2004) 3208–3213. doi:10.1021/ac035451r.

[110] G. Decher, Fuzzy Nanoassemblies: Toward Layered Polymeric Multicomposites, Science (80-.). 277 (1997) 1232–1237. doi:10.1126/science.277.5330.1232.

[111] S. Bai, Z. Wang, J. Gao, X. Zhang, Hydrogen-bonding-directed layer-by-layer polymer films: Substrate effect on the microporous morphology variation, Eur. Polym. J. 42 (2006) 900–907. doi:10.1016/j.eurpolymj.2005.06.033.

[112] L. Wang, Z. Wang, X. Zhang, J. Shen, L. Chi, H. Fuchs, A new approach for the fabrication of an alternating multilayer film of poly(4-vinylpyridine) and poly(acrylic acid) based on hydrogen bonding, Macromol. Rapid Commun. 18 (1997) 509–514. doi:10.1002/marc.1997.030180609.

[113] Y. Liu, J.C. Fanguy, J.M. Bledsoe, C.S. Henry, Dynamic coating using polyelectrolyte multilayers for chemical control of electroosmotic flow in capillary electrophoresis microchips, Anal. Chem. 72 (2000) 5939–5944. doi:10.1021/ac000932l.

[114] K. Boonsong, M.M. Caulum, B.M. Dressen, O. Chailapakul, D.M. Cropek, C.S. Henry, Influence of polymer structure on electroosmotic flow and separation efficiency in successive multiple ionic layer coatings for microchip electrophoresis, Electrophoresis. 29 (2008) 3128–3134. doi:10.1002/elps.200800186.

[115] S.T. Dubas, J.B. Schlenoff, Factors controlling the growth of polyelectrolyte multilayers, Macromolecules. 32 (1999) 8153–8160. doi:10.1021/ma981927a.

[116] R. Haselberg, F.M. Flesch, A. Boerke, G.W. Somsen, Thickness and morphology of polyelectrolyte coatings on silica surfaces before and after protein exposure studied by atomic force microscopy, Anal. Chim. Acta. 779 (2013) 90–95. doi:10.1016/j.aca.2013.03.066.

[117] S. Minko, D. Usov, C. Froeck, M. Stamm, M. Müller, A. Scholl, Lateral versus Perpendicular Segregation in Mixed Polymer Brushes, Phys. Rev. Lett. 88 (2002) 4.

doi:10.1103/PhysRevLett.88.035502.

[118] S. Minko, D. Usov, E. Goreshnik, M. Stamm, Environment-adopting surfaces with reversibly switchable morphology, Macromol. Rapid Commun. 22 (2001) 206–211. doi:10.1002/1521-3927(200102)22:3<206::AID-MARC206>3.0.CO;2-#.

[119] D. Julthongpiput, Y.H. Lin, J. Teng, E.R. Zubarev, V. V. Tsukruk, Y-Shaped Amphiphilic Brushes with Switchable Micellar Surface Structures, J. Am. Chem. Soc. 125 (2003) 15912–15921. doi:10.1021/ja038051u.

[120] D.M. Jones, J.R. Smith, W.T.S. Huck, C. Alexander, Variable Adhesion of Micropatterned Thermoresponsive of, Adv. Mater. 14 (2002) 1130–1134.

[121] Y.G. Takei, T. Aoki, K. Sanui, N. Ogata, Y. Sakurai, T. Okano, Dynamic Contact Angle Measurement of Temperature-Responsive Surface Properties for Poly(N-isopropylacrylamide) Grafted Surfaces, Macromolecules. 27 (1994) 6163–6166. doi:10.1021/ma00099a035.

[122] R. Israëls, F.A.M. Leermakers, G.J. Fleer, E.B. Zhulina, Charged Polymeric Brushes: Structure and Scaling Relations, Macromolecules. 27 (1994) 3249–3261. doi:10.1021/ma00090a018.

[123] J. Pyun, T. Kowalewski, K. Matyjaszewski, Synthesis of Polymer Brushes Using Atom Transfer Radical Polymerization, Macromol. Rapid Commun. 24 (2003) 1043–1059. doi:10.1002/marc.200300078.

[124] F. Liu, M.W. Urban, Recent advances and challenges in designing stimuli-responsive polymers, Prog. Polym. Sci. 35 (2010) 3–23. doi:10.1016/j.progpolymsci.2009.10.002.

[125] H. Zhang, X. Hou, F. Yang, L. Li, Y. Dadong, Y. Tian, L. Jiang, Bioinspired Artificial Single Ion Pump, J. Am. Chem. Soc. 135 (2013) 16102–16110. doi:10.1021/ja4037669.

[126] T. Kokubo, H. Takadama, How useful is SBF in predicting in vivo bone bioactivity?, Biomaterials. 27 (2006) 2907–2915. doi:10.1016/j.biomaterials.2006.01.017.

[127] T. Seki, J.-Y. Kojima, K. Ichimura, Light-Driven Dot Films Consisting of Single Polymer Chain, J. Phys. Chem. B. 103 (1999) 10338–10340. doi:10.1021/jp992062l.

[128] B.C. Bunker, B.I. Kim, J.E. Houston, R. Rosario, A.A. Garcia, M. Hayes, D. Gust, S.T. Picraux, Direct Observation of Photo Switching in Tethered Spiropyrans Using the Interfacial

Force Microscope, Nano Lett. 3 (2003) 1723–1727. doi:10.1021/nl034759v.

[129] R. Rosario, D. Gust, M. Hayes, F. Jahnke, J. Springer, A.A. Garcia, Photon-modulated wettability changes on spiropyran-coated surfaces, Langmuir. 18 (2002) 8062–8069. doi:10.1021/la025963l.

[130] R. Rosario, D. Gust, M. Hayes, J. Springer, A.A. Garcia, Solvatochromic Study of the Microenvironment of Surface-bound Spiropyrans, Langmuir. 19 (2003) 8801–8806. doi:10.1021/la0344332.

[131] M.Z. Bazant, B.D. Storey, A.A. Kornyshev, Double layer in ionic liquids: Overscreening versus crowding, Phys. Rev. Lett. 106 (2011) 6–9. doi:10.1103/PhysRevLett.106.046102.

[132] W. Qu, D. Li, A model for overlapped EDL fields, J. Colloid Interface Sci. 224 (2000) 397–407. doi:10.1006/jcis.1999.6708.

[133] B.D. Coday, T. Luxbacher, A.E. Childress, N. Almaraz, P. Xu, T.Y. Cath, Indirect determination of zeta potential at high ionic strength: Specific application to semipermeable polymeric membranes, J. Memb. Sci. 478 (2015) 58–64. doi:10.1016/j.memsci.2014.12.047.

[134] E.R. Nightingale, Phenomenological theory of ion solvation. Effective radii of hydrated ions, J. Phys. Chem. 63 (1959) 1381–1387. doi:10.1021/j150579a011.

[135] B.E. Conway, E. Ayranci, Effective ionic radii and hydration volumes for evaluation of solution properties and ionic adsorption, J. Solution Chem. 28 (1999) 163–192. doi:10.1023/A:1021702230117.

[136] B. Tansel, J. Sager, T. Rector, J. Garland, R.F. Strayer, L. Levine, M. Roberts, M. Hummerick, J. Bauer, Significance of hydrated radius and hydration shells on ionic permeability during nanofiltration in dead end and cross flow modes, Sep. Purif. Technol. 51 (2006) 40–47. doi:10.1016/j.seppur.2005.12.020.

[137] Y. Yukselen, A. Kaya, Zeta potential of kaolinite in the presence of alkali, alkaline earth and hydrolyzable metal ions, Water. Air. Soil Pollut. 145 (2003) 155–168. doi:10.1023/A.

[138] S.H. Behrens, D.G. Grier, The charge of glass and silica surfaces, J. Chem. Phys. 115 (2001) 6716–6721. doi:10.1063/1.1404988.

[139] V. Malyarchuk, F. Hua, N.H. Mack, V.T. Velasquez, J.O. White, R.G. Nuzzo, J.A. Rogers,

High performance plasmonic crystal sensor formed by soft nanoimprint lithography, Opt. Express. 13 (2005) 5669. doi:10.1364/OPEX.13.005669.

[140] R. Peng, D. Li, Electroosmotic flow in single PDMS nanochannels, Nanoscale. 8 (2016) 12237–12246. doi:10.1039/c6nr02937j.

[141] M.A. Brown, A. Goel, Z. Abbas, Effect of Electrolyte Concentration on the Stern Layer Thickness at a Charged Interface, Angew. Chemie - Int. Ed. 55 (2016) 3790–3794. doi:10.1002/anie.201512025.

[142] J. Morag, M. Dishon, U. Sivan, The governing role of surface hydration in ion specific adsorption to silica: An AFM-based account of the hofmeister universality and its reversal, Langmuir. 29 (2013) 6317–6322. doi:10.1021/la400507n.

[143] J. Mähler, I. Persson, A study of the hydration of the alkali metal ions in aqueous solution, Inorg. Chem. 51 (2012) 425–438. doi:10.1021/ic2018693.

[144] Dongqing Li, Chapter 2 Basics of electrical double layer, Volume 2, Academic Press, 2004. doi:10.1016/S1573-4285(04)80024-3.

[145] A. Esfandiar, B. Radha, F.C. Wang, Q. Yang, S. Hu, S. Garaj, R.R. Nair, A.K. Geim, K. Gopinadhan, Size effect in ion transport through angstrom-scale slits, Science (80-.). 358 (2017) 511–513. doi:10.1126/science.aan5275.

[146] P.M. Dove, C.J. Nix, on the Dissolution Kinetics of Quartz, Geochim. Cosmochim. Acta. 61 (1997) 3329–3340.

[147] M.C. Lin, C.J. Chu, L.C. Tsai, H.Y. Lin, C.S. Wu, Y.P. Wu, Y.N. Wu, D.B. Shieh, Y.W. Su, C.D. Chen, Control and detection of organosilane polarization on nanowire field-effect transistors, Nano Lett. 7 (2007) 3656–3661. doi:10.1021/nl0719170.

[148] C. Lee, W. Blanchard, C. Wu, Direct control of the electroosmosis in capillary zone electrophoresis by using an external electric field, Anal. Chem. 1523 (1990) 1550–1552. doi:Doi 10.1021/Ac00213a043.

[149] M.C. Murphy, I. Rasnik, W. Cheng, T.M. Lohman, T. Ha, Probing Single-Stranded DNA Conformational Flexibility Using Fluorescence Spectroscopy, Biophys. J. 86 (2004) 2530–2537. doi:10.1016/S0006-3495(04)74308-8.

[150] H. Lodish, A. Berk, P. Matsudaira, K. Monty, K. Matthew, L. Zipursky, J. Darnell, Molecular Cell Biology Types of epithelia, (2004).

[151] A. Alizadeh, M.E. Warkiani, M. Wang, Manipulating electrokinetic conductance of nanofluidic channel by varying inlet pH of solution, Microfluid. Nanofluidics. 21 (2017) 1–15. doi:10.1007/s10404-017-1892-9.

[152] M. Wang, A. Revil, Electrochemical charge of silica surfaces at high ionic strength in narrow channels, J. Colloid Interface Sci. 343 (2010) 381–386. doi:10.1016/j.jcis.2009.11.039.

[153] N. Bag, S. Bhattacharyya, P.P. Gopmandal, H. Ohshima, Electroosmotic flow reversal and ion selectivity in a soft nanochannel, Colloid Polym. Sci. 296 (2018) 849–859. doi:10.1007/s00396-018-4293-z.

[154] G.S. Manning, The molecular theory of polyelectrolyte solutions with applications to the electrostatic properties of polynucleotides, Q. Rev. Biophys. 11 (1978) 179. doi:10.1017/s0033583500002031.

[155] S.L. Llopis, J. Osiri, S.A. Soper, Surface modification of poly(methyl methacrylate) microfluidic devices for high-resolution separations of single-stranded DNA, Electrophoresis. 28 (2007) 984–993. doi:10.1002/elps.200600435.

[156] M. Wang, Q. Kang, E. Ben-Naim, Modeling of electrokinetic transport in silica nanofluidic channels, Anal. Chim. Acta. 664 (2010) 158–164. doi:10.1016/j.aca.2010.02.018.

[157] P.P. Gopmandal, S. Bhattacharyya, M. Banerjee, H. Ohshima, Electrophoresis of diffuse soft particles with dielectric charged rigid core grafted with charge regulated inhomogeneous polymer segments, Colloids Surfaces A Physicochem. Eng. Asp. 504 (2016) 116–125. doi:10.1016/j.colsurfa.2016.05.021.

[158] H. Chen, S.P. Meisburger, S.A. Pabit, J.L. Sutton, W.W. Webb, L. Pollack, Ionic strength-dependent persistence lengths of single-stranded RNA and DNA, Proc. Natl. Acad. Sci. 109 (2012) 799–804. doi:10.1073/pnas.1119057109.

[159] I. Wong, C.M. Ho, Surface molecular property modifications for poly(dimethylsiloxane) (PDMS) based microfluidic devices, Microfluid. Nanofluidics. 7 (2009) 291–306. doi:10.1007/s10404-009-0443-4.

[160] W.S. Bae, A.J. Convertine, C.L. McCormick, M.W. Urban, Effect of sequential layer-by-layer

surface modifications on the surface energy of plasma-modified poly(dimethylsiloxane), Langmuir. 23 (2007) 667–672. doi:10.1021/la062281f.

[161] B.G. De Geest, N.N. Sanders, G.B. Sukhorukov, J. Demeester, S.C. De Smedt, Release mechanisms for polyelectrolyte capsules, Chem. Soc. Rev. 36 (2007) 636–649. doi:10.1039/b600460c.

[162] P. Bertrand, A. Jonas, A. Laschewsky, R. Legras, Ultrathin polymer coatings by complexation of polyelectrolytes at interfaces: suitable materials, structure and properties Scheme of the electrostatic layer-by-layer self-assembly (ESA), Macromol. Rapid Commun. 21 (2000) 319–348. https://onlinelibrary.wiley.com/doi/pdf/10.1002/%28SICI%291521-3927%2820000401%2921%3A7%3C319%3A%3AAID-MARC319%3E3.0.CO%3B2-7.

[163] H.G.M. van de Steeg, M.A.C. Stuart, A. de keizer, B.H. Bijsterbosch, Polyelectrolyte Adsorption: A Subtle Balance of Forces, Langmuir. 8 (1992) 2538–2546. doi:10.1021/la00046a030.

[164] Z.L. Zhi, D.T. Haynie, Direct evidence of controlled structure reorganization in a nanoorganized polypeptide multilayer thin film, Macromolecules. 37 (2004) 8668–8675. doi:10.1021/ma049136y.

[165] E. Donath, D. Walther, V.N. Shilov, E. Knippel, A. Budde, K. Lowack, C.A. Helm, H. Möhwald, Nonlinear Hairy Layer Theory of Electrophoretic Fingerprinting Applied to Consecutive Layer by Layer Polyelectrolyte Adsorption onto Charged Polystyrene Latex Particles, Langmuir. 13 (1997) 5294–5305. doi:10.1021/la970090u.

[166] Y. Guo, W. Geng, J. Sun, Layer-by-layer deposition of polyelectrolyte-polyelectrolyte complexes for multilayer film fabrication, Langmuir. 25 (2009) 1004–1010. doi:10.1021/la803479a.

[167] S. Minko, M. Müller, M. Motornov, M. Nitschke, K. Grundke, M. Stamm, Two-level structured self-adaptive surfaces with reversibly tunable properties, J. Am. Chem. Soc. 125 (2003) 3896–3900. doi:10.1021/ja0279693.

[168] X. Hou, F. Yang, L. Li, Y. Song, L. Jiang, D. Zhu, A biomimetic asymmetric responsive single nanochannel, J. Am. Chem. Soc. 132 (2010) 11736–11742. doi:10.1021/ja1045082.

[169] M. Tagliazucchi, I. Szleifer, Stimuli-responsive polymers grafted to nanopores and other

nano-curved surfaces: Structure, chemical equilibrium and transport, Soft Matter. 8 (2012) 7292–7305. doi:10.1039/c2sm25777g.

[170] P.M. Biesheuvel, P. Stroeve, P.A. Barneveld, Effect of protein adsorption and ionic strength on the equilibrium partition coefficient of ionizable macromolecules in charged nanopores, J. Phys. Chem. B. 108 (2004) 17660–17665. doi:10.1021/jp047913q.

[171] T.D. Lazzara, K.H.A. Lau, A.I. Abou-Kandil, A.M. Caminade, J.P. Majoral, W. Knoll, Polyelectrolyte layer-by-layer deposition in cylindrical nanopores, ACS Nano. 4 (2010) 3909–3920. doi:10.1021/nn1007594.

[172] C.J. Roy, C. Dupont-Gillain, S. Demoustier-Champagne, A.M. Jonas, J. Landoulsi, Growth mechanism of confined polyelectrolyte multilayers in nanoporous templates, Langmuir. 26 (2010) 3350–3355. doi:10.1021/la903121e.

[173] H. Katayama, Y. Ishihama, N. Asakawa, Stable cationic capillary coating with successive multiple ionic polymer layers for capillary electrophoresis, Anal. Chem. 70 (1998) 5272–5277. doi:10.1021/ac980522l.

[174] R.R. Netz, D. Andelman, Neutral and charged polymers at interfaces, Phys. Rep. 380 (2003) 1–95. doi:10.1016/S0370-1573(03)00118-2.

[175] R.A. McAloney, M. Sinyor, V. Dudnik, M. Cynthia Goh, Atomic force microscopy studies of salt effects on polyelectrolyte multilayer film morphology, Langmuir. 17 (2001) 6655–6663. doi:10.1021/la010136q.

[176] C.C. Buron, C. Filiâtre, F. Membrey, C. Bainier, L. Buisson, D. Charraut, A. Foissy, Surface morphology and thickness of a multilayer film composed of strong and weak polyelectrolytes: Effect of the number of adsorbed layers, concentration and type of salts, Thin Solid Films. 517 (2009) 2611–2617. doi:10.1016/j.tsf.2008.10.036.

[177] J.F. Joanny, Polyelectrolyte adsorption and charge inversion, Eur. Phys. J. B. 9 (1999) 117–122. doi:10.1007/s100510050747.

[178] G. Decher, J. Schmitt, Fine-Tuning of the film thickness of ultrathin multilayer films composed of consecutively alternating layers of anionic and cationic polyelectrolytes, Trends Colloid Interface Sci. VI. 164 (2007) 160–164. doi:10.1007/bfb0116302.

[179] M. Muthukumar, Adsorption of a polyelectrolyte chain to a charged surface, J. Chem. Phys.

86 (2002) 7230–7235. doi:10.1063/1.452763.

[180] H. Alem, F. Blondeau, K. Glinel, S. Demoustier-Champagne, A.M. Jonas, Layer-by-layer assembly of polyelectrolytes in nanopores, Macromolecules. 40 (2007) 3366–3372. doi:10.1021/ma0703251.

[181] J.P. Derocher, P. Mao, J.Y. Kim, J. Han, M.F. Rubner, R.E. Cohen, Layer-by-layer deposition of all-nanoparticle multilayers in confined geometries, ACS Appl. Mater. Interfaces. 4 (2012) 391–396. doi:10.1021/am2014647.

[182] J. Li, R. Peng, D. Li, Effects of ion size, ion valence and pH of electrolyte solutions on EOF velocity in single nanochannels, Anal. Chim. Acta. 1059 (2019) 68–79. doi:10.1016/j.aca.2019.02.008.

[183] J. Li, D. Li, Electroosmotic flow velocity in DNA modified nanochannels, J. Colloid Interface Sci. 553 (2019) 31–39. doi:10.1016/j.jcis.2019.06.002.

[184] M.-S. Kang, C.R. Martin, Investigations of Potential-Dependent Fluxes of Ionic Permeates in Gold Nanotubule Membranes Prepared via the Template Method, Langmuir. 17 (2001) 2753–2759. doi:10.1021/la001186i.

[185] G. Xie, K. Xiao, Z. Zhang, X.Y. Kong, Q. Liu, P. Li, L. Wen, L. Jiang, A Bioinspired Switchable and Tunable Carbonate-Activated Nanofluidic Diode Based on a Single Nanochannel, Angew. Chemie - Int. Ed. 54 (2015) 13664–13668. doi:10.1002/anie.201505269.

[186] R. Karnik, R. Fan, M. Yue, D. Li, P. Yang, A. Majumdar, Electrostatic control of ions and molecules in nanofluidic transistors, Nano Lett. 5 (2005) 943–948. doi:10.1021/nl050493b.

[187] H. Daiguji, Y. Oka, K. Shirono, Nanofluidic diode and bipolar transistor, Nano Lett. 5 (2005) 2274–2280. doi:10.1021/nl051646y.

[188] H. Zhang, Y. Tian, L. Jiang, Fundamental studies and practical applications of bio-inspired smart solid-state nanopores and nanochannels, Nano Today. 11 (2016) 61–81. doi:10.1016/j.nantod.2015.11.001.

[189] B. Yameen, M. Ali, R. Neumann, W. Ensinger, W. Knoll, O. Azzaroni, Synthetic proton-gated ion channels via single solid-state nanochannels modified with responsive polymer brushes, Nano Lett. 9 (2009) 2788–2793. doi:10.1021/nl901403u.

[190] R. Peng, X.S. Tang, D. Li, Detection of Individual Molecules and Ions by Carbon Nanotube-Based Differential Resistive Pulse Sensor, Small. 14 (2018) 1–11. doi:10.1002/smll.201800013.

[191] Q. Pu, J. Yun, H. Temkin, S. Liu, Ion-enrichment and ion-depletion effect of nanochannel structures, Nano Lett. 4 (2004) 1099–1103. doi:10.1021/nl0494811.

[192] Z. Siwy, P. Apel, D. Dobrev, R. Neumann, R. Spohr, C. Trautmann, K. Voss, Ion transport through asymmetric nanopores prepared by ion track etching, Nucl. Instruments Methods Phys. Res. Sect. B Beam Interact. with Mater. Atoms. 208 (2003) 143–148. doi:10.1016/S0168-583X(03)00884-X.

[193] I. Vlassiouk, Z.S. Siwy, Nanofluidic diode, Nano Lett. 7 (2007) 552–556. doi:10.1021/nl062924b.

[194] X. Hou, H. Dong, D. Zhu, L. Jiang, Fabrication of stable single nanochannels with controllable ionic rectification, Small. 6 (2010) 361–365. doi:10.1002/smll.200901701.

[195] J.P. Hsu, Y.C. Chen, Y.M. Chen, S. Tseng, Influence of temperature and electroosmotic flow on the rectification behavior of conical nanochannels, J. Taiwan Inst. Chem. Eng. 93 (2018) 142–149. doi:10.1016/j.jtice.2018.10.013.

[196] W.K. Yen, W.C. Huang, J.P. Hsu, Ion current rectification behavior of a nanochannel having nonuniform cross-section, Electrophoresis. 41 (2020) 802–810. doi:10.1002/elps.201900396.

[197] J.P. Hsu, Y.M. Chen, S.T. Yang, C.Y. Lin, S. Tseng, Influence of salt valence on the rectification behavior of nanochannels, J. Colloid Interface Sci. 531 (2018) 483–492. doi:10.1016/j.jcis.2018.07.012.

[198] J.P. Hsu, Y.M. Chen, C.Y. Lin, S. Tseng, Electrokinetic ion transport in an asymmetric double-gated nanochannel with a pH-tunable zwitterionic surface, Phys. Chem. Chem. Phys. 21 (2019) 7773–7780. doi:10.1039/c9cp00266a.

[199] M. Zhang, X. Hou, J. Wang, Y. Tian, X. Fan, J. Zhai, L. Jiang, Light and pH cooperative nanofluidic diode using a spiropyran- functionalized single nanochannel, Adv. Mater. 24 (2012) 2424–2428. doi:10.1002/adma.201104536.

[200] P. Liu, G. Xie, P. Li, Z. Zhang, L. Yang, Y. Zhao, C. Zhu, X.Y. Kong, L. Jiang, L. Wen, A universal tunable nanofluidic diode via photoresponsive host–guest interactions, NPG Asia

Mater. 10 (2018) 849–857. doi:10.1038/s41427-018-0079-5.

[201] K. Ichimura, Light-Driven Motion of Liquids on a Photoresponsive Surface, Science (80-.). 288 (2000) 1624–1626. doi:10.1126/science.288.5471.1624.

[202] R. Peng, Y. Pan, Z. Li, S. Zhang, A.R. Wheeler, X. Tang, X. Liu, Ionotronics Based on Horizontally Aligned Carbon Nanotubes, Adv. Funct. Mater. 30 (2020) 1–14. doi:10.1002/adfm.202003177.

[203] W. Choi, Z.W. Ulissi, S.F.E. Shimizu, D.O. Bellisario, M.D. Ellison, M.S. Strano, Diameter-dependent ion transport through the interior of isolated single-walled carbon nanotubes, Nat. Commun. 4 (2013) 1–8. doi:10.1038/ncomms3397.

[204] S.J. Han, J. Tang, B. Kumar, A. Falk, D. Farmer, G. Tulevski, K. Jenkins, A. Afzali, S. Oida, J. Ott, J. Hannon, W. Haensch, High-speed logic integrated circuits with solution-processed self-assembled carbon nanotubes, Nat. Nanotechnol. 12 (2017) 861–865. doi:10.1038/nnano.2017.115.

[205] G. Hills, C. Lau, A. Wright, S. Fuller, M.D. Bishop, T. Srimani, P. Kanhaiya, R. Ho, A. Amer, Y. Stein, D. Murphy, Arvind, A. Chandrakasan, M.M. Shulaker, Modern microprocessor built from complementary carbon nanotube transistors, Nature. 572 (2019) 595–602. doi:10.1038/s41586-019-1493-8.

[206] Q. Cao, J. Tersoff, D.B. Farmer, Y. Zhu, S.J. Han, Carbon nanotube transistors scaled to a 40-nanometer footprint, Science (80-.). 356 (2017) 1369–1372. doi:10.1126/science.aan2476.

[207] A.I.M. Greer, I. Vasiev, B. Della-Rosa, N. Gadegaard, Fluorinated ethylene-propylene: A complementary alternative to PDMS for nanoimprint stamps, Nanotechnology. 27 (2016). doi:10.1088/0957-4484/27/15/155301.

[208] J. Li, D. Li, Polyelectrolyte adsorption in single small nanochannel by layer-by-layer method, J. Colloid Interface Sci. 561 (2020) 1–10. doi:10.1016/j.jcis.2019.11.116.

[209] J.P. Hsu, S.T. Yang, C.Y. Lin, S. Tseng, Ionic Current Rectification in a Conical Nanopore: Influences of Electroosmotic Flow and Type of Salt, J. Phys. Chem. C. 121 (2017) 4576–4582. doi:10.1021/acs.jpcc.6b09907.

[210] S. Dal Cengio, I. Pagonabarraga, Confinement-controlled rectification in a geometric nanofluidic diode, J. Chem. Phys. 151 (2019). doi:10.1063/1.5108723.

[211] W. Guan, R. Fan, M.A. Reed, Field-effect reconfigurable nanofluidic ionic diodes, Nat. Commun. 2 (2011) 2–9. doi:10.1038/ncomms1514.

[212] J.M. Perry, K. Zhou, Z.D. Harms, S.C. Jacobson, Ion transport in nanofluidic funnels, ACS Nano. 4 (2010) 3897–3902. doi:10.1021/nn100692z.

[213] Q. Liu, Y. Liu, B. Lu, Y. Wang, Y. Xu, J. Zhai, X. Fan, A high rectification ratio nanofluidic diode induced by an "ion pool," RSC Adv. 10 (2020) 7377–7383. doi:10.1039/c9ra09006a.

[214] Z. Zhang, X.Y. Kong, K. Xiao, G. Xie, Q. Liu, Y. Tian, H. Zhang, J. Ma, L. Wen, L. Jiang, A Bioinspired Multifunctional Heterogeneous Membrane with Ultrahigh Ionic Rectification and Highly Efficient Selective Ionic Gating, Adv. Mater. 28 (2016) 144–150. doi:10.1002/adma.201503668.

[215] L.J. Cheng, L.J. Guo, Ionic current rectification, breakdown, and switching in heterogeneous oxide nanofluidic devices, ACS Nano. 3 (2009) 575–584. doi:10.1021/nn8007542.

[216] T. Xiao, Q. Zhang, J. Jiang, J. Ma, Q. Liu, B. Lu, Z. Liu, J. Zhai, pH-Resistant Nanofluidic Diode Membrane for High-Performance Conversion of Salinity Gradient into Electric Energy, Energy Technol. 7 (2019) 1–8. doi:10.1002/ente.201800952.

[217] X. Sui, Z. Zhang, Z. Zhang, Z. Wang, C. Li, H. Yuan, L. Gao, L. Wen, X. Fan, L. Yang, X. Zhang, L. Jiang, Biomimetic Nanofluidic Diode Composed of Dual Amphoteric Channels Maintains Rectification Direction over a Wide pH Range, Angew. Chemie - Int. Ed. 55 (2016) 13056–13060. doi:10.1002/anie.201606469.

[218] Q. Zhang, Q. Liu, J. Kang, Q. Huang, Z. Liu, X. Diao, J. Zhai, Robust Sandwich-Structured Nanofluidic Diodes Modulating Ionic Transport for an Enhanced Electrochromic Performance, Adv. Sci. 5 (2018). doi:10.1002/advs.201800163.

[219] C.Y. Lin, J.P. Hsu, L.H. Yeh, Rectification of ionic current in nanopores functionalized with bipolar polyelectrolyte brushes, Sensors Actuators, B Chem. 258 (2018) 1223–1229. doi:10.1016/j.snb.2017.11.172.

[220] J.P. Hsu, H.H. Wu, C.Y. Lin, S. Tseng, Ion Current Rectification Behavior of Bioinspired Nanopores Having a pH-Tunable Zwitterionic Surface, Anal. Chem. 89 (2017) 3952–3958. doi:10.1021/acs.analchem.6b04325.

[221] Y. Wang, J. Zhai, Cell Junction Proteins-Mimetic Artificial Nanochannel System: Basic Logic

Gates Implemented by Nanofluidic Diodes, Langmuir. 35 (2019) 3171–3175. doi:10.1021/acs.langmuir.8b03986.

[222] Y. Bin Zheng, S. Zhao, S.H. Cao, S.L. Cai, X.H. Cai, Y.Q. Li, A temperature, pH and sugar triple-stimuli-responsive nanofluidic diode, Nanoscale. 9 (2017) 433–439. doi:10.1039/c6nr07339e.

[223] E.O. Gabrielsson, P. Janson, K. Tybrandt, D.T. Simon, M. Berggren, A four-diode full-wave ionic current rectifier based on bipolar membranes: Overcoming the limit of electrode capacity, Adv. Mater. 26 (2014) 5143–5147. doi:10.1002/adma.201401258.

[224] J. Gao, W. Guo, D. Feng, H. Wang, D. Zhao, L. Jiang, High-performance ionic diode membrane for salinity gradient power generation, J. Am. Chem. Soc. 136 (2014) 12265–12272. doi:10.1021/ja503692z.

[225] P. Waduge, R. Hu, P. Bandarkar, H. Yamazaki, B. Cressiot, Q. Zhao, P.C. Whitford, M. Wanunu, Nanopore-Based Measurements of Protein Size, Fluctuations, and Conformational Changes, ACS Nano. 11 (2017) 5706–5716. doi:10.1021/acsnano.7b01212.

[226] R. Vogel, G. Willmott, D. Kozak, G.S. Roberts, W. Anderson, L. Groenewegen, B. Glossop, A. Barnett, A. Turner, M. Trau, Quantitative sizing of nano/microparticles with a tunable elastomeric pore sensor, Anal. Chem. 83 (2011) 3499–3506. doi:10.1021/ac200195n.

[227] G.S. Roberts, S. Yu, Q. Zeng, L.C.L. Chan, W. Anderson, A.H. Colby, M.W. Grinstaff, S. Reid, R. Vogel, Tunable pores for measuring concentrations of synthetic and biological nanoparticle dispersions, Biosens. Bioelectron. 31 (2012) 17–25. doi:10.1016/j.bios.2011.09.040.

[228] W. Li, N.A.W. Bell, S. Hernández-Ainsa, V. V. Thacker, A.M. Thackray, R. Bujdoso, U.F. Keyser, Single protein molecule detection by glass nanopores, ACS Nano. 7 (2013) 4129–4134. doi:10.1021/nn4004567.

[229] W.H. Coulter, Means for counting particles suspended in a fluid. US Patent, 2656508, United States Pat. Off. Patentiert Am. 20 (1953) 1953. www.google.com/patents/US2656508.

[230] R.W. DeBlois, C.P. Bean, Counting and sizing of submicron particles by the resistive pulse technique, Rev. Sci. Instrum. 41 (1970) 909–916. doi:10.1063/1.1684724.

[231] R.W. DeBlois, R.K. Wesley, Sizes and concentrations of several type C oncornaviruses and

bacteriophage T2 by the resistive-pulse technique., J. Virol. 23 (1977) 227–233. doi:10.1128/jvi.23.2.227-233.1977.

[232] J. Larkin, R.Y. Henley, M. Muthukumar, J.K. Rosenstein, M. Wanunu, High-bandwidth protein analysis using solid-state nanopores, Biophys. J. 106 (2014) 696–704. doi:10.1016/j.bpj.2013.12.025.

[233] Y. Lin, Y.L. Ying, Y.T. Long, Nanopore confinement for electrochemical sensing at the single-molecule level, Curr. Opin. Electrochem. 7 (2018) 172–178. doi:10.1016/j.coelec.2017.12.002.

[234] B.M. Venkatesan, R. Bashir, Nanopore sensors for nucleic acid analysis, Nat. Nanotechnol. 6 (2011) 615–624. doi:10.1038/nnano.2011.129.

[235] G.F. Schneider, C. Dekker, DNA sequencing with nanopores, Nat. Biotechnol. 30 (2012) 326–328. doi:10.1038/nbt.2181.

[236] Y. Feng, Y. Zhang, C. Ying, D. Wang, C. Du, Nanopore-based fourth-generation DNA sequencing technology, Genomics, Proteomics Bioinforma. 13 (2015) 4–16. doi:10.1016/j.gpb.2015.01.009.

[237] J. Clarke, H.C. Wu, L. Jayasinghe, A. Patel, S. Reid, H. Bayley, Continuous base identification for single-molecule nanopore DNA sequencing, Nat. Nanotechnol. 4 (2009) 265–270. doi:10.1038/nnano.2009.12.

[238] D.W. Deamer, D. Branton, Characterization of nucleic acids by nanopore analysis, Acc. Chem. Res. 35 (2002) 817–825. doi:10.1021/ar000138m.

[239] X. Wu, Y. Kang, Y.N. Wang, D. Xu, D. Li, D. Li, Microfluidic differential resistive pulse sensors, Electrophoresis. 29 (2008) 2754–2759. doi:10.1002/elps.200700912.

[240] Y. Song, H. Zhang, C.H. Chon, X. Pan, D. Li, Nanoparticle detection by microfluidic Resistive Pulse Sensor with a submicron sensing gate and dual detecting channels-two stage differential amplifier, Sensors Actuators, B Chem. 155 (2011) 930–936. doi:10.1016/j.snb.2011.01.004.

[241] T. Zhou, Y. Song, Y. Yuan, D. Li, A novel microfluidic resistive pulse sensor with multiple voltage input channels and a side sensing gate for particle and cell detection, Anal. Chim. Acta. 1052 (2019) 113–123. doi:10.1016/j.aca.2018.11.049.

[242] Z. Liu, J. Li, J. Yang, Y. Song, X. Pan, D. Li, Improving particle detection sensitivity of a microfluidic resistive pulse sensor by a novel electrokinetic flow focusing method, Microfluid. Nanofluidics. 21 (2017) 1–11. doi:10.1007/s10404-016-1836-9.

[243] J. Li, D. Stein, C. McMullan, D. Branton, M.J. Aziz, J.A. Golovchenko, Ion-beam sculpting at nanometre length scales, Nature. 412 (2001) 166–169. doi:10.1038/35084037.

[244] H. Kwok, K. Briggs, V. Tabard-Cossa, Nanopore fabrication by controlled dielectric breakdown, PLoS One. 9 (2014). doi:10.1371/journal.pone.0092880.

[245] A.J. Storm, J.H. Chen, X.S. Ling, H.W. Zandbergen, C. Dekker, Fabrication of solid-state nanopores with single-nanometre precision, Nat. Mater. 2 (2003) 537–540. doi:10.1038/nmat941.

[246] B.N. Miles, A.P. Ivanov, K.A. Wilson, F. Dogan, D. Japrung, J.B. Edel, Single molecule sensing with solid-state nanopores: Novel materials, methods, and applications, Chem. Soc. Rev. 42 (2013) 15–28. doi:10.1039/c2cs35286a.

[247] W. Shi, A.K. Friedman, L.A. Baker, Nanopore Sensing, Anal. Chem. 89 (2017) 157–188. doi:10.1021/acs.analchem.6b04260.

[248] R. Gao, Y.L. Ying, B.Y. Yan, P. Iqbal, J.A. Preece, X. Wu, Ultrasensitive determination of mercury(II) using glass nanopores functionalized with macrocyclic dioxotetraamines, Microchim. Acta. 183 (2016) 491–495. doi:10.1007/s00604-015-1634-1.

[249] S.W. Kowalczyk, A.Y. Grosberg, Y. Rabin, C. Dekker, Modeling the conductance and DNA blockade of solid-state nanopores, Nanotechnology. 22 (2011). doi:10.1088/0957-4484/22/31/315101.

[250] G.R. Willmott, R. Chaturvedi, S.J.W. Cummins, L.G. Groenewegen, Actuation of Tunable Elastomeric Pores: Resistance Measurements and Finite Element Modelling, Exp. Mech. 54 (2014) 153–163. doi:10.1007/s11340-013-9795-5.

[251] G.R. Willmott, P.W. Moore, Reversible mechanical actuation of elastomeric nanopores, Nanotechnology. 19 (2008). doi:10.1088/0957-4484/19/47/475504.

[252] F. Haque, J. Li, H.C. Wu, X.J. Liang, P. Guo, Solid-state and biological nanopore for real-time sensing of single chemical and sequencing of DNA, Nano Today. 8 (2013) 56–74. doi:10.1016/j.nantod.2012.12.008.

[253] D. Stoddart, A.J. Heron, E. Mikhailova, G. Maglia, H. Bayley, Single-nucleotide discrimination in immobilized DNA oligonucleotides with a biological nanopore, Proc. Natl. Acad. Sci. U. S. A. 106 (2009) 7702–7707. doi:10.1073/pnas.0901054106.

[254] G.M. Cherf, K.R. Lieberman, H. Rashid, C.E. Lam, K. Karplus, M. Akeson, Automated forward and reverse ratcheting of DNA in a nanopore at 5-Å precision, Nat. Biotechnol. 30 (2012) 344–348. doi:10.1038/nbt.2147.

[255] H. Jin, D.A. Heller, J.H. Kim, M.S. Strano, Stochastic analysis of stepwise fluorescence quenching reactions on single-walled carbon nanotubes: Single molecule sensors, Nano Lett. 8 (2008) 4299–4304. doi:10.1021/nl802010z.

[256] H. Jin, D.A. Heller, M. Kalbacova, J.H. Kim, J. Zhang, A.A. Boghossian, N. Maheshri, M.S. Strano, Detection of single-molecule H2 O2 signalling from epidermal growth factor receptor using fluorescent single-walled carbon nanotubes, Nat. Nanotechnol. 5 (2010) 302–309. doi:10.1038/nnano.2010.24.

[257] J. Geng, K. Kim, J. Zhang, A. Escalada, R. Tunuguntla, L.R. Comolli, F.I. Allen, A. V. Shnyrova, K.R. Cho, D. Munoz, Y.M. Wang, C.P. Grigoropoulos, C.M. Ajo-Franklin, V.A. Frolov, A. Noy, Stochastic transport through carbon nanotubes in lipid bilayers and live cell membranes, Nature. 514 (2014) 612–615. doi:10.1038/nature13817.

[258] K. Besteman, J.O. Lee, F.G.M. Wiertz, H.A. Heering, C. Dekker, Enzyme-coated carbon nanotubes as single-molecule biosensors, Nano Lett. 3 (2003) 727–730. doi:10.1021/nl034139u.

[259] P. Chen, T. Mitsui, D.B. Farmer, J. Golovchenko, R.G. Gordon, D. Branton, Atomic layer deposition to fine-tune the surface properties and diameters of fabricated nanopores, Nano Lett. 4 (2004) 1333–1337. doi:10.1021/nl0494001.

[260] R. Wei, D. Pedone, A. Zürner, M. Döblinger, U. Rant, Fabrication of metallized nanopores in silicon nitride membranes for single-molecule sensing, Small. 6 (2010) 1406–1414. doi:10.1002/smll.201000253.

[261] M. Ayub, A. Ivanov, J. Hong, P. Kuhn, E. Instuli, J.B. Edel, T. Albrecht, Precise electrochemical fabrication of sub-20 nm solid-state nanopores for single-molecule biosensing, J. Phys. Condens. Matter. 22 (2010). doi:10.1088/0953-8984/22/45/454128.

[262] S. Xue, L.H. Yeh, Y. Ma, S. Qian, Tunable streaming current in a pH-regulated nanochannel by a field effect transistor, J. Phys. Chem. C. 118 (2014) 6090–6099. doi:10.1021/jp500996b.

[263] Y. Ma, Y.S. Su, S. Qian, L.H. Yeh, Analytical model for surface-charge-governed nanochannel conductance, Sensors Actuators, B Chem. 247 (2017) 697–705. doi:10.1016/j.snb.2017.03.080.

[264] R. Wei, V. Gatterdam, R. Wieneke, R. Tampé, U. Rant, Stochastic sensing of proteins with receptor-modified solid-state nanopores, Nat. Nanotechnol. 7 (2012) 257–263. doi:10.1038/nnano.2012.24.

[265] E.C. Yusko, J.M. Johnson, S. Majd, P. Prangkio, R.C. Rollings, J. Li, J. Yang, M. Mayer, Controlling protein translocation through nanopores with bio-inspired fluid walls, Nat. Nanotechnol. 6 (2011) 253–260. doi:10.1038/nnano.2011.12.

[266] V. Mussi, P. Fanzio, L. Repetto, G. Firpo, S. Stigliani, G.P. Tonini, U. Valbusa, " DNA-Dressed NAnopore" for complementary sequence detection, Biosens. Bioelectron. 29 (2011) 125–131. doi:10.1016/j.bios.2011.08.005.

[267] Y. Song, C. Wang, R. Sun, X. Pan, D. Li, Effect of induced surface charge of metal particles on particle sizing by resistive pulse sensing technique, J. Colloid Interface Sci. 423 (2014) 20–24. doi:10.1016/j.jcis.2014.02.018.

[268] S. Movahed, D. Li, Electrokinetic motion of a rectangular nanoparticle in a nanochannel, J. Nanoparticle Res. 14 (2012) 1–15. doi:10.1007/s11051-012-1032-0.

[269] R.A. Lucas, C.Y. Lin, L.A. Baker, Z.S. Siwy, Ionic amplifying circuits inspired by electronics and biology, Nat. Commun. 11 (2020) 1–9. doi:10.1038/s41467-020-15398-3.

[270] V.V.R. Nandigana, K. Jo, A. Timperman, N.R. Aluru, Asymmetric-Fluidic-Reservoirs Induced High Rectification Nanofluidic Diode, Sci. Rep. 8 (2018) 1–10. doi:10.1038/s41598-018-32284-7.

[271] J. Geng, K. Kim, J. Zhang, A. Escalada, R. Tunuguntla, L.R. Comolli, F.I. Allen, A. V. Shnyrova, K.R. Cho, D. Munoz, Y.M. Wang, C.P. Grigoropoulos, C.M. Ajo-Franklin, V.A. Frolov, A. Noy, Stochastic transport through carbon nanotubes in lipid bilayers and live cell membranes, Nature. 514 (2014) 612–615. doi:10.1038/nature13817.

[272] Z. Xie, J. Lei, M. Yang, Y. Li, X. Geng, S. Liu, J. Wang, Conical nanofluidic channel for

selective quantitation of melamine in combination with β-cyclodextrin and a single-walled carbon nanotube, Biosens. Bioelectron. 127 (2019) 200–206. doi:10.1016/j.bios.2018.12.020.

[273] H. Li, L. Zhou, Effects of Ambient Air and Temperature on Ionic Gel Gated Single-Walled Carbon Nanotube Thin-Film Transistor and Circuits, ACS Appl. Mater. Interfaces. 7 (2015) 22881–22887. doi:10.1021/acsami.5b05727.

[274] J. Li, D. Li, A surface charge governed nanofluidic diode based on a single polydimethylsiloxane (PDMS) nanochannel, J. Colloid Interface Sci. 596 (2021) 54–63. doi:10.1016/j.jcis.2021.03.126.

[275] R. Peng, D. Li, Fabrication of nanochannels on polystyrene surface, Biomicrofluidics. 9 (2015) 1–14. doi:10.1063/1.4918643.

[276] Q. Pu, J. Yun, H. Temkin, S. Liu, Ion-enrichment and ion-depletion effect of nanochannel structures, Nano Lett. 4 (2004) 1099–1103. doi:10.1021/nl0494811.

[277] R. Karnik, K. Castelino, C. Duan, A. Majumdar, Diffusion-limited patterning of molecules in nanofluidic channels, Nano Lett. 6 (2006) 1735–1740. doi:10.1021/nl061159y.

Appendices

Appendix A

Diffusion-limited patterning

As introduced in chapter 5, nanochannels can be modified by using LBL deposition of polyelectrolytes. The nanochannel size can be reduced, and surface charges can be modulated by using PB and DS solutions. To investigate the electrokinetic transport phenomena in partially coated nanochannels, diffusion limited patterning method is employed to generate opposite surface charges on the two halves[277].

In the surface modification, the PDMS nanochannels are connected to microchannels forming the nanofluidic chips and then modified with positively charged polyelectrolytes of PB by using the diffusion-limited method. Briefly, as shown in Figure A-1, the nanofluidic chip is filled with 0.1 M NaOH solution for 2 min after the plasma bonding process. Then, the chip is rinsed with DI-water to remove the residual NaOH solution for 3 times, each for 2 min. Afterward, DI-water is added into a "U" shape microchannel, and 5% PB solution is added into another microchannel. After leaving the chip standing for a certain time, DI-water is utilized to rinse the chip for 3 times and each for 2 min. Once the modification process is completed, the nanochannel will be partially coated with a PB layer, and the coated length depends on the diffusion time.

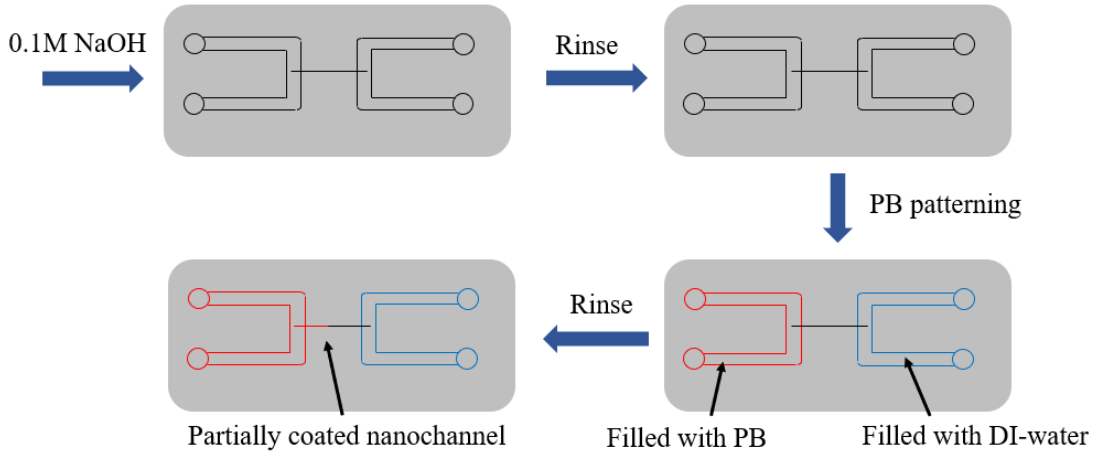

Figure A-1. Schematic diagram of the diffusion limited pattering process.

Measurement of the coated length

To measure the diffusion speed of the PB solution in the modified nanochannels, the fluorescent solution of FITC is used to indicate the coated length of the PB layer on the nanochannel surfaces. Since the modified nanochannel has opposite surface charges on the coated surface and uncoated surface, as shown in Figure A-2 (a), cations and anions will accumulate at different areas in the nanochannel when an electrical field is applied to the two sides of the nanochannel. In this work, the PB modified nanofluidic chip is filled with 1×10^{-4}M LiCl solution containing 100 μM FITC and connected to a DC power. Then, the fluorescent intensity along the nanochannel will be measured by using an optical microscope. Figure A-2 (b) shows the schematic diagram of the measurement system.

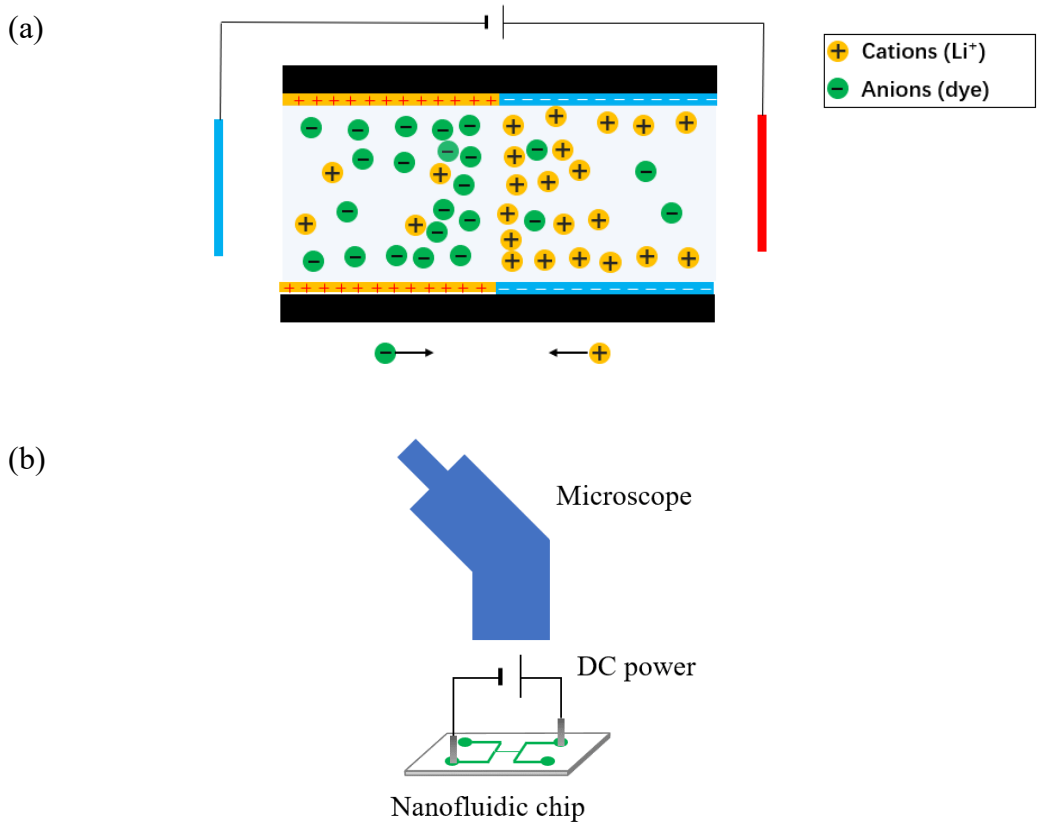

Figure A-2. (a) schematic diagram of the ion distribution in modified nanochannels under a forward electric field. (b) The fluorescent intensity measurement system.

Characterization of coated length in nanochannels

As introduced above, the surface charge will determine the ion distribution in the nanochannel. Anions that are the ions of FITC will mostly exist in the section of the nanochannel coated with PB layer due to the electrostatic interactions between the coated surface charges and the mobile ions. Only a few of them can exist in the section of the nanochannel with negative surface charges. As a result, the fluorescent intensity profile along the nanochannel will change corresponding to the PB coated length. The fluorescent intensity is relatively higher in the PB coated section of the nanochannel compared with that in the uncoated area. By measuring the fluorescent intensity profile, the coated length of the nanochannel can be obtained. Figure A-3 shows an example of the fluorescent intensity profile in the PB modified nanochannel measured by an optical microscope. The diffusion time is 45s. As one can see that the fluorescent intensity is relatively higher in the coated nanochannel area compared that in the uncoated area. The fluorescent intensity in microchannels is higher than that in nanochannels because the volume of FITC solution is extremely low in nanochannels.

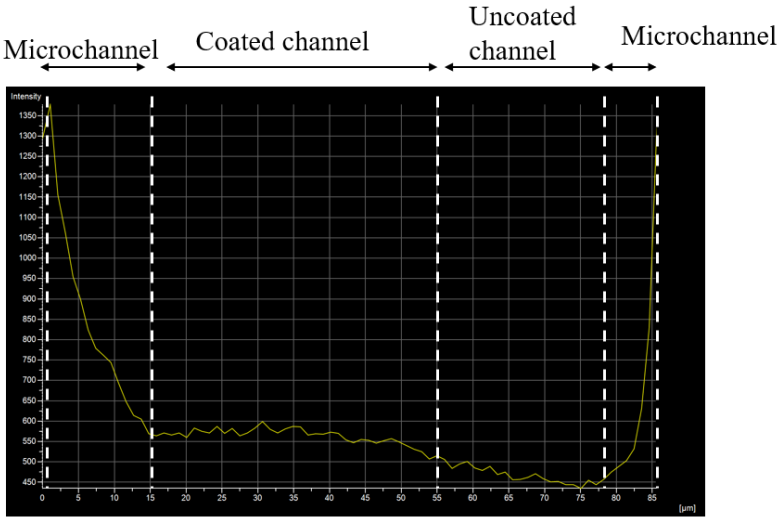

Figure A-3. An example of the fluorescent intensity profile of the PB modified nanochannel at the diffusion time of 45 s.

Figure A-4 shows the effects of the diffusion time on the PB coated length in nanochannels. As can be seen from the figure, the PB coated length is positively related to the diffusion time. Generally, the diffusion length should be linearly proportional to the diffusion time at the constant channel size. However, as shown in Figure A-4, the coated length increases dramatically at the low diffusion time and then gradually increases with the diffusion time further increases in both nanochannels with the sizes of 54 nm and 100 nm. This is because the nanochannel surfaces are negatively charged at the

initial state, and the positively charged PB molecules can enter the nanochannel easily. Once the entrance of the nanochannel is coated with PB layer, the surface charges become positive, thus inhibiting the transport of PB molecules through the nanochannel entrance. By comparing the results shown in Figure A-4 (b) and (c), it can be obtained that the coated length is proportional to the nanochannel size as well at the same diffusion time. A smaller nanochannel leads to a shorter coated length at the same diffusion time.

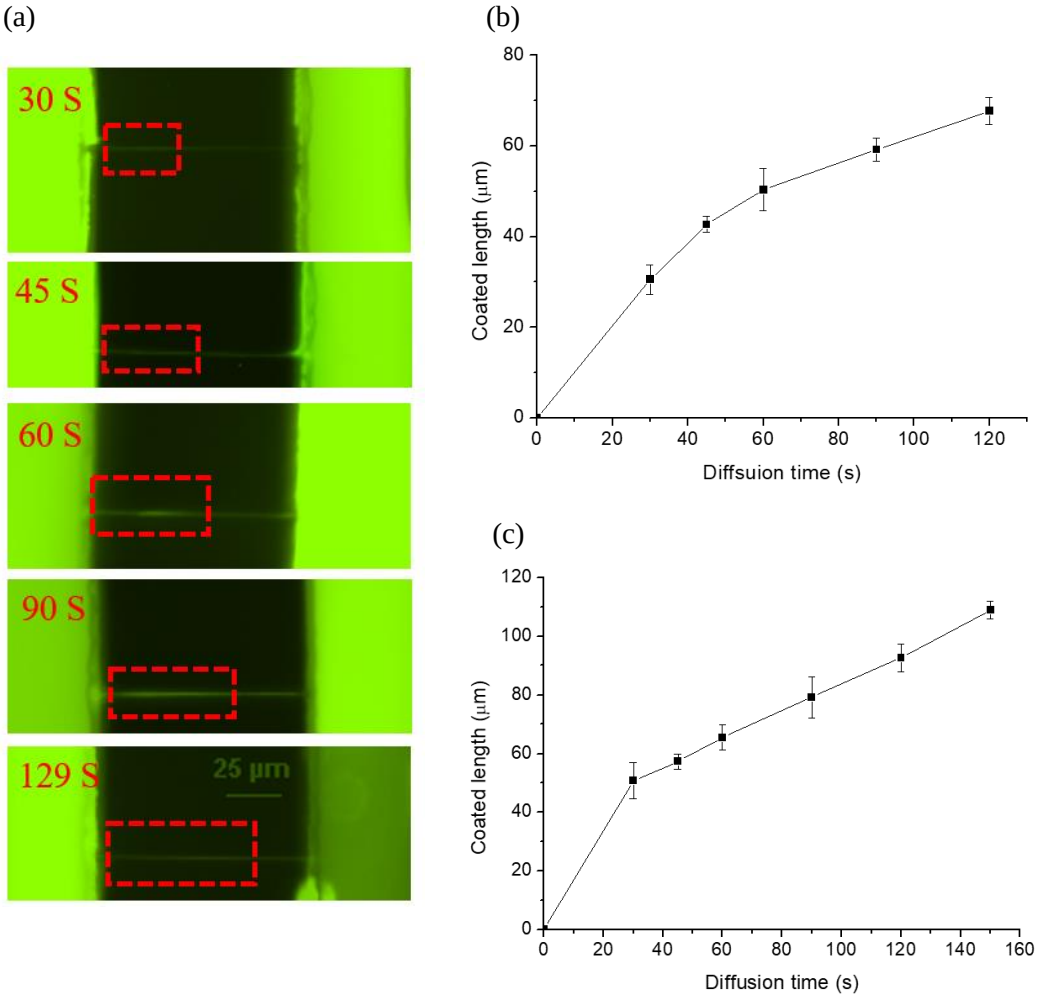

Figure A-4. (a) images of the FITC solution in modified nanochannels with different diffusion times. The PB coated section is marked by the red rectangle. (b) The coated length as a function of diffusion time in the nanochannel with depth of 54 nm. (c) The coated length as a function of diffusion time in the nanochannel with depth of 100 nm.

Appendix B

Ionic concentration effects on RPS signals

In the numerical simulation, ionic currents in nanochannels with different surface charges are calculated. The surface charge densities for the bipolar modified nanochannel are set as $\pm 5 \times 10^{-3}\ C/m^2$, respectively. For the positive nanochannel, the surface density is set as a uniform positive value of $5 \times 10^{-3}\ C/m^2$. For the negative nanochannel, the surface charge density is set as a uniform negative value of $5 \times 10^{-3}\ C/m^2$. The nanochannel length is 500 nm. This model is simulated with the bulk concentration of 10 mM and 100 mM, respectively. The relative permittivity of KCl solution, ε_r, is 80; the temperature T is 300 K; the density and the viscosity of the solution are $1 \times 10^3 kg/m^3$ and $1 \times 10^{-3}\ Pa \cdot s$, respectively; the diffusivities of K^+ and Cl^-, are $1.96 \times 10^{-9}\ m^2/s$ and $2.03 \times 10^{-9}\ m^2/s$, respectively. Figure B-1 shows the current change measured from nanochannel channels with different surface charges at the ionic concentration of 10 mM and 100 mM.

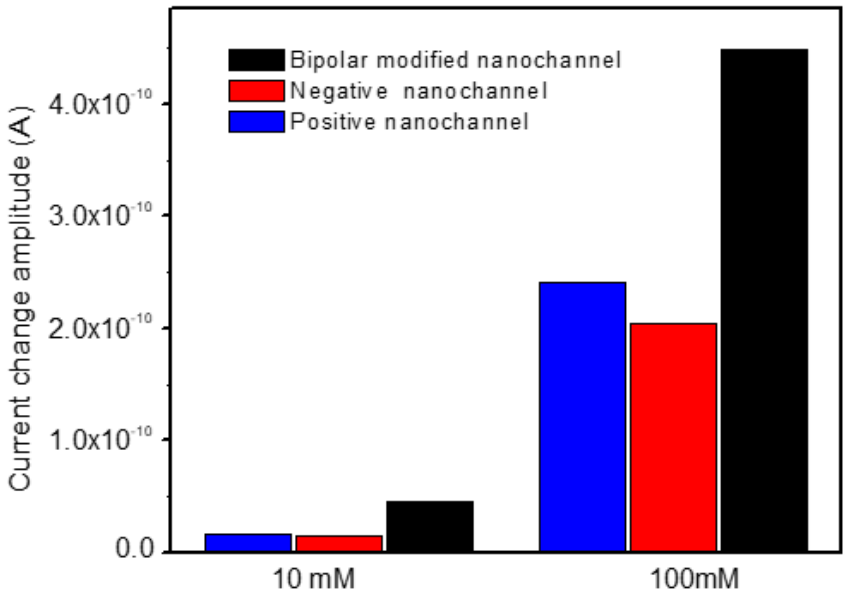

Figure B-1. Ionic current change amplitudes in modified nanochannels at the bulk concentration of 10 mM and 100 mM (Nanochannel length 500 nm).

Nanochannel length effects on rectification ratio

The nanochannel length will affect the effective electric field strength in the nanochannel when a constant electric voltage bias is applied. To better analyze the nanochannel length effects, an

experimental study about the effects of electric field strength on the performance of the bipolar modified nanochannel was conducted. In this experiment, the nanochannel length is 5000 nm, and the KCl solution of 10 mM was used as the sample solution. The total length of the main microchannels is 2 cm. The rectification ratio, which can be expressed as $f_{rec} = \left|\frac{I_{@+V}}{I_{@-V}}\right|$, was used to evaluate the current rectification performance of the bipolar modified nanochannel. When the nanochannel length is extremely small, such as 500 nm in the simulation, the ion accumulation or depletion could occupy most space of the nanochannel. As a result, a strong current rectification can be observed, and the exchange of counter-ions is accelerated with forward biased potential. A large promotion in ionic current and signal ratio can be observed. As the nanochannel length increases, ionic current rectification behaviors become less prominent, and the effective electric field decreases with the constant applied potential bias. Therefore, the enhancement ratio decreases correspondingly. However, the forward ionic current does not increase linearly with an increasing electric field strength in modified nanochannel. The increment in ionic current becomes gentle at high electric field strength. That means the promotion in ionic current in the modified nanochannel decreases as the applied electric field exceed a critical value. As shown in the following Figure B-2, the experimental results also illustrate that the ionic current rectification increases rapidly at low electric field strength. This increment becomes relatively gentle at high electric field strength. These results can explain the nanochannel length effects shown in Figure 6-9 (b). As the channel length increases from 3000~4000 nm, the effective electric field strength becomes smaller, and the current rectification reduces more significantly in the modified nanochannel. Hence, the decrease in the signal ratio is slightly steeper.

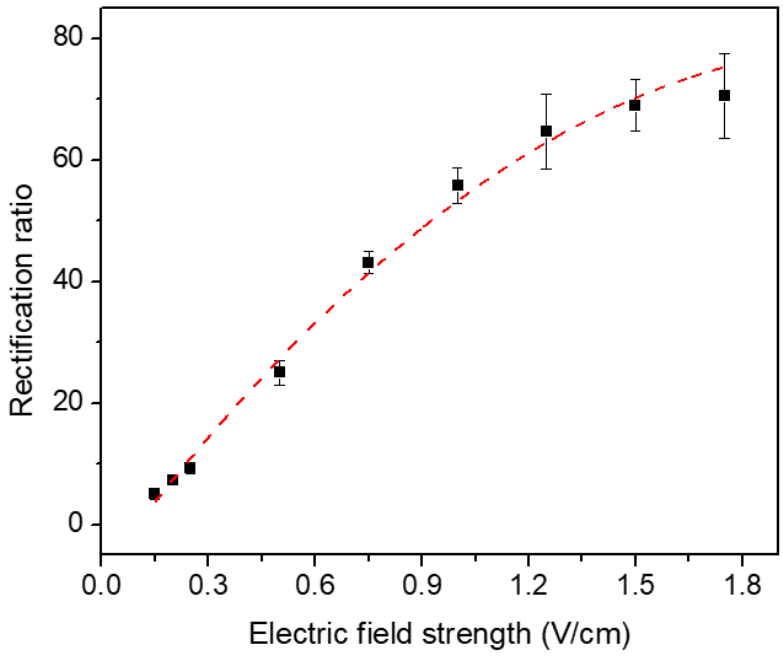

Figure B-2. The dependence of the ionic current rectification ratio on the applied electric field strength measured from a modified nanochannel with a 5 μm nanochannel.

In this work, the current rectification effects in the modified nanochannels were systematically measured. Each measurement was repeated at least three times. To simplify the figure, Figure 6-10 only shows an example of the current-voltage curve. Figure B-3 shows three current-voltage curves measured from the bipolar nanochannels modified with the same procedures. The results demonstrated an excellent reproducibility of the experiment.

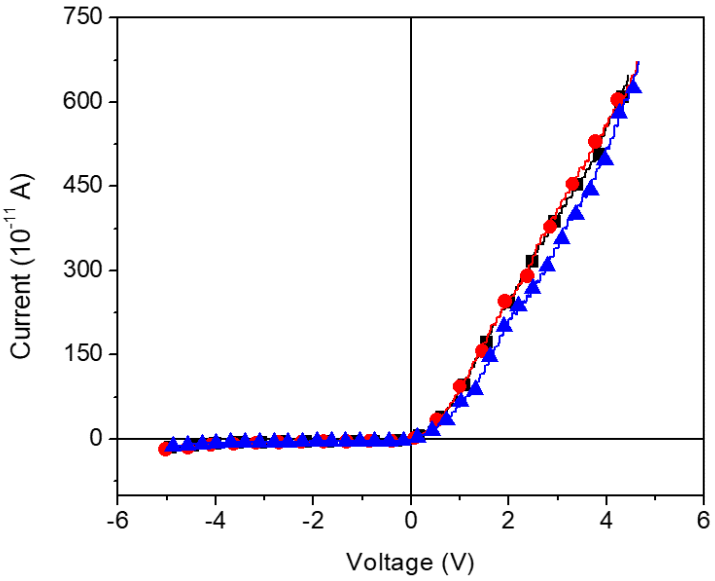

Figure B-3. The measured current-voltage curves from bipolar modified nanochannels.

The surface modification not only changes the surface charge of the nanochannel but also reduces the nanochannel size. The unmodified nanochannel used in this work is relatively larger compared with the small nanoparticles with a diameter of 5 nm. As a result, the RPS signals of nanoparticles are very small measured in unmodified nanochannel due to the low volume ratio of particles to the sensing channel. Figure B-4 shows an example of RPS signals measured in unmodified nanochannel. In this measurement, 0.1 M KCl solution containing nanoparticles of 5 nm is used as the sample solution. As shown in the figure, the signal-to-noise ratio is too small to determine the signal amplitude accurately. Therefore, only the results of the measurements for modified nanochannels with different surface charges are presented and compared at a small size.

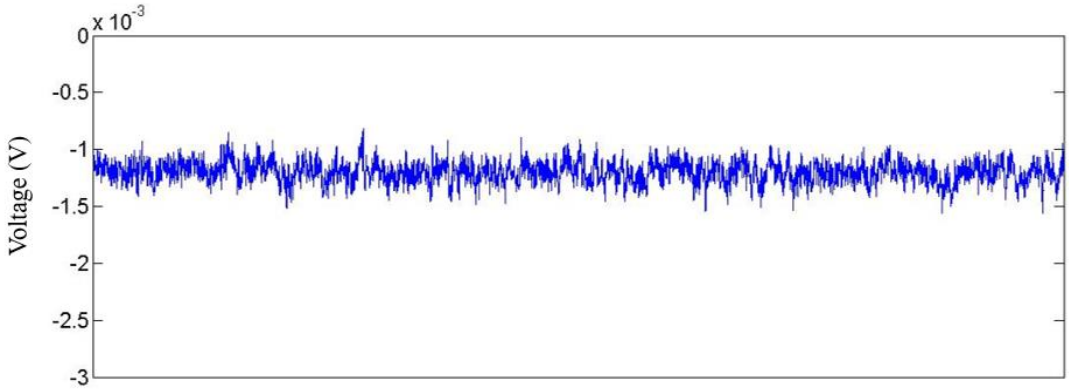

Figure B-4. An example of RPS signals of 5nm nanoparticles measured in unmodified nanochannel.